NASA Contractor Report 181945

DEVELOPMENT AND FABRICATION OF STRUCTURAL COMPONENTS FOR A SCRAMJET ENGINE

O. A. Buchmann

Contract NAS1-16097
March 1990

National Aeronautics and
Space Administration

Langley Research Center
Hampton, Virginia 23665-5225

NASA Contractor Report 181945

DEVELOPMENT AND FABRICATION OF STRUCTURAL COMPONENTS FOR A SCRAMJET ENGINE

O. A. Buchmann

AiResearch Los Angeles Division
Allied-Signal Aerospace Company
Torrance, California

Prepared for
Langley Research Center
under Contract NAS1-16097

March 1990

National Aeronautics and
Space Administration

Langley Research Center
Hampton, Virginia 23665-5225

FOREWORD

Many individuals at the NASA Langley Research Center and AiResearch contributed to this Scramjet structures program over the years. Mr. Hal Murrow was the NASA project manager during the final years of the program, and Mr. Bob McWithey before that. Additionally, Messrs. Paul Sandefur, Danny Barrows, and Henry Elksnin provided important technical coordination during the final phases of fabrication. The AiResearch program manager was Mr. Oscar Buchmann. The responsible program engineer during the full-scale fabrication efforts was Mr. Mike Lundberg. Messrs. Vic Arefian and Mike Faust were responsible for the earlier phases of the program and did much of the experimental work that provided the fabrication data base. All three also provided essential input to the original documentation that was used to support the preparation of this report.

CONTENTS

CONTENTS (Continued)

ILLUSTRATIONS

ILLUSTRATIONS (Continued)

ILLUSTRATIONS (Continued)

ILLUSTRATIONS (Continued)

ILLUSTRATIONS (Continued)

ILLUSTRATIONS (Continued)

ILLUSTRATIONS (Continued)

ILLUSTRATIONS (Continued)

ILLUSTRATIONS (Continued)

TABLES

1. INTRODUCTION

The NASA Hypersonic Research Engine (HRE) program (ref. 1), a major contributor to Scramjet technology development, led to the use of rectangular offset-fin, plate-fin coolant passages in hydrogen-cooled engine structures. This program culminated in the successful design, fabrication, and test of the first lightweight, hydrogen-cooled engine structure. The design life for the HRE cooled structures was 100 cycles and 10 hours, limited by creep and low-cycle fatigue.

Subsequent research at NASA-Langley led to a lightweight, fixed-geometry, modular, airframe integrated Scramjet concept promising high installed performance (net thrust) over a wide Mach number range. The Scramjet design study program (refs. 2 and 3). This program was an extension of the preliminary thermal-structural design of an airframe-integrated Scramjet study conducted by NASA (ref. 4). That study established the structural operating environment for the engine walls and the struts. A computer program for the transient thermal-structural analysis of a strut was developed as part of this work and was used as a check on design conditions. It defined an engine concept based on near-term metallic materials and manufacturing technology, with a life of 100 hours and 1000 cycles. Emphasis was placed on the engine thermal-structural design. Figures 1 and 2 show the general engine configuration. Figure 3 and Table 1 show the nominal structural design conditions for the engine and life cycle behavior as a function of cooling jacket ΔT.

The advanced fabrication techniques program for hydrogen-cooled engine structures (ref. 5) was a direct precursor of this program and was undertaken to evaluate key features identified in the Scramjet design study. Coolant passage geometries, material systems, and joining processes that will produce long-life hydrogen-cooled structures for application to a scramjet were developed. The results were used to establish the final design details for the strut and the baseline fabrication processes for the current program.

The program covered in this report consisted of four tasks: Task 1 (strut leading edge design verification), Task 2 (heat transfer performance), Task 3 (fabrication of fuel injection strut), and Task 4 (flat panel evaluation). Task 2 involved the design of a heat transfer test specimen for evaluation of pin-fin and channel coolant passage geometries using air in lieu of hydrogen. Section 2 provides an additional summary of each program task. In Task 4, the concept for a structural test panel was designed. This test panel incorporated important, typical features of an engine sidewall, including support structure, cooling jacket, and coolant manifolds. Its mounting system accommodates simultaneous structural and thermal loading. The main program activity, however, was in Tasks 1 and 3; discussion of these constitutes the bulk of this report. Section 2 provides an additional summary of each program task.

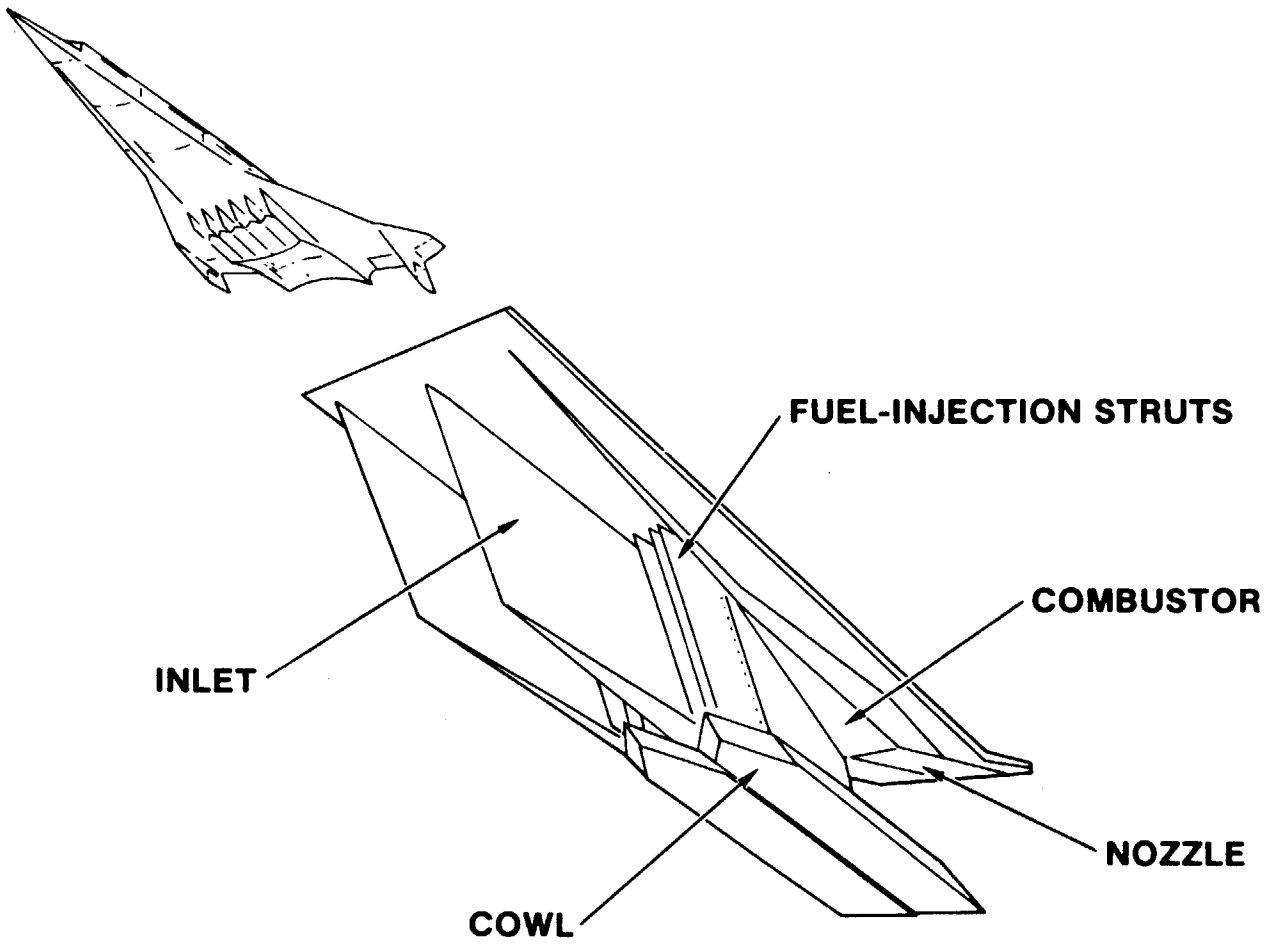

Figure 1. Scramjet Reference Design

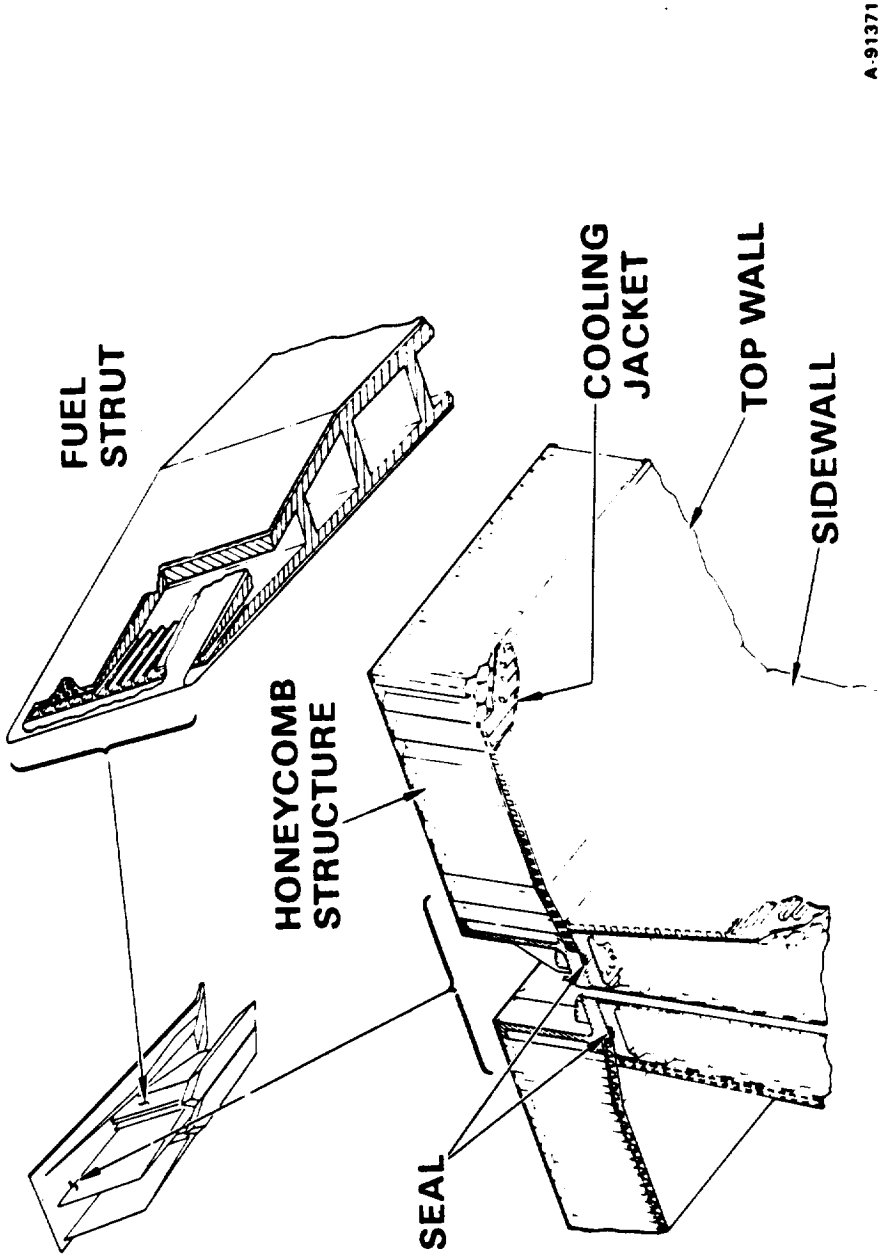

Figure 2. Features of Scramjet Cooled Structure

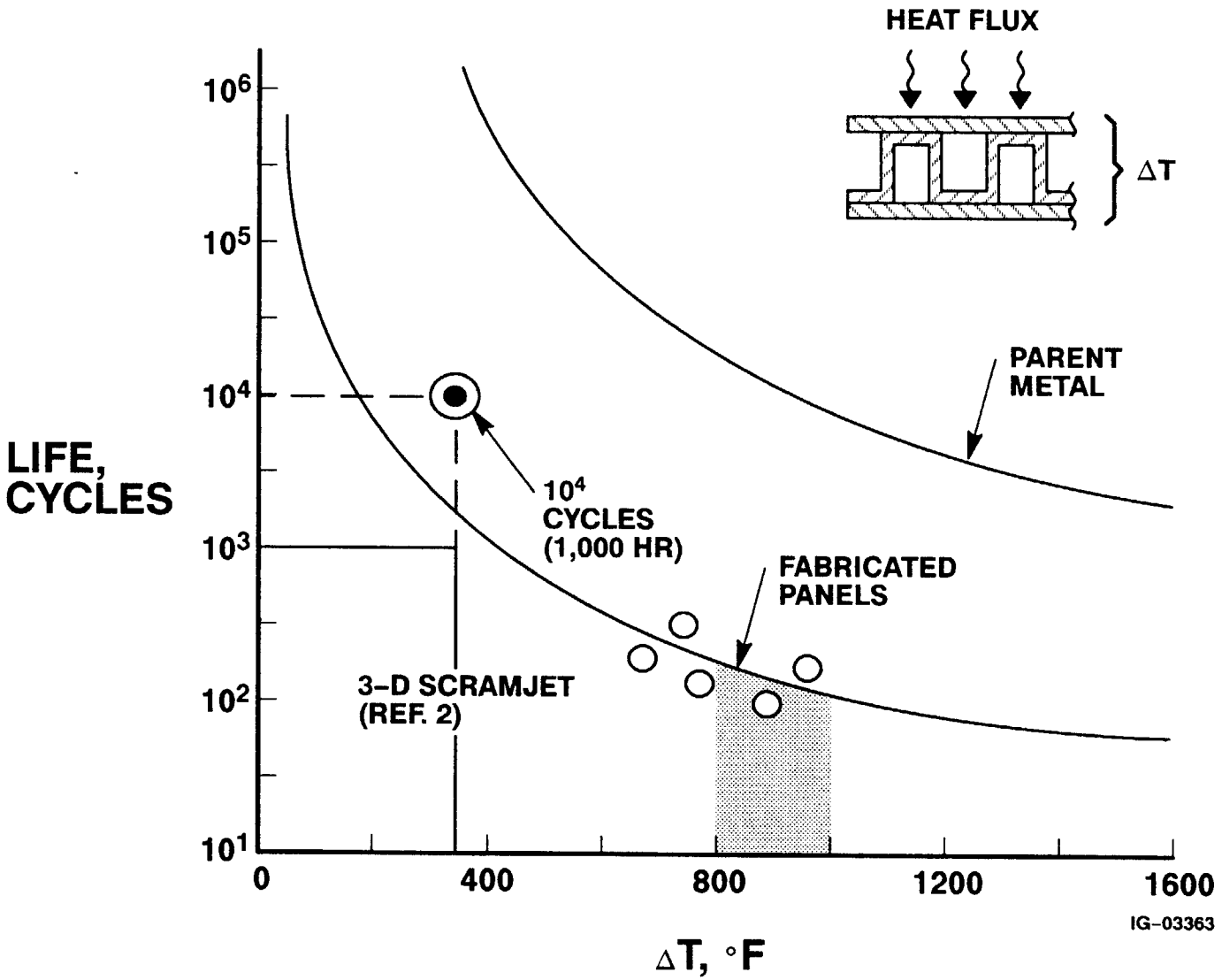

Figure 3. Program Goal

TABLE 1 DESIGN CONDITIONS	
Life	100 Hrs, 1000 Cycles
Deflections	< 5% Area, 0.4°
Metal Temperature	< 1600°F
Hydrogen Inlet Outlet Coolant Ø	 1000 psia, -360°F 750 psia, 1140°F < 1.0

A fuel injection strut was selected for fabrication development because the struts are among the most critical of the engine features. The basic function of the struts is the in-stream injection of fuel (hydrogen) at four distinct stations on each of the three struts. Although they span the full engine height, from the top wall to the cowl, they provide no structural tie between the two. The top wall serves as the primary support for the strut; the cowl allows free span-wise motion and restrains lateral, axial, and twisting loads.

Figure 4 (taken from ref. 2) shows the design pressure loads used for the struts, based on the assumption of an asymmetrical engine unstart at M = 5.1. This condition was used because it is the most severe aerodynamic loading. The high net load on the side strut led to its selection for this program. Figure 5 (from ref. 2) shows the heating rates used in the design, taken at the M = 10 operating condition. This is the highest thermal loading and served to define the cooling requirements, and the creep-rupture and low-cycle-fatigue performance. Although the heating rates are somewhat lower for the side strut than for the center strut, the side strut was judged the most severe combined-load case. Tables 2 and 3 list the heat loads and fluxes for both kinds of struts.

The struts, therefore, were specified to combine severe structural and performance requirements with severe volume constraints and complex mechanical assembly. This combination of requirements places demands on design efficiency, the fits and tolerances of detail parts, and both guided and constrained development and detailed investigations. Table 4 lists the important concerns that result from these requirements.

The development effort, as described in the report, extends through delivery of one set of three major subassemblies: the Inconel 718 support structure assembly and the forward and aft cooling jacket assemblies. Ni-201 is the pin-fin material of the aft jacket and Ni-200, of the forward jacket.*

*Ni-201 is preferred because of its lower carbon content and the expected increase in ductility (not verified on this program). Ni-200 was used because it is more readily available in small quantities.

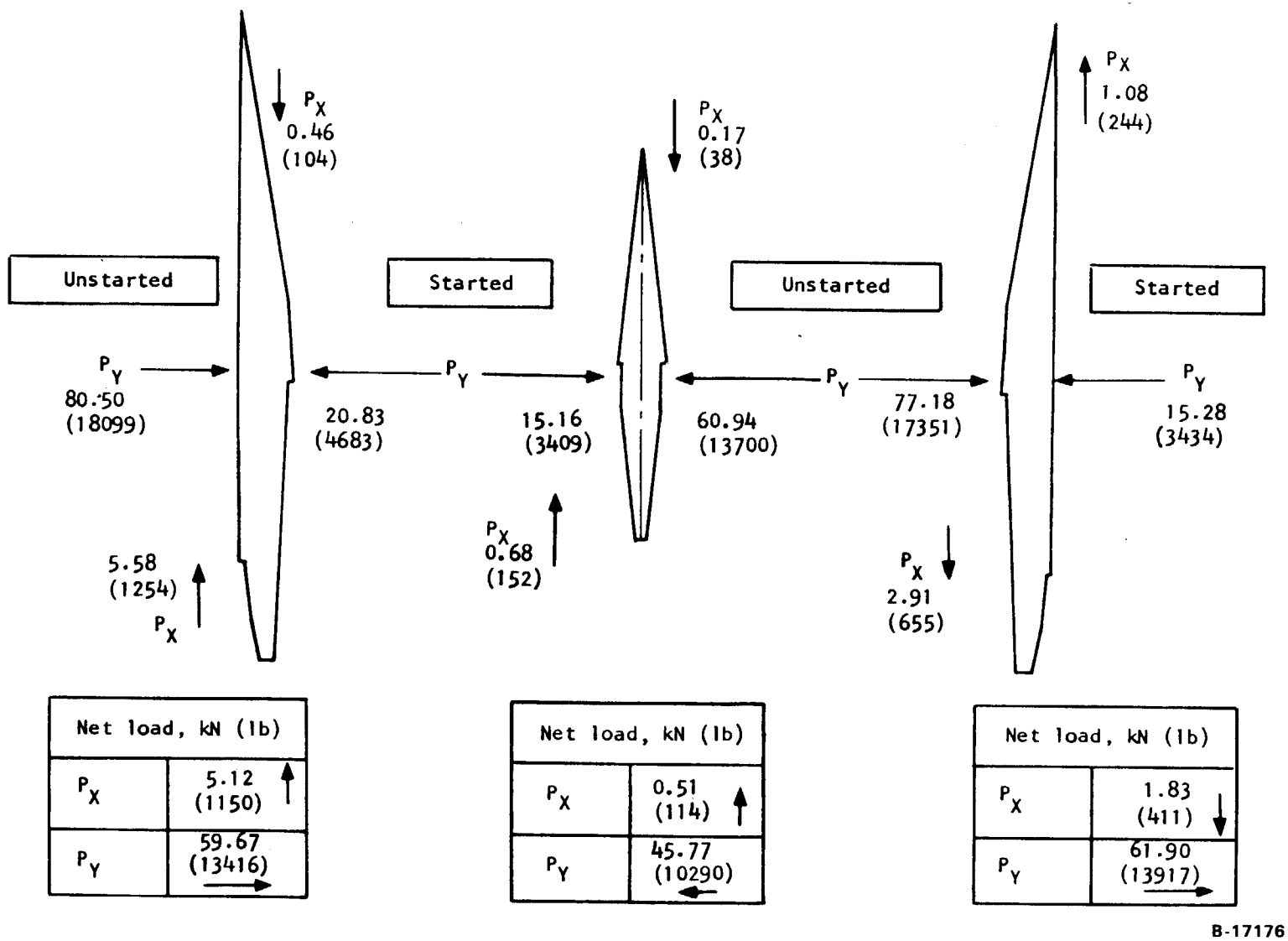

Figure 4. Strut Loads, Transient Unstart Conditions

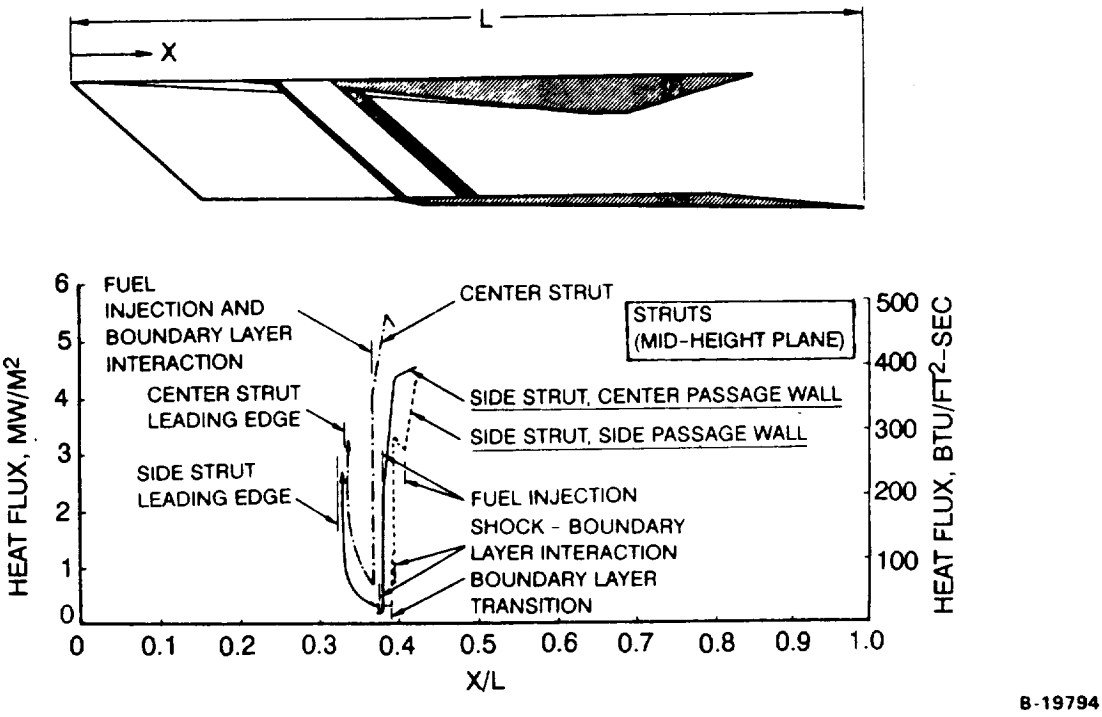

Figure 5. Aerodynamic Heating Rates on Fuel Injection Struts at Maximum Heating Condition (Reference 2)

TABLE 2

STRUT HEAT LOADS
($M\infty = 10$, $q\infty = 1500$, 2-G TURN, $\Phi_f = 1.5$)

Location	Maximum Flux	Average Flux	Heat Load
	Btu/sec-ft^2		Btu/sec
Center strut	480	231	454
Side strut, center	400	184	548
Side strut, side	380	132	392

TABLE 3

LEADING EDGE HEAT FLUXES
($M\infty = 10$, $q\infty = 1500$, 2-g TURN, $\phi_f = 1.5$)

Location	Heat Flux, Btu/sec-ft^2	
	0.8 mm (0.030-in.) radius	1.3 mm (0.050-in.) radius
Side strut	1718	1331
Center strut	2313	1792

TABLE 4

DESIGN CONSIDERATIONS

Thermal

- Creep life and cycle life under high heat flux loading
- Transient structural ΔT's

Configuration

- Multiple fuel injection stations
- Separation of internal hydrogen flows
- Flow distribution and pressure drop

TABLE 4 DESIGN CONSIDERATIONS (Continued)
Structural – long, slender body under severe loads • Thermal • Aero (unstart) • Pressure containment Manufacturing • Sequenced multi-stage assembly • Dimensional control • Process control • Inspectability

Section 4 describes the various development efforts undertaken in support of full-size strut fabrication, including a series of manufacturing investigations. Most of the experimental work that used subelements of specific features of the strut have been included in Section 4 to provide a common reference for subsequent discussions. Many of the tests were derived from experience gained in fabricating two partial-length struts. Some of the tests were generic or in direct support of the basic partial- and full-length strut efforts, (e.g. development of tooling, definition of process parameters and their application, and inspection requirements). As a result of this grouping of activities, discussions in Section 4 sometimes precede the discussion of the experiences in Sections 5 and 6 that were the cause of the investigations, as in the case of the partial-length struts.

Sections 5 and 6 review the manufacturing experience with the struts. As noted, the partial-length struts identified many of the manufacturing subtleties that characterize the strut and provided important input to the manufacturing investigations. The results described in Sections 4 and 5 led to many of the processing and tooling methods that were applied on the full-length struts. The detail data provided in Section 4 (and, to a lesser extent in Section 5) are used as a common reference and are not repeated in Section 6. Instead, Section 6 provides a narrative of the manufacturing sequences and shows where additional effort might be needed to facilitate fabrication.

1.1 Symbols

C_p	Specified heat at constant pressure, Btu/lb°F
E	Young's modulus, lb/in.^{2}
F	Load or force, lb
F_{ty}	Yield strength, lb/in.^{2}
F_{tu}	Ultimate strength, lb/in.^{2}
K_e	Stress reduction factor due to elastic constraint, dimensionless
K_f	Effective stress concentration factor in fatigue, dimensionless
K_t	Theoretical stress concentration factor, dimensionless
P	Pressure, lb/in.^{2}
t	Time, hrs
T	Temperature, °F, and joint thickness, in.
ΔT	Temperature difference, °F
σ	Stress, lb/in.^{2}
τ	Shear stress, lb/in.^{2}
ϕ	Equivalence ratio, dimensionless. Engine ϕ (ϕ_f) is actual fuel flow/fuel flow for stoichiometric combustion; coolant ϕ (ϕ_c) is coolant flow/actual fuel flow to the engine.
w	Mass flow rate, lb/sec

1.2 Abbreviations

EDM	Electrical discharge machining
FL	Full length, with reference to a strut of full-size cross section
LCF	Low cycle fatigue
LE	Leading edge
PCM	Photochemical machining

PL	Partial length, with reference to a strut of full-size cross section
psid	Pressure, lb/in.^{2} differential
psig	Pressure, lb/in.^{2} gage
RT	Room temperature
TPS	Thermal protection system

2. SUMMARY

Results of the previous studies (references 2 through 6) indicated that the basic goal of increasing the life of hydrogen-cooled structures two orders of magnitude relative to that of the Hypersonic Research Engine could be reached with available technology. Estimated life based on extrapolations of creep-rupture and low cycle fatigue tests (ref. 5), is 19,000 cycles for the channel coolant passage and 16,000 cycles for the pin-fin coolant passage configurations, Figure 6, using Nickel 201. Additional research is required to establish the fatigue characteristics of dissimilar-metal coolant passages (Nickel 201/Inconel 718) and to investigate possible embrittling effects of the hydrogen coolant.

The program described here focused on fabrication of a full-size fuel injection strut based on the previously developed design (ref. 2) and fabrication techniques (ref. 5).

2.1 Task 1 – Verification of Strut Leading Edge Design

The leading edges are exposed to stagnation line heat fluxes that range from 900 to 1800 Btu/sec-ft^2 (ref. 2). This is the most severe loading on any of the engine components. By using direct impingement cooling with cryogenic hydrogen, a sharp, 0.050-in. radius leading edge can be used at these heat fluxes. Nickel 201, a high thermal conductivity material, was selected for the leading edges primarily to obtain a life in excess of 1000 cycles. Although this material has good low cycle fatigue performance, its creep strength is low. As a result, metal temperatures must be lower than temperatures for superalloys. The high thermal conductivity of the nickel, on the other hand, minimizes ΔT in the face sheet and allows operation at coolant temperatures approaching those when using superalloys that have much higher, allowable creep strengths but relatively lower thermal conductivities.

The objective of this task was to evaluate the fabricability and structural performance of the selected leading edge design. The efforts included the following:

(a) Final definition of the detailed design of the impingement-cooled strut leading edge.

(b) Fabrication of partial length specimens of the strut leading edge using the previously selected materials and fabrication techniques (refs. 2 and 5).

(c) Tests of the combined creep and thermal fatigue performance of the strut leading edge stagnation region using a structural model based on structural simulation (see para. 4.3). This model is simple and allows rapid, bench-top evaluation of materials and processing effects.

2.2 Task 2 – Heat Transfer Performance of Pin-Fin Cooling Jacket

The work of this task involved the design of a test unit for evaluation of the heat transfer and pressure drop performance of the photoetched channel and pin-fin cooling passages selected for the engine cooling jacket. The task was terminated with the preparation of an engineering drawing. The coolant passages are formed by PCM, with channel depths and/or pin heights in the range of 0.02 to 0.03 in. Figure 3 shows typical test panels incorporating these passages (fabricated under the ref. 5 effort).

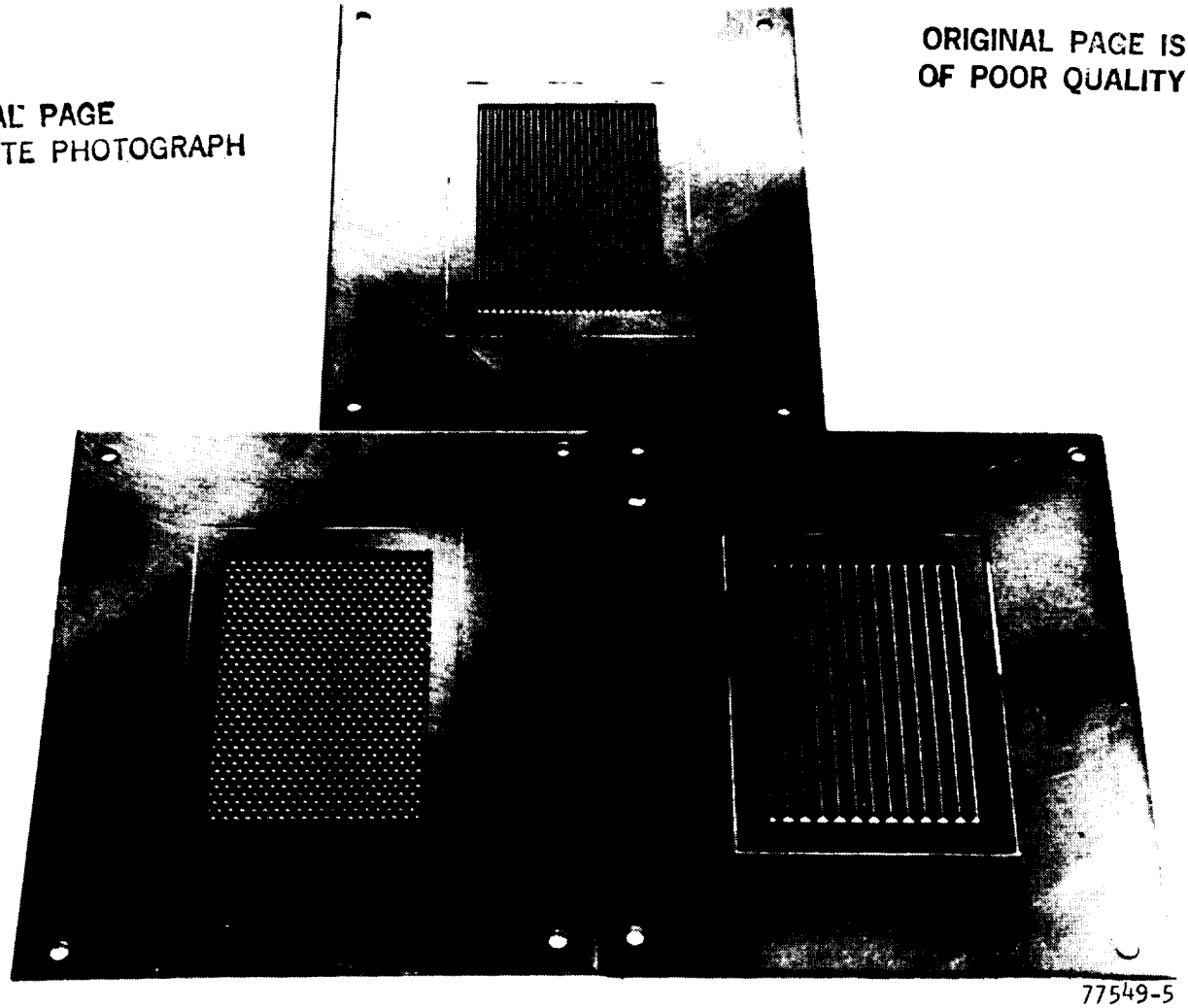

77549-5
F-34927

Figure 6. Photochemically Machined Pin-Fin and Channel Coolant Passage Panels

2.3 Task 3 – Fabrication of Fuel Injection Strut

The strut design used as the basis of this task was taken from the engine design (ref. 2) and is suitable for thermal and structural testing in a hot gas wind tunnel at NASA-Langley. The following design, development, fabrication, and test efforts were completed: (1) the finalization of the design of the strut and the definition of interfaces for use with the wind tunnel, (2) the development of the tooling and fabrication procedures required to fabricate a side strut (versus the center of the three struts) and a mounting adapter, (3) the fabrication and delivery to NASA of all components, including major subassemblies of a full-size strut, and (4) the nondestructive inspection and testing of these components prior to delivery.

The overall accomplishments or technological contributions from the program generally reflect the specific design features of the reference strut, but also include important generic data. The broad areas in which the program provided valuable data include:

- Successful completion and delivery of the three major strut subassemblies: the Inconel 718 support structure, and the forward and aft Nickel 201 cooling jackets
- Development of design, materials, and manufacturing data for this type of thermal-structural engine component, with much of the data derived in case-specific investigations
- Development of forming and joining techniques that allow successful assembly of sheet-metal-type components to essentially machining-type tolerances
- Manufacturing feasibility of this type of strut
- Validation of the strut pressure containment concept

Figure 7 shows the full-size strut assembly.

2.4 Task 4 – Flat Panel Evaluation of Engine Sidewall

This task developed the design of a thermal-structural test panel. The panel is representative of the flat surfaces and structure of the engine (ref. 2) and is composed of cooling jackets, manifolds, and supporting structure. It was designed to allow experimental evaluation of the transient thermal and structural performance of such cooled, flat panels. The task was terminated with the preparation of an engineering drawing.

FOLDOUT FRAME 2

ORIGINAL OF POOR

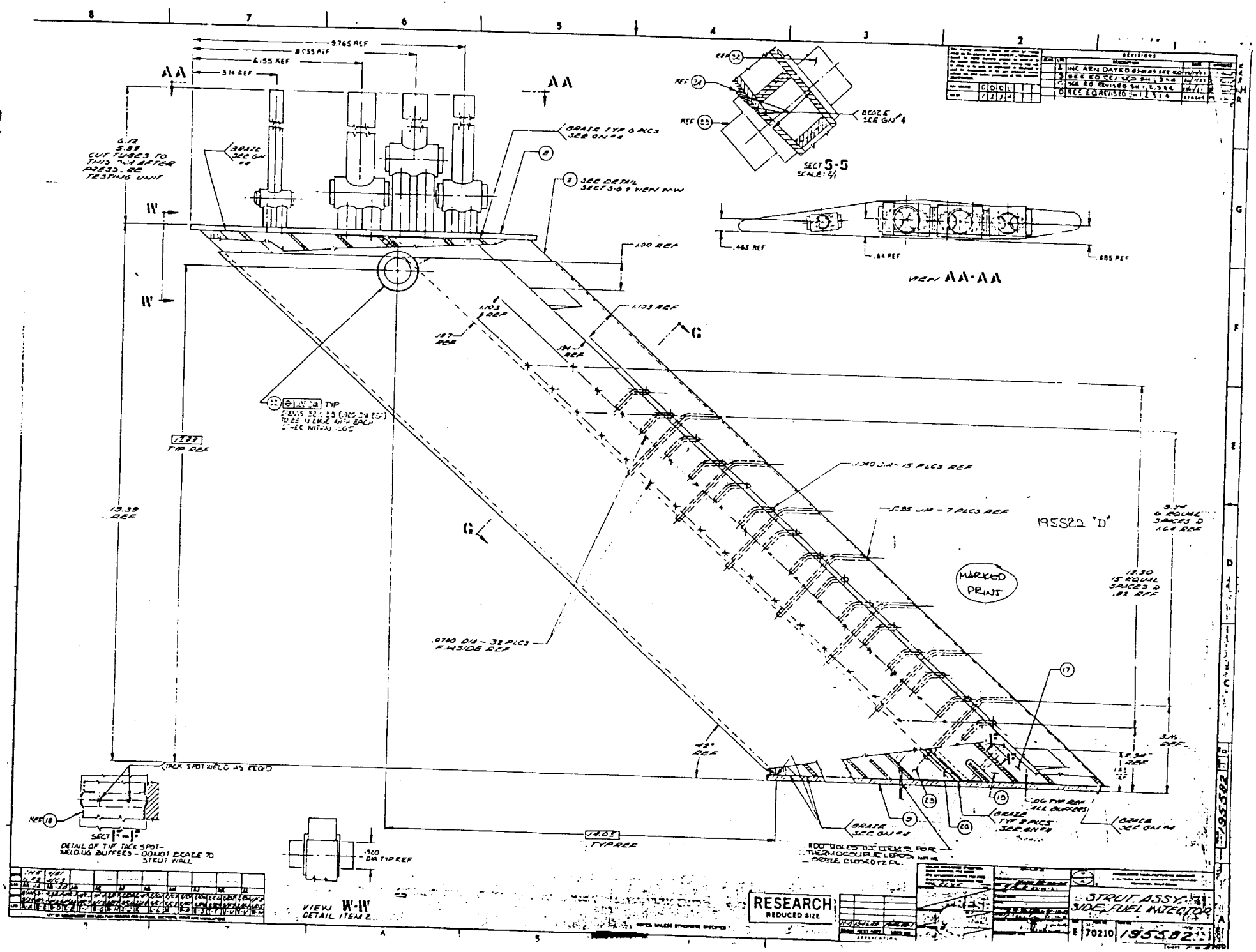

FRAME 1

FOLDOUT FRAME 2

ORI
OF

AGE IS
UALITY

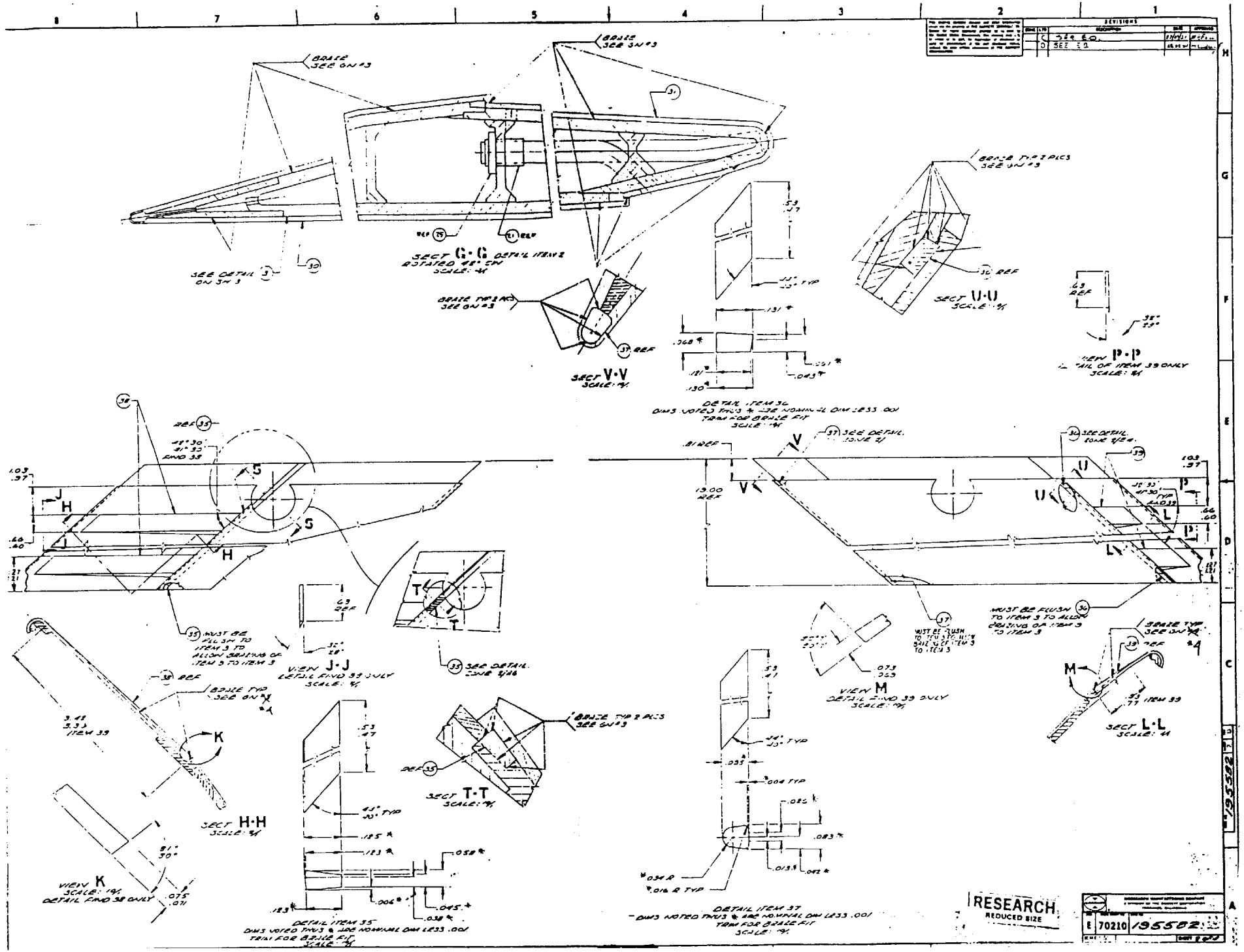

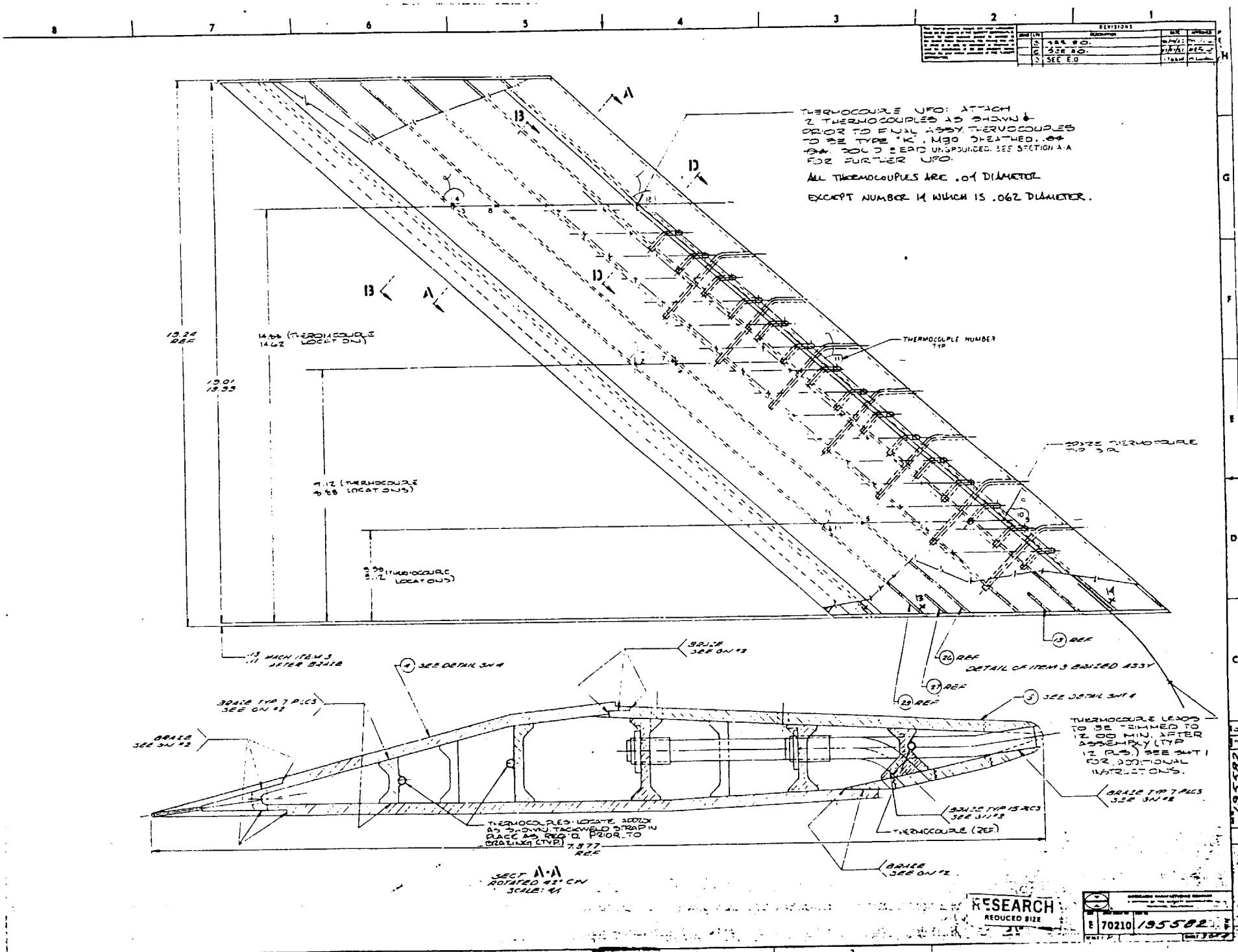
THERMOCOUPLE LEADS TO BE TRIMMED TO 12.00 MIN. AFTER ASSEMBLY (TYP 12 PLS.) SEE SHT 1 FOR ADDITIONAL INSTRUCTIONS.
THERMOCOUPLE NUMBER TYP
SECT A-A ROTATED 43° CW SCALE: 1/4
DETAIL OF ITEM 3 BRAZED ASSY
RESEARCH
REDUCED SIZE
70210
195582

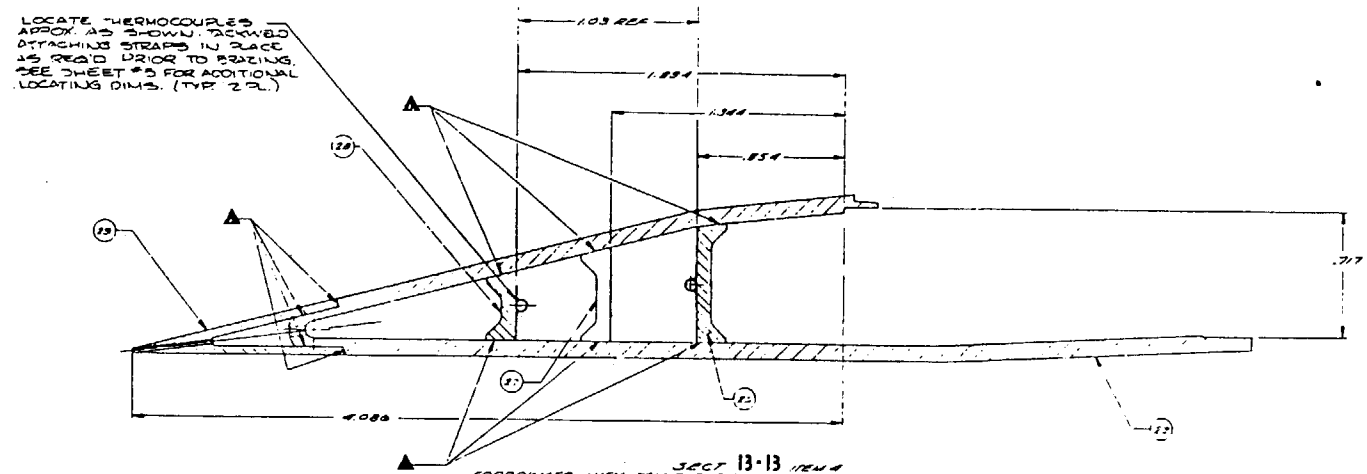

SECT 13-13 ITEM 4
COORDINATE WITH ITEM 5 FOR A BRAZE FIT AS SHOWN IN SECT A-A, SH 3. REPLACE .015 BRAZE ECH (AMS 4788) IN JOINTS MARKED THUS ▲ AND TACKWELD TOGETHER AS SHOWN

NOTE: ASSEMBLE & TACKWELD THERMOCOUPLES TO LOCATIONS SHOWN ON SHEET 3 BEFORE ASSEMBLY.

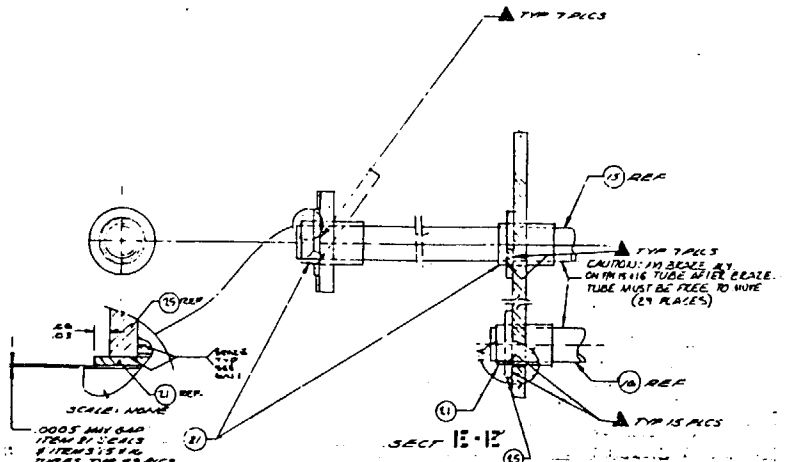

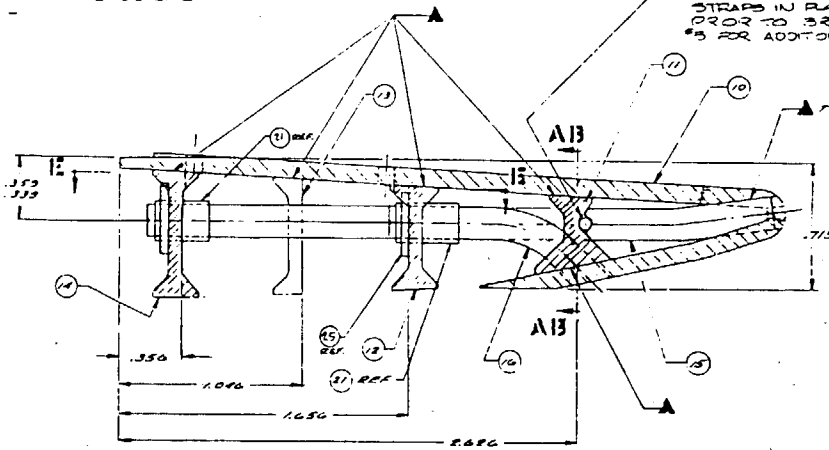

SECT D-D ITEM 5
COORDINATE WITH ITEM 4 FOR A BRAZE FIT AS SHOWN IN SECT A-A, SH 3. REPLACE .015 BRAZE ECH (AMS 4788) IN JOINTS MARKED THUS ▲ AND TACKWELD TOGETHER AS SHOWN

NOTE: ASSEMBLE & TACKWELD THERMOCOUPLES

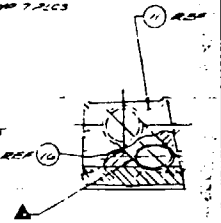

SECT A13-A13
TYP 15 PLCS

RESEARCH
REDUCED SIZE

REVISIONS			
LTR	DESCRIPTION	DATE	APPROVED
B	SEE E.O.		
C	SEE E.O.		
D	SEE E.O.		

8 7 6 5 4 3 2 1

G F E D C B A

3. TASKS 2 AND 4 – COOLED TEST PANEL DESIGN

Preliminary designs of two types of panels were prepared: one for use in evaluating the basic heat transfer and friction characteristics of pin-fin cooling jackets (Task 1); the other, for evaluating the structural performance of a cooled, flat engine panel under combined thermal and pressure loads (Task 4). The important design considerations used in formulating the designs are summarized below.

3.1 Task 2 – Heat Transfer Performance of Pin-Fin Cooling Jackets

The test unit is approximately 6 in. by 6 in. and features a single passage (of known thermal characteristics) sandwiched between two pin-fin test surfaces. Water and air are the test fluids. Large water flow rates are used in the known passage to provide a large thermal capacity rate (WC_P) relative to the airflow used in the pin-fin passages. By this means, the contribution of the water side to experimental uncertainty is minimized. The water and air passages are oriented in a cross-flow configuration to facilitate manifolding. The high-capacity rate of the water will also minimize cross-flow effects on the data. Figure 8 shows the test unit. Figure 9 shows the arrangement of the fluid passages in the test unit.

The design Reynolds number for the air was matched to the nominal Reynolds number for hydrogen in the strut at the design point (15,000). The design point was taken from reference 2. Mach numbers were kept sufficiently low so that shock losses and compressibility effects are minimal. On the air side, Reynolds numbers are 5000 to 20,000 (in the turbulent regime) to enhance predictability. Table 5 lists the test conditions formulated as part of this effort.

Following completion of the design, this task was terminated and no hardware was built.

3.2 Task 4 – Flat Panel Evaluation of Engine Sidewall

A cooled panel that is representative of an engine sidewall was designed with the objective of assessing the transient thermal and structural performance of the cooled flat panels. Pressure and thermal loads for an unstart condition (Figures 6 and 7 of ref. 2) served as the basis for the design. Pressures peak at 130 psia, with a sidewall top-bottom average peak of 100 psia; heat fluxes peak at 350 Btu/ft^2-sec, with an average peak of 250 Btu/ft^2-sec.

FOLDOUT FRAME 2

ORIGIN
OF PO

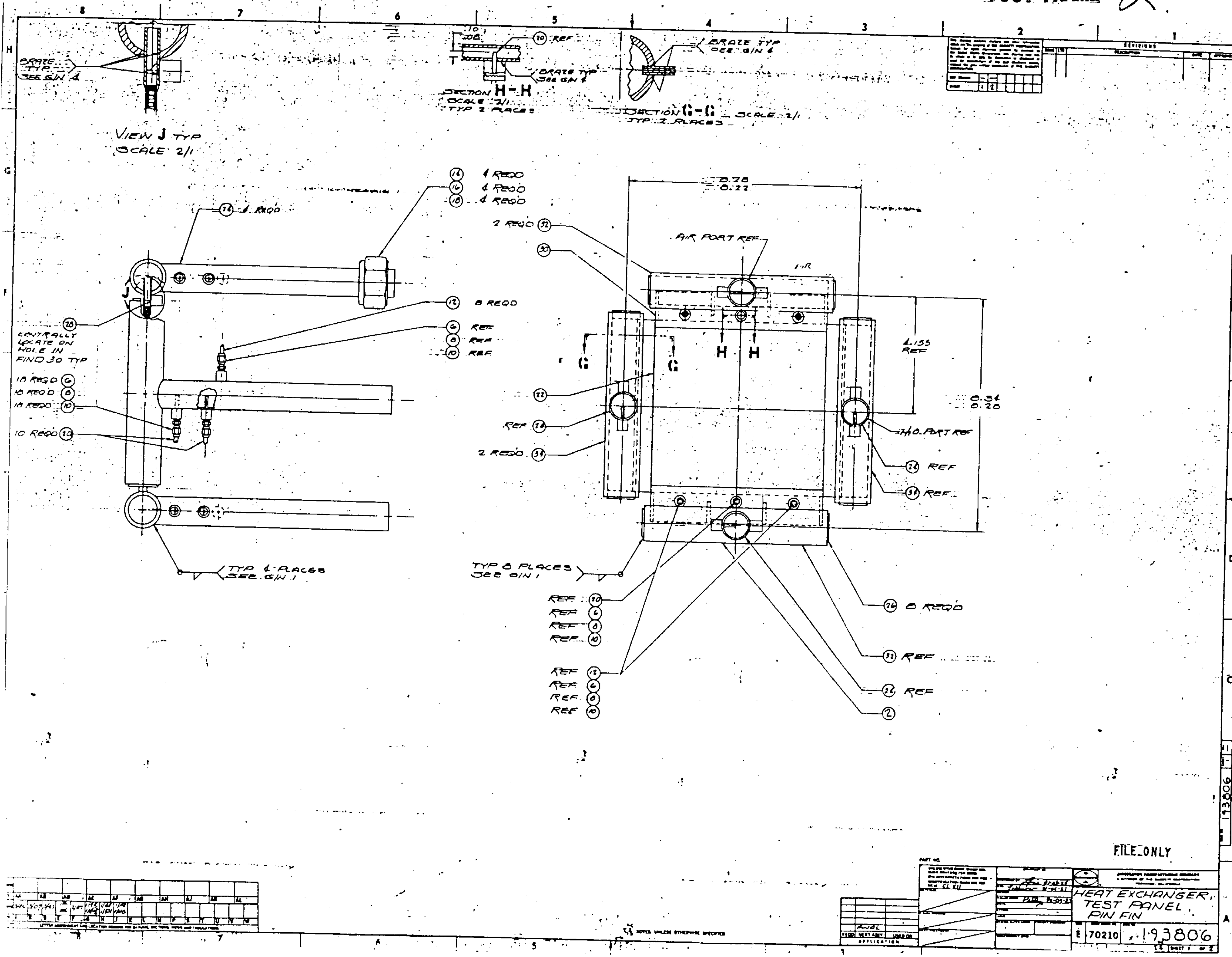

FILE ONLY

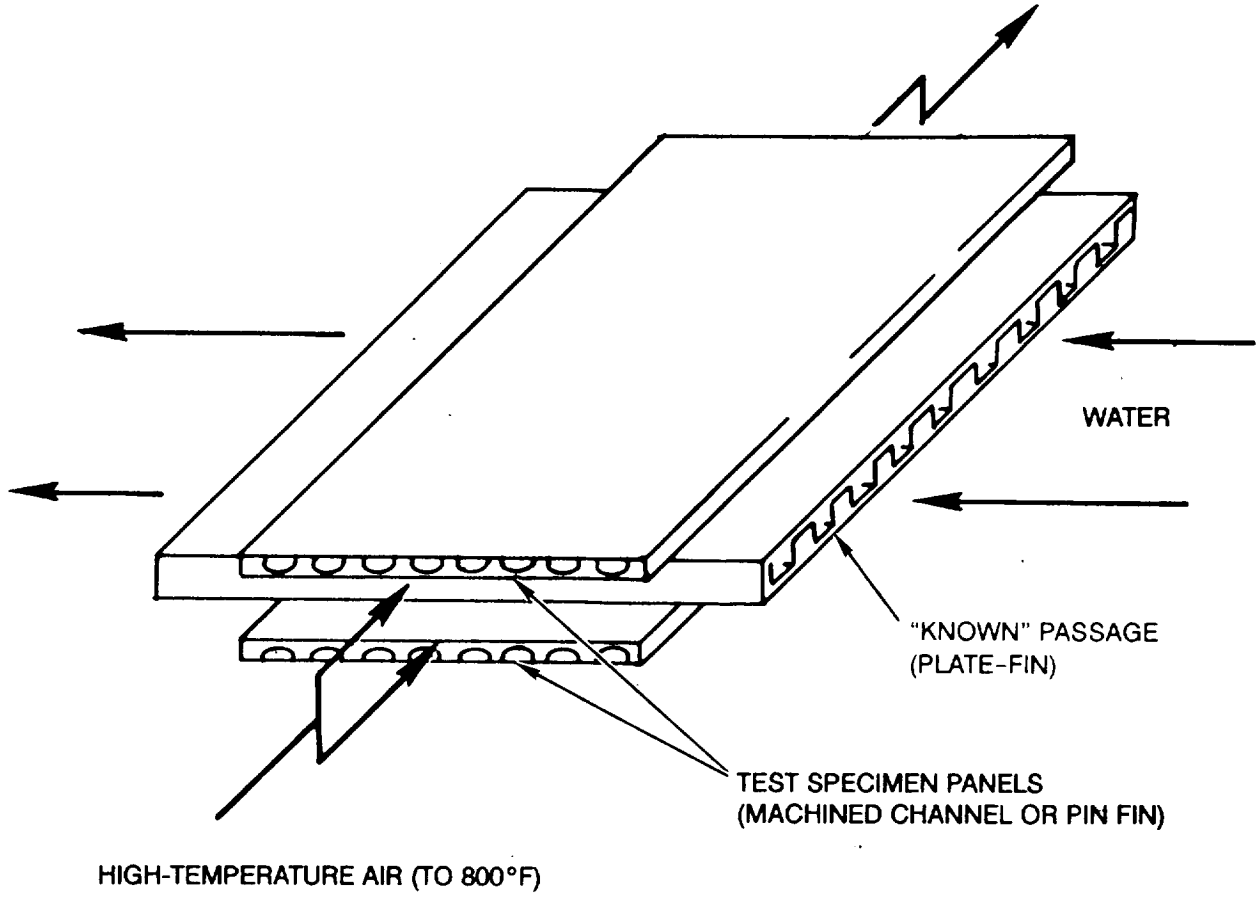

Figure 9. Flow Configuration of Heat Transfer Performance Test Unit

TABLE 5*

TEST CONDITIONS

Test Condition	Air Side			Water Side		
	Flow Rate (lbm/min)	T_{IN} (°F)	P_{IN} (psia)	Flow Rate (lbm/min)	T_{IN} (°F)	P_{IN} (psia)
ISOTHERMAL PRESSURE DROP TESTS						
1	1.75	70	450	20	70	120
2	2.17	↓	↓	30	↓	↓
3	2.79			35		
4	3.49			45		
5	4.40			55		
6	5.59			70		
7	6.98	↓	↓	90	↓	↓
HEAT TRANSFER TESTS						
1	2.5	600	450	50	70	120
2	3.1	↓	↓	50	↓	↓
3	4.0			70		
4	5.0			70		
5	6.3			90		
6	8.0			90		
7	10.0	↓	↓	90	↓	↓

*Tests were not conducted

The test panel design includes inlet and outlet manifolds, edge closures, honeycomb stiffening members, and support brackets.

Thermal tests require a heat source capable of providing the typical operational heat loads. The most suitable existing heat source at the time of the study was a carbon filament heater, with a flux of approximately 190 Btu/sec-ft^2, located at the Structures Directorate of the NASA Langley Research Center. Alternatives that were reviewed included surface combustors and gas burners. A review of past experience, however, has shown the porous surface combustor to have much lower heat flux capabilities than needed and to be unreliable and susceptible to flashbacks at elevated temperatures. Gas burners were judged unattractive because of their potential uncertainties in applied thermal loads and control and limited heat flux capabilities.

The design features a photochemically machined Ni-201 channel TPS surface supported by Hastelloy X honeycomb sandwich structure. Figure 10 is a layout of the test panel. The facesheet channels are 0.0255 in. high (0.0225-in. radius), 0.045-in. wide at the base, and 0.0615 in. center-center; the facesheet thickness is 0.0165 in., giving a total thickness of 0.042-in. The honeycomb sandwich is 2.25-in. high, with 0.003-in. cell walls and 0.06-in. facesheets. The cooling jacket facesheet is brazed directly to the honeycomb facesheet.

The mounting system for the panel is based on a series of pinned connections. These allow free thermal growth. Coolant inlet is provided by two manifolds, one on each side, with the flow toward the single outlet manifold. This was done to permit a more clear-cut evaluation of the manifold region in mid-panel than is possible with the edge effects associated with the end manifolds for flow across the entire panel length.

After the conceptual design was completed, this task was terminated and no hardware was built.

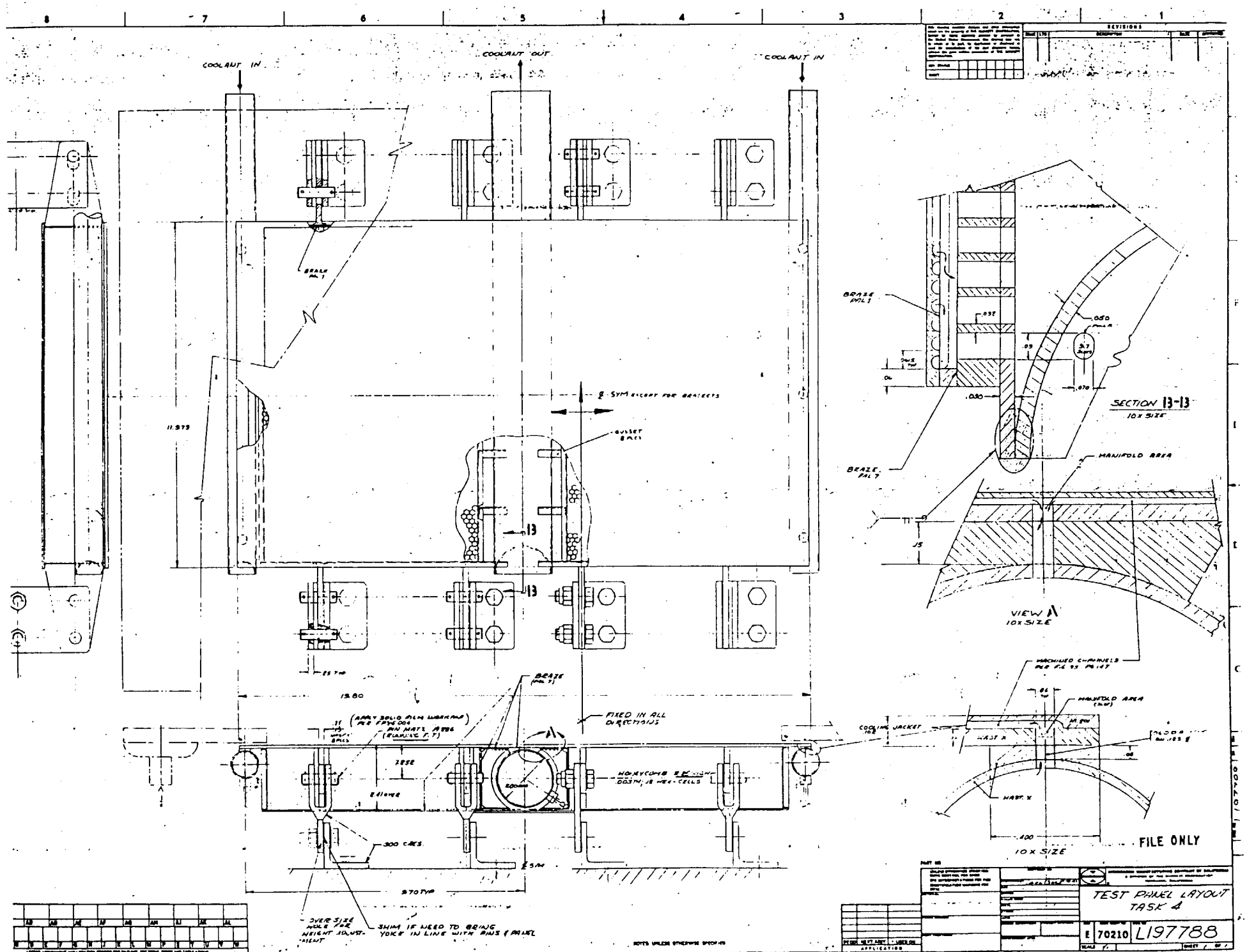

4. FUEL INJECTION STRUT DEVELOPMENT

4.1 Configuration

The design of the full-scale side strut features a final assembly consisting of a number of brazed subassemblies, as summarized in Table 6. Figure 11 shows the general configuration of the strut; Figure 12 shows the sequence of brazing operations; additional details on the assembly operations are shown in Figures 13, 14, 15, and 16. Table 7 shows the temperature and pressure schedules used for strut brazing. Temperature histories from the furnace runs are shown in Figures 17 through 20. PL strut records are included for those operations that were not performed on the FL strut. These records incorporate the modifications and refinements that resulted from the various development efforts discussed in Sections 4, 5, and 6. Figure 21 shows a cutaway model of the strut. Some of these figures show internal details that represent early strut designs, and they are included to conveniently highlight the main features.

TABLE 6

FABRICATION SEQUENCE FOR THE FUEL INJECTION STRUT

INCO-718 Support Structure
Tool design and fabrication
Form and hot size skin
Fabricate leading edge insert
Assemble and braze strut body
Detail parts fabrication
Cooling jacket/support structure braze
Cooling Jacket Assembly
PCM pin-fin face sheets
Assemble and braze
Form and hot size
Support Structure Assembly and Braze
Final assembly and braze
Final pressure test/hold
Ship to NASA

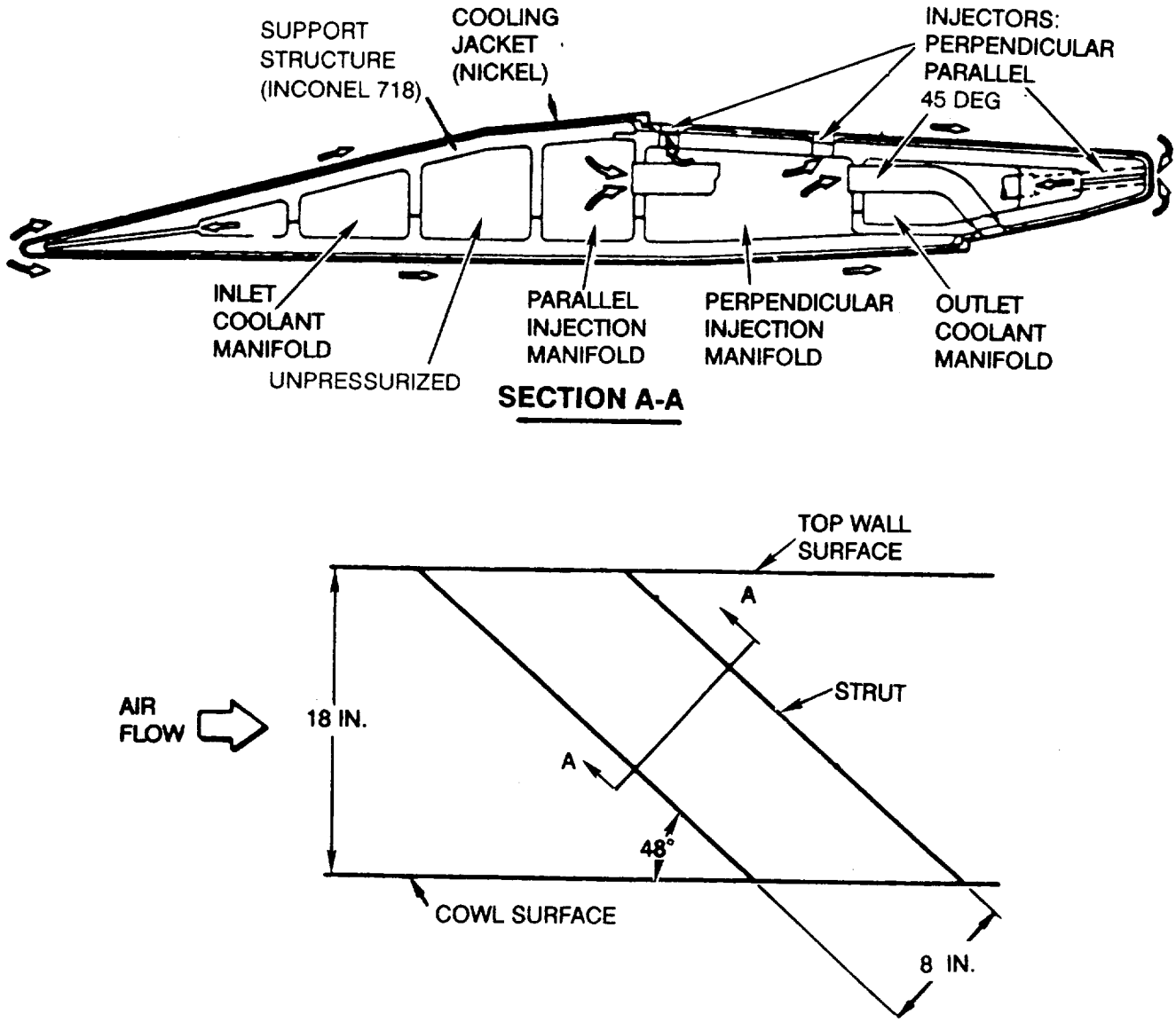

Figure 11. Side Strut Assembly

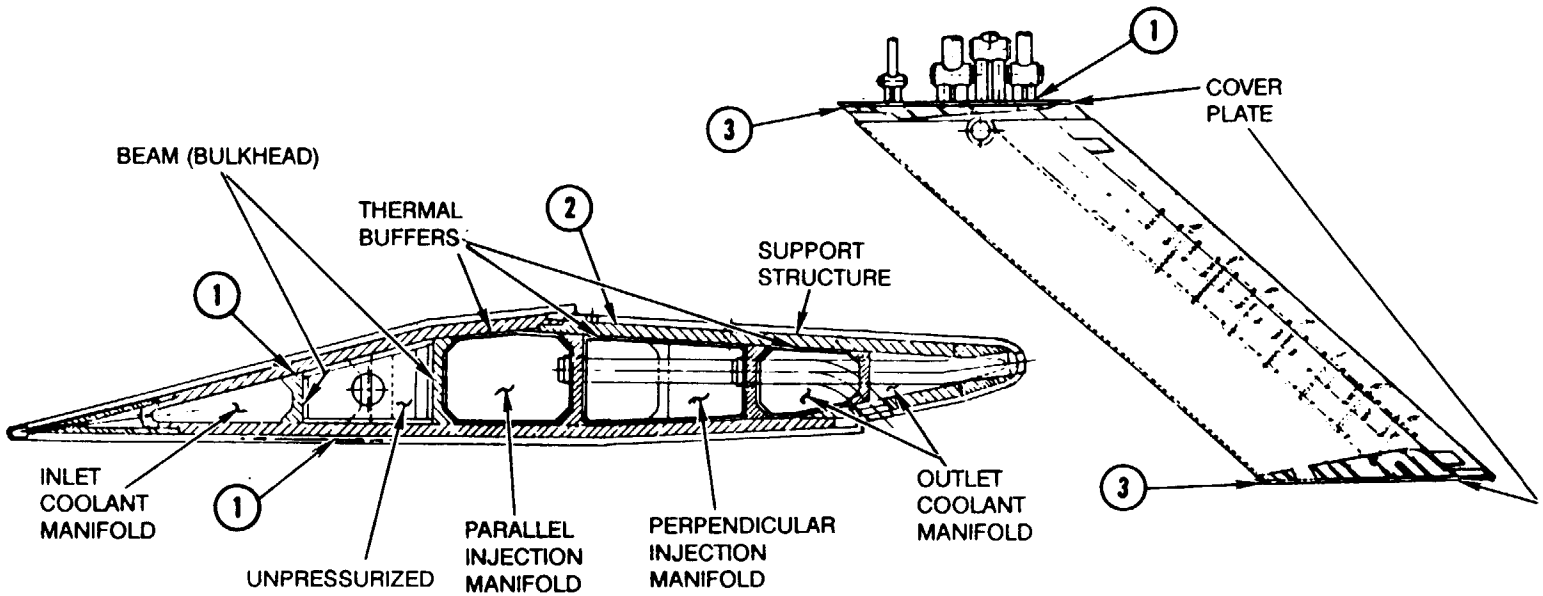

BRAZE TEMPERATURES

SEQUENCE	JACKET	SUPPORT STRUCTURE	COVER PLATE	ASSEMBLY
1	2070	2070	2070	-
2	-	-	-	1935 (JACKET-SUPPORT STRUCTURE)
3	-	-	-	1800

B-19641

Figure 12. Strut Assembly Features

- SINGLE SANDWICH CONSTRUCTION
- PCM PIN-FIN COOLANT PASSAGE
- Ni-201 PIN-FIN SHEET 0.035 IN.
- Ni-201 BACK SHEET 0.010 IN.
- 50% Au-25% Pd-25% Ni (PALNIRO 1) 0.0015-IN. BRAZE FOIL
- BRAZE IN VACUUM BAG (2070°F)
- HOLOGRAPHIC PRESSURE TEST

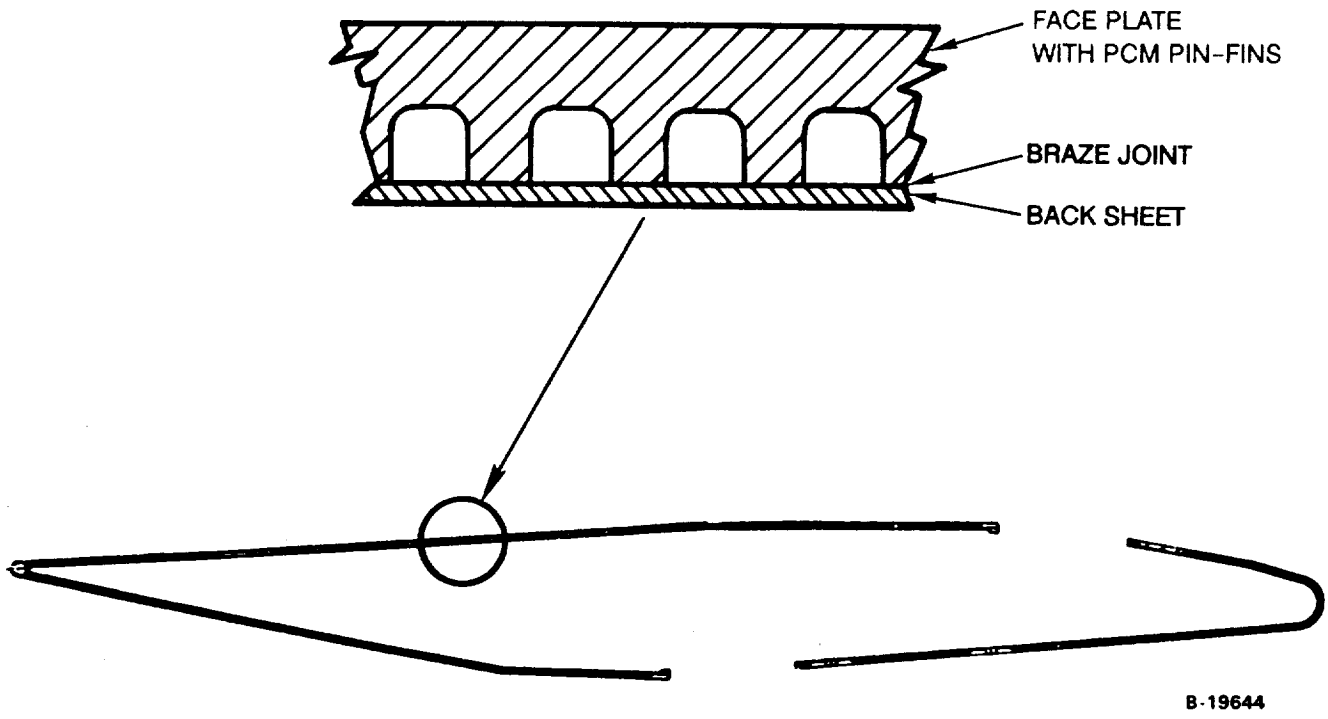

Figure 13. Jacket Assembly

- INCONEL 718 BEAMS AND WALLS
- TYPE 347 STAINLESS STEEL BUFFERS
- 50 Au, 25 Pd, 25 Ni (PALNIRO 1) 0.001-IN. BRAZE FOIL
- BRAZE IN VACUUM BAG (2070°F)
- AGE HARDEN
- HOLOGRAPHIC PRESSURE TEST

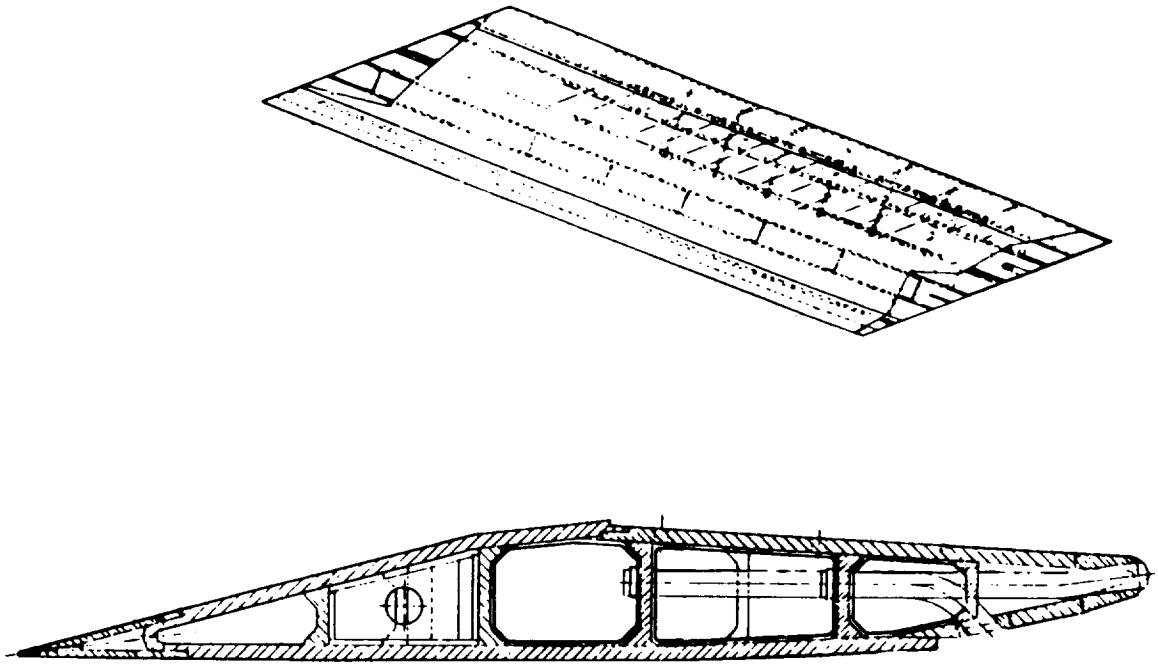

B-19640

Figure 14. Support Structure Assembly

- BRAZE JACKETS TO SUPPORT STRUCTURE
- 70 Au-8 Pd-22 Ni (PALNIRO 7) 0.001-IN. BRAZE FOIL
- BRAZE IN VACUUM (1935°F)

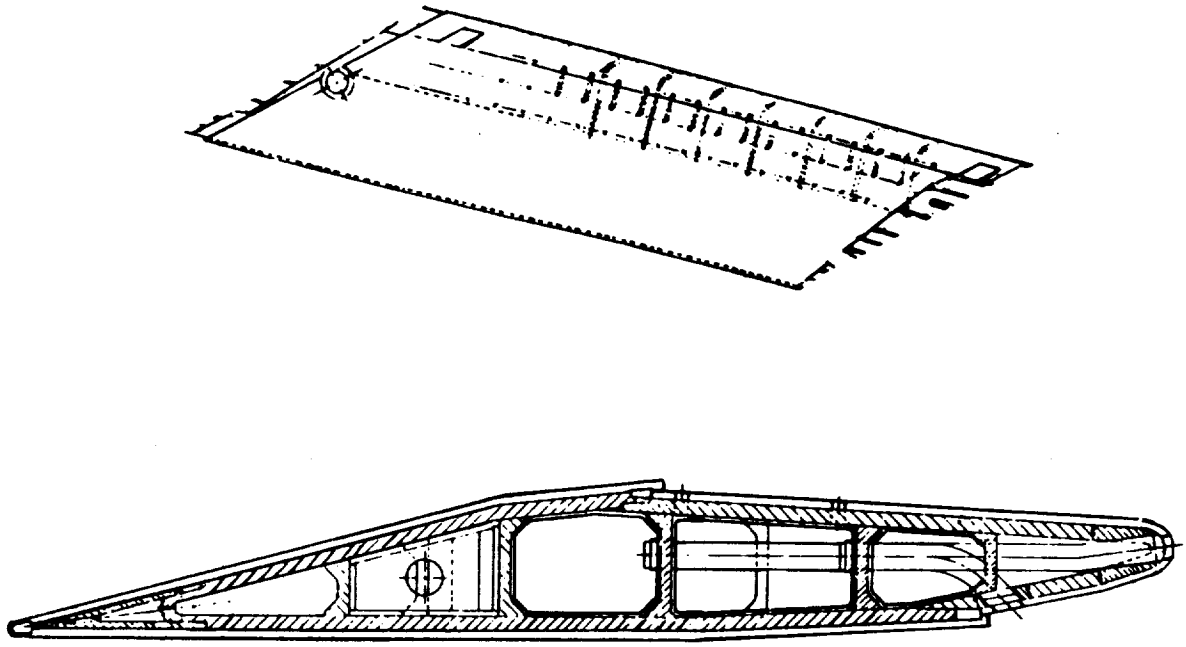

B-19639

Figure 15. Final Assembly, First Stage

- BRAZE COVER PLATES TO JACKET-SUPPORT STRUCTURE ASSEMBLY
- 82 Au-18 Ni (NIORO), 0.001-IN. BRAZE FOIL (1800°F)
- AGE HARDEN FOR SUPPORT STRUCTURE PROPERTIES
- HOLOGRAPHIC PRESSURE TEST
- ASSEMBLE INTERFACE HARDWARE

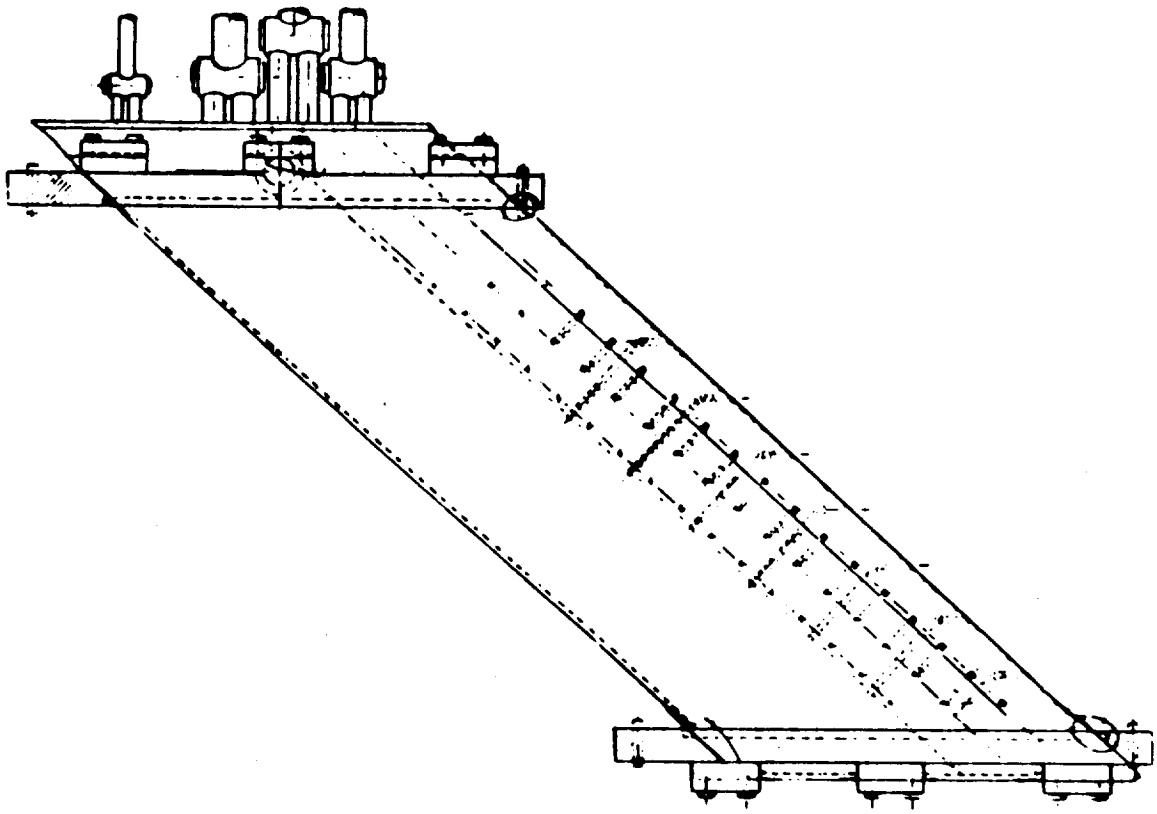

B-19638

Figure 16. Final Assembly, Second Stage

TABLE 7

STRUT BRAZE SCHEDULES

---------- BRAZE SCHEDULE ---------- FORM E1835-1 ---

NAME: STRUT/COVER PLATE

1	SPECIFICATION:	MIL-B-7883, GRADE B(WBS-88)		
2	TOOL NO:	GRAPHITE SUPPORT PLATE AND SPACER BARS		
3	NO. OF SPRINGS:			
4	SPRING COMPRESSION:			
5	NO. OF BELLOWS:			
6	BRAZING ALLOY SPEC.:	AMS 4787		
7	BINDER TYPE:	N.B.500, AIRSPRAY 014		
8	SOAK TEMP:	1690+/-10F	TIME	45 +/- 5 MIN.
9	BRAZE TEMP:	1800+/-10F	TIME	5 MIN.+/-30 SEC.
10	DELTA T:	250F TO 1200F, 150F - 1690F, 50F - 1800F.		
11	HEATING RATE:	TO MAINTAIN DELTA T		
12	COOLING RATE:	TO MAINTAIN DELTA T		
13	ATMOS. FURNACE NO.:	8		
14	GAS FLOW RATE:	500 C.F.H. ARGON		
15	POST BRAZE TREAT:			
16	INDUCTION HEATER NO.:		COIL NO:	
	TIME:		AMPS:	
17	OTHER:			
18	VACUUM FURNACE:			
19	ALUM. SALT BATH:			
20	TORCH:			

R E M A R K S

USE SPACER BARS TO SUPPORT TRAILING EDGE OF STRUT. USE REFRASIL BETWEEN PART AND SPACER BARS AND SUPPORT PLATE. SUPPORT TUBES USING SPACER BLOCKS AND REFRASIL. PLACE 2 THERMOCOUPLES APPROX. 2 CONTINUED
INCHES INSIDE STRUT THROUGH TUBES AND 2 IN CONTACT WITH NICKEL JACKET. AFTER CLOSING RETORT, EVACUATE RETORT TO APPROX. 30" HG AND BACKFILL TO AMBIENT PRESSURE WITH ARGON. REPEAT THIS PROCEDURE A TOTAL OF 4 TIMES BEFORE STARTING HEAT INPUT.

TABLE 7

STRUT BRAZE SCHEDULES
(Continued)

---------- BRAZE SCHEDULE ---------- FORM E1835-1 ---

NAME: STRUT BODY/JACKETS

1	SPECIFICATION:	MIL-B-7883, GRADE B(WBS-88)		
2	TOOL NO:			
3	NO. OF SPRINGS:			
4	SPRING COMPRESSION:			
5	NO. OF BELLOWS:			
6	BRAZING ALLOY SPEC.:	AMS 4786		
7	BINDER TYPE:	N.B. 500.		
8	SOAK TEMP:	1800+/-10F	TIME	45 +/- 5 MIN.
9	BRAZE TEMP:	1930+/-10F	TIME	5 MIN.+/-30 SEC.
10	DELTA T:	250F TO 1200F. 150F- 1800F.50F -1930F.		
11	HEATING RATE:	TO MAINTAIN DELTA T'S		
12	COOLING RATE:	FURNACE COOL TO 750F. AIR COOL TO ROOM TEMPERATURE.		
13	ATMOS. FURNACE NO.:	8		
14	GAS FLOW RATE:	300+/-20 C.F.H.- ARGON		
15	POST BRAZE TREAT:			
16	INDUCTION HEATER NO.:		COIL NO:	
	TIME:		AMPS:	
17	OTHER:			
18	VACUUM FURNACE:			
19	ALUM. SALT BATH:			
20	TORCH:			

R E M A R K S

POSITION PART AND FIXTURE APPROXIMATELY 6" ABOVE FURNACE HEARTH AND SUPPORT AS NECESSARY TO PREVENT MOVEMENT DURING BRAZING. EVACUATE PRESSURE BAG FIXTURE TO 30" HG., THEN EVACUATE RETORT CONTINUED

TO 30" HG. AND BACKFILL TO AMBIENT PRESSURE WITH ARGON. PURGE AND FILL VACUUM BAG WITH ARGON SEVERAL TIMES TO PREVENT CONTAMINATION. BACKFILL PRESSURE BAG FIXTURE TO 4" HG. AND MAINTAIN FROM AMBIENT TO 1500F. AT 1500F. ADJUST THE PRESSURE TO 30" HG. AND MAINTAIN UNTIL PART HAS COOLED TO 1800F AFTER BRAZING. AT 1800F. ADJUST THE PRESSURE TO 4" HG. AND MAINTAIN UNTIL RETORT IS OPENED.

TABLE 7

STRUT BRAZE SCHEDULES
(Continued)

---------- BRAZE SCHEDULE ---------- FORM E1835-1 ---

NAME: STRUT BODY. ASSLY.

1	SPECIFICATION:	MIL-B-7883. GRADE B(WBS-88)		
2	TOOL NO:			
3	NO. OF SPRINGS:			
4	SPRING COMPRESSION:			
5	NO. OF BELLOWS:			
6	BRAZING ALLOY SPEC.:	AMS 4784		
7	BINDER TYPE:	N.B. 500. AIRSPRAY 014		
8	SOAK TEMP:	1965+/-10F	TIME	45 +/-5 MIN.
9	BRAZE TEMP:	2080+/-10F	TIME	5 MIN.+/-30 SEC.
10	DELTA T:	250F TO 1200F.THEN 150F TO 1965F.50F-2070F		
11	HEATING RATE:	TO MAINTAN DELTA T		
12	COOLING RATE:	COOL DOWN RATE FOR HEAT REATMENT SHALL OVERRIDE THE DELTA TEMP. REQUIREMENT.		
13	ATMOS. FURNACE NO.:	8		
14	GAS FLOW RATE:	300+/-20 C.F.H.- ARGON		
15	POST BRAZE TREAT:			
16	INDUCTION HEATER NO.:		COIL NO:	
	TIME:		AMPS:	
17	OTHER:			
18	VACUUM FURNACE:			
19	ALUM. SALT BATH:			
20	TORCH:			

R E M A R K S

POSITION PART AND FIXTURE APPROXIMATELY 6" ABOVE FURNACE HEARTH. SUPPORT AS NECESSARY TO PREVENT MOVEMENT DURING BRAZING. EVACUATE PRESSURE BAG FIXTURE TO 30" HG.. EVACUATE RETORT TO 30" HG. AND CONTINUED
BACKFILL TO AMBIENT PRESSURE WITH ARGON. PURGE AND FILL VACUUM BAG WITH ARGON SEVERAL TIMES TO PREVENT CONTAMINATION. MANTAIN 30" HG. IN PRESSURE BAG FIXTURE FROM AMBIENT TEMPERATURE TO 1000F. AT 1000F ADJUST PRESSURE TO 20" HG. AND MAINTAIN UNTIL PART COOLS TO 1000F AFTER BRAZING.

.

HEAT TREAT PER HT-71 CONCURRENTLY WITH THE BRAZE CYCLE AS FOLLOWS:
1) COOL FROM BRAZE TEMPERATURE AT 600F/HR. MINIMUM TO 1400 +/-25F AND HOLD FOR 8 HRS.
2) COOL FROM 1400 +/-25F AT APPROXIMATELY 100F/HR. TO 1200 +/-25F AND HOLD UNTIL A TOTAL AGING TIME OF 20 HRS. IS REACHED (1400F PLUS FURNACE COOL PLUS 1200F EQUALS 20 HRS.).
3) FROM 1200F COOL TO ROOM TEMPERATURE AT ANY CONVENIENT RATE.

.

REBRAZE NO.1 AND 2 - SAME PROCEDURE AS THE ORIGINAL BRAZE AS INDICATED ABOVE.

.

********** HYDROGEN CLEANING CYCLE **********
HYDROGEN CLEAN PRIOR TO BRAZING AT 1700F - 1750F TEMPERATURE AND HOLD FOR 30 MINUTES. HEAT UP AND COOL DOWN RAMPS TO BE THE SAME AS THE BRAZING RAMPS SPECIFIED ABOVE.

TABLE 7

STRUT BRAZE SCHEDULES
(Continued)

---------- BRAZE SCHEDULE ---------- FORM E1835-1 ---

NAME: AFT JACKET ASSLY.

1	SPECIFICATION:	MIL-B-7883. GRADE B(WBS-88)		
2	TOOL NO:			
3	NO. OF SPRINGS:			
4	SPRING COMPRESSION:			
5	NO. OF BELLOWS:			
6	BRAZING ALLOY SPEC.:	AMS 4784		
7	BINDER TYPE:	N.B. 500. AIRSPRAY 014		
8	SOAK TEMP:	1965 +/-10F	TIME	45 +/-5 MIN.
9	BRAZE TEMP:	2080 +/-10F	TIME	5 MIN.+/-30 SEC.
10	DELTA T:	250F TO 1200F. 150F - 1965F. 50F - 2070F.		
11	HEATING RATE:	TO MAINTAIN DELTA T'S		
12	COOLING RATE:	TO MAINTAIN DELTA T'S		
13	ATMOS. FURNACE NO.:	8		
14	GAS FLOW RATE:	300+/-20 C.F.H.- ARGON		
15	POST BRAZE TREAT:			
16	INDUCTION HEATER NO.:		COIL NO:	
	TIME:		AMPS:	
17	OTHER:			
18	VACUUM FURNACE:			
19	ALUM. SALT BATH:			
20	TORCH:			

R E M A R K S

POSITION PART AND FIXTURE APPROXIMATELY 6" ABOVE FURNACE HEARTH AND SUPPORT AS NECESSARY TO PREVENT MOVEMENT DURING BRAZING. EVACUATE PRESSURE BAG FIXTURE TO 30" HG.. THEN EVACUATE RETORT

CONTINUED

TO 30" HG. AND BACKFILL TO AMBIENT PRESSURE WITH ARGON. PURGE AND FILL BAG WITH ARGON SEVERAL TIMES TO PREVENT CONTAMINATION. BACK-FILL PRESSURE BAG FIXTURE TO 3" HG. AND MAINTAIN FROM AMBIENT TO 1965F. AT 1965F. ADJUST PRESSURE TO 30" HG. AND MAINTAIN UNTIL PART HAS COOLED TO 1965F AFTER BRAZING. AT 1965F. ADJUST PRESSURE TO 3" HG. AND MAINTAIN UNTIL RETORT IS OPENED.

TABLE 7

STRUT BRAZE SCHEDULES
(Continued)

---------- BRAZE SCHEDULE ---------- FORM E1835-1 ---

NAME: FORWARD JACKET ASSY

1	SPECIFICATION:	MIL-B-7883, GRADE B(WBS-88)
2	TOOL NO:	
3	NO. OF SPRINGS:	
4	SPRING COMPRESSION:	
5	NO. OF BELLOWS:	
6	BRAZING ALLOY SPEC.:	AMS 4784
7	BINDER TYPE:	N.B. 500, AIRSPRAY 014
8	SOAK TEMP:	1965 +/-10F TIME 45 +/-5 MIN.
9	BRAZE TEMP:	2080 +/-10F TIME 5 MIN.+/-30 SEC.
10	DELTA T:	250F TO 1200F, 150F - 1965F, 50F - 2070F.
11	HEATING RATE:	TO MAINTAIN DELTA T'S
12	COOLING RATE:	TO MAINTAIN DELTA T'S
13	ATMOS. FURNACE NO.:	8
14	GAS FLOW RATE:	300+/-20 C.F.H.- ARGON
15	POST BRAZE TREAT:	
16	INDUCTION HEATER NO.:	COIL NO:
	TIME:	AMPS:
17	OTHER:	
18	VACUUM FURNACE:	
19	ALUM. SALT BATH:	
20	TORCH:	

R E M A R K S

POSITION PART AND FIXTURE APPROXIMATELY 6" ABOVE FURNACE HEARTH AND SUPPORT AS NECESSARY TO PREVENT MOVEMENT DURING BRAZING. EVACUATE PRESSURE BAG FIXTURE TO 30" HG., THEN EVACUATE RETORT CONTINUED
TO 30" HG. AND BACKFILL TO AMBIENT PRESSURE WITH ARGON. PURGE AND FILL PRESS. BAG WITH ARGON SEVERAL TIMES TO PREVENT CONTAMINATION. BACKFILL PRESSURE BAG FIXTURE TO 3" HG. AND MAINTAIN FROM AMBIENT TO 1965F. AT 1965F, ADJUST PRESSURE TO 30" HG. AND MAINTAIN UNTIL PART HAS COOLED TO 1965F AFTER BRAZING. AT 1965F, ADJUST PRESSURE TO 3" HG. AN MAINTAIN UNTIL RETORT IS OPENED.

TABLE 7

STRUT BRAZE SCHEDULES
(Continued)

---------- BRAZE SCHEDULE ---------- FORM E1835-1 ---

REBRAZE FOR RAILS
NAME: FORWARD JACKET ASSY

1	SPECIFICATION:	MIL-B-7883, GRADE B(WBS-88)		
2	TOOL NO:	1/2" GRAPHITE AND .012" INCO 625 VAC. BAG.		
3	NO. OF SPRINGS:			
4	SPRING COMPRESSION:			
5	NO. OF BELLOWS:			
6	BRAZING ALLOY SPEC.:	AMS 4786		
7	BINDER TYPE:	N.B. 500, AIRSPRAY 014		
8	SOAK TEMP:	1800 +/-10F	TIME	45 +/-5 MIN.
9	BRAZE TEMP:	1930 +/-10F	TIME	5 MIN.+/-30 SEC.
10	DELTA T:	250F TO 1200F, 150F - 1800F, 50F - 1930F.		
11	HEATING RATE:	TO MAINTAIN DELTA T'S		
12	COOLING RATE:	TO MAINTAIN DELTA T'S		
13	ATMOS. FURNACE NO.:	8		
14	GAS FLOW RATE:	300+/-20 C.F.H.- ARGON		
15	POST BRAZE TREAT:			
16	INDUCTION HEATER NO.:		COIL NO:	
	TIME:		AMPS:	
17	OTHER:			
18	VACUUM FURNACE:			
19	ALUM. SALT BATH:			
20	TORCH:			

R E M A R K S

POSITION PART AND FIXTURE APPROXIMATELY 6" ABOVE FURNACE HEARTH AND SUPPORT AS NECESSARY TO PREVENT MOVEMENT DURING BRAZING. EVACUATE PRESSURE BAG FIXTURE TO 30" HG., THEN EVACUATE RETORT CONTINUED
TO 30" HG. AND BACKFILL TO AMBIENT PRESSURE WITH ARGON. PURGE AND FILL PRESS. BAG WITH ARGON SEVERAL TIMES TO PREVENT CONTAMINATION. BACKFILL PRESSURE BAG FIXTURE TO 3" HG. AND MAINTAIN FROM AMBIENT TO 1800F. AT 1800F, ADJUST PRESSURE TO 30" HG. AND MAINTAIN UNTIL PART HAS COOLED TO 1800F AFTER BRAZING. AT 1800F, ADJUST PRESSURE TO 3" HG. AN MAINTAIN UNTIL RETORT IS OPENED.

FOLDOUT FRAME 2.

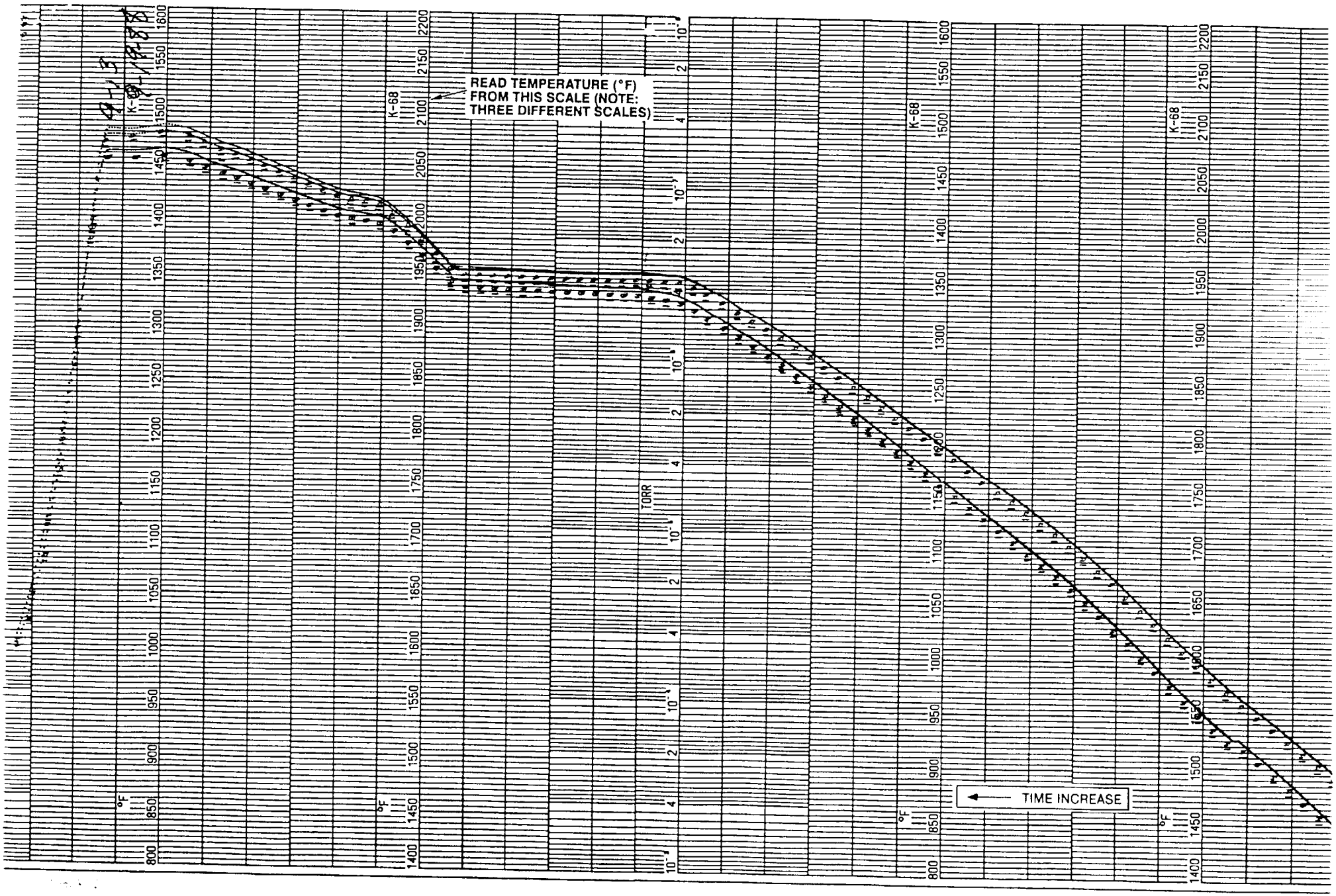

B-19493

FOLDOUT FRAME 2

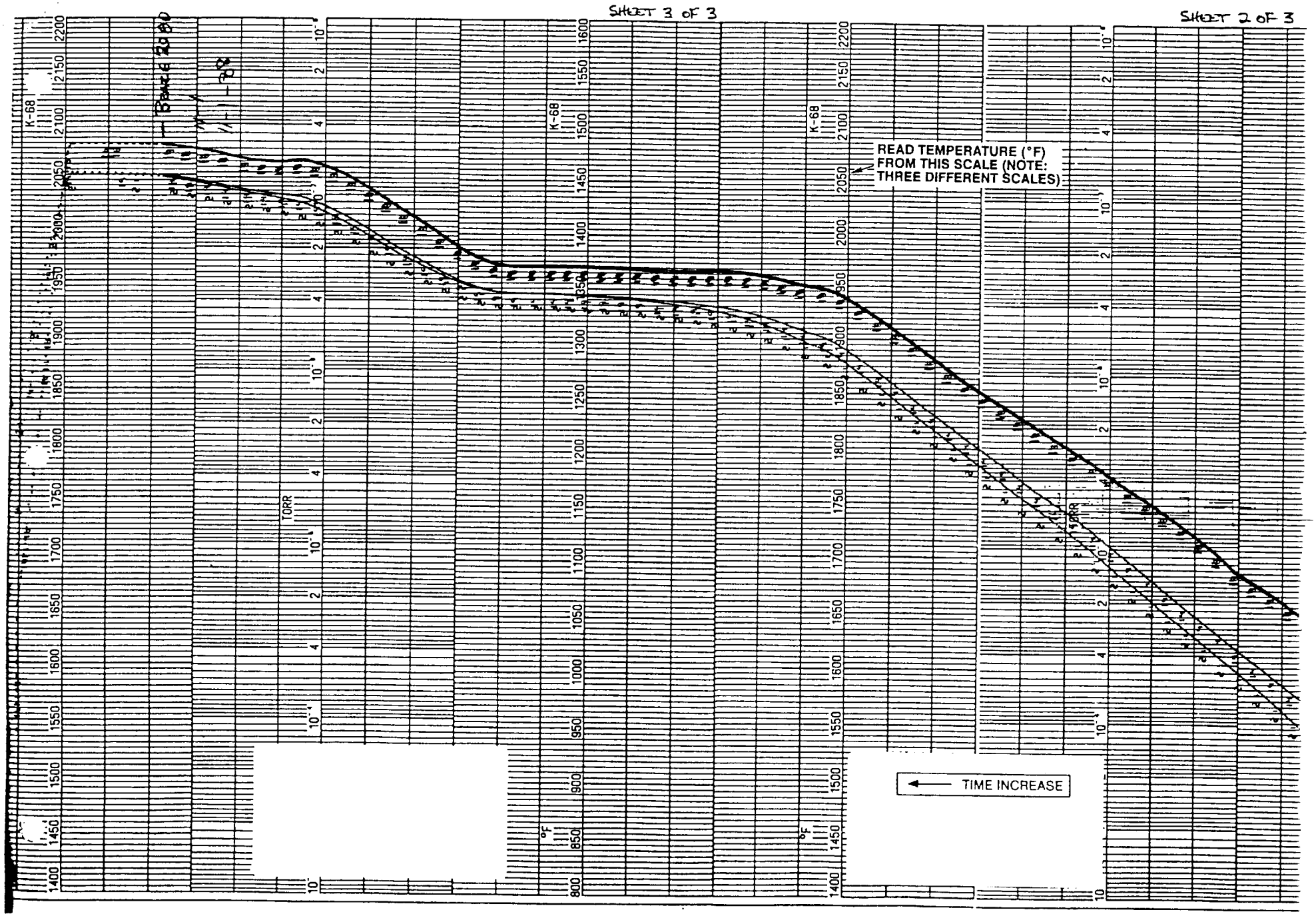

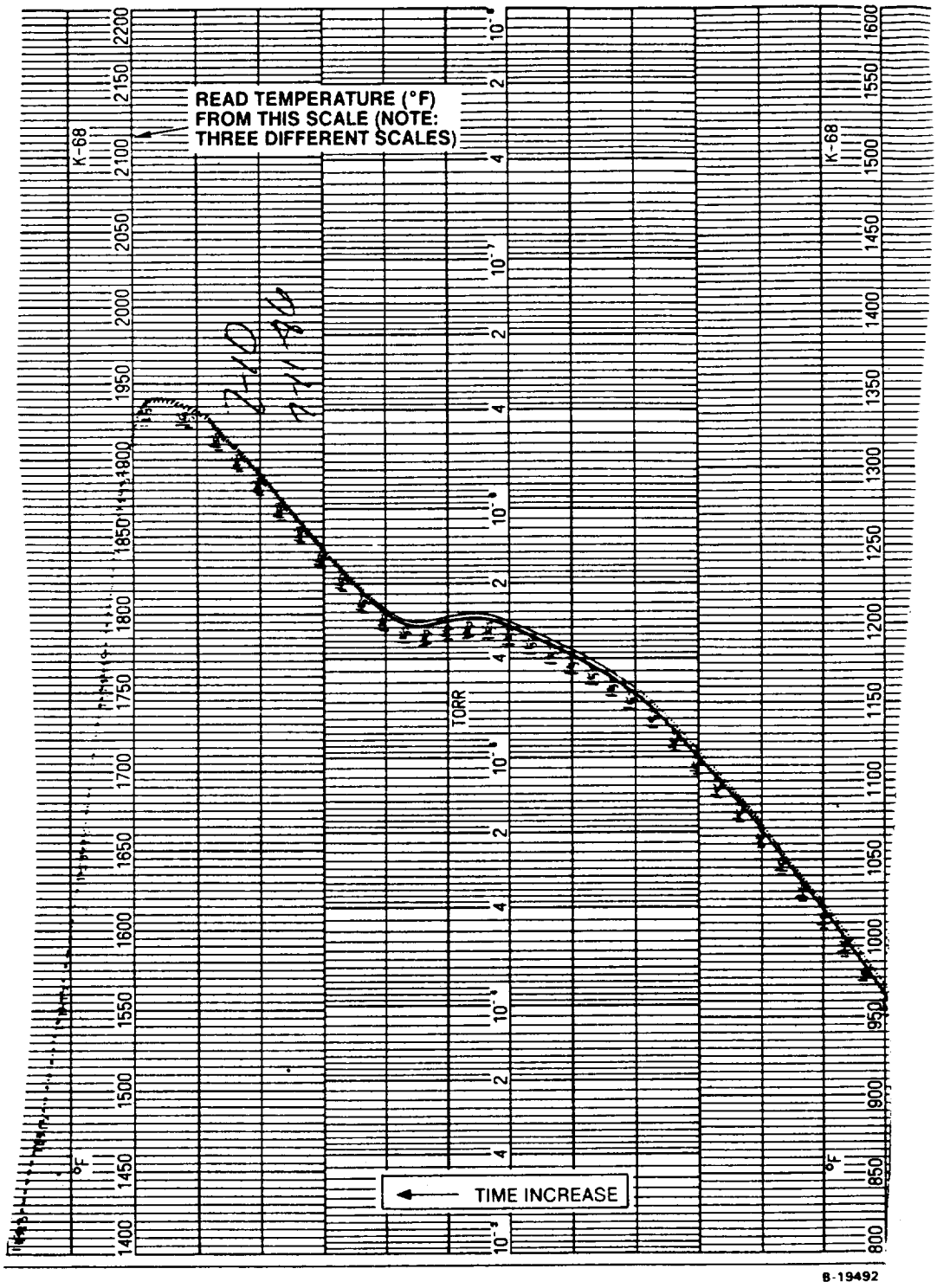

Figure 19. Braze Cycle Temperature History for PL Cooling Jacket-to-Support Structure with Palniro 7 Filler Alloy

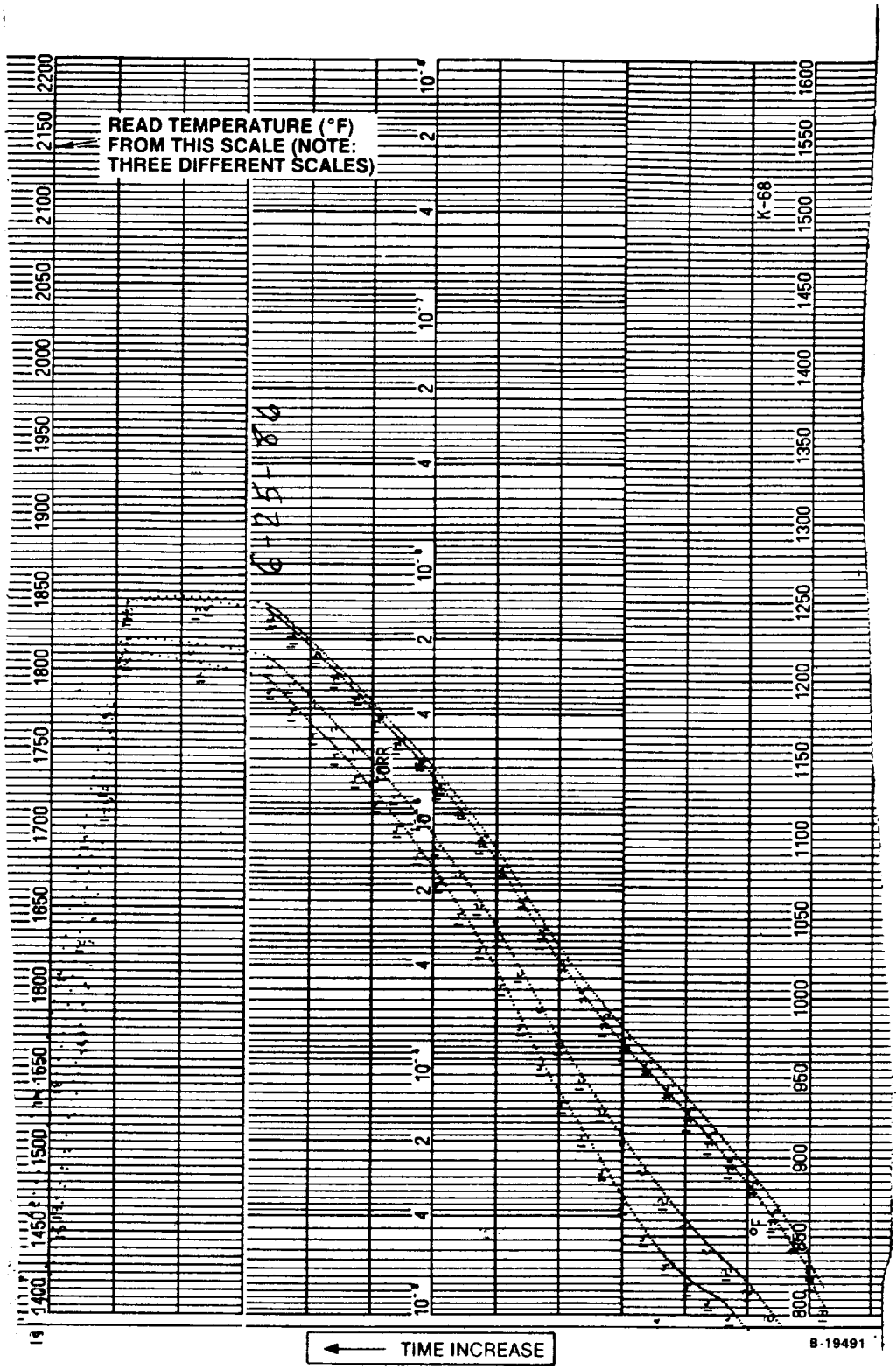

Figure 20. Braze Cycle Temperature History for PL Strut Cover Plate – Support Structure with Nioro Filler Alloy

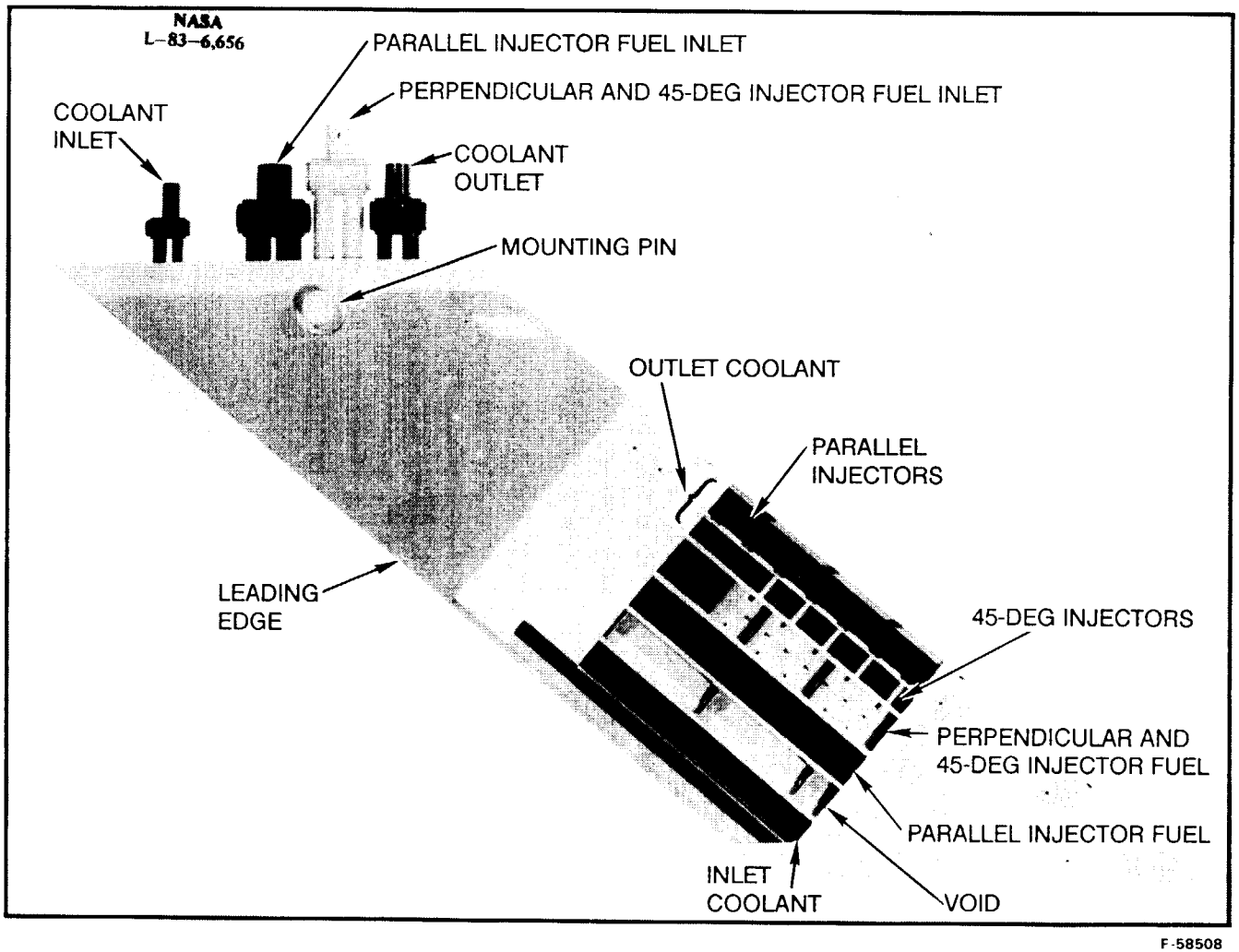

Figure 21. Strut Assembly Model

The design provides for independent fabrication of the cooling jacket and support structure as the forward and aft sections. Fabrication of the formed support structures involved grinding the material blanks flat to final thickness, brake forming to the general shape of the wall contour, and hot forming the rough shaped walls into the precise shape for brazing the walls and bulkheads (wire EDM was used to generate the hot forming mandrel). After final machining, the Inco-718 support-structure elements were braze-assembled in a single operation.

The cooling jackets have photochemically machined (PCM) Ni-201 pin-fin surfaces, 0.035-in. thick overall, that are brazed in the flat to a 0.010-in.-thick Ni-201 back sheet. The brazed subassemblies were pressure tested and holographically evaluated for braze voids under pressure load prior to delivery. The holography technique employed uses a double exposure of the test item at two different internal pressures. With this technique, discontinuities in the resulting interference fringes are used to locate braze voids (deflection differences).

The strut final assembly includes the assembled support structure and cooling jackets, mounting pins, and top and bottom cover plates. The assembly is bolted and mechanically sealed against the wind tunnel wall. Figure 22 is a layout of the strut installation and shows the design of the mounting system.

The strut will be installed for the wind tunnel tests such that the tunnel walls are approximately 0.50 in. from the first set of fuel injectors at the top and 0.34 in. from the bottom fuel injectors. If forms a clearance fit with the top and bottom wind tunnel walls; the top is attached with pins. Tunnel wall seals (Item 7 in Figure 22) are clamped on each side, top and bottom (Items 2 and 3), and they restrain the strut laterally. The bottom is not fixed in the span-wise direction to allow it to expand and contract and to accommodate installation tolerances. Since the bottom surface is shielded from the hot gases, the bottom cover plate need not be cooled, and a simple solid plate can be used instead of a cooled plate.

The mounting pins at the top have a diameter of 0.92 in. and 1.4-in.-diam. collars, which are brazed to the support structure (see sketch under para. 4.2.2). These pins are large enough to accommodate and distribute the induced loads into the strut structure through the strut bulkheads. To improve the load carrying capability of the support structure in the area of mounting pins, the thicknesses of the bulkheads of the parallel fuel injector manifold were locally increased from 0.08 to 0.17 in., for a length of 1.00 in. Figure 23 (Drawing 195588) shows one of these bulkheads. The increased bulkhead thickness almost doubles the section modulus of the structure at the mounting pin attachment points.

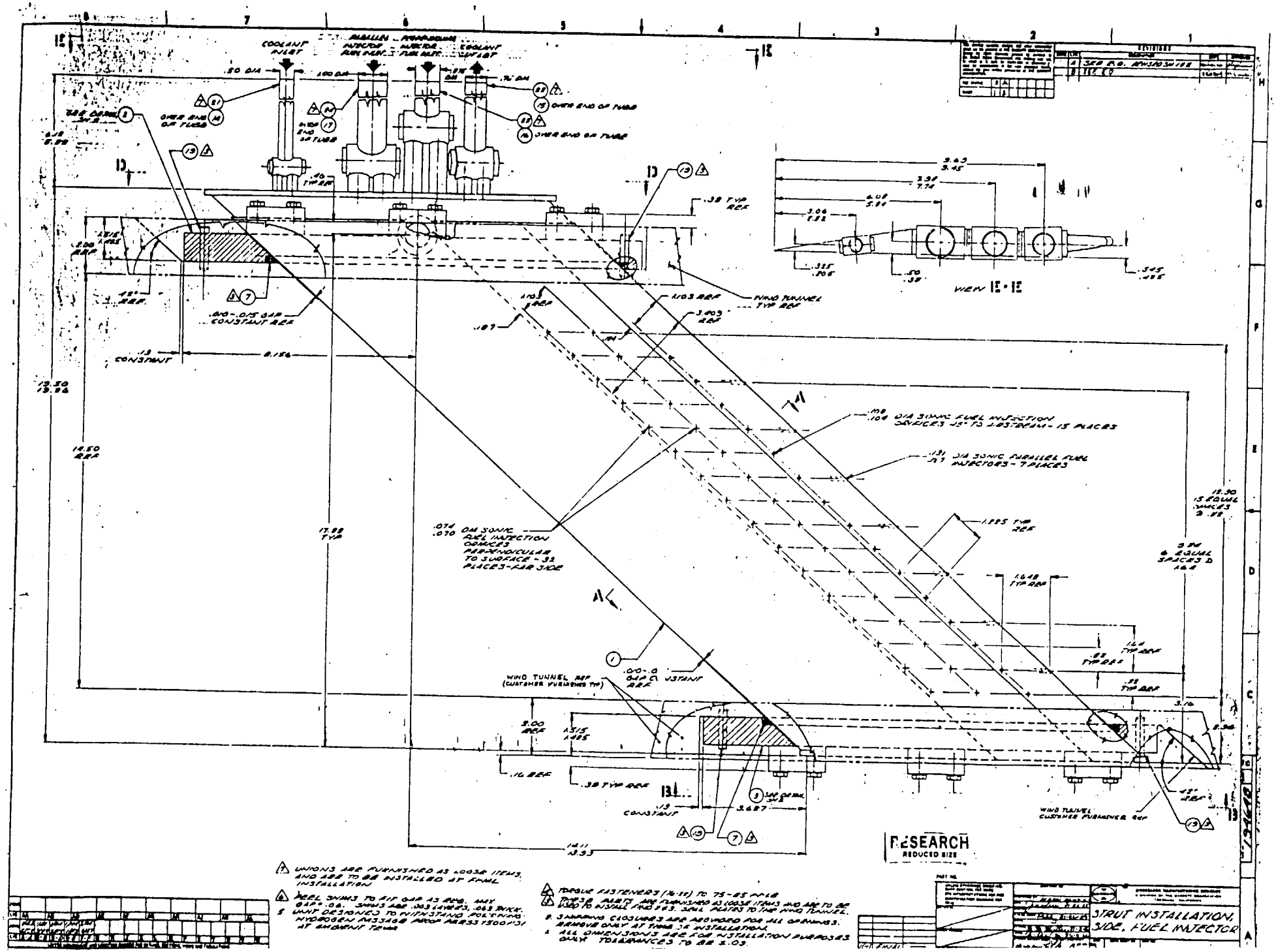

⚠ UNIONS ARE FURNISHED AS LOOSE ITEMS, AND ARE TO BE INSTALLED AT FINAL INSTALLATION

⚠ REEL SHIMS TO FIT GAP AS REQ. MAT GAP = .06. SHIMS ARE .063 (AMS5523, .063 THICK, 5 UNIT DESIGNED TO WITHSTAND BOILING HYDROGEN AMS5508 PROOF PRESS 1500 PSI AT AMBIENT TEMP

TORQUE FASTENERS (¼-28) TO 75-85 IN-LB

⚠ THESE PARTS ARE FURNISHED AS LOOSE ITEMS AND ARE TO BE USED TO INSTALL AND FIT STRUT SEAL PLATES TO THE WING TUNNEL.

B SHADING CLOSEOUTS ARE REQUIRED FOR ALL OPENINGS. REMOVE ONLY AT FINAL INSTALLATION.

A ALL DIMENSIONS ARE FOR INSTALLATION PURPOSES ONLY TOLERANCES TO BE ± .03

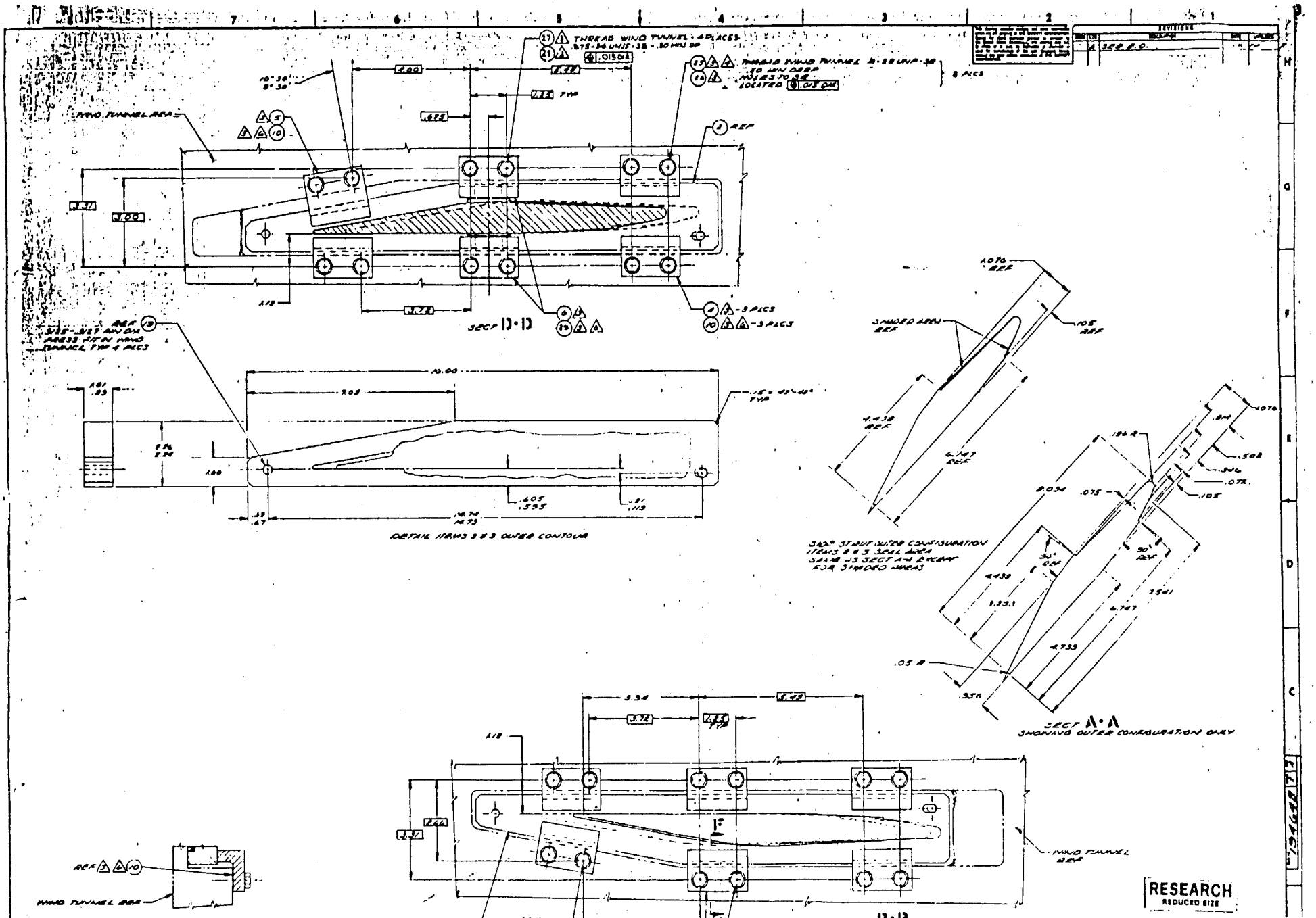

FOLDOUT FRAME 2.

ORIGINAL PAGE IS
OF POOR QUALITY

REVISIONS				
ZONE	LTR	DESCRIPTION	DATE	APPROVED
	R			

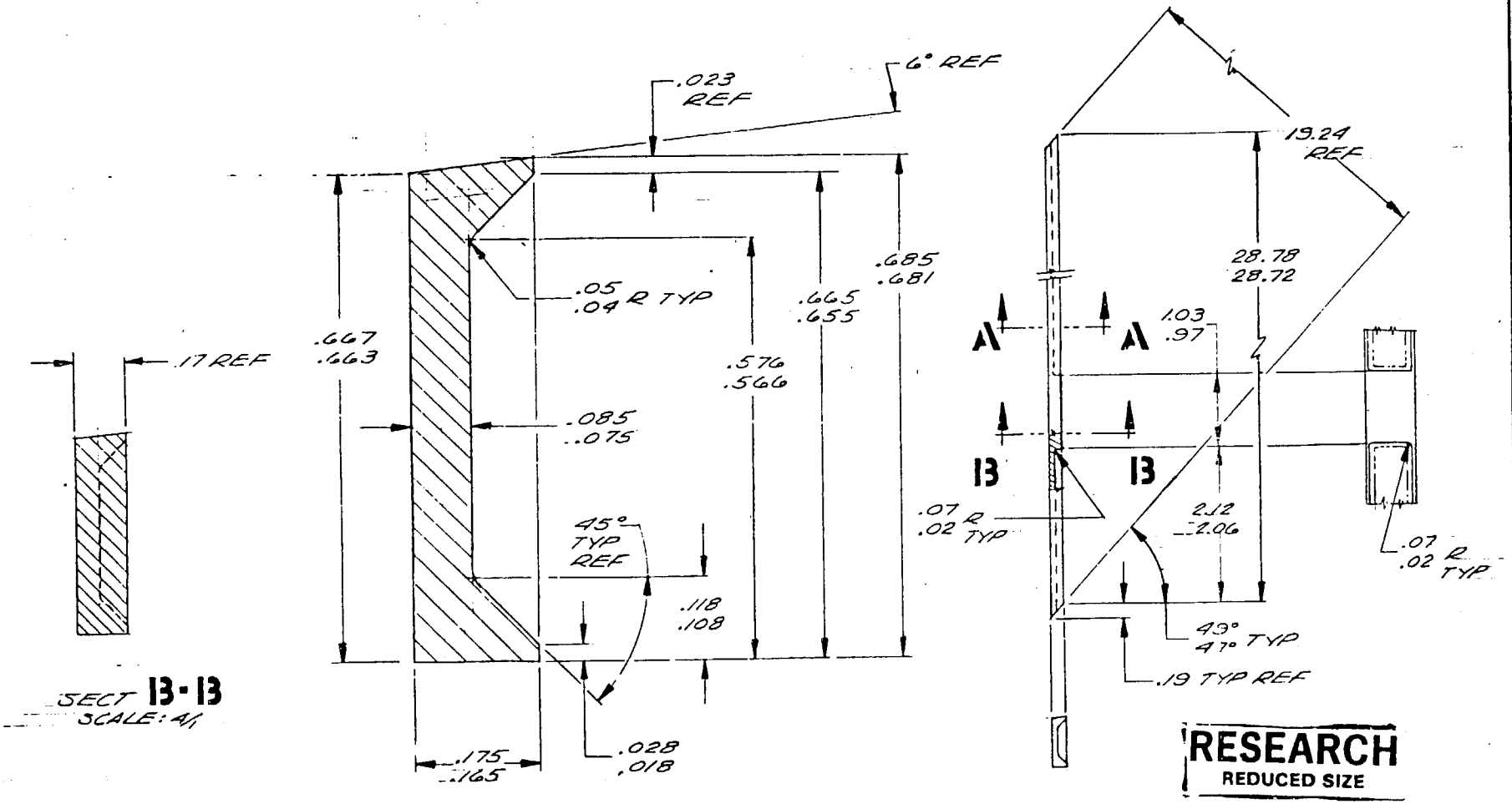

SECT B-B
SCALE: 4/1

SECT A-A
SCALE: 10/1

RESEARCH
REDUCED SIZE

195588

PART NO. 195588-1

UNLESS OTHERWISE SPECIFIED:
BURR CONTROL PER SCRS, CLB
STD INTERPRETATIONS PER PBB
IDENTIFICATION MARKING PER
MC16, EC XII

MATERIAL .19 PLATE
NICKEL ALLOY

CONTRACT NO.

PREPARED BY MASA/ 82-09-25
CHK J. Paul 82-10-12
DES SR
VALUE ENGR

AIRESEARCH MANUFACTURING COMPANY
A DIVISION OF THE GARRETT CORPORATION
TORRANCE, CALIFORNIA

BEAM, CHANNEL,

4.2 Design Investigations

The basic design of the strut was defined as part of a previous study (ref. 2). Design activity in this program was limited to modifications to facilitate manufacturing, to accommodate interfaces with the planned NASA-Langley wind tunnel, and to selectively reexamine critical design features.

4.2.1 Sealing. – High temperature seal material is required for the gasket that forms the seal between the strut and the seal retaining block that bolts to the wind tunnel wall. Since some seepage through the seal was judged acceptable, commercially available, square-braided ceramic fiber, 0.25-in. by 0.25-in., was selected.

4.2.2 Strut mounting. – The strut mounting pin design accommodates the thermally and aerodynamically induced loads on the strut, and forms an important interface with the tunnel. The plate that provides sealing at the strut-tunnel wall interface supports the strut loads and substitutes for a pin and ball mounting system at the bottom of the strut. The seal plate is sized to allow unrestrained spanwise movement and to resist lateral and airstream direction loads.

The loads imposed on the strut are defined in ref. 2. These loads represent upper limit values that were obtained with an analysis that considered the top pin support to be rigid. Hinge action and the flexibility of the adjacent engine structure were ignored.

The loading on the hinge pin, as shown below, will result in bending and shear stresses at the braze joint. From ref. 2, the resultant of the vertical and horizontal loads is:

$$F = (42000^2 + 19000^2)^{1/2}$$

$$F = 46{,}700 \text{ lb}$$

The pin reaction is:

$$P = (46{,}700)\left(\frac{0.8}{1.75}\right) = 21{,}350 \text{ lb}$$

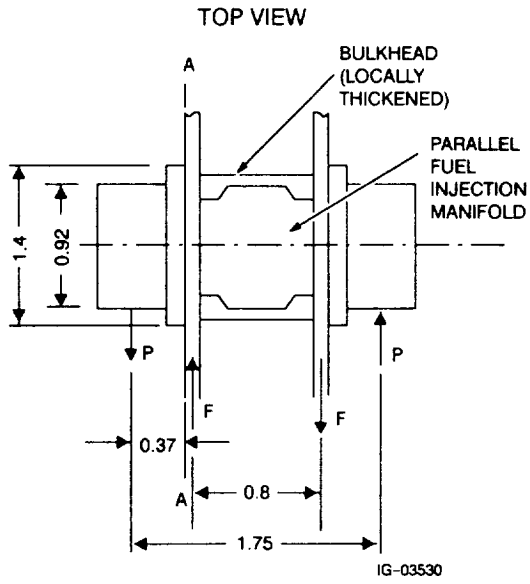

Bending moment at plane AA is:

$$M = (21{,}350)\ (0.37) = 7900 \text{ in.-lb}$$

Stresses at plane AA:

$$\sigma_b = \frac{M}{Z} = \frac{7{,}900}{(0.0982)(1.4)^3} = 29{,}300 \text{ psi (bending)}$$

$$\tau = \frac{21{,}350}{(\pi/4)\ (1.4)^2} = 13{,}870 \text{ psi (shear)}$$

Equivalent stress:

$$\sigma_e = \left[29{,}300^2 + (3)\ (13{,}870)^2\right]^{1/2} = 37{,}900 \text{ psi}$$

Since the braze joint strength will approach parent metal strength (over 100,000 psi), the simplified analysis above was judged sufficient to indicate that the hinge pin design can support the imposed loads. Specifically, the seal analysis in ref. 2 considered hinge rotation and engine top wall flexibility. The resulting strut deflections from that analysis were considerably lower than had been previously obtained in the rigid pin analysis, as indicated by the seal gap changes. The lower deflections obtained with the more inclusive model correspond to lower actual loads on the hinge pin than the ones used above.

The strut mounting design is shown in Figure 22. The pin is free to move spanwise, and the lateral loads will be carried by the top and bottom seals and seal plates. Contact stresses of a few thousand psi can be expected and will be borne by solid regions of the cooling jacket assembly.

4.2.3 Coolant flow distribution. – Flow distribution within the cooling jacket was another critical design area that was reviewed. The analysis covered: (1) side-to-side flow distribu-

tion and (2) top-to-bottom flow distribution. The preliminary analysis of flow distribution and manifolding is reported in ref. 2, pp. 63-87.

4.2.3.1 Side-to-side distribution: Flow distribution, pressure drop, and heat transfer analyses were conducted on the side and center passages, which have different heating rates and heat loads, to estimate the maximum metal temperatures. Uniform spanwise (top-to-bottom) flow was assumed for this analysis (but separately examined and adjusted later). A strut cross section is shown in Figure 24.

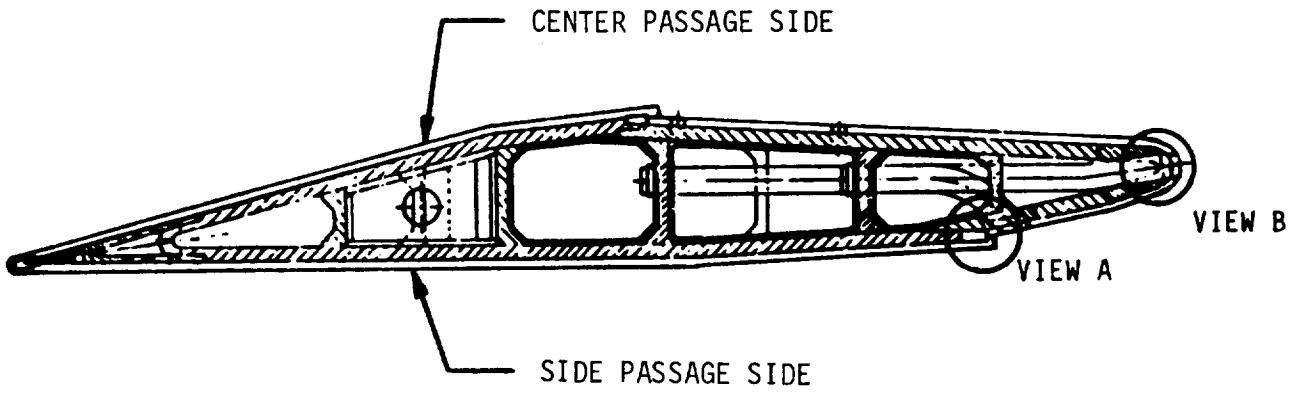

Figure 24. Strut Cross Section

The total heat input on the center passage side is 39-percent greater than on the side passage side when the perpendicular fuel injectors are in operation. During this phase of operation, the tendency is for a percentage of the total mass flow of coolant to shift from the center passage side to the side passage side because of the resulting differences in coolant temperatures and densities between the two passages. Ignoring this tendency could result in unacceptable metal temperatures along the trailing edge of the center passage. These temperatures can be controlled by restricting flow in the side passage, thereby forcing a sufficient amount of coolant in the center passage side during this operating condition.

Three configurations of the side passage were evaluated: (1) no restriction – identical passages for both passages, (2) a large, uniform flow restriction sufficient to produce equal fluid outlet temperatures (i.e., match flow rates to heat loads), and (3) localized restrictions to partially match flows to heat loads. The results of the analysis are given in Table 8.

TABLE 8

STRUT CENTER AND SIDE PASSAGE FLOW DISTRIBUTION, PRESSURE DROP, COOLANT OUTLET TEMPERATURE, AND MAXIMUM METAL TEMPERATURE

Type of Flow Restriction in the Side Passage	Passage	Flow Rate,(1) lb/sec	Pressure Drop, psi	Coolant Outlet Temperature,(4) °F	Approximate Maximum Metal Temperature,(6) °F
Case 1: None	Side	0.05470	136.2	605	880
	Center	0.04530	136.2	1315	1560
Case 2: Large Restriction	Side(2)	0.04147	104.4 + ΔP_R	925	1210
	Center	0.05853	173.4	925	1190
Case 3: Restriction in Accessible Locations	Side(3)	0.05188	144.1(5)	660	930
	Center	0.04812	144.1	1210	1460

NOTES:
(1) Total flow = 0.100 lb/sec.
(2) Requires a flow restriction pressure drop of 69 psi ($= \Delta P_R$). This is best achieved by using a more restrictive pin-fin surface in the side passage.
(3) Restrict the flow as follows:
  (a) Block every other slot in trailing edge.
  (b) Block every other hole at entrance to pin-fin surface in the aft jacket assembly.
  (c) Replace the five slots in forward jacket assembly with 126 0.030-in.-diam holes.
(4) Mixed coolant outlet temperature = 925°F.
(5) Total pressure drop from inlet manifold to outlet manifold is 161 psi.
(6) Design objective is 1200°F.

For Case 1, the maximum coolant outlet temperature is 1315°F at the center passage trailing edge, and the maximum metal temperature in this region is 1560°F. Tunnel test conditions would need to be reduced for satisfactory operation of the strut.

For Case 2, the coolant outlet temperatures are made equal by increasing the pressure drop in the side passage by 69 psi. The coolant outlet temperatures are now the same as the mixed temperature of 925°F and the maximum metal temperature is 1210°F. This solution was selected, fabricated, and used in the full-length strut. The pin-fin surfaces are 0.040 in. high in the side passage versus 0.030 in., in the center passage.

For Case 3, the solution was judged high risk for both analysis and fabrication and itself experimental. Therefore, it was rejected in favor of Case 2.

4.2.3.2 Top-to-bottom flow distribution: One corner of the strut is vulnerable to overheating as a result of the combined effects of the angled installation and flow skewing due to the pressure drop gradient in the pin-fin coolant passages. The region of potential overheating is in the lower left-hand corner, as indicated in Figure 25. In this region, the flow will take the path of least resistance – path 2. The reasons for this are as follows (comparing path 2 to path 1):

(a) The effective coolant free-flow area is about 15 percent greater because the pins are inline.

(b) Flow length is about 23 percent shorter.

(c) Friction factor is about 10 percent smaller.

(d) The hydraulic radius is about 15 percent greater.

(e) The specific volume is inversely proportional to the flow because the heat input is relatively independent of coolant temperature and, therefore, approximately constant. As a result, the maldistribution is aggravated by the increased temperature rise of the reduced flow (for reasons (a) through (d)), i.e., the increased specific volume and associated increased pressure drop.

Using these factors in combination and ignoring interactions, the flow through path 2 would be estimated at about twice that in flow path 1, resulting in high metal temperatures at the exit of path 1. The solution implemented in the full-length strut hardware was to add 12 horizontal flow dividers into the pin-fin surface, to give 13 one-inch wide channels. These channels will limit flow maldistribution to less than 10 percent and will produce acceptable metal temperatures. See Figure 26.

4.2.4 Heating at fuel injectors. – The angled fuel injectors on the side-passage side (45 degrees aftward to the air stream) are the most critical of the fuel injectors due to the combination of high heat fluxes and the already high coolant temperature in the surrounding cooling jacket.

Results of a thermal analysis around these fuel injectors are summarized in Figure 27. The nonlinear temperature gradients around the injection ports are expected to cause a maximum temperature differential of 400°F in the Nickel 201 cooling jacket, and 800°F between the cooling jacket and the Inconel 718 support structure. These temperature differences are larger than those in an uninterrupted cooling jacket at the same location and heat flux because of the increased length of conduction path, skin surface to coolant. The skin temperatures (and ΔT's) are nearly the same with and without fuel injection because the injected fuel temperature is approximately the same as the nozzle metal temperature without injection.

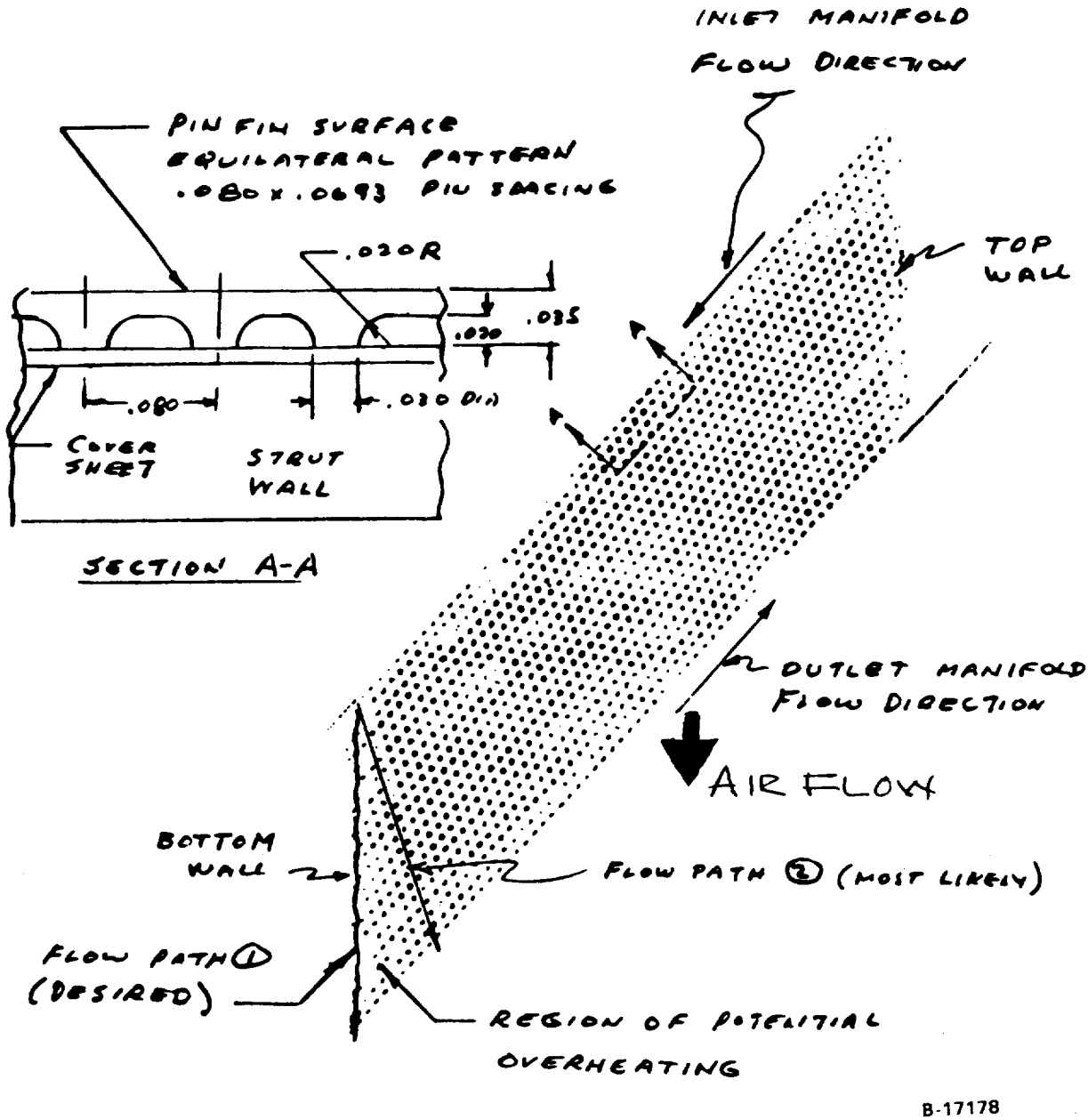

Figure 25. Pin-Fin Coolant Surface

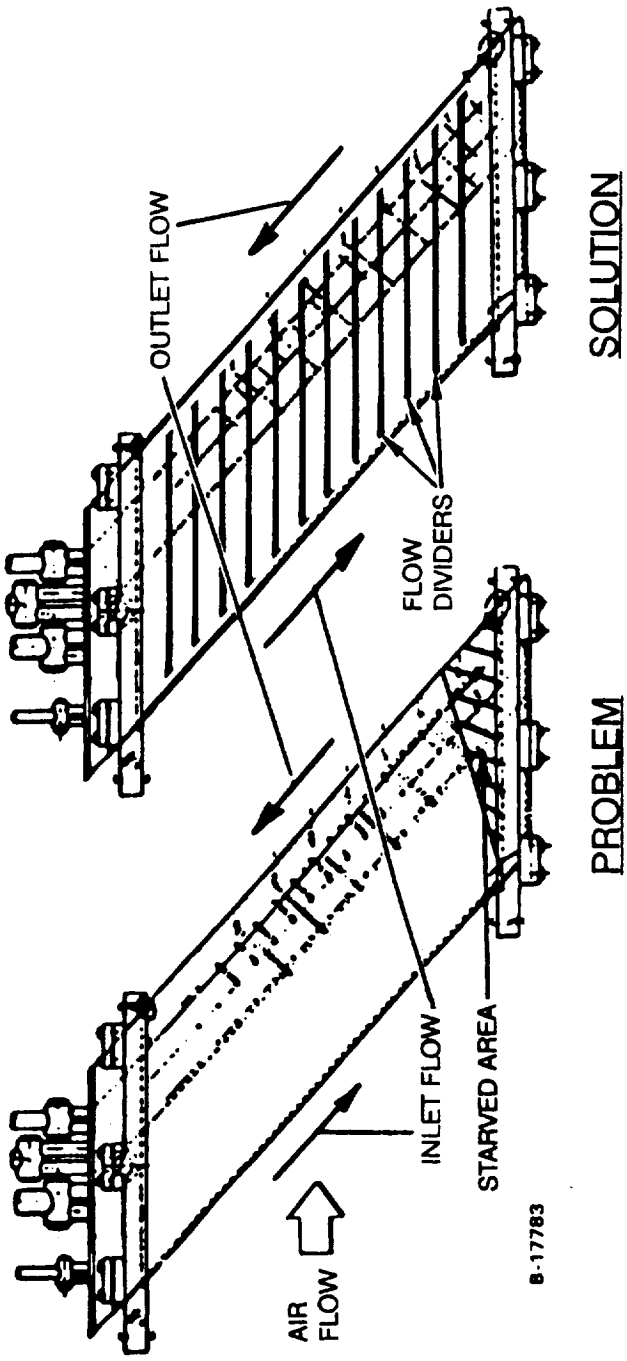

Figure 26. Solution for Top-to-Bottom Flow Distribution

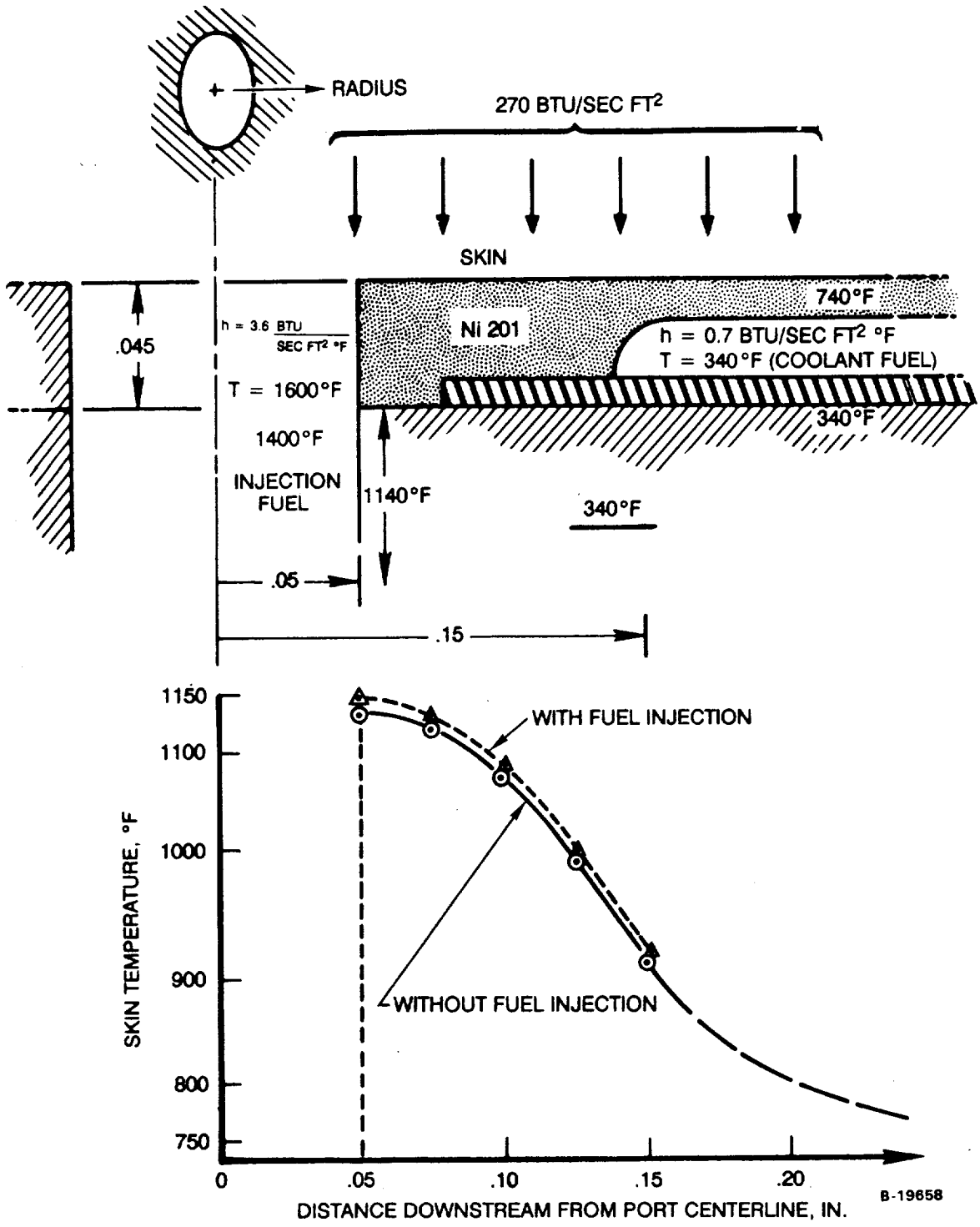

Figure 27. Temperature Distribution Around the 45° Fuel Injector Port

The thermal expansion coefficients of Nickel 201 and Inconel 718 are close, as shown in Figure 28, and the effect of the difference in material thermal expansion on the overall stress will be small. Thermal stresses in the strut, however, will result from constraint of hot local regions by the large, surrounding cool regions.

To estimate the thermal stress and the expected life of the Nickel 201 skin in the region around the perpendicular fuel injector ports, the hot region was assumed to be elastically constrained by the cooler surrounding region. This localized loading has the effect of a stress concentration, and a stress concentration factor (K_t) can be formulated as the ratio of maximum local stress to the nominal stress (calculated by elementary formulas). Detailed finite element stress analyses typically show that plastic thermal stresses occur with stress concentration factors of $K_t \leq 2.0$. Furthermore, correlations of calculated cyclic lives with test results have shown the effective stress concentration factors for ductile materials to be less than the theoretical values (see also ref. 5). To reflect this, an effective fatigue concentration factor, K_f, was formulated for use in place of K_t. For the ductile Nickel 201, $K_f = 1.2$ was assumed. Also, the full $E\alpha\ \Delta T$ stress is not realized, because the cool material surrounding the higher temperature region is elastic and does not offer complete constraint against thermal expansion. The resulting stress will be reduced by a factor of K_e, between 0.5 and 1.0, for the lower constraint condition. A conservative factor of 0.95 was used in the analysis.

Ref. 5 recommended a stress concentration factor, K_f, of 1.7 for application to a range of materials. Specifically, this value was used to generate comparative LCF estimates that led to selection of nickel as the hot skin. It was also used in LCF data reduction. It gave good correlation for the uniaxial loading used in the tests. $K_f = 1.2$ was judged more representative for use with the nickel hot skin. A simplified analysis based on apparent elastic stress, as defined below, was used to estimate LCF.

The properties of Nickel 201 at the 740°F mean temperature were used ($\alpha = 8.3 \times 10^{-6}$ in./in.-°F; $E = 26.6 \times 10^6$ psi). The calculated apparent elastic stress for the 800°F temperature difference near the injector port is:

$$\sigma = K_e K_f\ E\ \alpha\ \Delta T = (0.95)(1.2)(26.6 \times 10^6)(8.3 \times 10^{-6})(800) = 201{,}400 \text{ psi}$$

This stress was checked against the maximum elastic stress for the desired LCF. A low-cycle fatigue life of approximately 1,000 cycles can be expected for a total strain of 0.01, or 1 percent (ref. 5). The apparent elastic stress at this strain is then:

$$\sigma = \epsilon E = 266{,}000 \text{ psi}$$

Since the allowable stress for 1.0-percent strain is greater than the conservatively calculated $E\ \alpha\ \Delta T$ stress, a life of over 1,000 cycles is expected for the region around the 45-deg fuel injector ports.

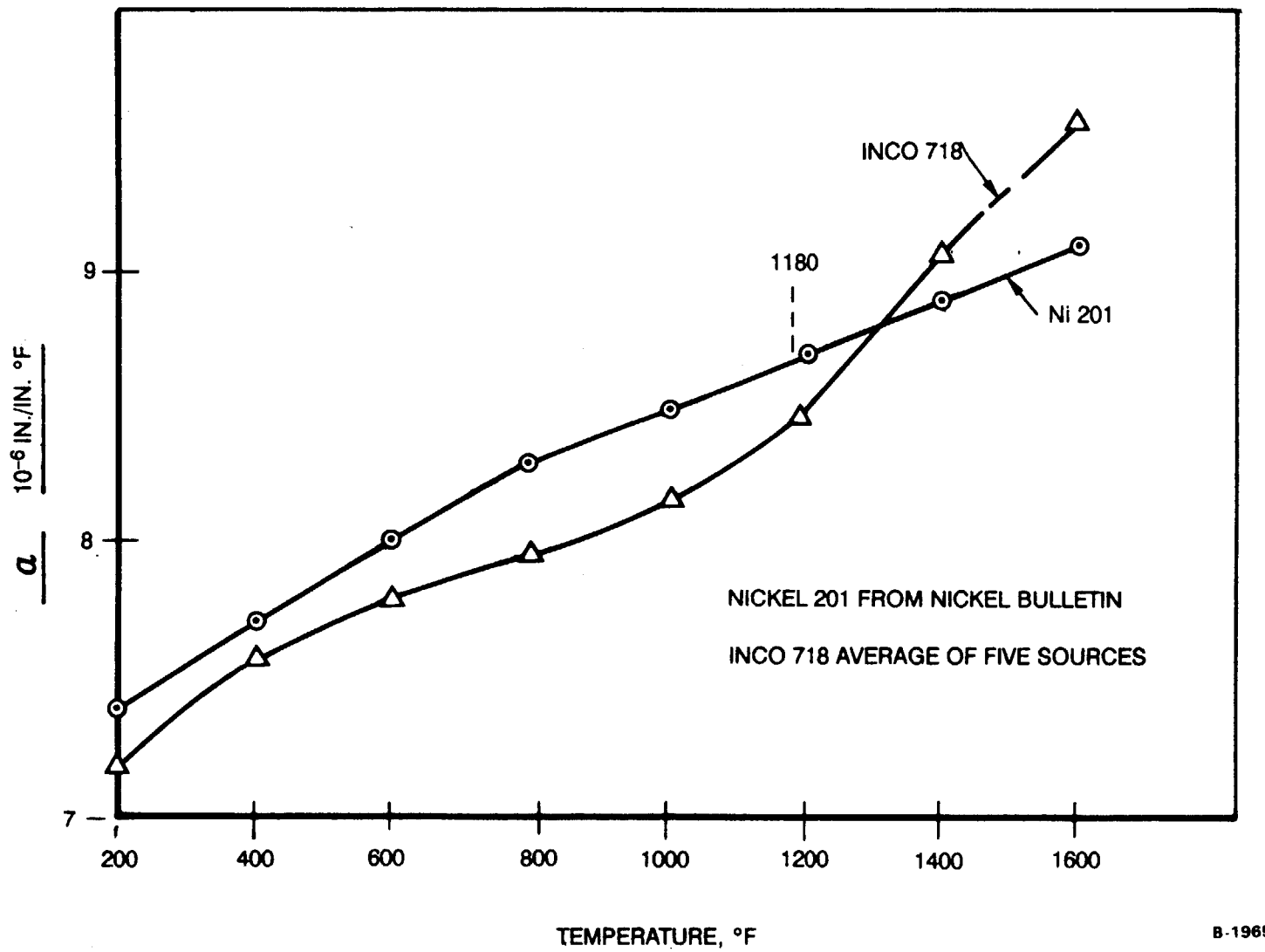

Figure 28. Coefficient of Thermal Expansion (α) for Nickel 201 and Inconel 718

4.2.5 Braze joint design.-The strut support structure is a brazed Inconel 718 assembly consisting of walls and beams. Figure 29 is a generic sketch of the assembly. Details of the beam and fuel tube configurations were subsequently changed to reflect fabrication and test experience as discussed below (para. 4.2.5.1).

Palniro 1 braze filler alloy is placed in all of the joints prior to vacuum brazing at 2080°F. The aft three beams are penetrated by fuel injection tubes, and in the aft-most beam, the penetrations cause the braze joint on one side to be interrupted along the length. Braze assembly of the cooling jackets follows strut body brazing and is with Palniro 7 filler alloy at 1935°F, as shown in Figure 12. The top and bottom ends of the strut are closed by flat plates that are brazed to the assembly with Nioro filler alloy during a third braze operation at 1800°F.

After brazing, an internal hydrostatic proof pressure test to 1500 psig at room temperature is required. (This was subsequently changed to 1050 psig, consistent with planned wind tunnel conditions.) All of the internal chambers are pressurized simultaneously, except for the unpressurized space between the first and second beams from the leading edge. This pressure loading subjects beam braze joints to combined bending and tension loading.

4.2.5.1 Braze joint strength: During an initial pressure test of a partial length strut (see Section 5), the braze joint on the aft beam separated at 1200 psig. The aft two chambers were cut from the strut, and the fuel tube openings in the remainder of the strut were closed with epoxy-cemented plugs. When this remainder was tested, the epoxy-cemented plugs were dislodged at 1700 psig. After the plugs were replaced, the braze joint of the most forward of the two beams separated at 450 psig.

The design of the braze joints was based on available data for Nioro and Palniro 1 braze joint strengths. Typical data for these alloys are shown in Table 9. The tensile tests confirm that Palniro 1 braze joint strengths of 120 ksi can be obtained.

Confirmation of Nioro braze joint strength was obtained by a burst test on a rectangular-chamber specimen that simulated the most severely loaded end closure plate joint. Table 10 shows the test results. The associated test specimen configuration is sketched on p. 60. The 5200-psig burst pressure, and the calculated (a simplified plate plastic bending analysis) stress of 122 ksi are consistent with the Nioro braze strength shown in Table 9.

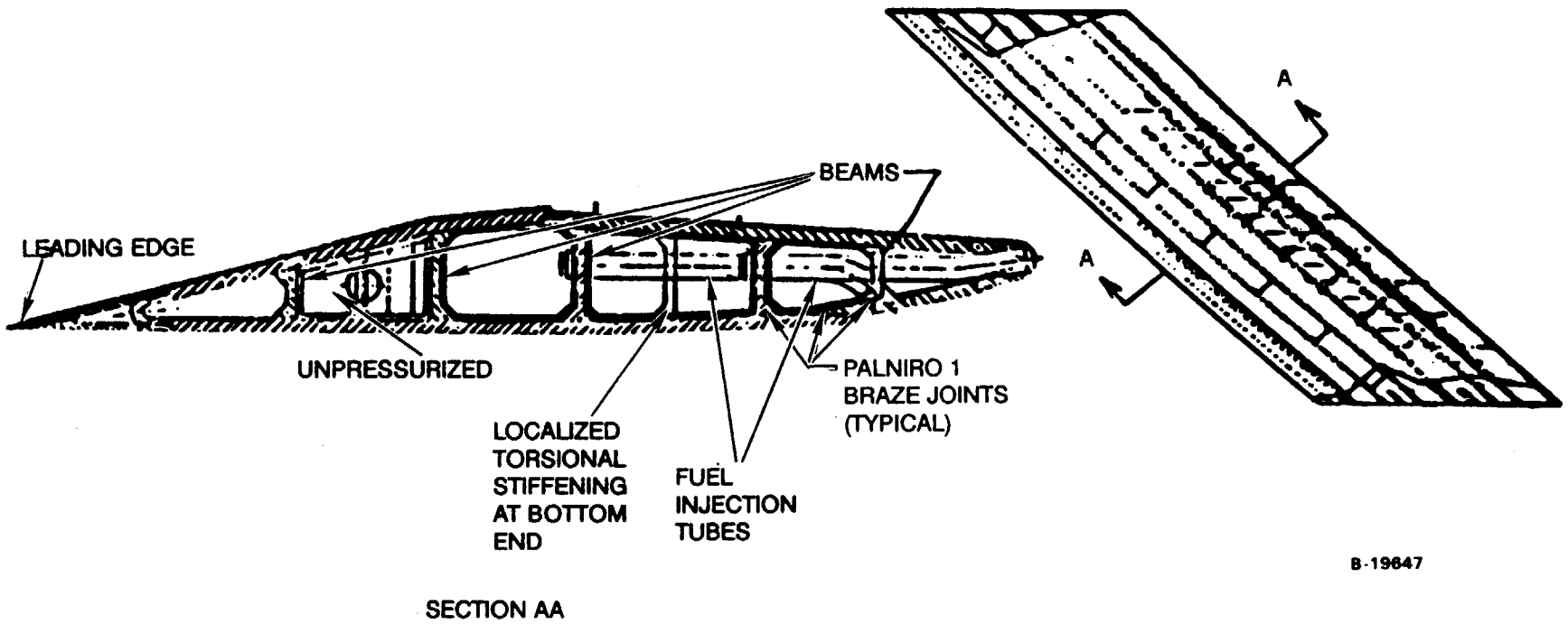

Figure 29. Strut Configuration for First Braze Cycle

TABLE 9

BRAZE JOINT DESIGN STRENGTH

Filler Alloy	Nioro		Palniro 1
Temperature	1000°F		RT
Braze alloy metal			
Fty, ksi	99.5[3]		105[3]
Ftu, ksi	115[3]		122[3]
Braze joints			
Fty, ksi[1]	107.2[4]	61.7[4]	–
Ftu, ksi[2]	194.7[4]	103.1[4]	–

NOTES:

(1) 0.004 clearance joint after tempering, AISI 410 stainless-steel base material

(2) Same as (1) but in the "as brazed condition"

(3) Data from Western Gold and Platinum Company data sheets

(4) Data from "Further evaluation of Ni-Cr-B and 82Au-18Ni brazing alloys," Welding Research Supplement, December 1958

TABLE 10

NIORO JOINT STRENGTH
RECTANGULAR-CHAMBER PRESSURE TEST

Test pressure at burst	5200 psig
Calculated stress at 1500 psig	51 ksi
Calculated stress at burst	122 ksi
Joint strength	> 115 ksi

Table 11 shows the results of the partial-length strut pressure test and the calculated stress. The maximum test pressure of 1700 psig was far short of the expected burst pressure of 4800 psig, and corresponds to a calculated stress of 43 ksi at burst.

TABLE 11 PALNIRO-1 JOINT STRENGTH PARTIAL-LENGTH STRUT PRESSURE TEST	
Calculated burst pressure (design)	4800 psig
Test pressure at burst	1700 psig
Calculated stress at 1700 psig	43 ksi

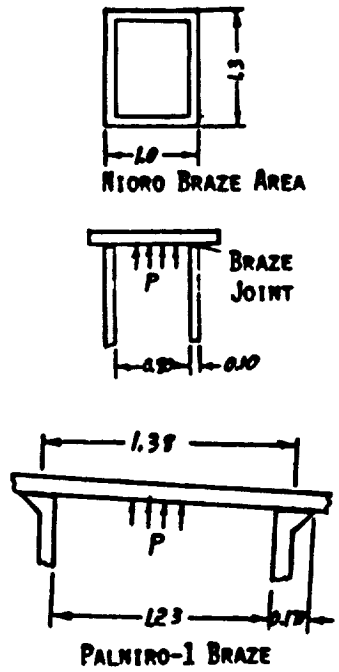

The apparently low Palniro braze joint strengths indicated by strut pressure test results were further investigated by metallurgical examination, and tensile tests on specimens cut from the strut assembly. Four specimens were machined to obtain a straight load path for tensile machine tests and to avoid the eccentricity inherent in the full joint (see sketch below). The results of these tests are shown in Table 12. The strength range from 42 to 60.7 ksi was again below expectation.

TABLE 12 PALNIRO-1 BRAZE JOINT TENSILE-MACHINE TEST RESULTS
60.7 ksi
53.7 ksi
52.2 ksi
42.0 ksi
NOTES:
(1) Ultimate strength at room temperature
(2) Straight joint specimens from strut beams

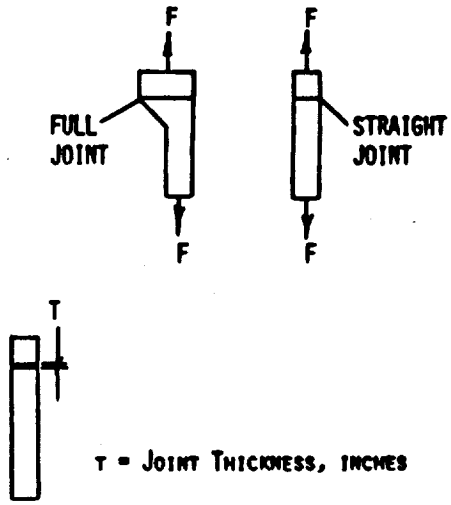

Four rectangular-chamber pressure test specimens were also brazed, as shown above. Two joint clearances were used. These specimens burst at a pressure above 8000 psig, when welds on the specimen chambers fractured. Braze joint tensile-machine specimens were cut from the chambers, and the tensile test results are shown in Table 13.

TABLE 13 PALNIRO-1 JOINT STRENGTH RECTANGULAR CHAMBER PRESSURE TEST	
T = 0.0043 in.*	T = 0.0087 in.*
123.8 ksi	129.8 ksi
114.8 ksi	133.7 ksi
*Braze joint gap as set up.	

Metallurgical examination of the strut braze joints showed porosity, while the pressurized chamber braze joints are practically free of porosity. Braze joint cross sections are compared in Figures 30 and 31. This porosity reduced joint strength. In addition, enlarged, machined holes in the aft beam, to facilitate assembly of the fuel distribution tubes, resulted in increased local stresses that combined with the reduced strength to cause fracturing at a low pressure.

4.2.5.2 Stress analysis: As a result of the low strength demonstrated by the strut pressure tests, additional stress analyses were performed on the strut structure. A two-dimensional finite element ANSYS model was made of the strut cross section, as shown in Figure 32. The 1000-psig internal pressure loading is the normal operating maximum. The displacement plot is highly exaggerated and makes the bending at various locations readily apparent.

The 2D analysis indicates that the highest stresses in braze joints occur at beams 3, 4, and 5 as identified in Figure 32, with a maximum of 74.7 ksi at beam 4. Equivalent (Von Mises) stress contours for these beams are shown in Figures 33, 34, and 35. Beam 5 (aft beam) stresses are relatively low because the effects of the fuel tube penetrations are not included in the 2D model. The stress contours show the expected stress concentrations at the sharp corner joints between the beams and the outer shell structure; however, the maximums are well below expected room temperature yield strength. This elastic analysis indicates that for a 1500-psig proof pressure, and for operation at normal pressure and at 1000°F, very localized stresses will approach the yield strength.

After the 2D analysis was completed, a 3D ANSYS model was made of a representative section of the aft beam to evaluate the effect of the openings for fuel tube penetrations. Three views of the model are shown in Figure 36. The model is for a 2.37-in. length of the beam, and is made with 1550 STIF45 solid elements. Loading is applied to the beam by imposing the 2D model displacements at each node of the braze joint faces.

Figures 37 and 38 show the stress distribution in the 3D model for the 2D model displacement loading. This type of loading results in similar stress distributions in the two models, and the loading on the 3D model is considered representative of the type of loading that results from strut internal pressure.

Transverse section stress plots for the 3D model show very localized peak stresses at braze joint sharp corners, with a maximum stress of 89.3 ksi. The 2D and 3D ANSYS

CROSS SECTIONS THROUGH BEAM 4

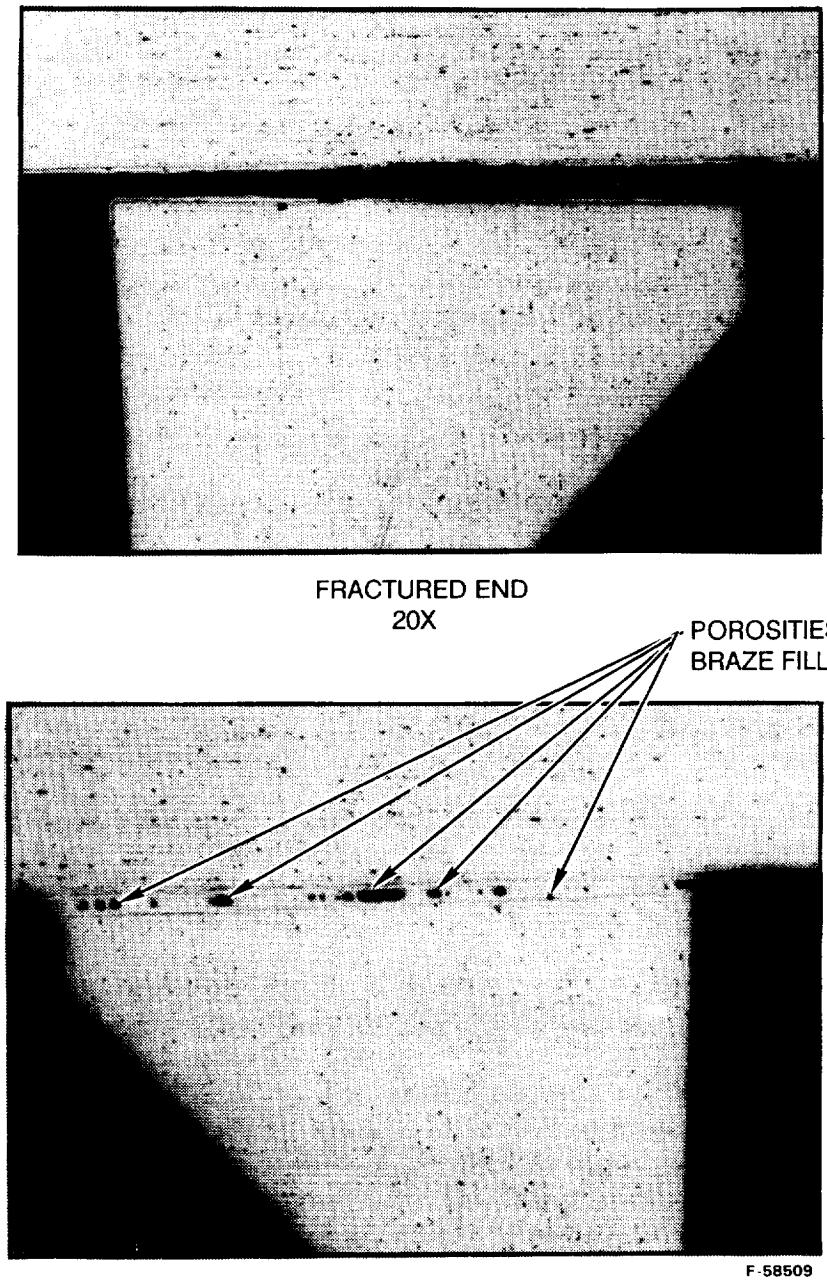

Figure 30. Strut Aft Beam Braze Joint Cross Sections

CROSS SECTION OF BURST SAMPLES

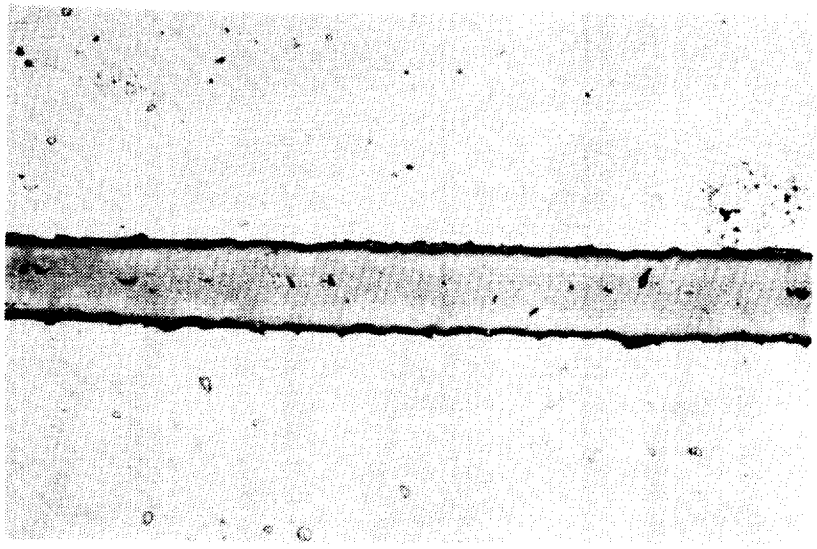

0.0043 GAP
100X

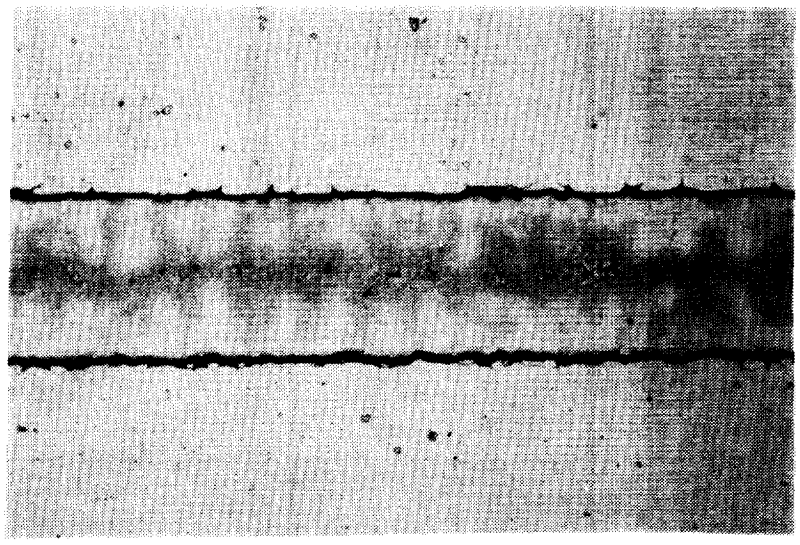

0.0087 GAP
100X

Figure 31. Pressurized Chamber Specimen Braze Joints (Note the Lack of Porosity)

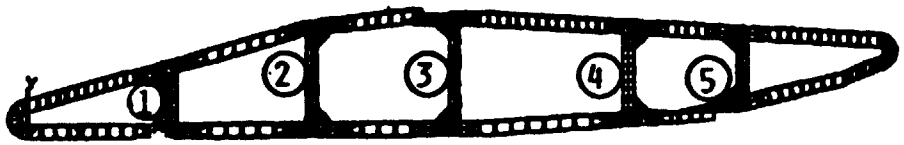

MODEL

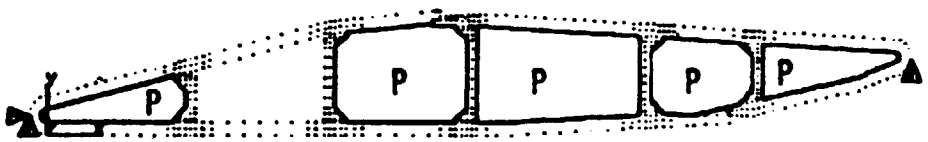

P = 1000 PSIG

BOUNDARY CONDITIONS AND LOADING

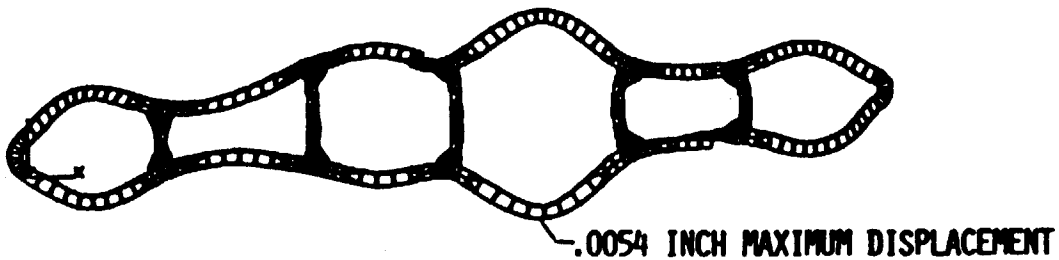

EXAGGERATED DISPLACEMENT PLOT

B-17180

Figure 32. Strut 2D ANSYS Analysis

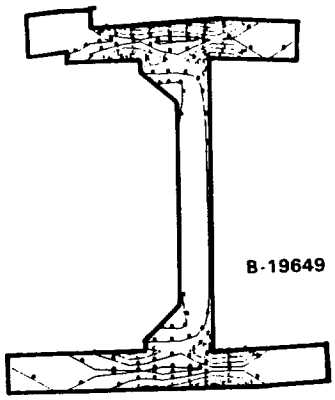

Figure 33. Beam 3 Joint Equivalent Stress Plot for 2D ANSYS Model Analysis – 66.2-ksi Maximum Stress at 1000 psig

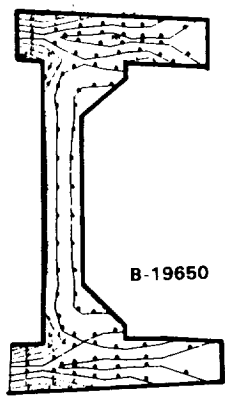

Figure 34. Beam 4 Joint Equivalent Stress Plot From 2D ANSYS Model Analysis – 74.7-ksi Maximum Stress at 1000 psig

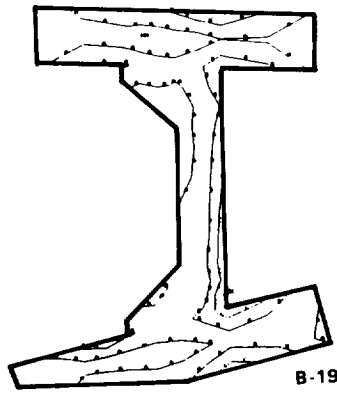

Figure 35. Beam 5 Joint Equivalent Stress Plot From 2D ANSYS Model Analysis – 44.4-ksi Maximum Stress at 1000 psig

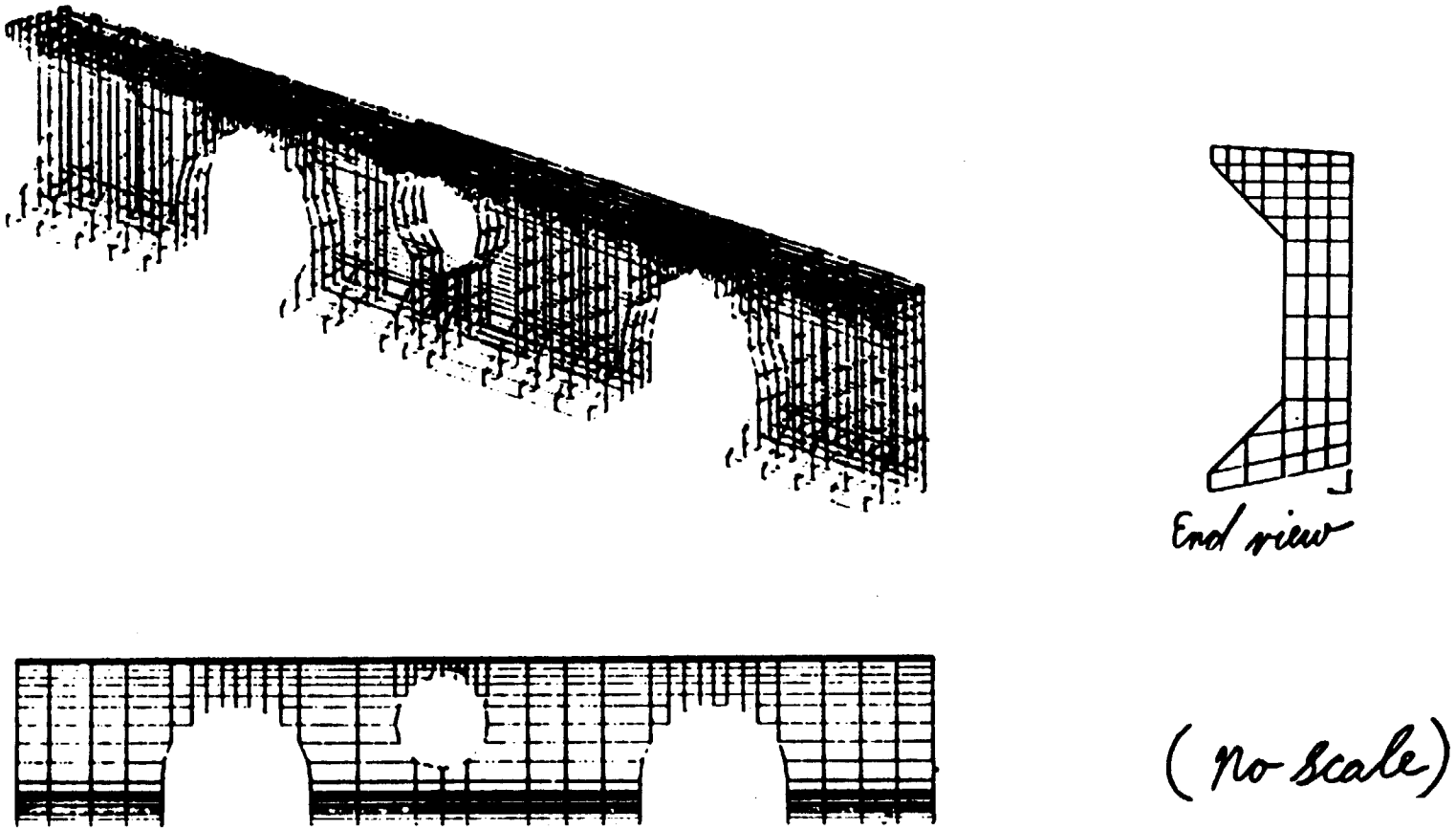

Figure 36. Three Views of ANSYS 3D Finite Element Model of a Portion of Beam 5

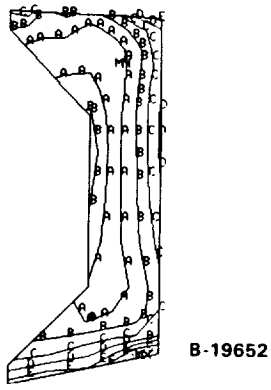

Figure 37. Beam 5 Equivalent Stress from 3D ANSY Model Analysis at Section Z = 1.49-Maximum Stress 84.4 ksi

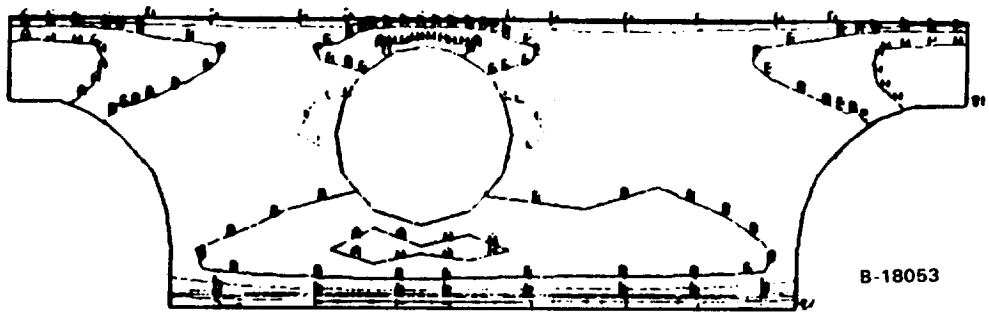

Figure 38. Beam 5 Equivalent Stress from 3D ANSY Model Analysis at Section X = 0.02-Maximum Stress 84.4 ksi

model stresses and deformations for similar sections are compared in Figures 39 and 40. Although the stress patterns in the 3D sections are similar to the 2D model stress patterns, the 3D model stresses are higher, and vary along the length, because of the hole and two arches that penetrate the beam. These penetrations also cause reduced beam stiffness, and the 2D model displacements applied to the 3D model result in a lower load per unit length; thus, the 3D model stresses must be increased by a factor to obtain magnitudes corresponding to an applied pressure load of 1000 psig.

The average loads per unit length for the two models were compared by considering the nodal forces at the braze joint boundaries. This comparison resulted in a factor of 1.86 that must be applied to the 3D model to obtain the same loading per unit length as for the 2D model with 1000-psig internal pressure. When this factor is applied, the peak stresses are as shown in Figures 41 and 42. These peak stresses will cause local yielding. They must be reduced to provide margins that accommodate variability which results in less than full design strengths. The strut pressure tests indicate that with full-strength braze joints (approximately double the strength actually obtained) a proof pressure of 1500 psig can indeed be sustained.

Emphasis in this review was placed on the braze joint strength required to contain the strut internal pressure. Additional loads are caused by temperature and aerodynamic pressure (ref. 2), and the joint must accommodate the combined loading in a fatigue environment. These additional loads are within the capability of the joints.

4.2.5.3 Summary: The strut braze joint structural design review showed the following:

(a) Based on this investigation, the reason for the 450-psig break in the beam joint on the third pressure cycle (1200, 1700, 450 psig) is likely the high localized plastic stresses that developed in the porous braze joints.

(b) The strut was designed to be structurally efficient. Design margins are low, and full design strengths of materials and joints are required to meet performance objectives. (Margins are in addition to design factors, i.e., 1.5 proof and 2.5 burst factors.)

(c) Except for the aft beam, the joint stresses are acceptable, but see item (d).

(d) Joint quality was improved (porosity reduced) in lieu of reducing joint stress to accommodate lower strength values.

(e) Enlarged penetrations in the aft beam were eliminated.

(f) Penetrations of the aft beam were reinforced with additional material, particularly by making integral injector port passages in the aft beam, as illustrated in Figure 43. The beam was redesigned in accordance with Figure 43, fabricated, and used in the full-length strut. The improved design has an increased braze joint area and better braze joint symmetry. Fuel tube assembly was also facilitated with this revised design.

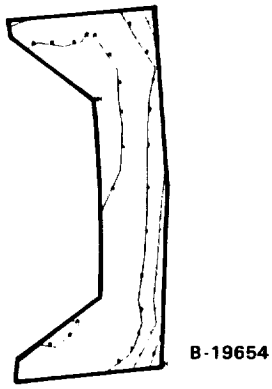

Figure 39. Deformed Shape and Equivalent Stress for 2D ANSYS Model of Beam 5

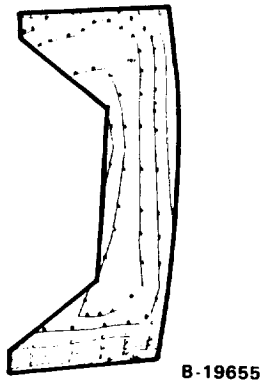

Figure 40. Deformed Shape and Equivalent Stress for 3D ANSYS Model of Beam 5

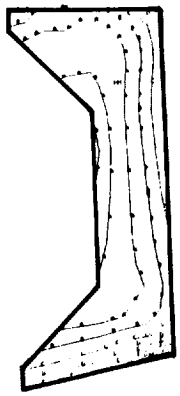

Figure 41. Transverse Cross Section Equivalent Stress for 3D ANSYS Model with Application of a 1.86 Factor to Obtain Correspondence of Loading with the 2D Model at 1000 psig

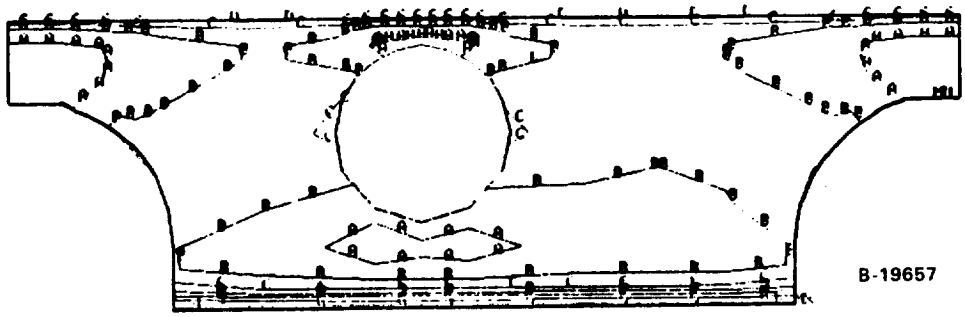

Figure 42. Longitudinal Cross Section Equivalent Stress for 3D ANSYS Model with Application of a 1.86 Factor to Obtain Correspondence of Loading with the 2D Model at 1000 psig

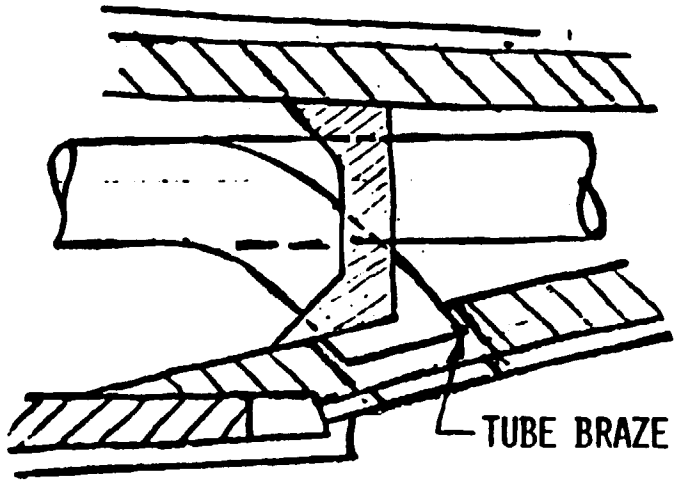

PREVIOUS DESIGN

- WEAKENED BRAZE JOINT
- DIFFICULT TUBE FIT AND ASSEMBLY

IMPROVED DESIGN

- REINFORCED BRAZE JOINT AND CENTER HOLE
- SIMPLIFIED FIT AND ASSEMBLY

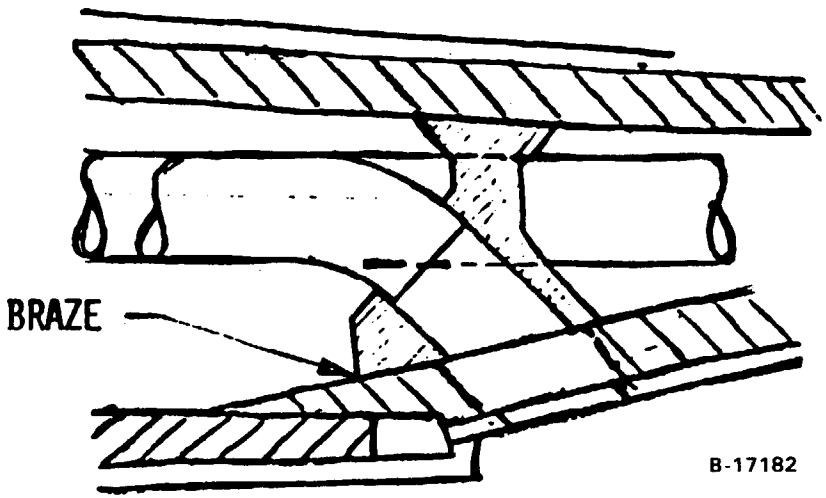

Figure 43. Aft Beam 45-Deg Injector Tube Interface

4.3 Task 1 – Verification of Strut Leading Edge Design

Two aspects of the leading edge design were selected for verification:

(a) Fabrication, including preparation of pressure test specimens to provide an overall assessment of the critical braze joints

(b) Low cycle fatigue performance of the leading edge stagnation region

4.3.1 Fabrication Evaluation.

4.3.1.1 Design: The test specimen was a full-scale cross section of the leading edge tip region. The span was 3 in. and the cord length was 2 in. These dimensions are large enough to provide simulation of leading edge design features, but small enough to allow use of relatively simple fixtures and tools. Span-wise effects were not evaluated because of the greatly increased tooling requirements. Instead, the small test specimens were intended, in part, to guide design of the full-length tools and procedures.

The cooling jacket consisted of a PCM pin-fin heat exchange surface brazed to a 0.010-in.-thick backplate. This initial braze was performed in a flat state. After brazing, the subassembly was pressure tested and holographically examined for structural integrity before it was formed and brazed to an Inco-718 support structure. The Inco-718 braze surfaces were ground flat.

Figure 44 shows a set of detail parts for the test specimen.

4.3.1.2 Fabrication development – cooling jackets: Initially, sample specimens of the Ni-201 cooling jacket pin-fin were prepared by PCM to verify acceptability of the artwork. Figure 45 shows two pin-fin cooling jacket surfaces as etched on a single Ni-201 material blank. Palniro 1 filler alloy foil, 0.001-in. thick, was used to braze the jacket assembly. Several formed jacket assemblies were sectioned after forming, and the leading edge radius was examined. Forming mandrels were adjusted until the design radius of 0.050-in. was obtained. Then, the brazed jackets were formed (see Figure 46) and brazed to solid Inco-718 support structures (see Figure 44) to develop fixturing and brazing techniques. Palniro 7 filler alloy, 0.001 in. thick, was used. The Inco-718 braze surfaces were nickel-plated to enhance alloy flow and wetting. The Ni-201 surfaces were left unplated. A loading of 10 psi was used during the braze cycle. The brazed specimen was sectioned and the braze quality evaluated.

Figure 47(a) is a photomicrograph of pin-fin-to-back sheet and back sheet-to-support structure joints. Figure 47(b) is a macro through the tip of the specimen. Both sections are from the same specimen. The pin-fin joint shows good alloy flow. Voids are present in the Palniro 7 braze joint between the jacket and the Inco-718 structure.

Examination indicated that the as-brazed apparent thickness of the filler metal was about 0.002 in.; the original thickness of the braze alloy foil was 0.001 in. This apparent

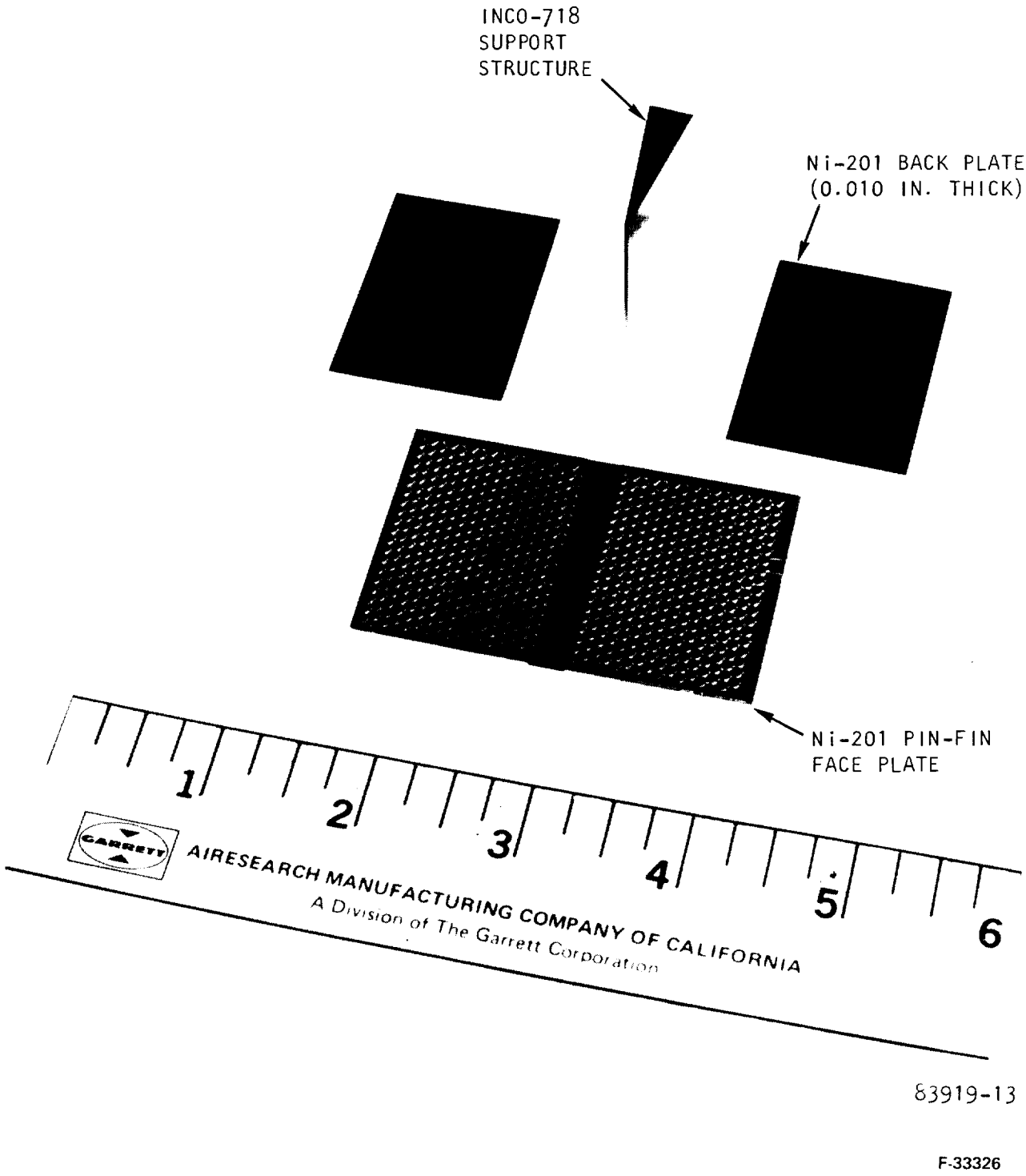

Figure 44. Leading Edge Test Specimen Details

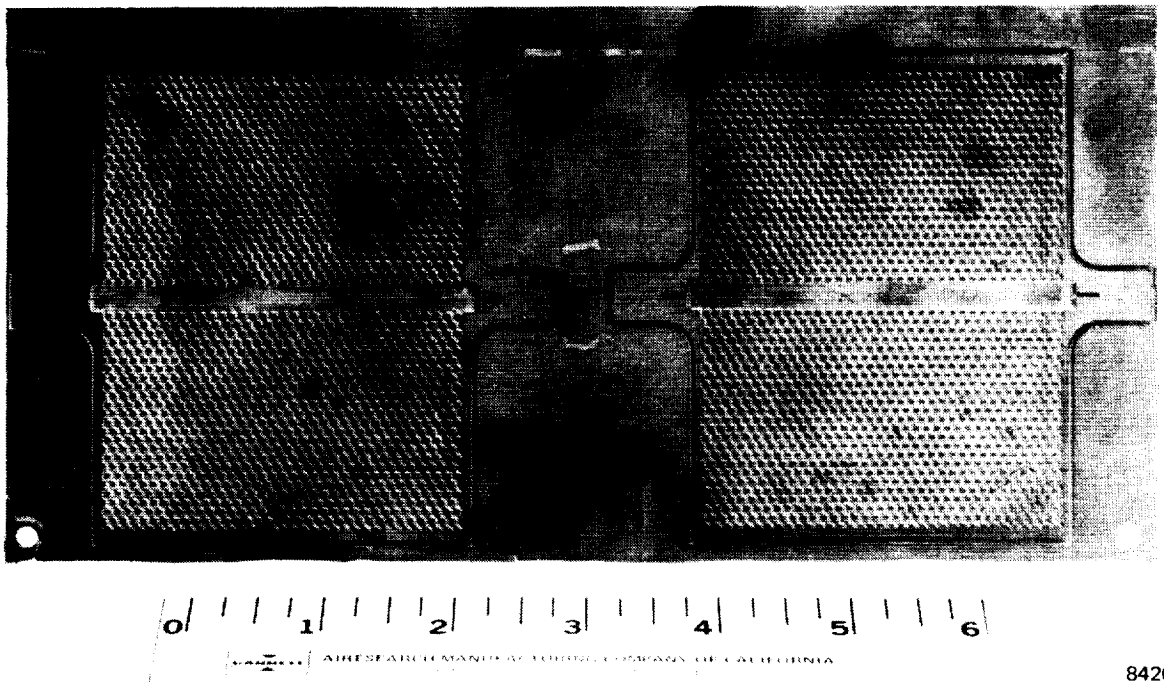

84205-1
F-33544

Figure 45. Pin-Fin Cooling Jacket Face Plate

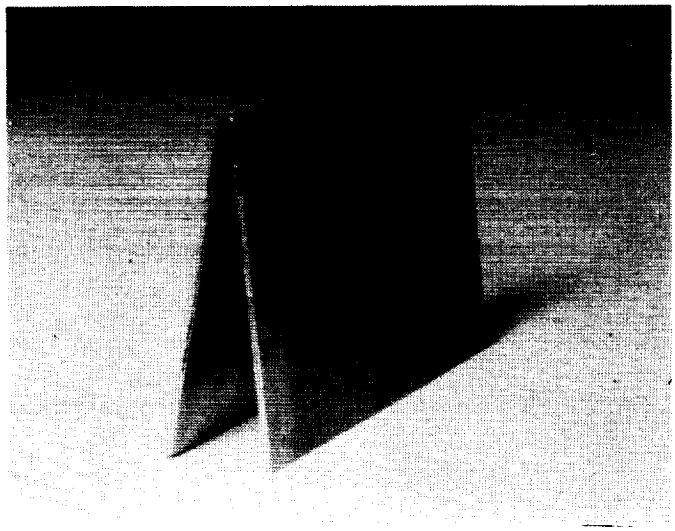

F-34901

Figure 46. Formed Strut Leading Edge Cooling Jacket Assembly

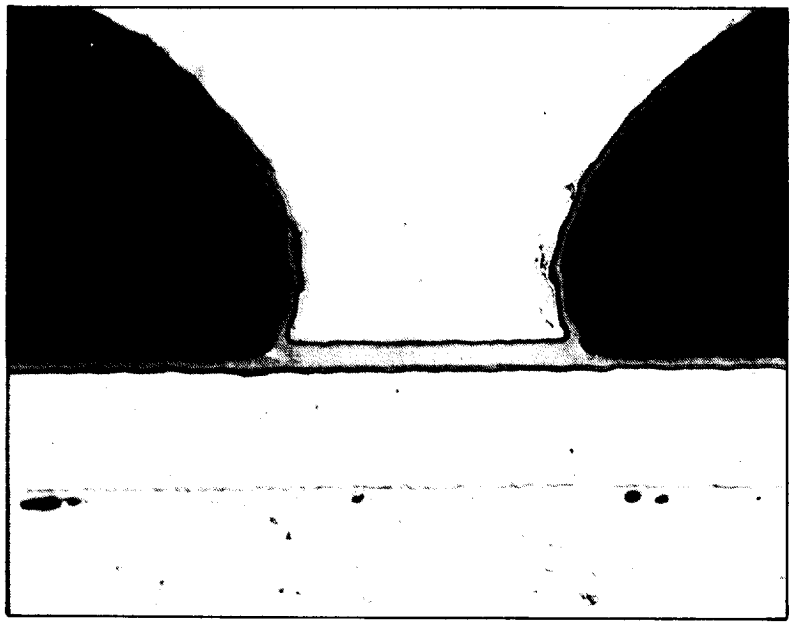

a. Cooling Jacket Assembly Braze Joint

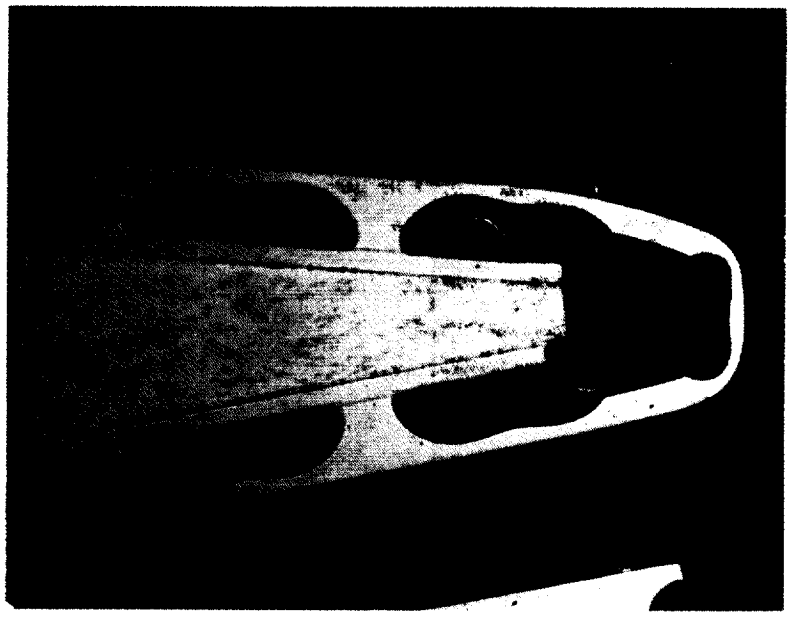

b. Inco-718 Support Structure-to-Cooling Jacket Assembly Braze Joint

F-33988

Figure 47. Sections from Leading Edge Test Specimen

increase in thickness of braze joints generally can be observed in other micrographs as well. It appears to represent an equilibrium for the conditions and materials used. It is considered apparent because of (1) obliteration of the interface between filler and parent metal as a result of interalloying and (2) surface tension effects, which influence wetting of the parent metal by the filler. That the net thickness of the brazement does not increase proportionally to the apparent increase in joint thickness gives some support to point (1). With regard to point (2), the two sections from the panel specimen in Figure 48 show excellent wetting, with all surfaces covered with filler. The combined filler thicknesses in void areas as shown in Figure 48(b) are approximately the same as the total apparent thickness in a complete joint, Figure 48(a). Figure 48(a) shows some minor additional growth under the joint and has a measured thickness of 0.0025 in. Thus, the 0.002-in. to 0.0025-in. observed joint thicknesses appear to represent an equilibrium range for the general configuration and conditions used.

In joints formed by flat, unetched surfaces, as in brazing the Ni-201 cooling jacket assembly to the Inco-718, the joint thickness was also 0.002 in., but braze voids were generally noted. Initially, it was assumed that the observed voids were not structurally critical and, therefore, were acceptable. Subsequent work on the partial length strut (Section 5) led to further investigation and development to improve the joint design. On subsequent specimens, in the interim, the braze loading was increased to 1 atm, which served to reduce the extent of observed voids.

The brazed, flat jacket assemblies intended for pressurization tests were X-rayed and holographically inspected under pressure. Figure 49 is included to show results for a panel with two unbrazed pins, indicating good resolution for the method. The unbrazed areas appear as small white spots, as marked. Holography was used throughout to verify the integrity of joints. Additional attention to flatness of the joint surfaces and to pin orientation (tip up or down) during brazing generally yielded satisfactory brazed assemblies.

As part of the investigation, two pin-fin face plates, that were distorted because of material removal from one side during PCM, were stress relieved. Following stress relief, the tip of each pin was inked and a printed impression of the array was made. Only about 70-percent contact of the mating surfaces was observed. The face plates were then subjected to a second stress relief cycle at 1700°F for 10 min and at a 1 atm load. Imprinting showed 100 percent contact of the pin-fins of one face plate whereas a number of pin-fins on the other failed to indicate contact. This plate was lapped to obtain 100 percent contact. Both face plates were then assembled and brazed as test specimens.

After brazing, holographic pressure testing showed three unbrazed pins in each panel, one of which is shown in Figure 50. The braze misses appear as bull's eyes. The panel was sectioned and metallographically studied, Figure 48 above.

One sample cooling jacket assembly was brazed using additional Palniro 1 filler alloy (0.0015-in. foil vs 0.0010-in. foil) to evaluate the effect of the increased filler alloy on the occurrence of pin-braze voids. The pin-fin face plate for this specimen was stress-relieved and lapped. Also, the specimen was fixtured for braze with the pin-fin braze joints facing

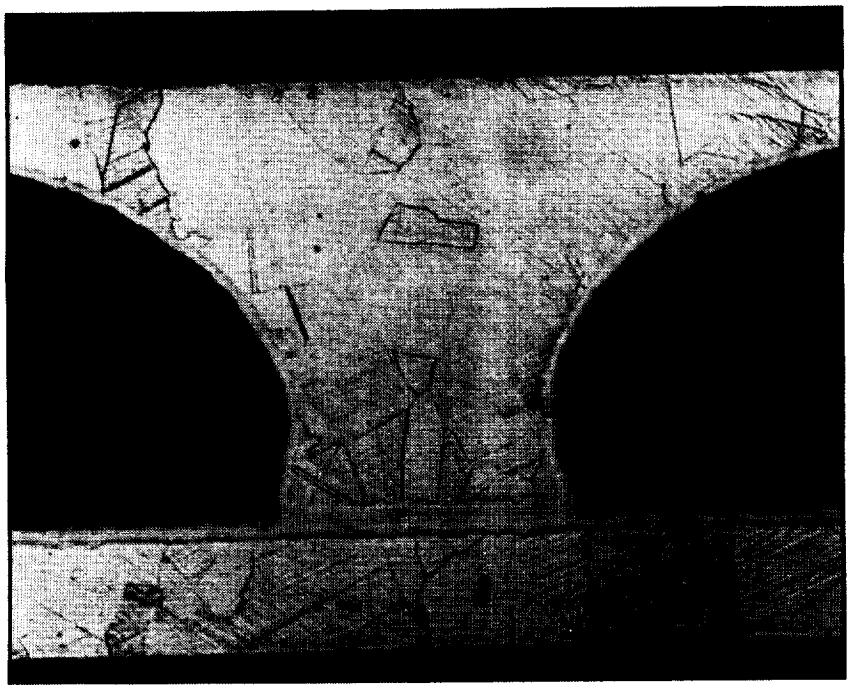

(a) Brazed Pin-Fin

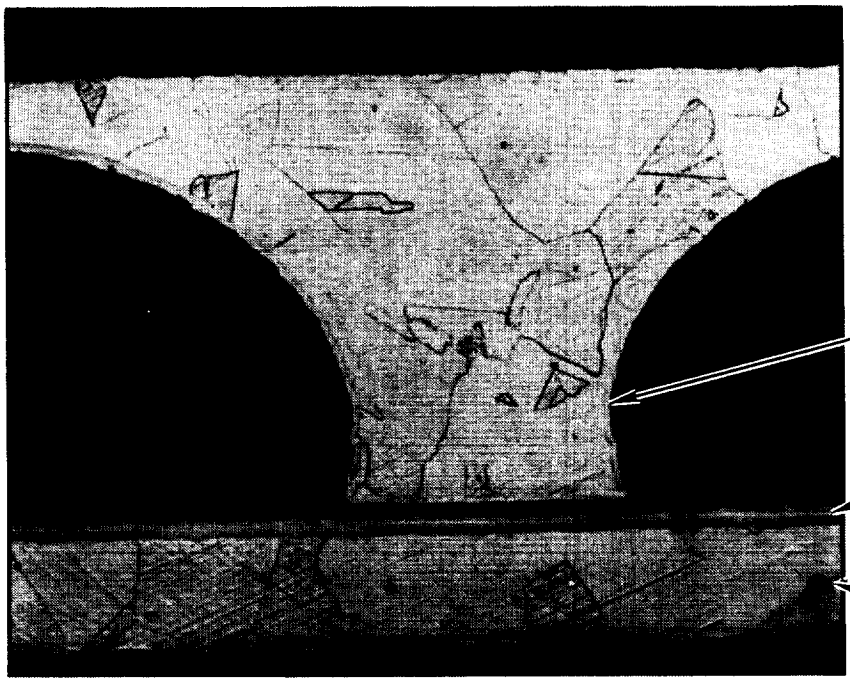

(b) Unbrazed Pin-Fin

F-35449

Figure 48. Section from Cooling Jacket Braze Specimen

ORIGINAL PAGE
BLACK AND WHITE PHOTOGRAPH

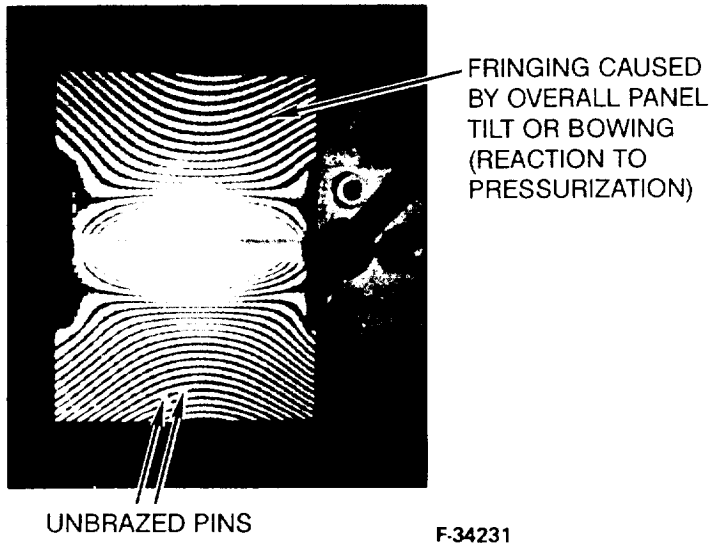

Figure 49. Hologram of Cooling Jacket Assembly Showing Two Unbrazed Pin-Fins

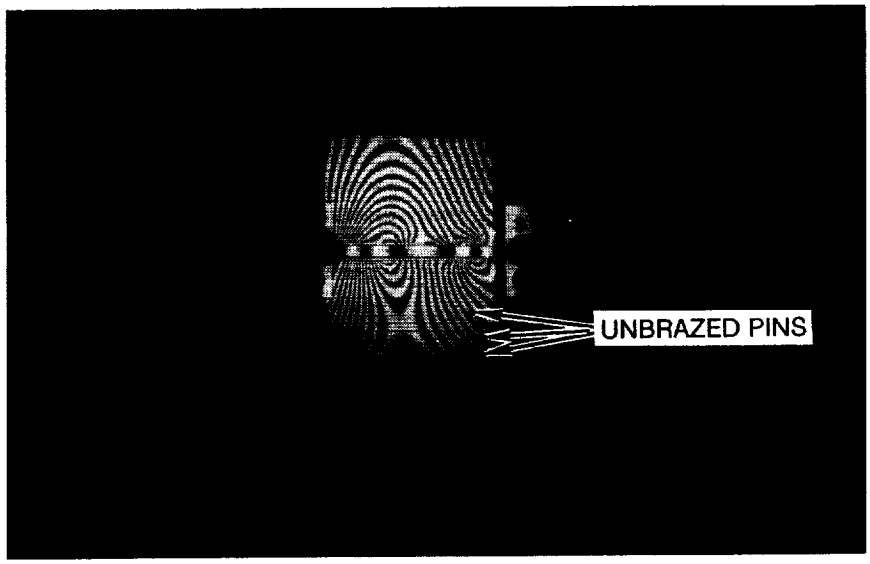

Figure 50. Hologram of Cooling Jacket Assembly Showing Three Unbrazed Pin-Fins

up, as used previously. The face plate was supported by a flat graphite plate and the braze load applied to the back sheet by a pressurized bellows.

After brazing, the specimen was radiographically examined. Excess filler alloy occurred only at one edge, suggesting an out-of-flat positioning of the fixtured specimen during brazing. It was then pressure-tested and holographically examined. A typical hologram of the specimen, Figure 51, indicates completely brazed joints.

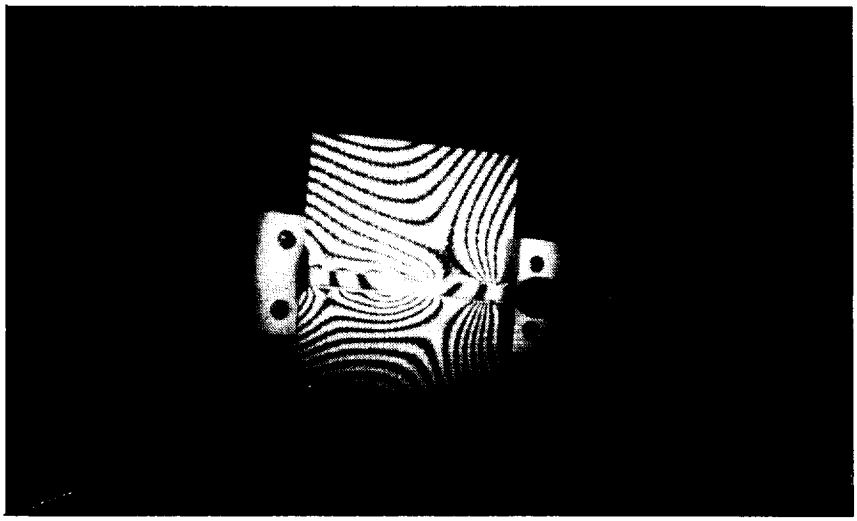

F-35856

Figure 51. Hologram of Cooling Jacket Brazed with 0.0015-in. Filler Alloy Foil, Pins Facing Up (No Braze Voids)

A second cooling jacket assembly was brazed using the increased 0.0015-in. filler alloy foil. The specimen was fixtured with the tips of the pin-fins facing down, sitting on the filler alloy and the back sheet.

After brazing, the specimen was radiographically examined. Excess filler alloy accumulated only at the first row of pins adjacent to the headers. The specimen was pressure-tested and holographically inspected. The holograms showed a sound and completely brazed structure (see Figure 52). Because of the location and minimal amounts of excess filler alloy, the specimen was used in the assembly of a leading edge test specimen.

A third cooling jacket assembly was brazed, pins facing down, using 0.0015-in. Palniro 1 foil and a stress-relieved and lapped pin-fin face plate. The header bars contained separated strips of braze foil to reduce the total amount of filler alloy.

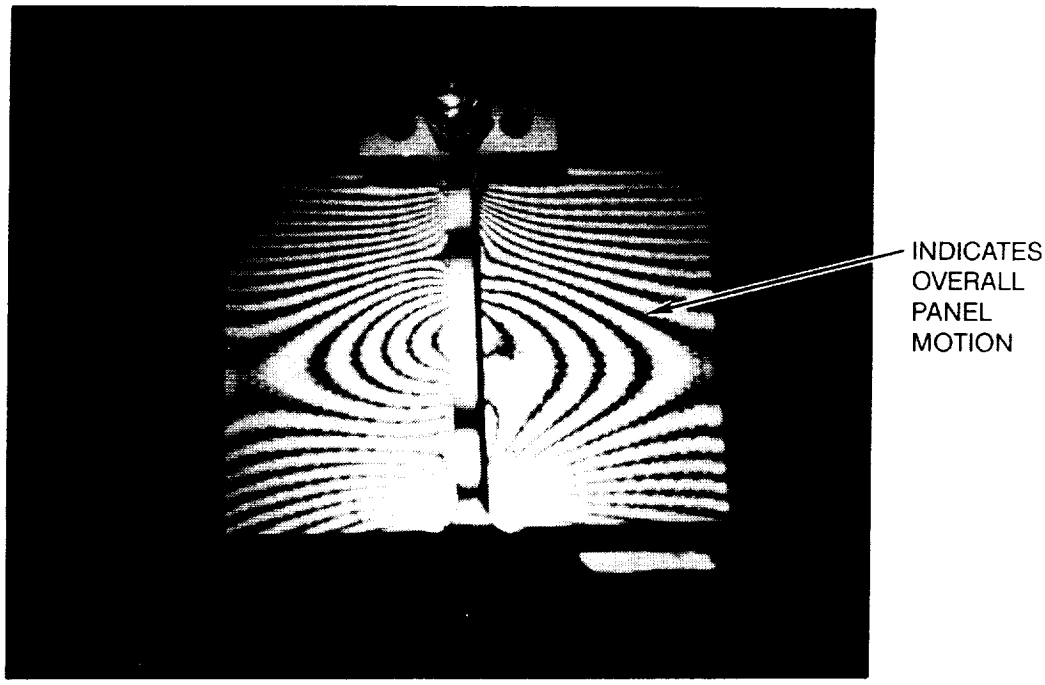

F-36080

Figure 52. Hologram of Cooling Jacket Brazed with 0.0015-in. Filler Alloy Foil, Pins Facing Down (No Braze Voids)

After brazing, the specimen was radiographically examined (Figure 53). Results indicated a very satisfactory braze without evidence of plugged areas. The pressure test and holography showed a completely brazed structure (Figure 54). The specimen was subsequently used in the assembly of a leading edge test specimen.

A fourth cooling jacket assembly was brazed using the 0.0015-in.-thick filler alloy over the pin-fins, pin-fins facing down, as on the previous assembly. To simplify the alloying procedure, instead of applying varying amounts of alloy to the header bars via stripping, a uniform 0.0005-in. layer of foil was applied to half the header bar width. Radiographic examination after brazing showed no plugging and holography, a completely brazed structure (Figure 55).

The cooling jackets for use in the leading edge test units were then machined to open the backsheet over the leading edge cavity. Slots for coolant return at the ends were electrodischarge machined (EDM). The jackets were then formed to the leading edge design configuration. Figure 56 shows the slots in the completed jacket along with the remaining parts of the assembly.

4.3.1.3 Fabrication development—Inco-718 support structure: To generate the leading edge inlet coolant channels, several sample parts were PCM'd. Excellent etched surfaces were obtained, with sharp and well-defined features and with no surface erosion due to photo-resistant separation. The resultant channel width and depth, however, did not meet the specifications. Development of the PCM process continued, while a parallel effort was

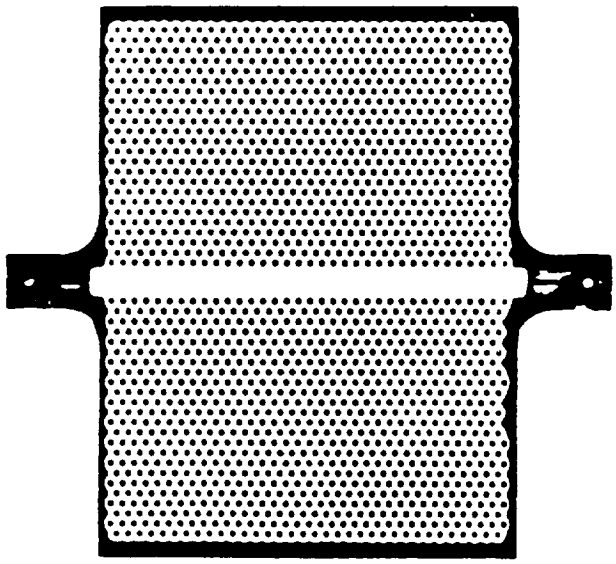

Figure 53. Radiograph of Cooling Jacket Brazed with 0.0015-in. Filler Alloy Foil Over the Pin-Fin Area, Strips of Foil at the Headers (No Plugging Between Fins or Excess Buildup of Filler Alloy)

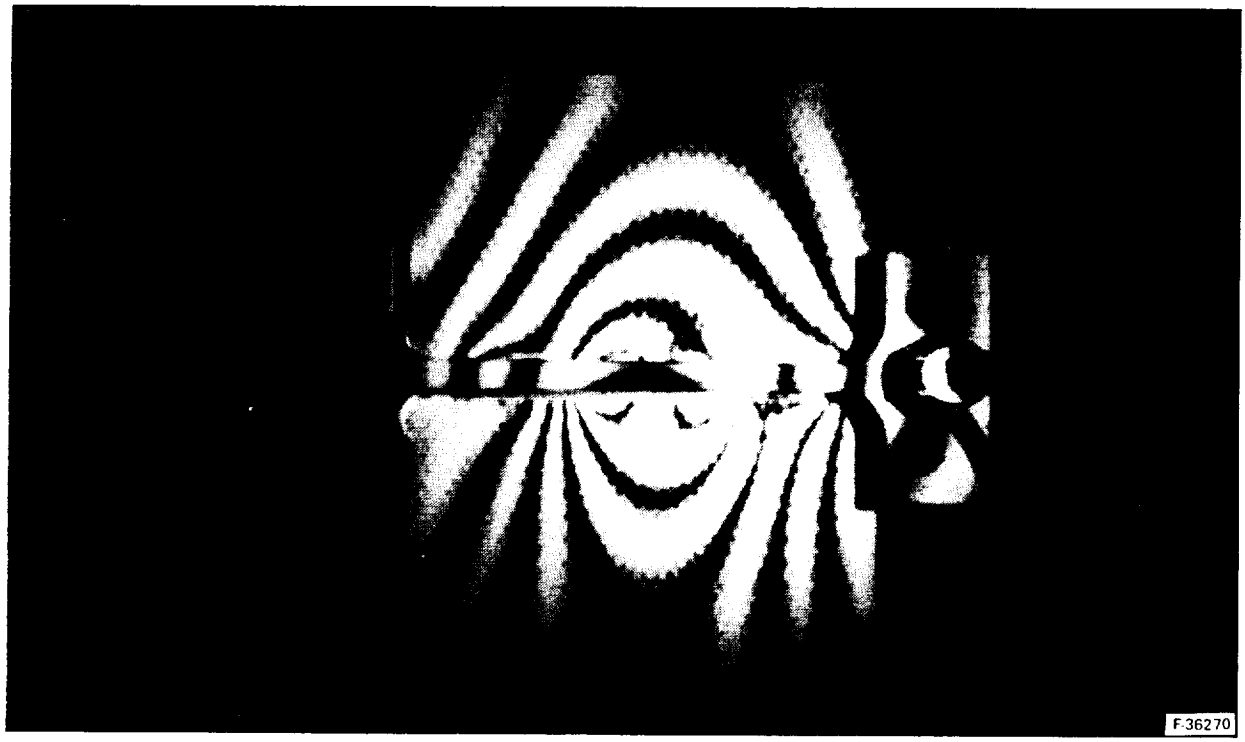

Figure 54. Hologram of Cooling Jacket Brazed with 0.0015-in. Filler Alloy Foil over the Pin-Fin Area, Strips of Foil at the Headers (No Braze Voids)

F-60424

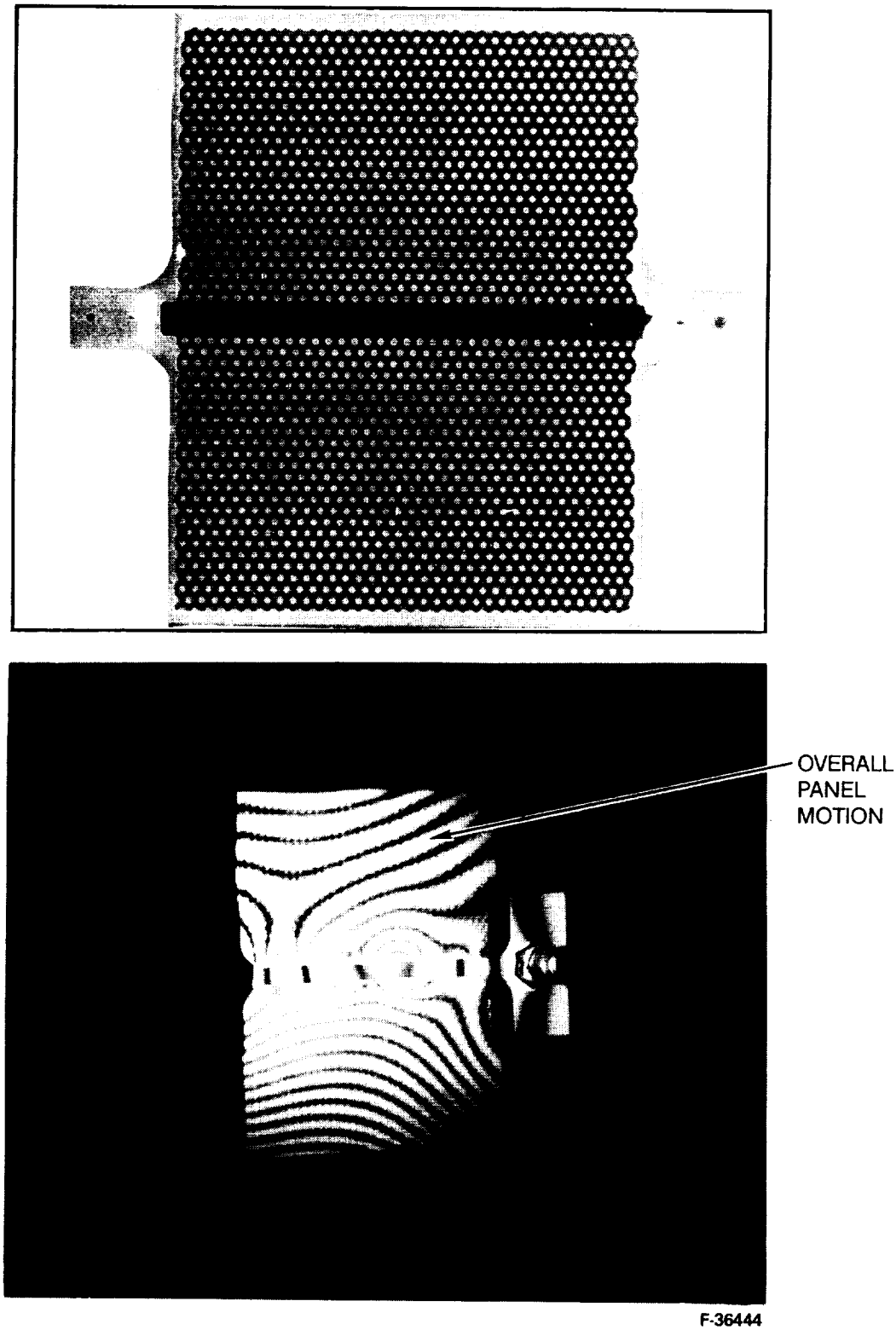

Figure 55. Radiographic and Holographic Results for Cooling Jacket Brazed with 0.0015-in. Filler Alloy Foil Over the Pin-Fin Area, 0.0005-in. Foil at Headers (No Braze Alloy Plugging or Braze Voids)

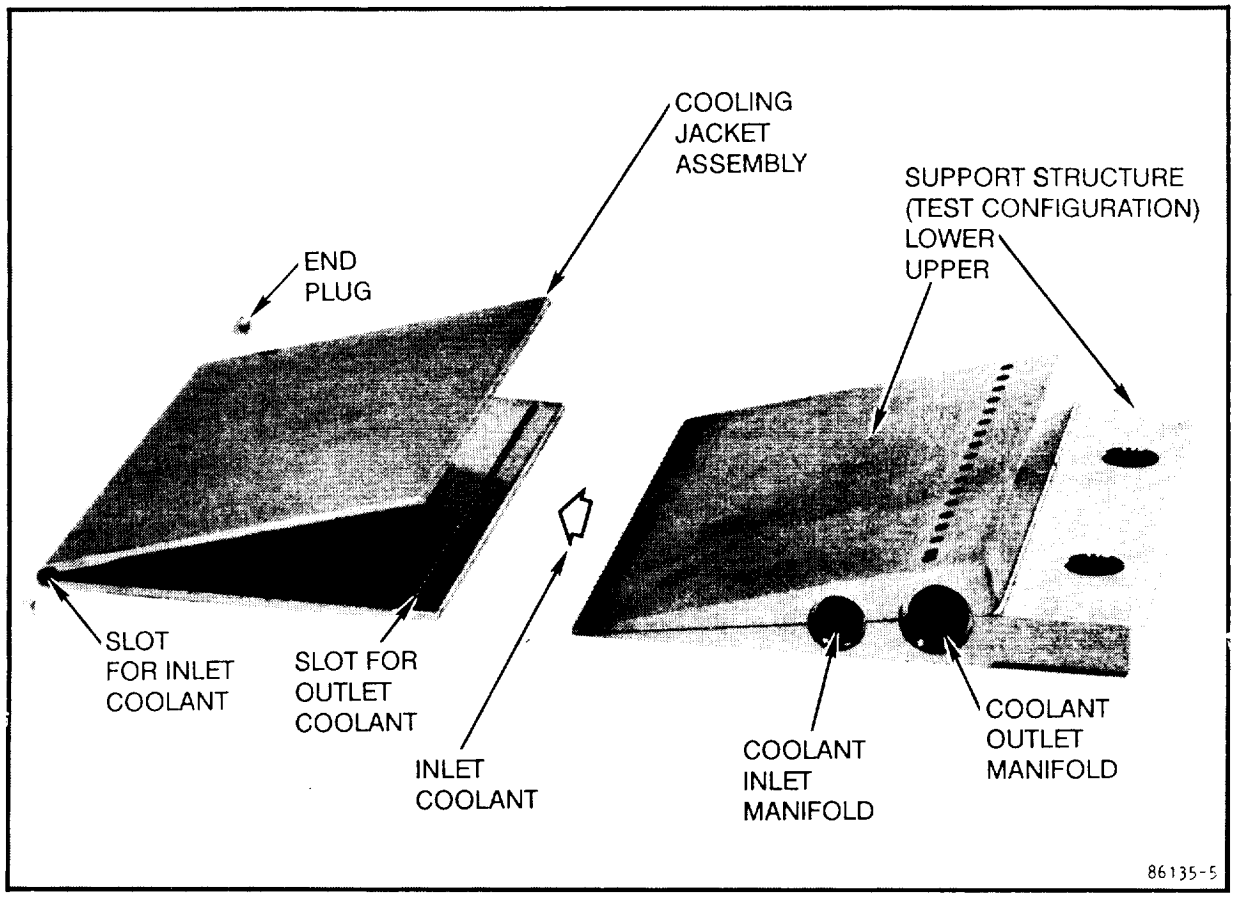

Figure 56. Detail Parts of Strut Leading Edge Test Specimen

undertaken to evaluate the use of EDM. This process was then selected to avoid delays. The EDM effort was subsequently perfected and used on certain features of partial and full-size struts. Figure 57 shows the EDM features as applied to the leading edge test specimen (upper support structure half). The two support structure halves (upper and lower) as shown in Figure 56, were brazed, final machined, and brazed to the cooling jacket.

4.3.1.4 Assembly: A dry assembly of the detail parts (Figure 56) for fit-up examination is shown in Figure 58.

Palniro 7 filler alloy, 0.0005-in. thick, was used to vacuum-furnace braze the cooling jacket-to-structure joint. A photograph of the as-brazed specimen is shown in Figure 59. The two straps on either side of the jacket were used to fixture the jacket in contact with the structure during brazing. This method of fixturing the specimen was satisfactory. No deformation or damage to the leading edge occurred. The specimen appeared to be well brazed. The specimen was sectioned and metallographically examined. Results indicated good wetting and flow with no braze joint porosity. A photomicrograph of a section through typical braze joints is shown in Figure 60.

Three additional specimens were brazed using the previously discussed cooling jackets. Results generally indicated satisfactory brazing. When additional filler alloy was added to areas showing a relative lack of alloy (on the sides), localized plugging of the pin fins along the edges occurred.

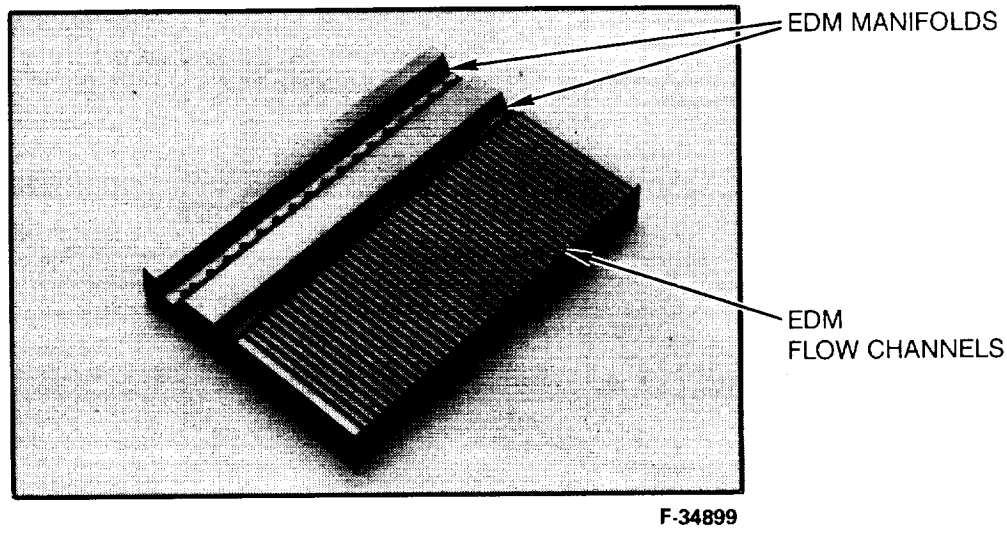

Figure 57. Inconel 718 Strut Leading Edge
Support Structure (Upper Half)

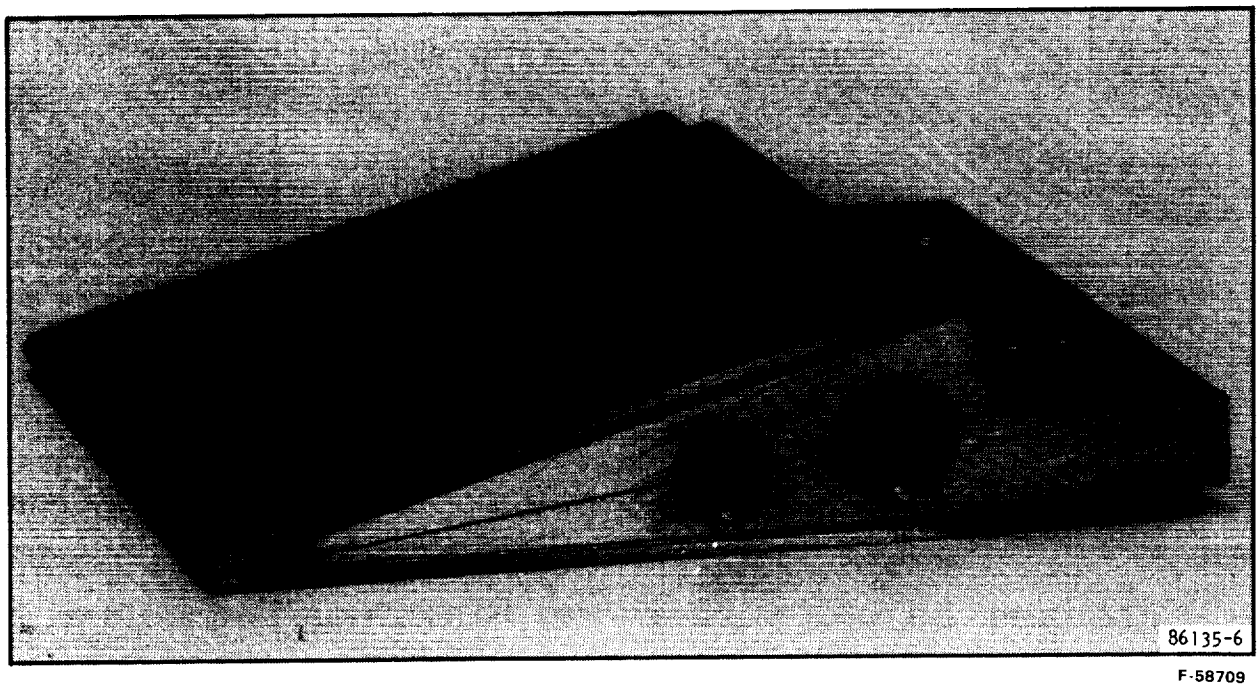

Figure 58. Dry Assembly of Strut Leading Edge Test Specimen

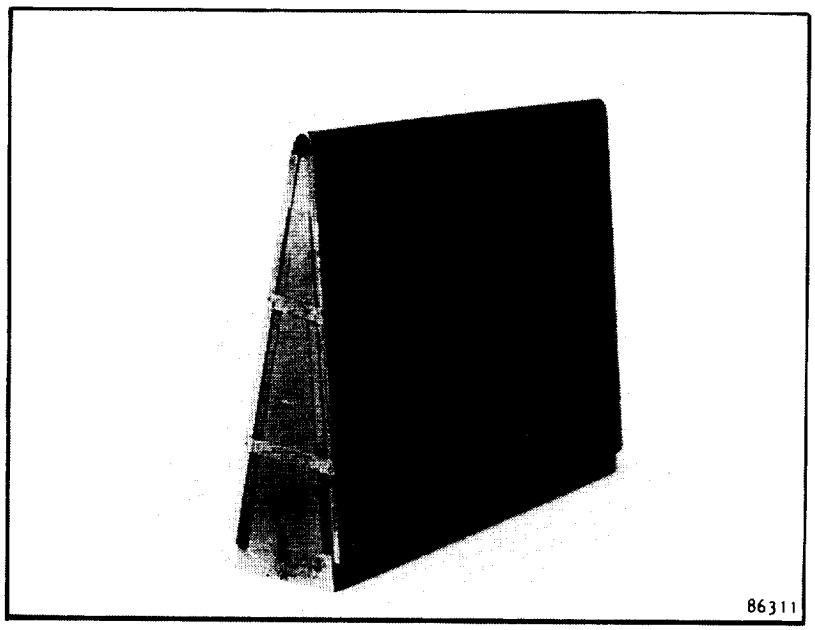

F-60403

Figure 59. Brazed Strut Leading-Edge Test Specimen (3 in. Long)

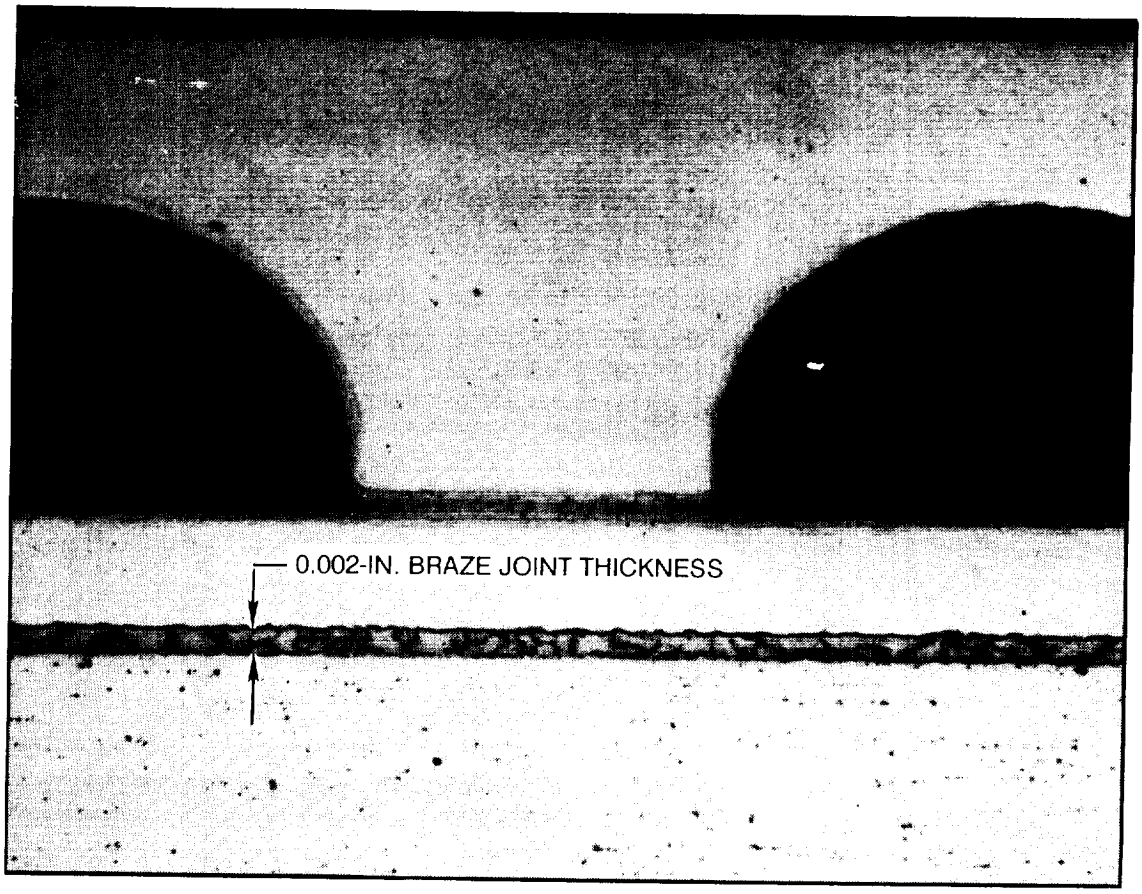

F-36733

Figure 60. A Section Through the Strut Leading Edge Braze Specimen

The fourth specimen had manifolds added, as provided by the original design, to permit pressure testing.* Figure 61 shows the brazed assembly. The specimen was successfully pressure tested to 1500 psig and holographically examined in increments to 1250 psig. No joint voids were noted. Holograms at 1250 psig are shown in Figure 62.

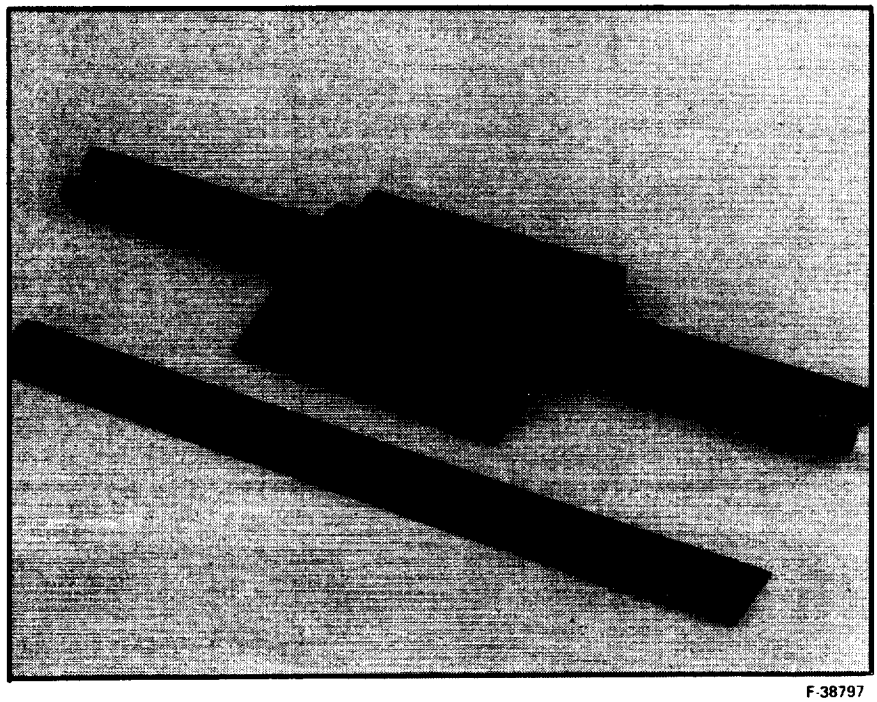

Figure 61. Manifolded Strut Leading Edge Specimen

This satisfactorily concluded the activity on fabrication development under this task. The manufacturing processes and techniques for fabrication, assembly, and brazing were subsequently applied and further developed as part of the full-scale, partial- and full-length strut work.

4.3.2 Low cycle fatigue testing. – Initial plans called for laser beam heating, using an existing numerically controlled cutting table, to cycle the leading edge tip at fluxes that induce design temperature differences at design temperatures. This method of heating proved

*Originally, the leading edge specimen had been designed to serve a dual purpose: (1) to develop and verify fabrication techniques, and (2) to evaluate low-cycle-fatigue (LCF) life of the Nickel 201 leading edge using a high-intensity laser beam. The test plan was subsequently revised and new Nickel 201 specimens were fabricated for LCF testing using electrical resistance heating. Because of this initial testing requirement, inlet and outlet manifolding were provided.

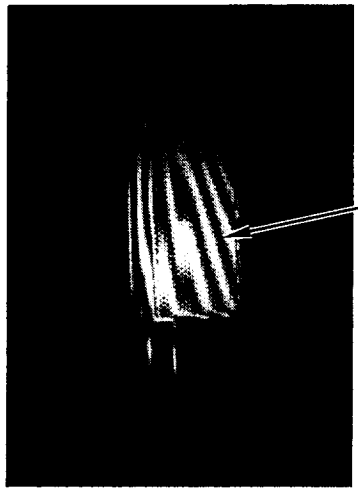

a. SIDE 1 AT 1250 PSIG

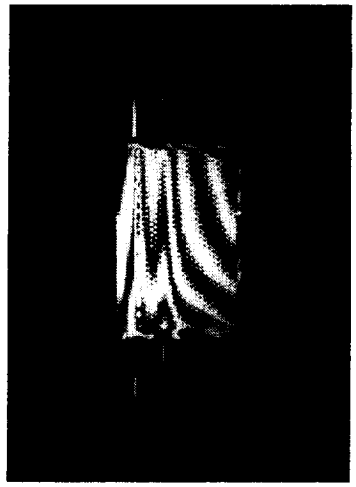

b. SIDE 2 AT 1250 PSIG

F-39477

Figure 62. Leading-Edge Assembly Holograms (No Braze Voids)

impractical. Heating control was difficult, and the intended temperature levels could not be maintained consistently, nor could the required steady-state distributions be obtained.

Several alternate heating techniques were evaluated, including wind tunnel, focused quartz lamp, rastered electron beam, acetylene-oxygen or hydrogen-oxygen torch, and electrical resistance. Electrical resistance heating was selected as the simplest and most practical. Wind tunnel testing would require cycling the facility over a thousand times and was rejected for that reason. Focused quartz lamp and torch heating do not produce the desired heat fluxes. Focused quartz lamp heating, however, was considered a viable backup because it can impose heat loads on the test specimens that are adequate for low cycle fatigue testing. Electron beam heating can produce the desired heat fluxes, but must be operated in a vacuum chamber, which severely limits testing flexibility.

The most important consideration in the leading edge test is the generation of representative thermally induced strains at leading edge operating conditions. The strut leading edge experiences high, localized aerodynamic heating during operation. The most intense heating occurs in a narrow band that extends along the length of the leading edge. Thermal expansion of the leading edge is restrained by the adjacent Nickel 201 sheet material, and the support structure. Cyclic operation with this restraint condition results in a thermally induced strain cycle that can include both plastic and creep damage components.

Two-dimensional finite element computer models of a transverse section and a longitudinal portion of the leading edge were used to determine the stresses and displacements that result from pressure and thermal loads. The temperature distribution for the center strut, instead of the side strut, was used for this modelling because the center strut is the more critical of the two with respect to LCF life. The center strut leading edge is subjected to higher heat fluxes and, consequently, higher face sheet temperatures (1100°F vs 580°F for the side strut leading edge). Elastic analysis results showed that the longitudinal compressive stress is dominant for maximum leading edge temperatures above 1000°F. Cross-sectional temperature differences of less than 200°F have a very small effect on stress (and total strain). The maximum longitudinal stress was obtained for any heated length greater than 0.5 in. Consequently, any heating pattern of greater length will give the required stress. A 1.0-in. heated length, located centrally with respect to the 3.0-in. specimen length, was used.

At 1400°F, short-time creep due to thermal loading is also a major factor in determining the leading-edge life. Stress relaxation times were calculated for three strut leading edge test temperatures and are listed in Table 14. These temperatures cover the expected operational range. Pressure-induced tensile and bending stresses are small in comparison with the thermal stresses. Therefore, constant pressure can be used in this type of test, with temperature cycling only.

TABLE 14

LEADING-EDGE STAGNATION LINE
STRESS RELAXATION TIMES

		Stress (psi) After		
Test Temperature, °F	*Initial Stress, psi	1 min	6 min	60 min
1000	12,100	12,000	11,900	10,700
1200	10,200	9,900	9,000	5,900
1400	7,000	4,500	2,600	1,100

*Initial stress = Yield strength at temperature

TABLE 15

LEADING EDGE LCF TESTING

Test Temperature, °F	Test Pressure, psi	Number of Test Points	Heated Length Per Test, in.	Hold Time, min	Estimated Cycles to Fracture
1000	1000	2	1	6	440
1200	1000	2	1	6	300
1400	1000	2	1	6	220

Table 15 gives the expected LCF life for the leading edge, based on results of the reverse bending fatigue tests performed on Ni-201 at 1400°F (ref. 5), at the three test temperatures. A 6-min hold time was selected to obtain significant stress relaxation at the higher temperatures. The analysis for thermal cycling from ambient to elevated test temperatures with hold time predicted an LCF life that was consistent with the life predictions obtained by extrapolating reverse bending fatigue test data on Ni-201 at 1400°F (ref. 5). This close agreement supports the use of analytical techniques to evaluate structural performance of the engine at conditions that may differ from the specific and limited test conditions.

The following discussion documents experience with laser heating tests and presents test data for the electrical heating tests. Laser heating with the available equipment

proved to be unsatisfactory for this LCF testing. Instead, electrical resistance heating was used. The analysis results above also served as the basis for defining subsequent tests.

4.3.2.1 Laser heating tests: The parameters in Table 15 were used as a goal in setting up the tests. Gaseous nitrogen was selected as the coolant for the internal cooling passages. Small-scale calibration tests were run on nickel sheet material to determine the degree of beam focus required to produce the desired thermal loads. Water-cooled baffles were used to control beam coverage across the leading edge and to absorb beam spillage.

Several calibration test specimens, using 0.015-in. Ni-201 brazed to Inconel-718 support plates, were fabricated and instrumented with thermocouples (Figure 63). Figure 64 is a photograph of the test setup which shows the laser beam crosshead and the temperature recording equipment. During the calibration tests, the laser was operated at maximum power in order to obtain the desired 1400°F minimum surface temperature with the expanded beam diameters used to spread the heated zone. An optical radiometer was mounted on the laser crosshead to measure the surface temperature of the heated area.

Static crosshead tests were run using a raw laser beam, a focused beam, and a slightly defocused beam (approximately 3/4 in. below the focal point), with beam diameters of 0.15 to 0.50 in. The specified temperature of 1400°F was not recorded during any of the test runs. With an expanded beam diameter of approximately 0.28-in., the maximum surface temperature was 1000°F. At maximum power settings, however, the instability of beam power was unacceptable, because it resulted in relatively large fluctuations of the surface temperature (up to 100°F). The maximum power with stable operation gave a surface temperature of approximately 800°F. Higher surface temperatures were obtained when smaller beam diameters were used, but this resulted in a departure from the 0.50-in. heated length requirement.

Further tests were run using numerical control to provide programmed scanning with a more highly focused beam. The test specimen was fixtured 0.5 in. below the laser beam focal point. The rate of travel was varied manually to a maximum of 300 in./min. During this initial test series, no temperatures above 600°F were recorded. The test specimen was then placed at the laser beam focal point, and testing was resumed. At a mid-range power setting, a sudden temperature rise beyond 1600°F was indicated on the back surface of the test specimen. Examination of the specimen indicated that a 1-in.-long slit was burned through the part.

Additional calibration test specimens were prepared and tested to determine the laser beam power, distance from focal point, and the scanning rate required to induce the desired heat fluxes on the leading edge fatigue test specimens (Figure 44). Results of the calibration tests with repetitively scanned laser beam indicated that surface temperatures in excess of 1400°F can be obtained. The test length, however, was not heated to a constant and uniform temperature. Both temporal and spatial variations of several hundred degrees occurred over the beam raster length. Specifically: (1) At a given point along the laser beam traverse path, relatively large fluctuations of the surface temperature (approximately 200°F with the maximum rate of travel) were recorded. This was due to the heat

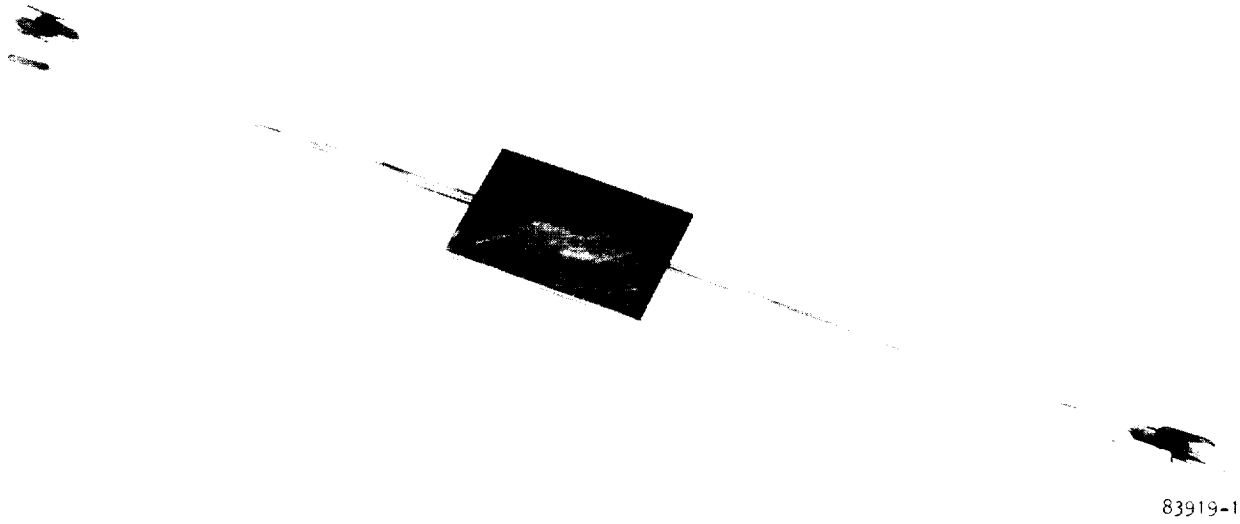

83919-1

a. Ni-201 SIDE

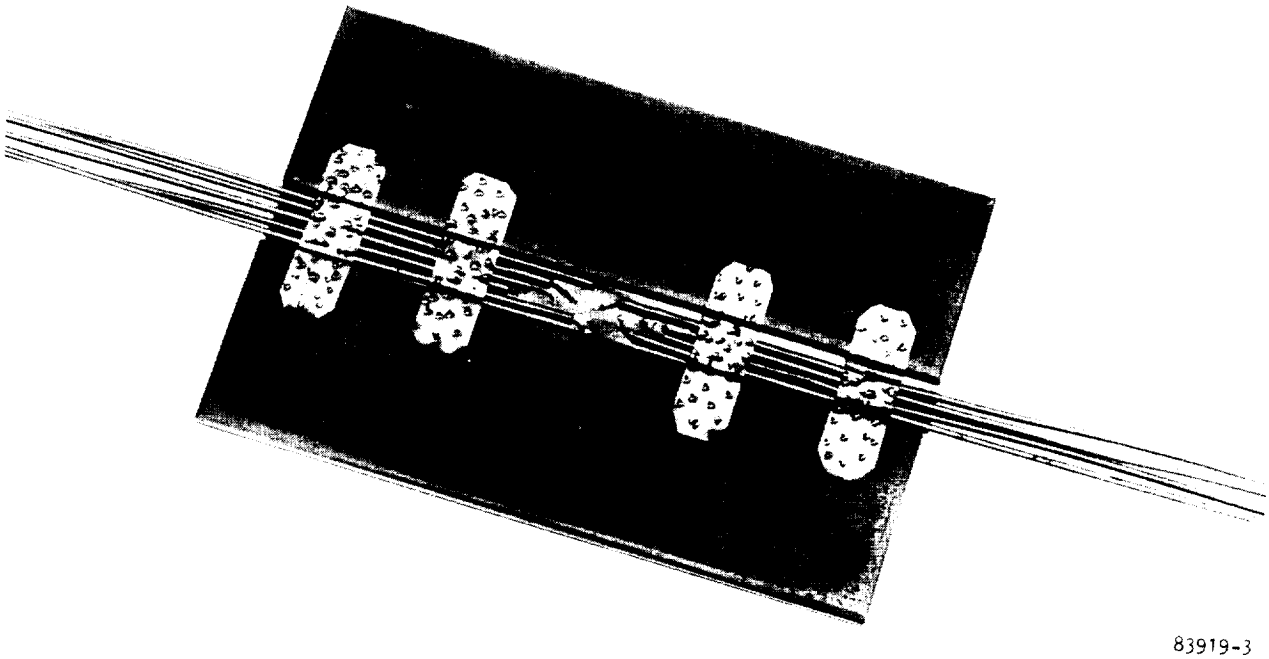

83919-3

b. INCO-718 SIDE

F-33327

Figure 63. Laser Calibration Test Specimen

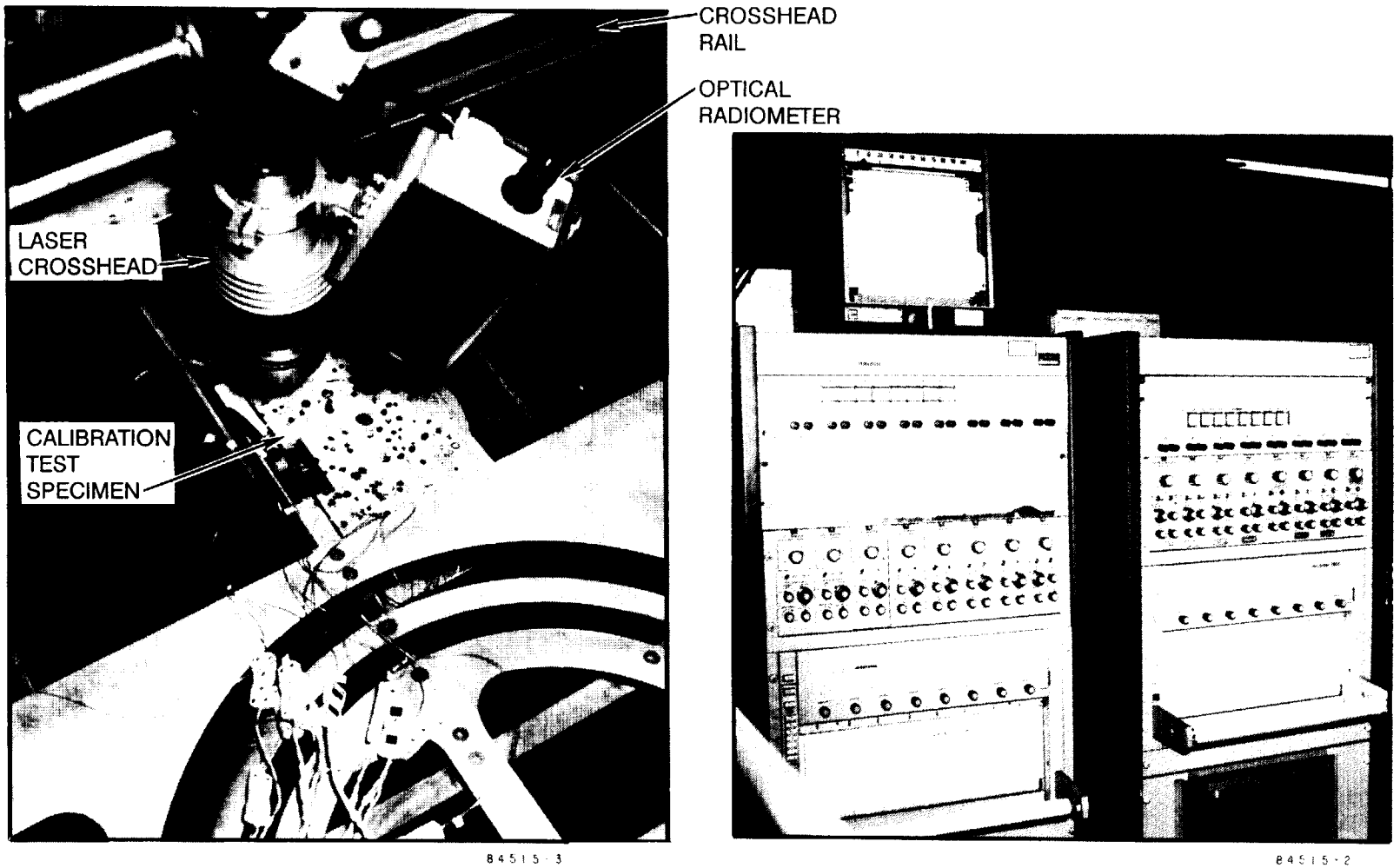

A. CALIBRATION TEST SETUP

B. TEMPERATURE RECORDING EQUIPMENT

F-33989

Figure 64. Laser Calibration Test Setup

loss from the heated area in the time interval required for the laser beam to repetitively impart energy to a point on the travel path; (2) The peak maximum temperature occurred at the ends of the heated length, where the beam momentarily stopped as the direction of travel was reversed. Masking that intercepts the laser beam at the ends of the travel was used to reduce this effect; (3) A constant energy input at a level required to obtain a 1400°F mean temperature resulted in a slowly rising mean temperature that preceded burnthrough. Examinations of the test pieces between runs have shown sites of incipient melting in the heated region when no excessive temperatures were recorded by the thermocouples. The surface temperature at the point of beam impingement was not directly measured by the thermocouples and was considerably hotter than the indicated value.

When a new calibration specimen was installed and tested at the same conditions as before, temperatures were 600° to 1000°F lower than before. This apparently is due to the effect of surface degradation with time. This degradation (i.e., slowly rising temperatures during testing) occurred even after specimens were preoxidized.

Given the interactions of beam power, distance from focal point, travel rate, and surface degradation, as seen in the above calibration tests, there did not appear to be a straightforward procedure to reliably produce a given minimum-maximum oscillation of the surface temperature with readily available equipment.

4.3.2.2 Electrical resistance heating: The critically heated portion of the leading edge is formed, 0.015-in.-thick sheet metal. A relatively simple and inexpensive test specimen was designed for the electrical-resistance heating tests, (see Figure 65). To simulate the actual fabrication processing experienced by a leading edge, the 0.015-in.-thick Nickel 201 sheet metal specimen was PCM'd to thickness and subjected to a pseudo-braze cycle—specifically, to a Palniro 1 cycle to simulate the pin-fin cooling jacket brazing and, following mill-cutting and forming into a 0.25-in. radius curve at the test section, to a Palniro 7 cycle to simulate brazing of the cooling jacket to the Inco-718 structure. The test specimen was then brazed between water-cooled, flat, copper heat sink plates using a low-temperature silver alloy. These copper plates also formed the electrical connections. A curved specimen was used to counter the buckling tendency of a flat sheet. Such buckling causes a nonrepresentative stress relaxation.

Both thermal and stress analyses were conducted to determine specimen size, predicted temperature distribution, and electrical heating current requirements. Results of the thermal analysis for a 0.50-in.-wide test section are presented in Figure 66 for two test specimen maximum temperatures as noted, and compared to calibration data points. The results indicate that a representative temperature distribution can be obtained using electrical resistance heating. For a given width of the test section, there is a minimum length of the narrow heated band required to obtain the maximum thermally induced strain. Increases in length of the band beyond this length do not change the maximum thermally induced strains. To limit the electrical heating current to approximately 1,000 amp, a minimum heated length of 1.5 in. was selected.

The test setup is shown in Figure 67. The test equipment consisted of a power supply (Sorenson dc power supply Model DCR20-1000), programmer (Data-Track

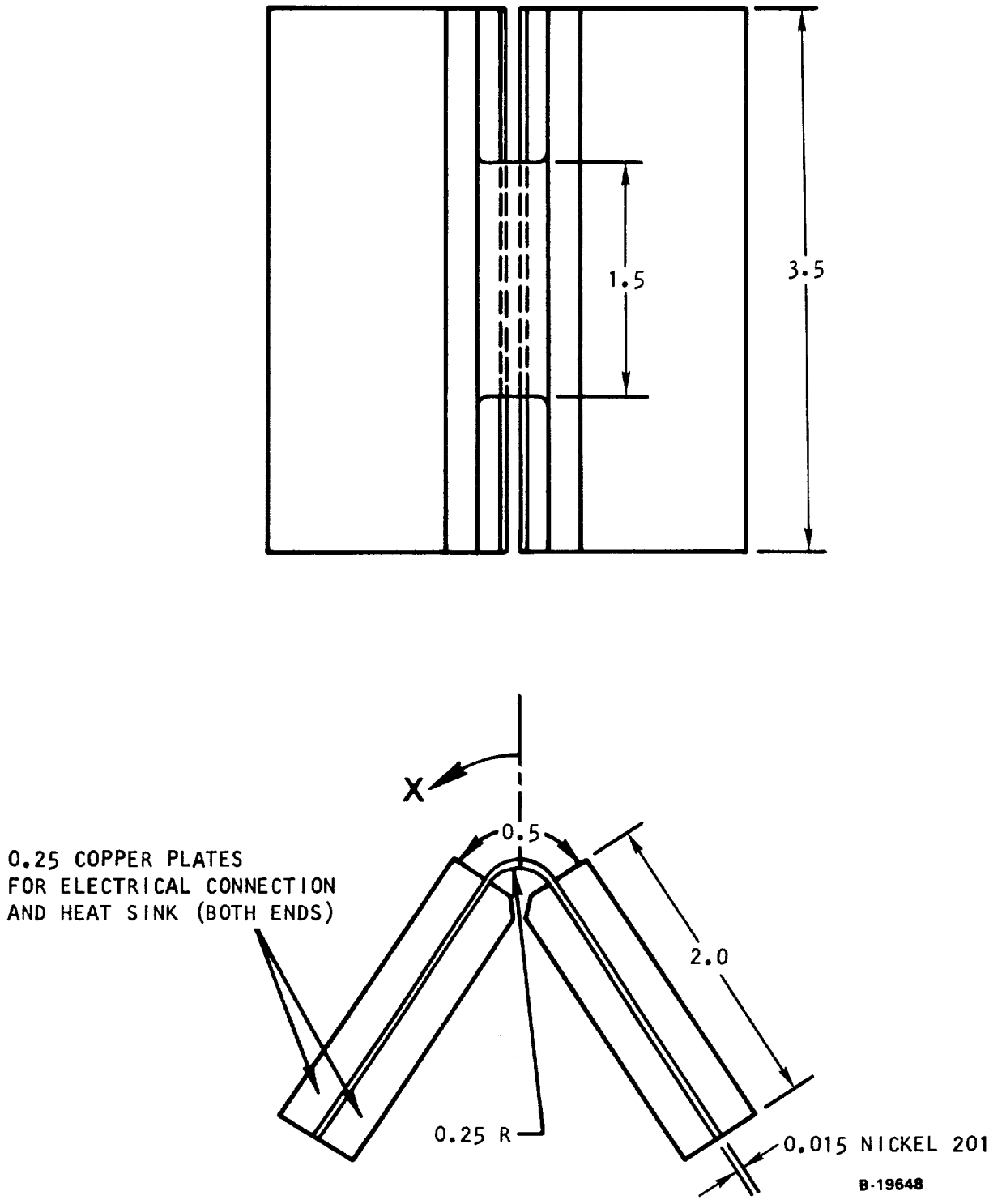

Figure 65. Electrical Resistance Heating Specimen for Combined Low Cycle Fatigue and Creep Testing

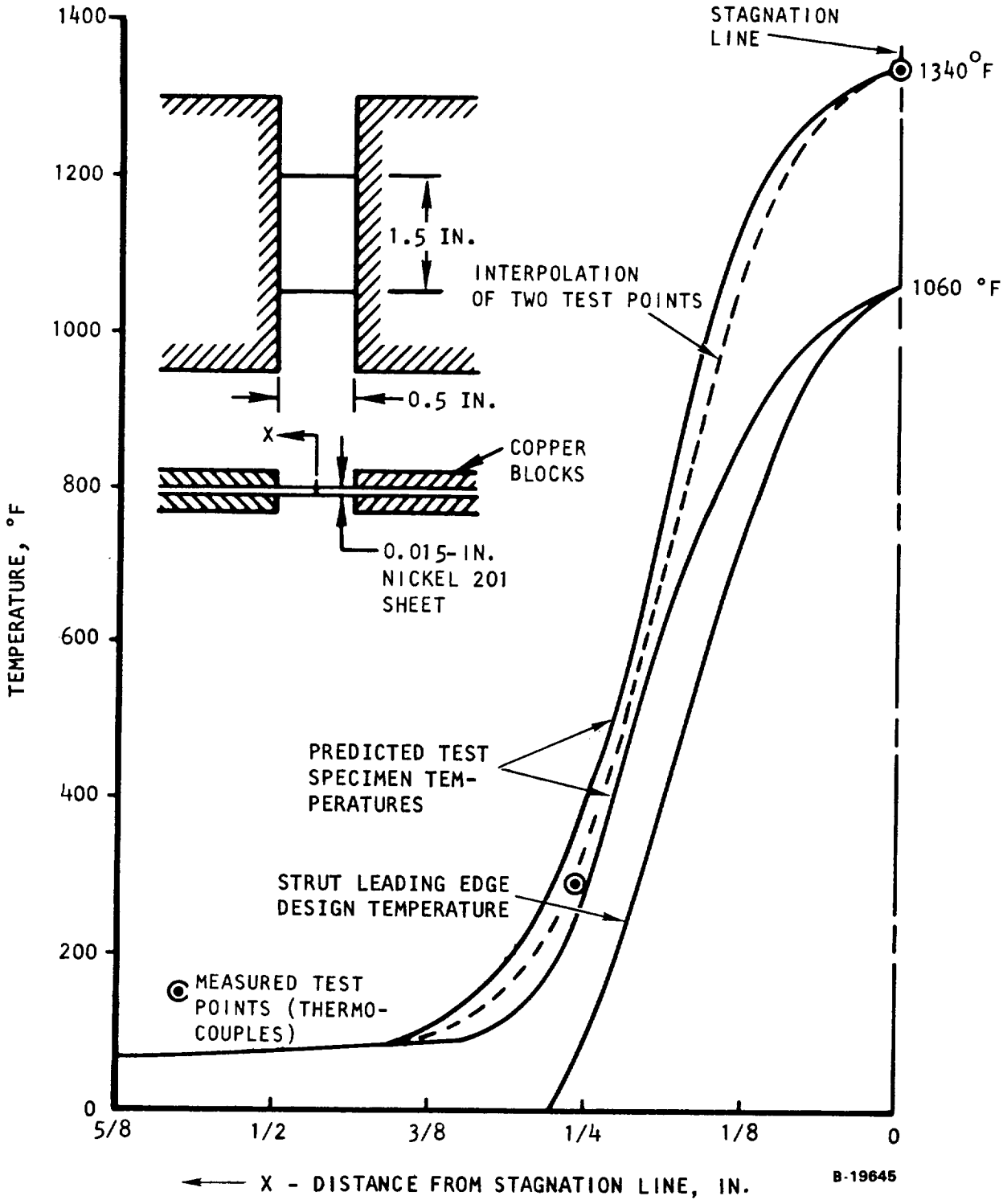

Figure 66. Strut Leading Edge LCF Test Specimen Temperature Distribution Using Electrical Resistance Heating

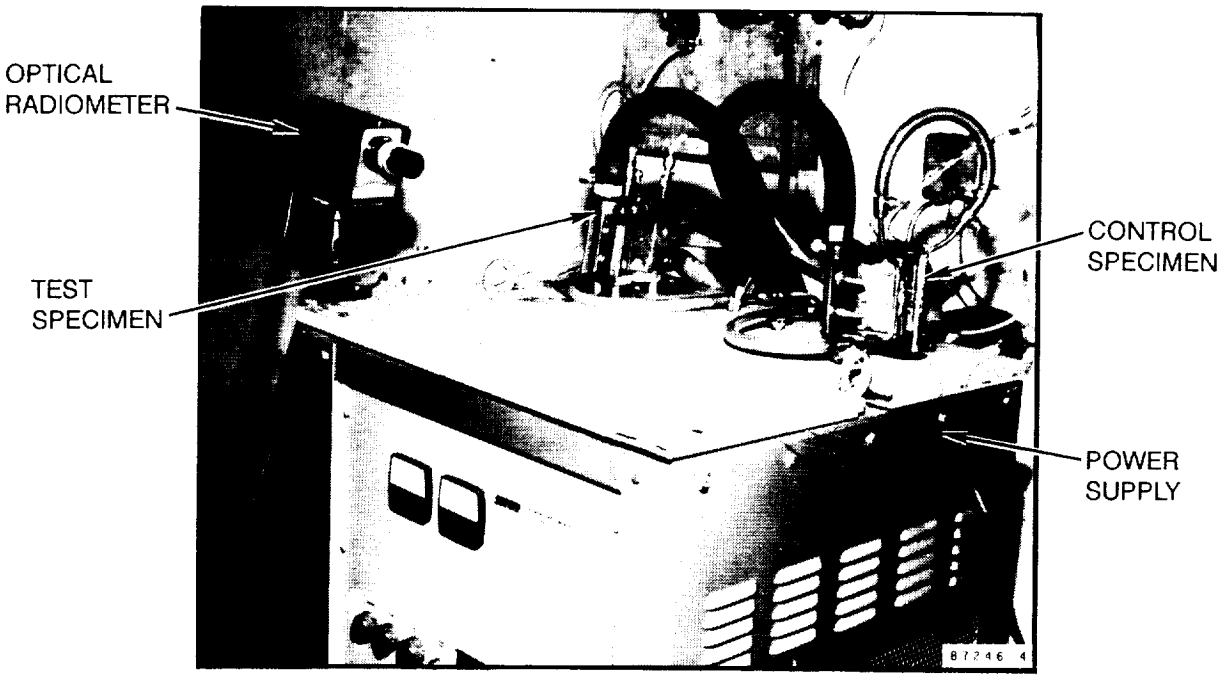

a. ELECTRICAL RESISTANCE HEATING TEST SETUP

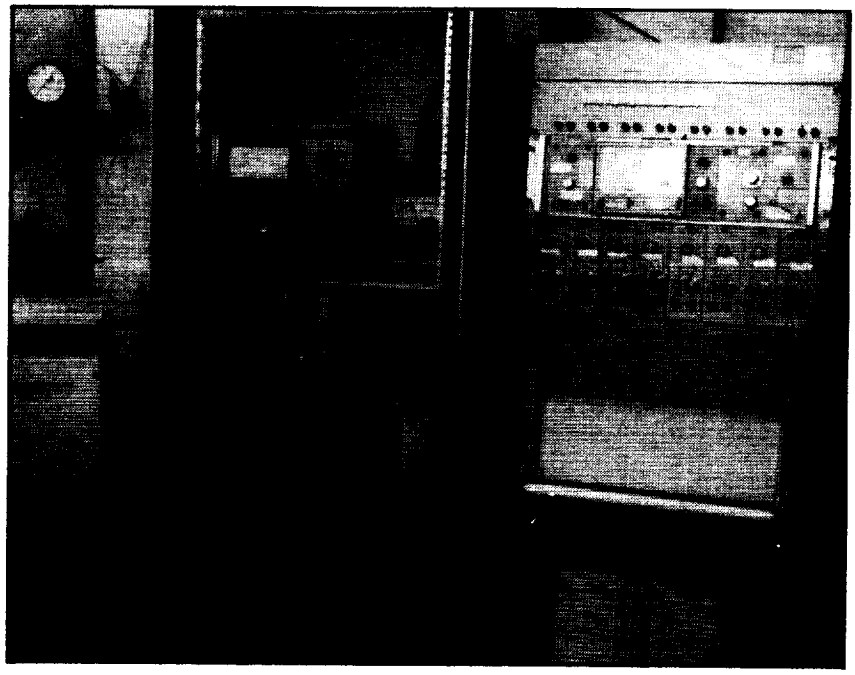

b. CONTROL (LEFT) AND TEMPERATURE RECORDING (RIGHT) EQUIPMENT

F-38060

Figure 67. Nickel 201 LCF Test Setup Using Electrical Resistance Heating

Model 5600), recorder (Gould Brush 2800, 8 channel), and an optical radiometer (Ircon Model 300T5H). A control specimen was installed in series with the test specimen and contained seven thermocouples for monitoring and controlling the test specimen temperature. Three thermocouples were on the stagnation line; the remaining four thermocouples were installed along the transition lines from the curved test section to the flat mounting sections, and midway between the centerline and the transition lines, to obtain a measure of the temperature distribution across the formed test section. Figure 68 shows the control specimen, and Figure 69, the test specimen. It was identical to the test specimen in configuration and processing. Both specimens have the basic features shown in Figure 65. Convective water cooling of the copper plates was used to provide the desired simulation of temperature gradient around an actual leading edge.

The optical radiometer was used to supplement thermocouple measurements and provide actual temperature readings of the test specimen. Thermocouples were not used on the test section to avoid damage to the material in the tested area. The programmer provided for the cyclic heating of the test section to the desired test temperature. The cycle consisted of heating the test pieces to test temperature in approximately 1 min, maintaining a constant test temperature for 6 min, followed by a 1-min cool-down to ambient temperature. The central stagnation line thermocouple was recorded to monitor and verify the test temperature.

Based on results of a calibration test, the estimated temperature distribution around the test section is shown in Figure 70 (see also Figure 66). For comparison, the anticipated temperature distribution in the face sheet outer fibers, around the leading edge of the center strut, is also presented. As may be seen, a close simulation of the leading edge temperature distribution and, therefore, the thermally-induced strain levels, can be obtained using electrical resistance heating.

During actual cooled operation of the leading edge, a temperature difference exists through the leading edge material thickness that is not simulated using isothermal test conditions. Results of elastic analysis, however, show that cross-sectional temperature differences have a relatively small effect on stress (and total strain). A constant temperature test at the face sheet outer wall temperature, therefore, provides a conservative estimate for the LCF capability of the Nickel 201 leading edge.

A calibration test cycle is shown in Figure 71. The test specimen was heated to 1390°F (channel 2) and maintained at temperature for 6 min. Water cooling of the copper heat sink plates adjacent to the test specimen test section maintained the nickel specimen edge sections at approximately 250°F (channels 1 and 3) to provide the desired temperature gradient across the 0.50-in.-wide test section. Following a 1-min cool-down period, the cycle was repeated.

A single test specimen was then run to conclude this activity. Figure 72 shows a typical test cycle. After 48 cycles, two ripples developed across the 0.25-in. radius test section. The number of ripples increased to three after 112 cycles. After 162 cycles, the start of a longitudinal crack was noted over the top ripple. After 214 cycles, testing was concluded because the crack propagation had resulted in a nonuniform heating pattern

ORIGINAL PAGE
BLACK AND WHITE PHOTOGRAPH

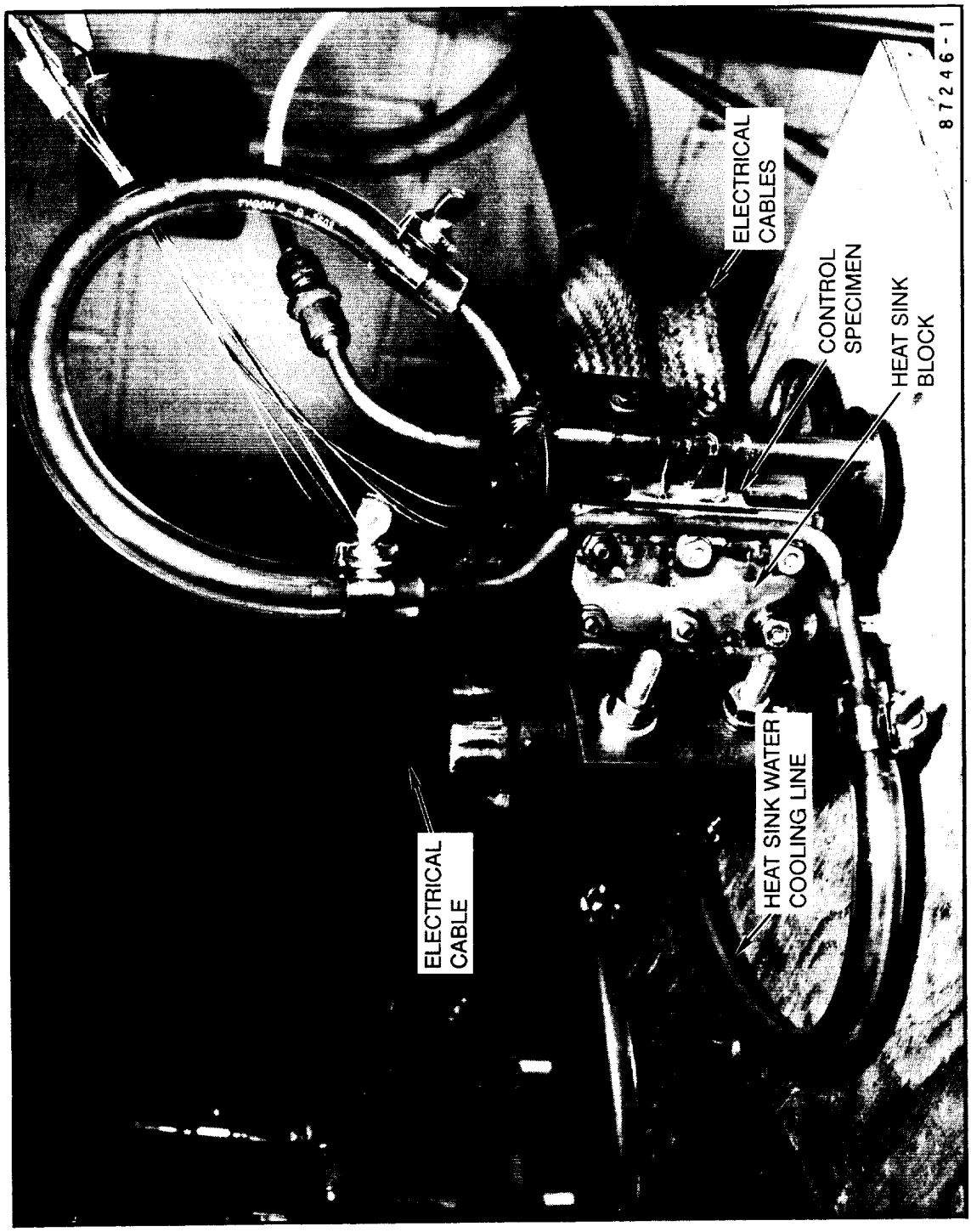

Figure 68. Control Specimen Instrumentation, Electrical Resistance Heating Test Setup

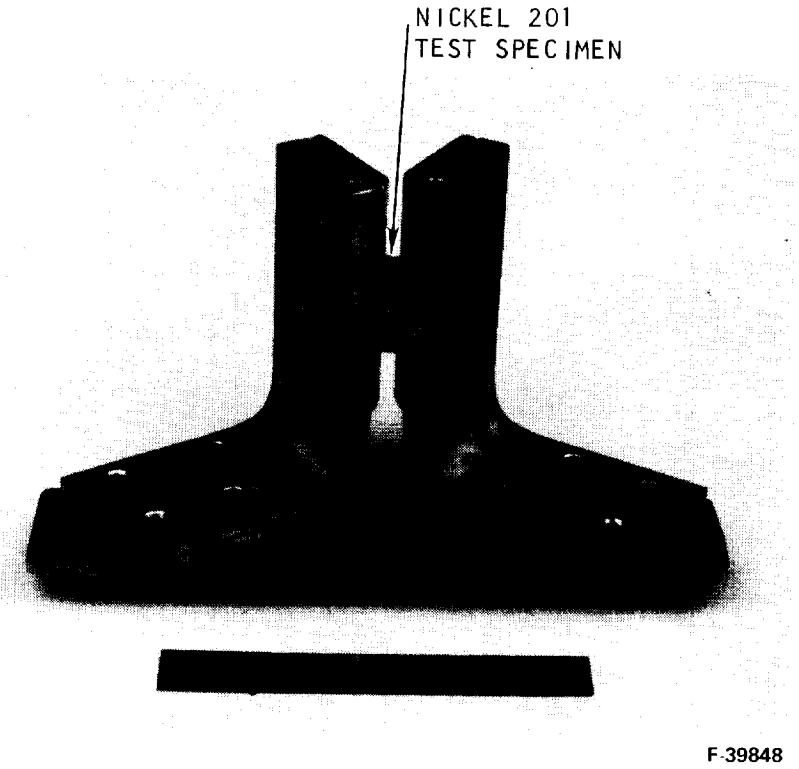

Figure 69. LCF Test Specimen, Electrical Resistance Heating

along the test section. A photograph of the test specimen after testing is presented in Figure 73.

LCF results were judged within the general design range, but are indicative only. The data are too limited for use as a design basis. Additionally, for future tests aimed at developing a statistical design basis, the specimen design would be reviewed. Flattening of the curved test section along the intensely heated band was noted after relatively few cycles, due to creep deformation. A tighter radius is required to resist flattening and thus prevent buckling of the test section. Since buckling is not expected in the actual leading edge (0.05-in. radius)*, this will provide more directly applicable design data. The important simulation parameters are temperature and temperature gradient and these are well modeled. If it is subsequently determined that buckling is a consideration, varying degrees of resistance to buckling can be obtained by adjusting the test specimen radius.

*Requires verification, but is consistent with experience on HRE, ref. 1.

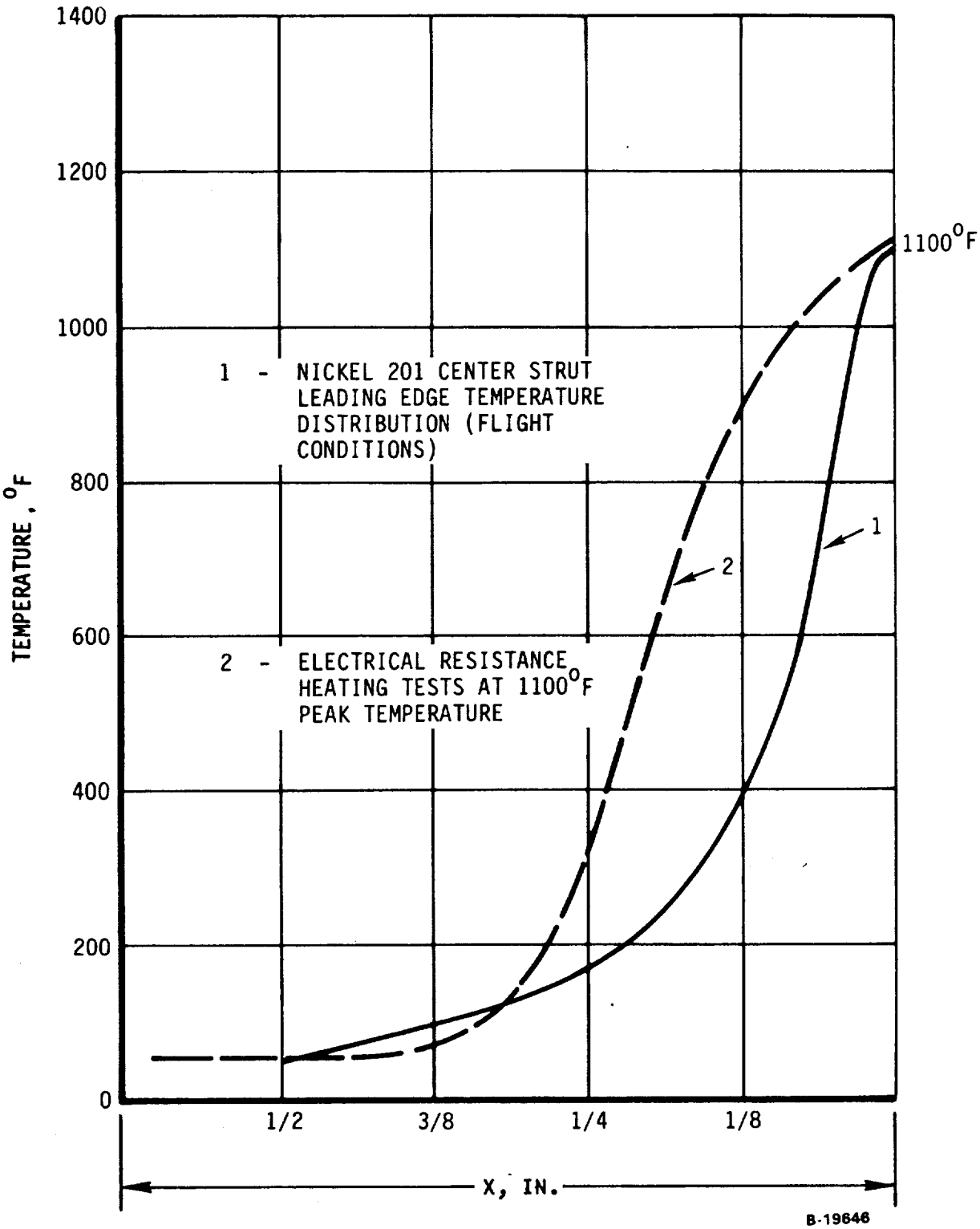

Figure 70. LCF Test Specimen Temperature Distribution Using Electrical Resistance Heating

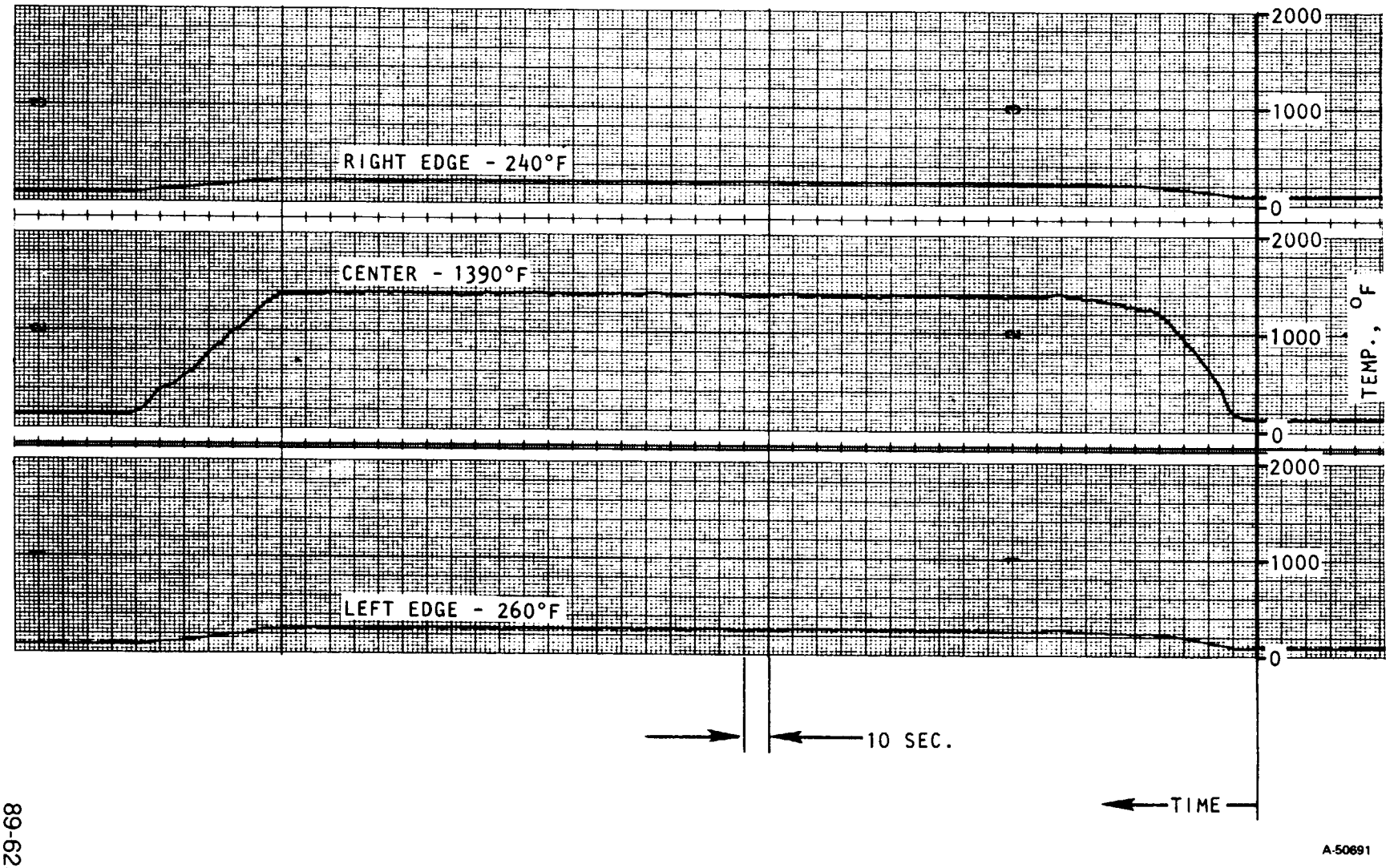

Figure 71. A Combined LCF and Creep Calibration Test Cycle Using Electrical Resistance Heating

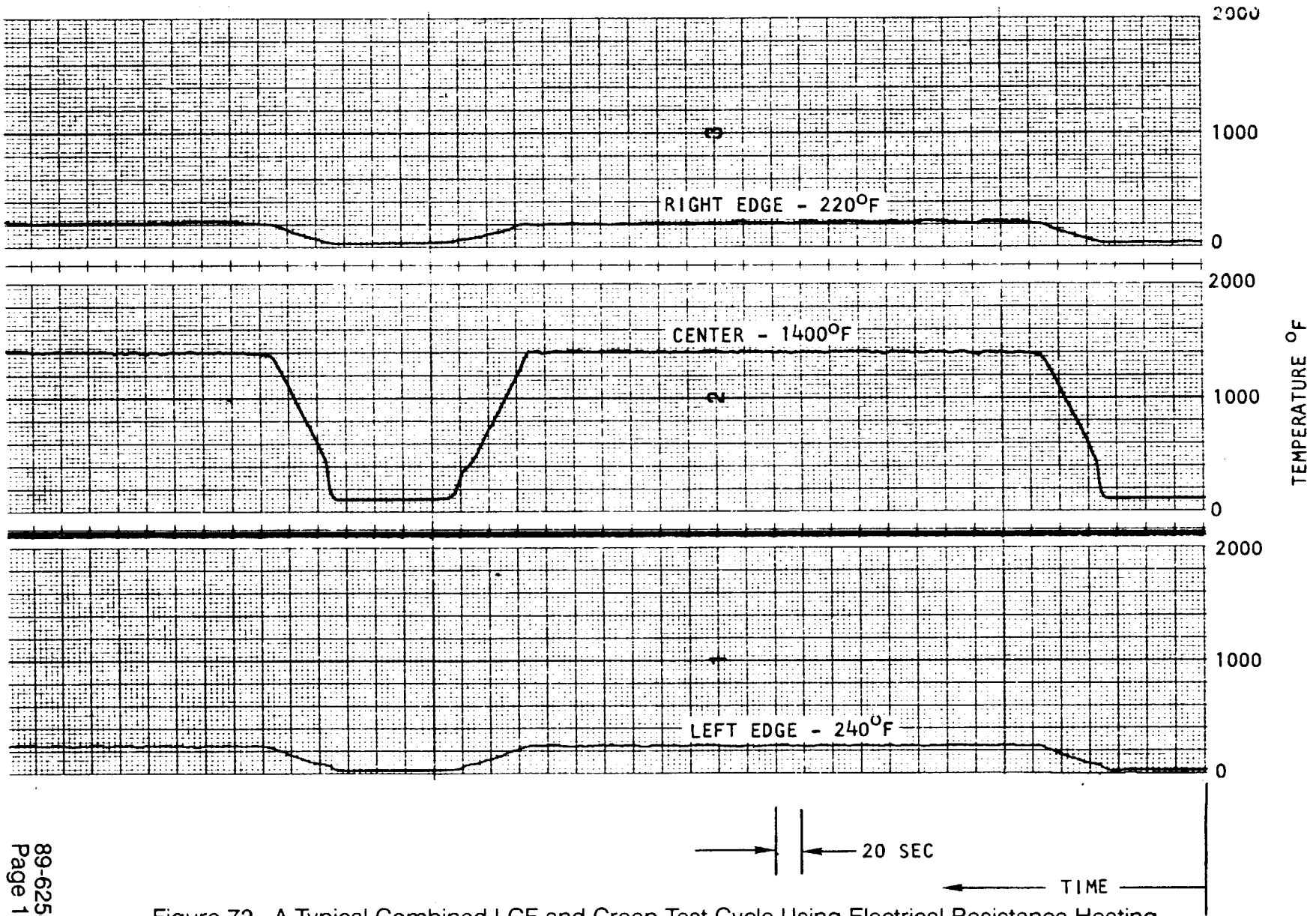

Figure 72. A Typical Combined LCF and Creep Test Cycle Using Electrical Resistance Heating

ORIGINAL PAGE
BLACK AND WHITE PHOTOGRAPH

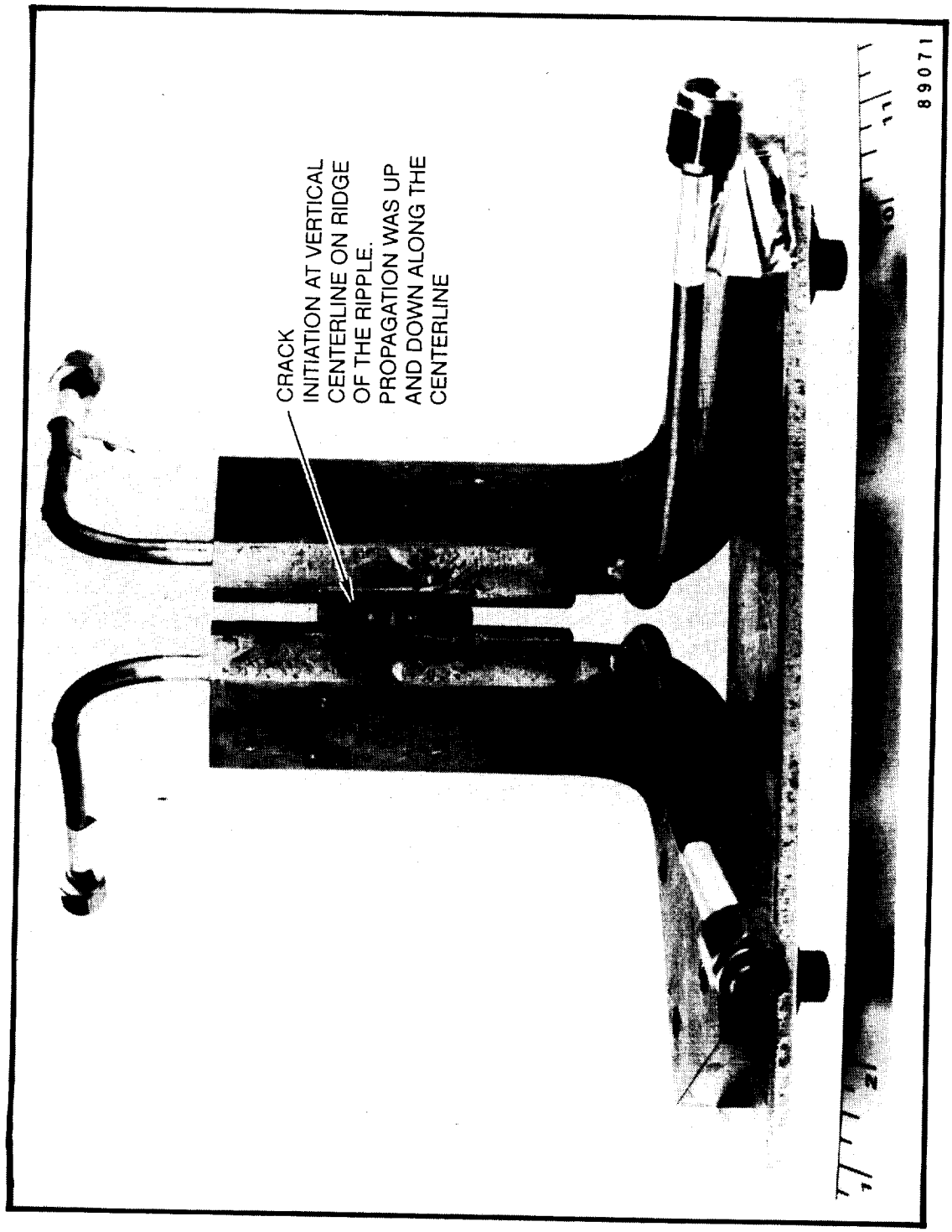

Figure 73. Nickel 201 Electrical Resistance Heating Test Specimen After 214 Combined LCF and Creep Cycles

4.4 Task 3 — Fabrication Investigations

A number of targeted, developmental evaluations resulted from experience in fabricating parts and assemblies of the partial and full-length struts. These were often in parallel with ongoing strut work. They are grouped here for convenience and continuity.

Three basic areas of concern emerged during fabrication of the two partial-length struts (see Section 5): (1) The cooling jacket pin-fin passages were becoming plugged with braze alloy when the jacket was brazed to the support structure, (2) Voids were observed between the cooling jacket and the support structure (also second stage), and (3) The support structure strength of the beam-to-wall braze joints in the support structure were lower than anticipated (first-stage braze, Palniro 1).

The initial study plan is shown in Figure 74. It varies a number of parameters during the different brazing stages. An overview of the baseline brazing parameters, established by experience with the partial-length struts or the development work in ref. 5, is presented in Table 16. Also noted are the observed deficiencies which led to some of the investigations. For Item 5, quantities and placement of alloy were varied in an examination of the beam-to-wall joints. Joint strength was tested and the braze void area examined. A parallel effort for Item 3 in the investigation dealt with eliminating plugging in the cooling jacket passage during the brazing of the jacket to the strut body, as well as finding means for eliminating the jacket-to-body braze voids. The parameters that were varied in making the braze included alloy thickness, stopoff application and oxidation, braze temperature, pressure loading, and surface roughness.

The overlap joints (Item 2) of the front and aft cooling jackets were also simulated in order to avoid plugging. A cross section of the strut body (Item 5) was exposed to one atmosphere of pressure during a simulated second-stage braze cycle at 1935°F to determine the wall deflections. In addition, for Item 6, sections of the leading and trailing edges from the second PL strut were capped and pressurized to rupture to determine the structural effects of the leading and trailing edge holes in these parts.

The results of the investigations are individually summarized in the following paragraphs. Additional investigations, stemming, in part, from the results of the initial evaluations and, in part, from ongoing manufacturing experience are included with the appropriate items. Outlines of the specific issues that were being addressed by the investigations are included in Tables 17, 18, 19, and 20.

NO.	TEST ITEM	FOIL THICKNESS	NUMBER OF TEST SPECIMENS									NOTES
			STOP-OFF				IN BRAZE HOT SIZE	STAGED BRAZE LOADING	BRAZE TEMP	SURFACE ROUGH-NESS	PRESSURE TEST	
			SLURRY (PAINT)	OXIDATION PRE	OXIDATION POST	NONE						
1	FLAT PANEL (JACKET BRAZE)											
	(a) 1 IN. x 3 IN. (NEW PIN FIN)	.001 IN.	–	4	–	–	–		OK	–	–	
	(b) 1 IN. x 3 IN. (OLD PIN FIN)	.001 IN.	–	3	–	2	–		OK	–	–	
2	JACKET CROSSOVER JOINT	OK	–	2	2	2	–		SELECT	–	–	
3	STRUT END (L.E. AND T.E. BRAZE)											
	(b) 1 IN. x 3 IN. (EA END) (OLD FIN)	.001 EACH	–	4	–	4	–		OK	–	–	.0007 NOT OK OK VOID PLUGGED .0005 .001
	(c) 1 IN. x 3 IN. (EA END) (NEW FIN)		–	8	–	–	4		2	2	–	
	(d) 2 IN. x 4 IN. (EA END) (OLD FIN)		–	–	–	4	–		OK	–	–	
	(e) NO. 1 P.L. STRUT) (OLD FIN)		–	8	–	–	FROM 'STOP-OFF'		OK	OK	–	
4	NOT ASSIGNED	–	–	–	–	–	–		–	–	–	
5	BEAM-TO-WALL BRAZE JOINTS*						(HIGH TEMP LOAD)					
	(a) SUPPLEMENTAL FILLER (WIRE/FOIL)(OLD BEAM)	–		–	–	–	2x (USE NO. 2 STRUT)		–	–	–	
	(b) BEAM SHAPES (NEW BEAM)	–	–	–	–	–	OK (FROM ABOVE)		–	–	–	
6	DESIGN ISSUES											
	(1) L.E. AND T.E. HOLE STRESSES	–	–	–	–	–	–		–	–	2 (1 EA)	
	(2) INJECTION TUBE PENETRATION (INTERNAL LEAKAGES)	–	–	–	–	–	–		–	–	–	STRESS ANALYSIS LEAK ESTIMATE

IW-05077

Figure 74. Manufacturing Investigation Plan

TABLE 16

BASELINE BRAZING PARAMETERS*

Jacket Braze	Support Structure Braze	Jacket-to-Support Structure Braze
• Palniro 1 foil thickness = 0.001 in. • No braze filler slurry • One atmosphere load at braze temperature • Selected for investigation because deficiences were correctable – No plugging – Good filleting • Investigate to correct isolated voids	• Palniro 1 foil thickness = 0.001 in. • Braze filler slurry added • 10-psi braze load • Selected for investigation because deficiencies were correctable – Braze voids in beam joints – Undesired brazing of thermal buffers to support structure • Investigate to correct braze voids • Use alternate assembly sequence to correct buffer brazing	• Palniro 7 foil thickness = 0.001 in. • Braze slurry added • 10-psi braze load • Selected for investigation because deficiencies were correctable – Good strength in no-void joints – Braze voids in jacket-support structure joints – Plugging of previously brazed cooling jacket pin-fin joints

*Columns are independent and read vertically only.

TABLE 17 PIN-FIN PASSAGE PLUGGING	
Test Item 1	• Prevent braze alloy migration into pin-fins at the leading and trailing edges, crossover joints, and top and bottom edges – Oxidation of panel before braze – Chrome plating/oxidation before braze • Determine plugging potential during cooling jacket braze – Braze samples with 0.001-in. Palniro-1 filler alloy – Braze samples with 0.0015-in. Palniro-1 filler alloy
Test Item 2	• Prevent crossover joint plugging at jacket/support structure braze – Reproduce plugging using sample with braze alloy foil and slurry
Test Item 3	• Prevent pin-fin plugging at jacket/support structure braze – Braze samples with braze foil only – Braze samples with braze foil and slurry

TABLE 18 VOID REDUCTION IN JACKET/SUPPORT STRUCTURE BRAZEMENT
Test Item 3
• Hot isostatic pressing (HIP) of sample with voids • Braze pressure loading increase from 10 psi to 15 psi (full vacuum) – Braze end section wedge samples – Braze samples to cleaned-up partial length strut areas and evaluate holographically • Add grooves on back of cooling jacket – Braze flat sample without grooves – Braze flat sample with grooves – Braze equivalent stiffness (to cooling jacket) samples to wedge samples

TABLE 19 STRENGTH OF BEAM-TO-WALL BRAZEMENT
Test Item 5
• Verify braze joint strength – Simulate beam-to-wall joint with samples – Tensile test samples • Reduce braze joint porosity after brazing – Hot isostatic pressing (HIP) of sample • Improve beam-to-wall joint design at 45-deg fuel injector tube penetration

TABLE 20 DESIGN ISSUES
Test Item 6
• Determine structural effect of coolant holes on support structure – Burst test leading edge section of partial length strut 2 – Burst test trailing edge section of partial length strut 2 • Improve braze joint design of seal for fuel-injector tube penetration of beams – Use sleeve and washer design

4.4.1 Flat panel (test Item 1). – To inhibit braze alloy flow into the pin-fins during the second stage of brazing, various methods of oxidation of the nickel pin-fin cooling jacket were tested. First, flat plates of Nickel 201 were oxidized in air at from 1000° to 1800°F. All had a small amount of Palniro 1 braze alloy placed on the surface and were exposed to the 2070°F braze cycle. In all cases, the braze alloy flowed freely over the surface. This result was further verified by brazing a number of pin-fin specimens. Figure 75 shows photomicrographs of the resulting pin-fin braze joints. Wetting by the filler is evident throughout. Subsequently, sections of nickel sheet stock were chrome-plated to a 25- to 50-μ in. thickness and then oxidized at 1500°F for 30 min. They were similarly brazed at 2070°F. Some increase in resistance to braze alloy flow was observed. Figure 76 shows results from one of the braze panels. They are typical of the three panels that were brazed. It was concluded that neither method would be beneficial or would be used on the full-length strut.

Samples of the two pin-fin geometries (center and side passage configurations) were then repeatedly brazed without any plugging at the first level of brazing (jacket assembly) using 0.001-in.-thick Palniro 1 braze alloy. Radiographs showed some plugging

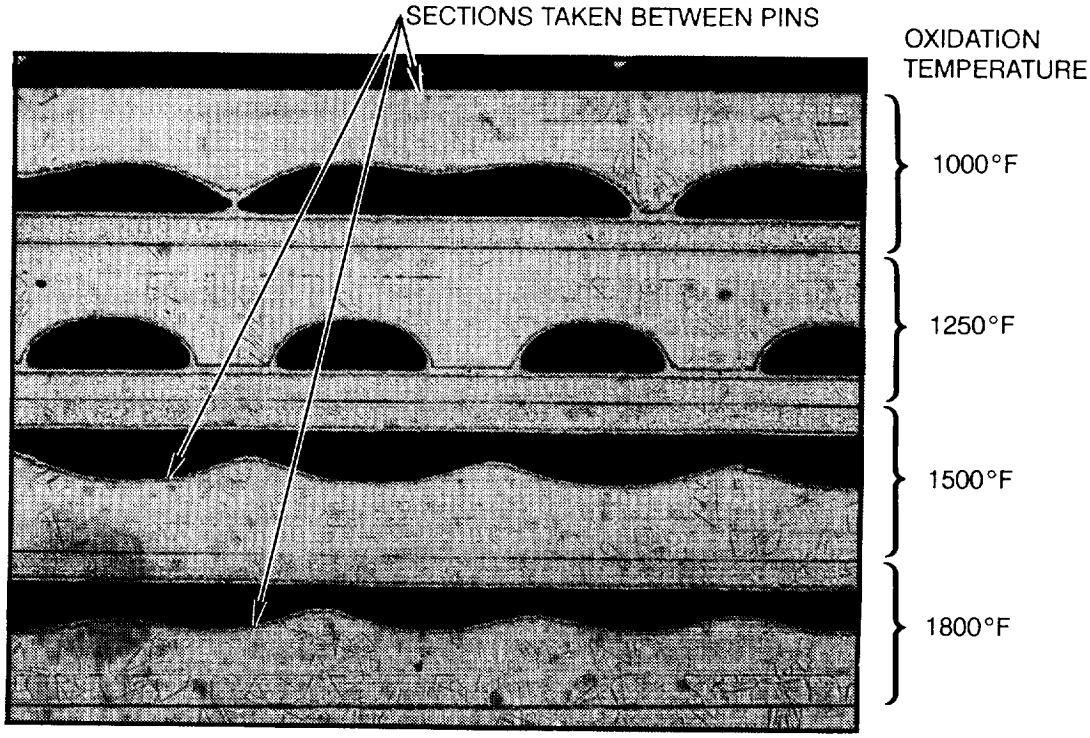

Figure 75. Braze Alloy Flow in Four Preoxidized Pin-Fin Cooling Jacket Coupons

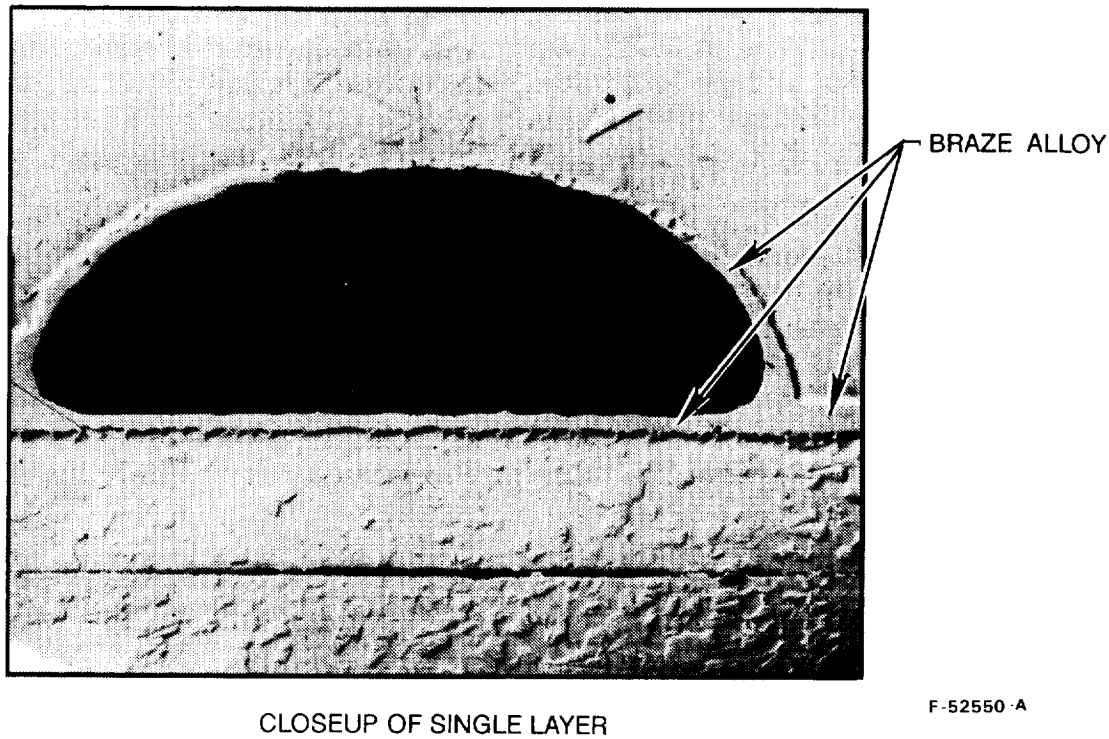

Figure 76. Braze Alloy Flow in Chrome-Plated Preoxidized Pin-Fin Cooling Jacket Coupon

adjacent to the flow dividers when they were brazed with 0.015-in.-thick braze alloy. As a result, the 0.001-in. Palniro 1 braze alloy was used for the full-length strut.

4.4.2 Jacket crossover joint (test Item 2). – In an attempt to reproduce the plugging that was observed in the second partial-length strut, a sample was fabricated that simulated the basic geometry of the crossover joint between the forward and aft jackets. Brazing was with Palniro 7 braze slurry and 0.001-in.-thick foil. Figure 77 includes a photo of the sample and an X-ray of the completed part. The test specimen configuration incorporates a solid coolant passage end piece, as used in the full-length strut. This was judged important in the simulation because it represents a potential and relatively large source of excess filler alloy that can contribute to plugging. Little accumulation of braze alloy was observed in this area of the brazed sample. Since the alloy accumulation in the second partial-length strut was minimal, it was decided to discontinue this investigation and to concentrate on eliminating the excess alloy conditions observed at the leading and trailing edges. The full-length jacket crossover joint was brazed using only the 0.001-in. braze foil. Furthermore, the test Item 3 evaluation below showed that at assembly supplementary braze slurry should not be added to the support structure with Palniro 7 filler alloy because of the potential for pin-fin plugging. Therefore, as a precaution, no supplementary braze slurry was added to this joint when the full-length jacket was brazed.

4.4.3 Strut assembly brazement (test Item 3). – To determine the cause of the pin-fin plugging at the second stage of brazing, several cooling jacket coupons were brazed to Inconel 718 wedges. No plugging was observed with the use of only braze foil. Figure 78 is a comparison of the two types of wedge samples. Subsequent braze tests and X-ray examination showed that only samples that used braze slurry to supplement the foil demonstrated any plugging of the cooling jacket (slurry had been used with PL2). The full-length strut assembly brazement, therefore, should use only the 0.001-in. Palniro 7 braze foil without the added braze slurry.

As part of this item, hot isostatic pressing (HIP) was performed on a section of the second partial-length strut as a possible means of reducing the braze void area between the cooling jacket and the strut body. The strut section was subjected to 15,000 psi at 950°C for 1 hr. Ultrasonic and holographic examination showed no reduction in void area (Figure 79). As a result, HIP is not considered an available option for use in full-length strut repair.

In another approach to eliminating the braze voids between the jacket and the support structure, the pressure loading was increased to 15 psi during the brazing of the coupons to the wedges. This additional loading was applied periodically during the high-temperature portion of the braze cycle in order to creep-form the nickel cooling jacket to the shape of the support structure. Sectioning of this wedge sample confirmed the presence of braze gaps up to 0.003-in., Figure 80, but typically the gaps were from 0.001 to 0.002 in. In general, the gaps observed in this sample were smaller than those on the second partial-length strut.

A third approach to eliminating the braze voids entailed brazing the leading and trailing edge jacket sections to the first partial-length strut after the original jacket was removed

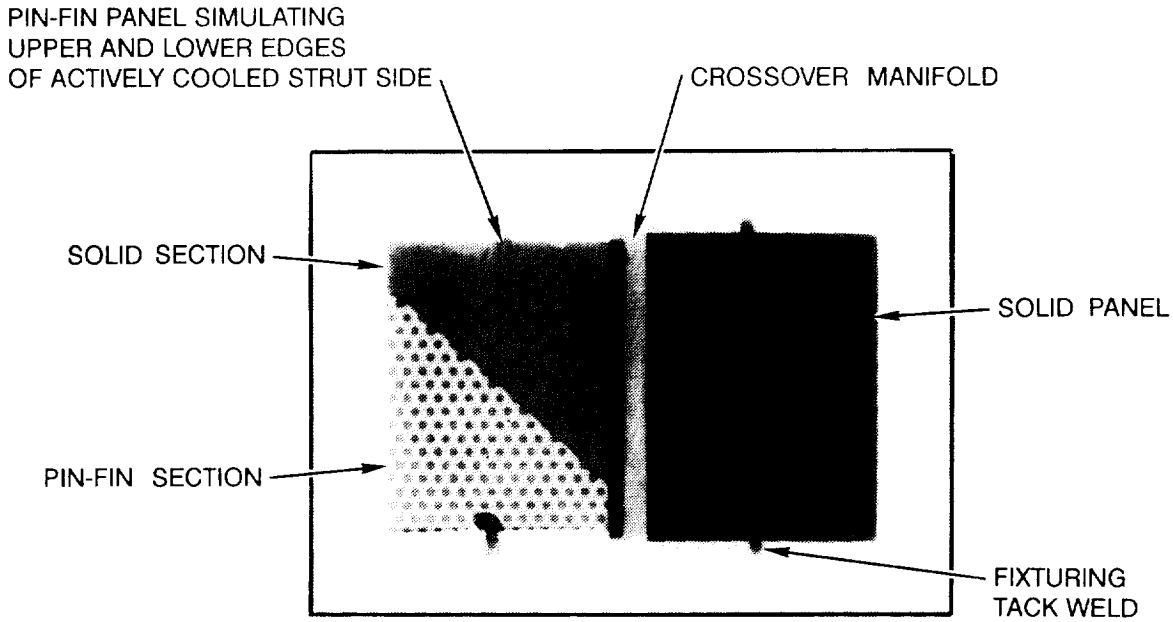

X-RAY OF TEST SAMPLE

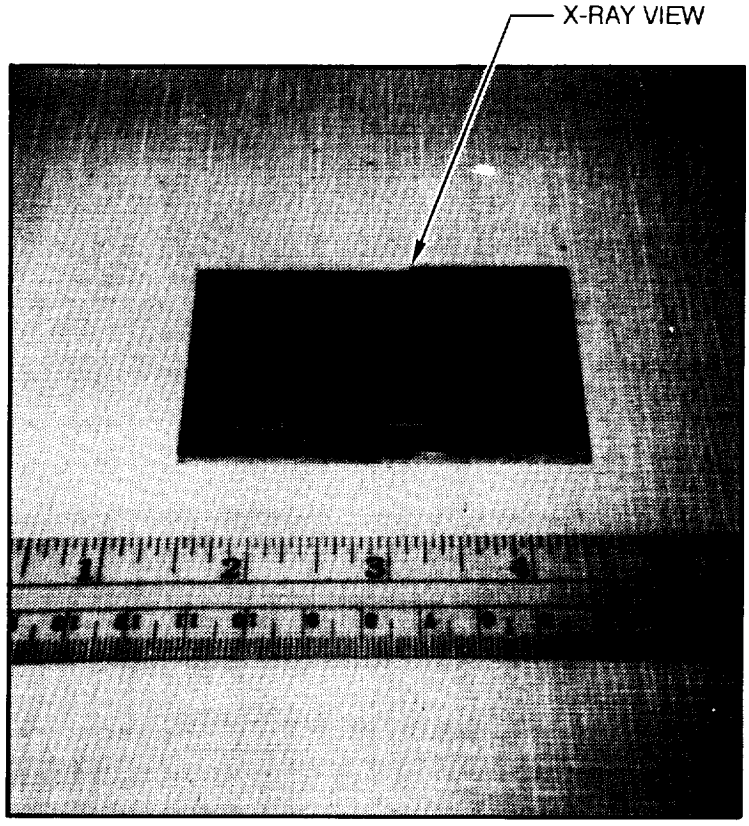

Figure 77. Test Sample and X-ray of Jacket Crossover Joint

ORIGINAL PAGE
BLACK AND WHITE PHOTOGRAPH

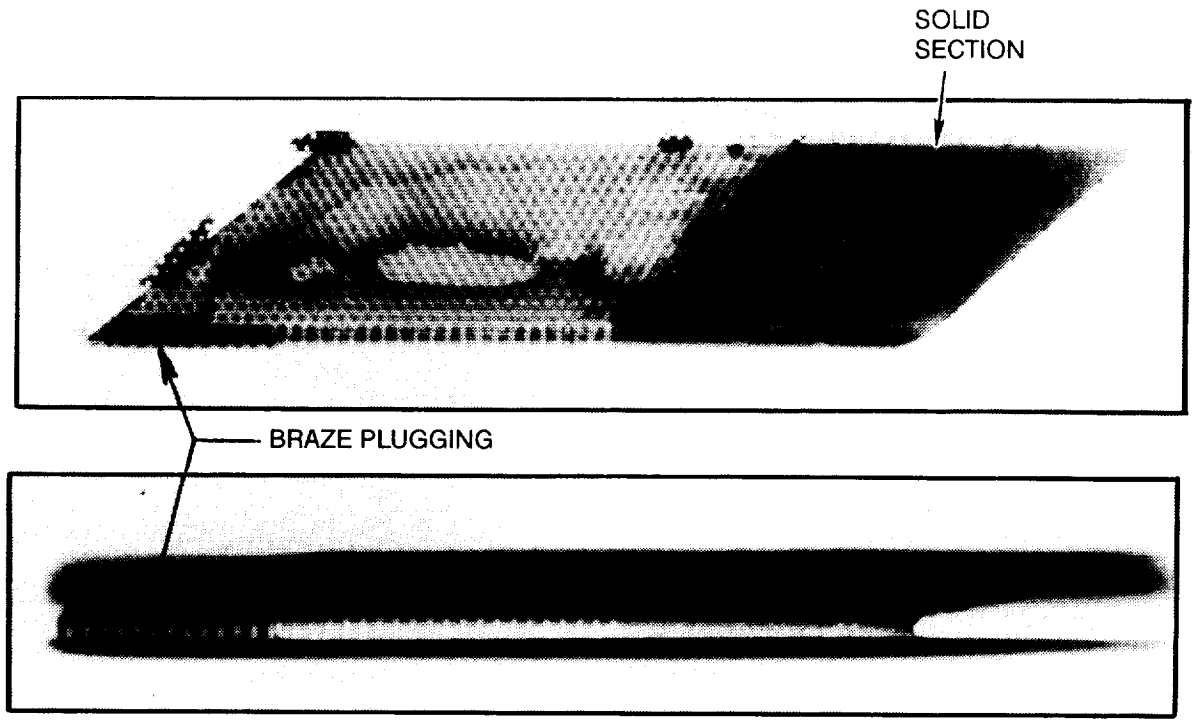

SAMPLE WITH BRAZE POWDER SLURRY (PLUGGING)

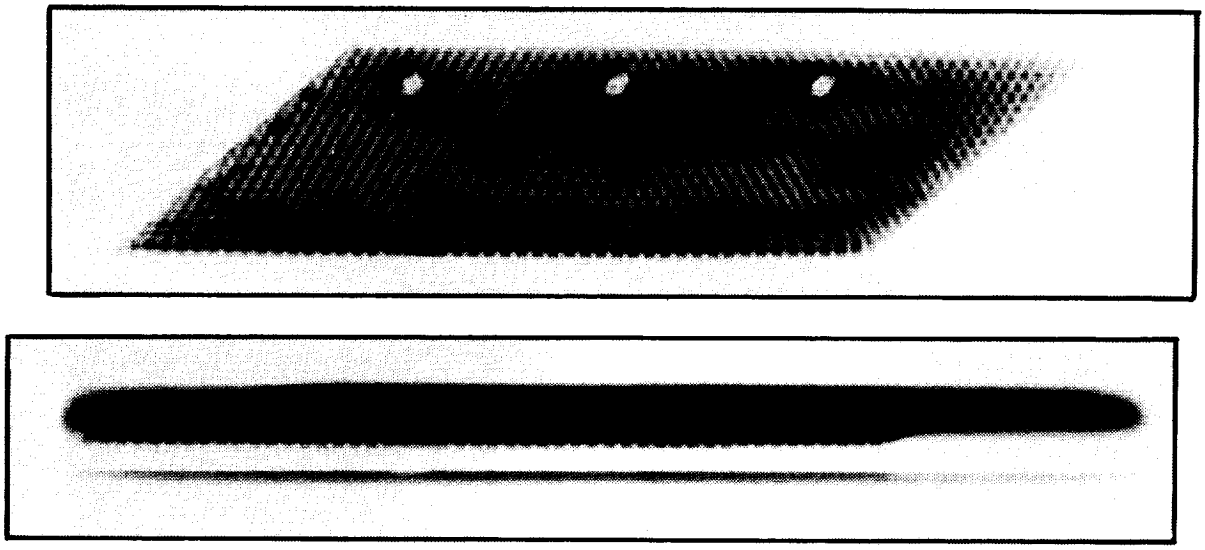

SAMPLE WITHOUT BRAZE ALLOY SLURRY (NO PLUGGING)

F-52548-A

Figure 78. X-ray Comparison of Braze Plugging of Wedge Samples

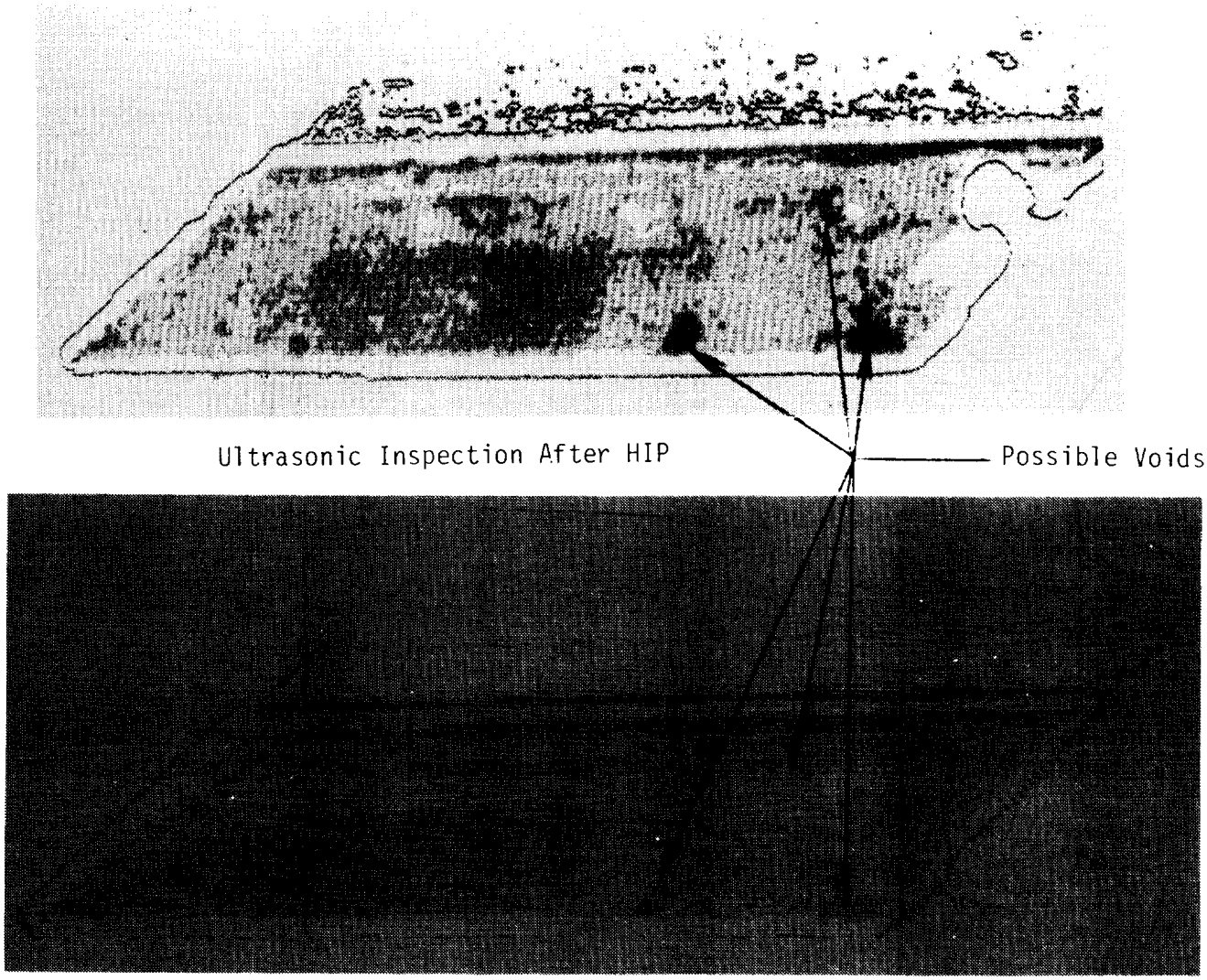

Figure 79. Evaluation of HIP to Reduce Voids in Jacket – Support Structure Joint

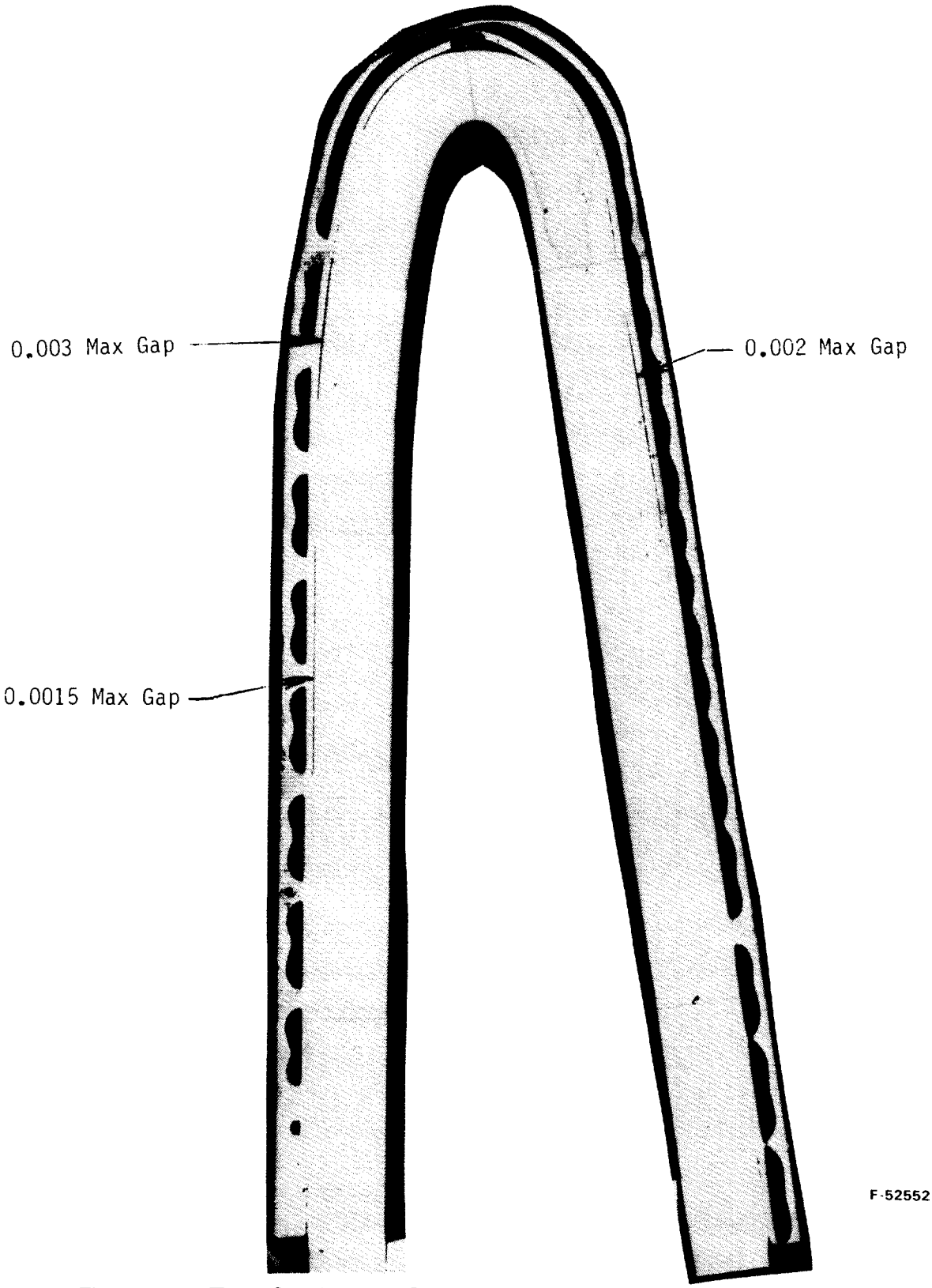

Figure 80. Test Section of Cooling Jacket-Support Structure Trailing Edge Braze Joint

by machining. For this test, 15-psi loading was applied from 1500°F up to the braze temperature of 1925°F and back down to 1800°F. Holographic examination of the leading edge jacket section revealed a void approximately 1/4 in. wide and 1/2 in. long.

At this point, the elimination of jacket-to-support structure braze voids was not resolved. Based on these results, hot-sizing of the pin-fin cooling jackets was specified for the full-size strut. Samples with various surface treatments were exposed to the temperature cycle to make sure the nickel jacket would not bond to the Inconel 718 structure during the sizing operation. No bonding occurred. The surface treatments considered were oxidizing the support structure and application of stop-off to either the jacket or the support structure. Oxidation of the structure was selected due to the possibility of flaking of the stop-off and its trapping in the pin-fins.

To further evaluate the design of the jacket-to-structure braze joint, two flat nickel panels were brazed to Inconel plates. One specimen included grooves (Figure 81), and one specimen did not. After brazing, these test specimens were examined for braze voids by X-ray and holography and then sectioned and metallographically evaluated. Figures 82, 83, and 84 show results for the two types of panels. The grooved panel was uniformly well brazed. Figure 83 shows the grooves as generally light lines; dark regions along the lines are due to filter alloy buildup in the grooves; dark lines along the edges of the grooves indicate large fillets of filler alloy. The ungrooved sample brazed poorly, with extensive, contiguous void areas. A cut across the width of the sample was made through both the light and dark areas shown in Figure 84 and is shown in Figure 82. The light areas in Figure 84 correlated well with the amount of voids shown in Figure 82. The joint gaps averaged 0.0025 in. for both the grooved and ungrooved samples.

As a next step, grooved, equivalent thickness nickel panels were formed and brazed to wedges that simulated the leading and trailing edges of the strut body. After brazing, the wedge specimens were examined for braze voids by X-ray, holography, and sectioning.

Figures 85 and 86 show the test specimens prior to brazing. Figures 87 and 88 show sections of two sets of the brazed forward and aft wedges. Examination of both micros and macros indicated that the braze joints, where made, were satisfactory and not prone to void formation. The relatively large gaps at the leading edge resulted from incomplete forming and poor fit-up of the panel and indicated the need for improved cold-form tooling. Specifically, the throat dimension (at the location corresponding to the coolant inlet slot) of the test piece was approximately 0.040 in. compared to the tool dimension of 0.026 in. Subsequent hot sizing was expected to, but did not, correct this condition. As a result, the cold-form tooling for the forward jacket was redesigned from a male punch forming into rubber to a coining die which utilizes a male-female die set to form the leading edge. The punch tooling for the trailing edge was retained since the observed results were judged satisfactory.

Finally, the susceptibility to a collapse of the cooling jacket at the breaks in the side contours of the strut was evaluated. A previously fabricated pin-fin cooling jacket specimen was used. The solid header bar was cut off on one side of the cooling jacket assembly to simulate the long, unstiffened area encountered in the full-length strut. No difficulties

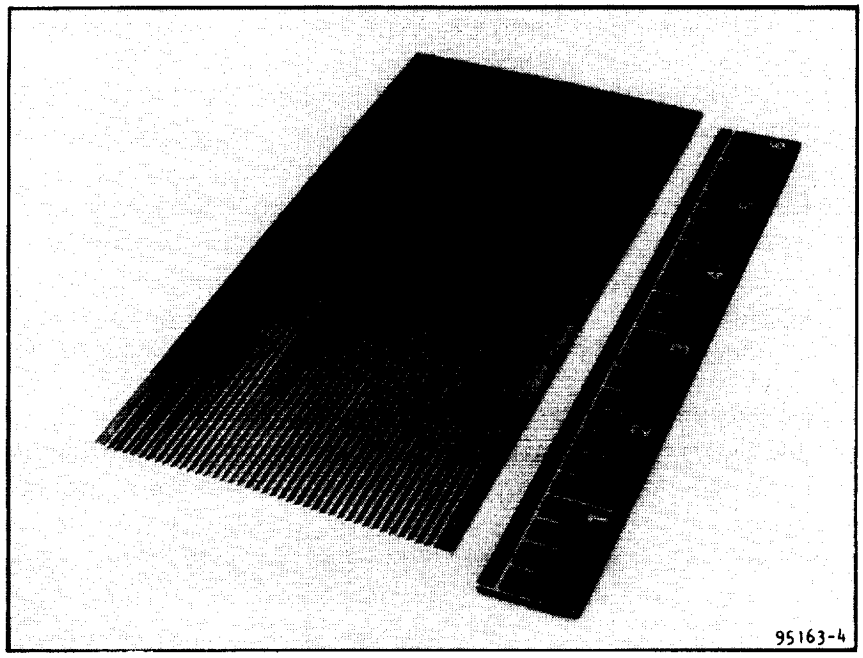

F-58711

Figure 81. Grooved Flat Specimen (0.005-in.-deep and 0.025-in.-wide groove)

were encountered for bend angles of 5 to 45 deg at the required radius. Figure 89 is a section through a typical bend. It shows no buckling of the face plate or damage to the braze joints. As a result, no internal stiffening ribs were used at bends in the strut contour.

4.4.4 Beam-to-wall brazement (test Item 5).—Simulated beam-to-wall braze joint samples were fabricated to verify achievement of adequate joint strength. Results of this investigation are discussed in para. 4.2. Tensile-tested beam joints showed that with supplementary braze alloy, joint strength values of 60 ksi minimum can be obtained. Stress analysis based on a modified beam design showed that tne new design would withstand the 1500-psig proof pressure with braze joint strengths of 60 ksi. The full-length strut was brazed using the supplementary braze alloy and a continuous argon purge of 300 ft^3/hour during brazing to sweep out vapor from the binder that is used to apply filler alloy slurry.

As in the case of the cooling jacket-to-strut body joint, a HIP process was performed on a section of the second partial-length strut that included a beam-to-wall braze joint to determine the possibility of braze void reduction. An insignificant increase in joint strength was observed when compared to the same beam braze joint prior to the HIP process. HIP, therefore, is not considered an appropriate rework procedure.

A sample was constructed and tested to determine if the strut body could withstand a 15-psi load during second stage brazing at 1925°F (jacket-to-support structure) as a general means of improving joint quality. Minimal deflection between beams was observed (approximately 0.002 in.). Subsequently, this loading was used in the last braze

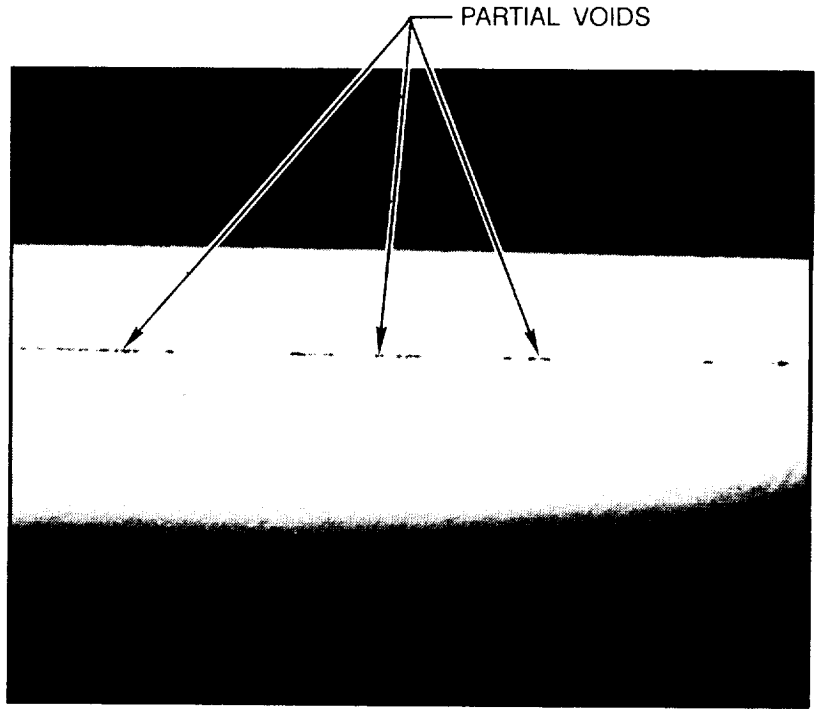

PARTIAL VOID
(DARK AREA IN X-RAY, FIGURE 84)

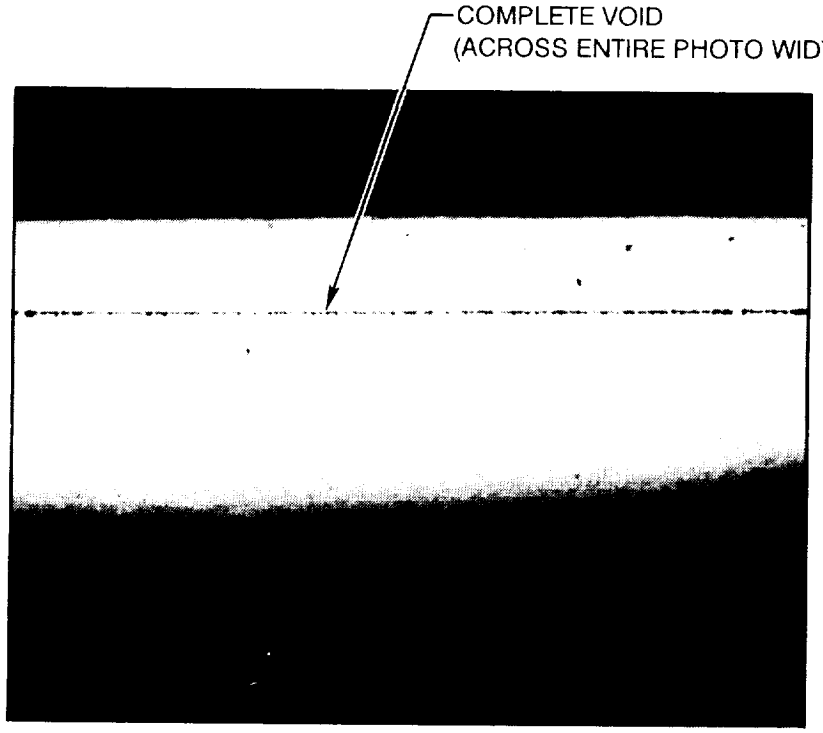

COMPLETE VOID
(LIGHT AREA IN X-RAY, FIGURE 84)

Figure 82. Braze Joint, Ungrooved Flat Sample

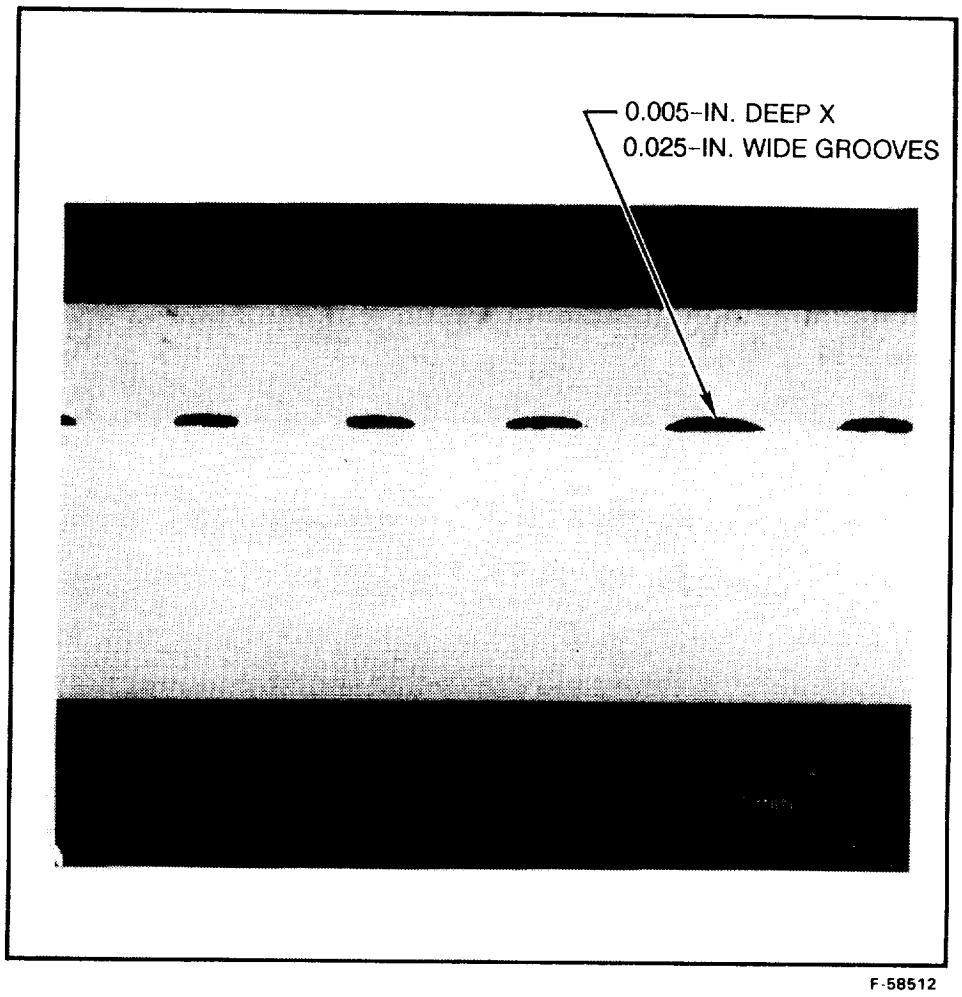

Figure 83. Braze Joint, Grooved Flat Sample (No Voids)

test under test Item 3 (brazing of the simulated jacket to the strut wedge). The 15-psi loading was also used during rebraze of the full-length support structure to fill starved braze joints.

4.4.5 Design issues (test Item 6). – Burst tests were run on leading and trailing edge specimens. The tests were designed to determine the structural effect of the coolant holes in the leading and trailing edges of the strut body. The specimens ruptured at approximately 2900 psig and 2750 psig, which is well above the 1500-psig proof pressure requirement. The support structure ruptures occurred in the cooling jacket, probably in a void area between the cooling jacket and the body. The support structure was not deformed. Figures 90 and 91 show the burst test specimens after rupture. Thus, the holes in the leading and

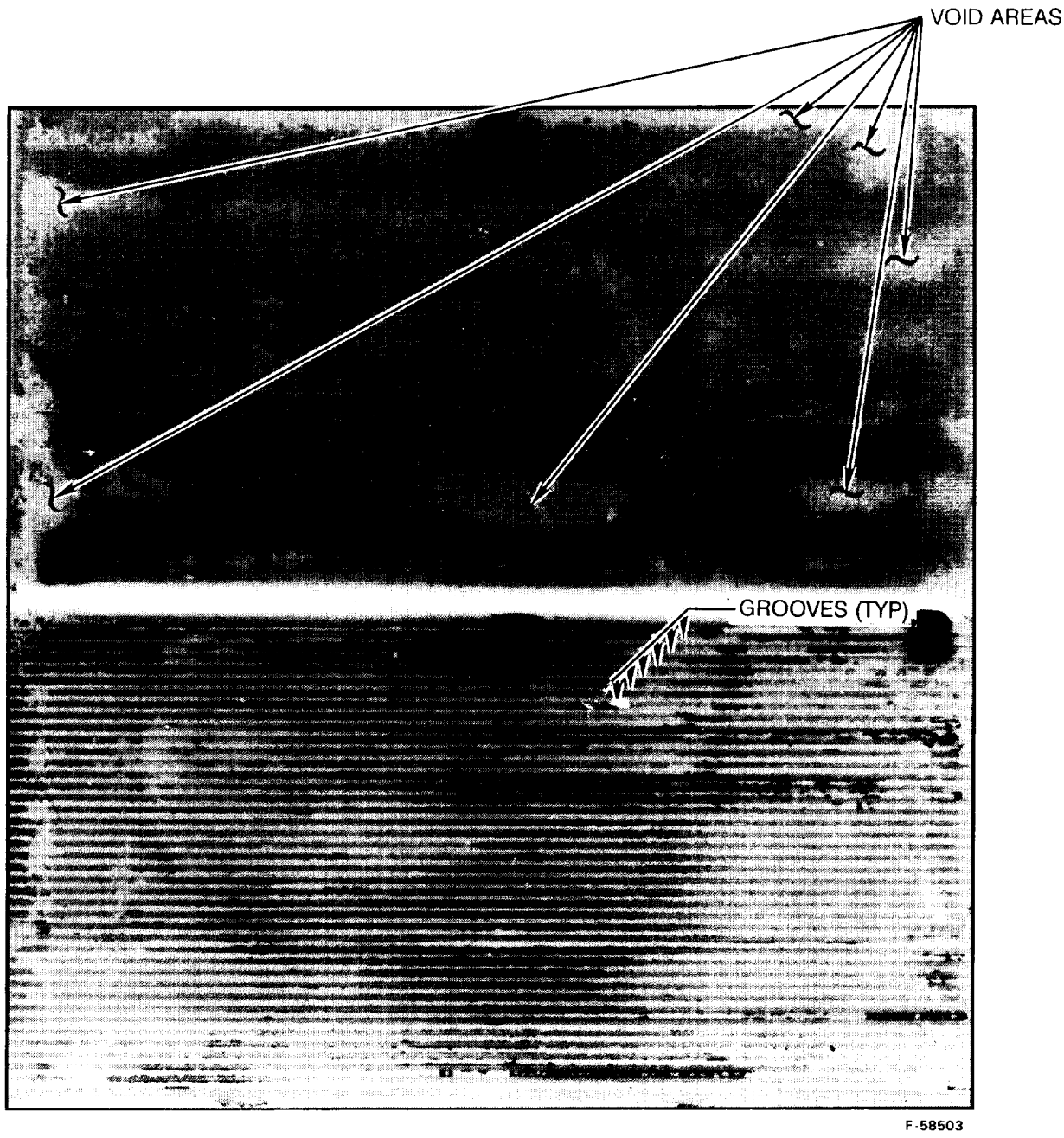

Figure 84. X-Ray of Both the Ungrooved (Top) and Grooved (Bottom) Braze Samples. Void Areas, Including Grooves in Grooved Panel, Are Light.

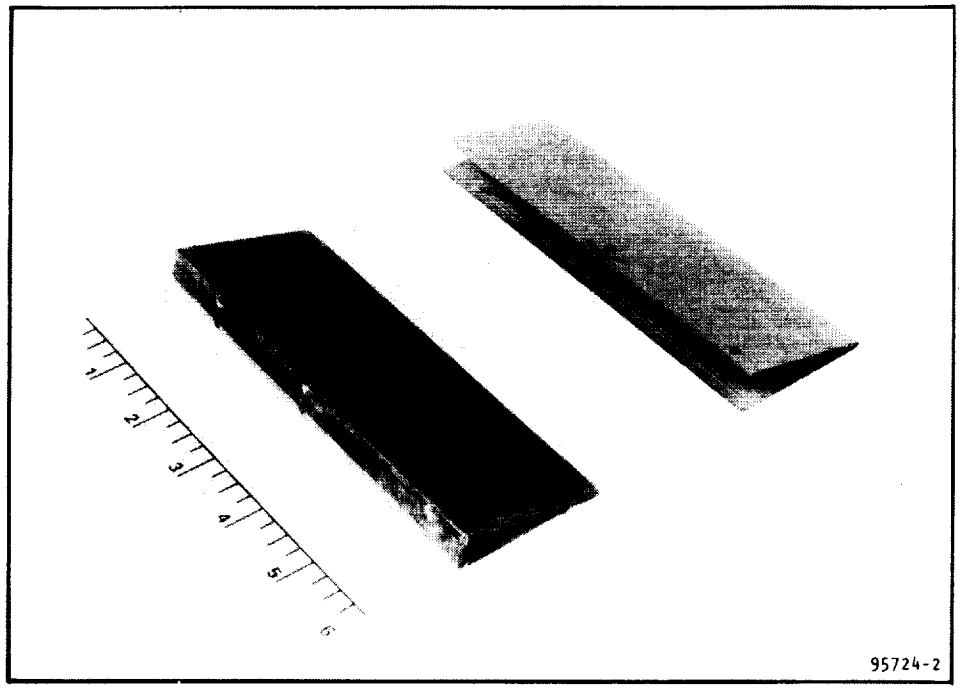

F-58712

Figure 85. Forward Strut Wedge Specimen Parts Using a Grooved Panel

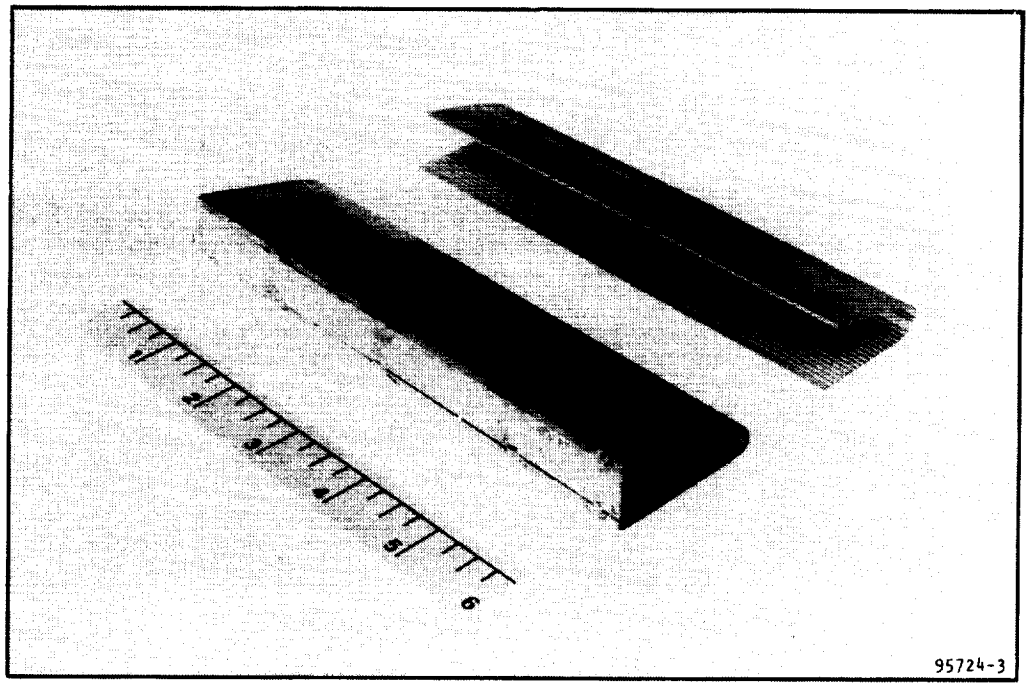

F-58713

Figure 86. Aft Strut Wedge Specimen Parts Using a Grooved Panel

ORIGINAL PAGE IS
OF POOR QUALITY

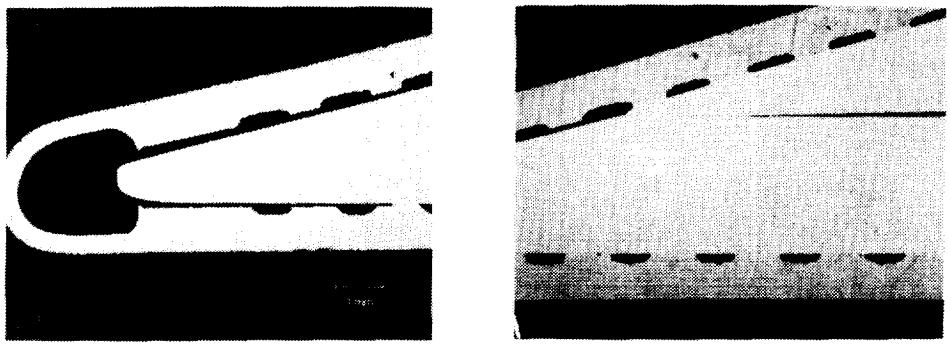

Figure 87. Braze Joints of Forward Strut Wedge Test Specimens

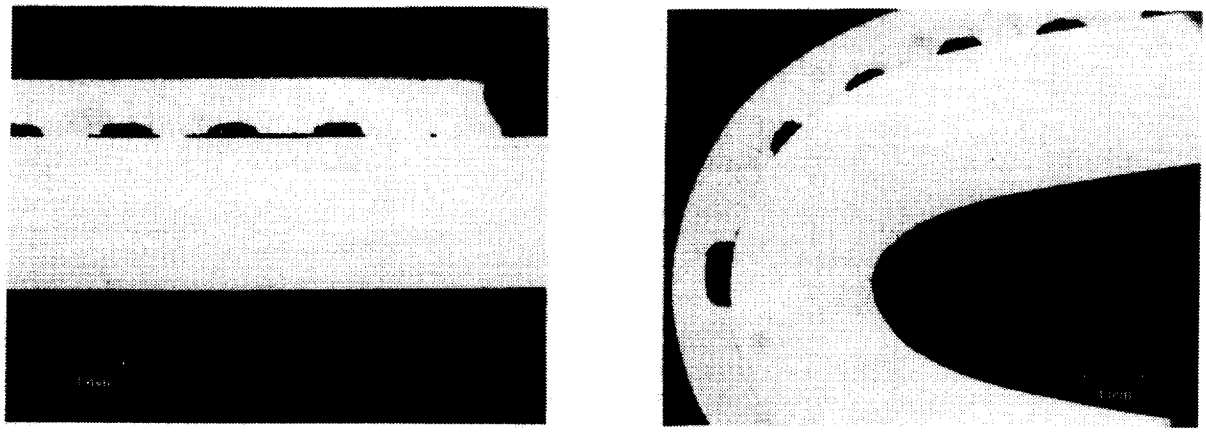

Figure 88. Braze Joints of Aft Strut Wedge Test Specimens

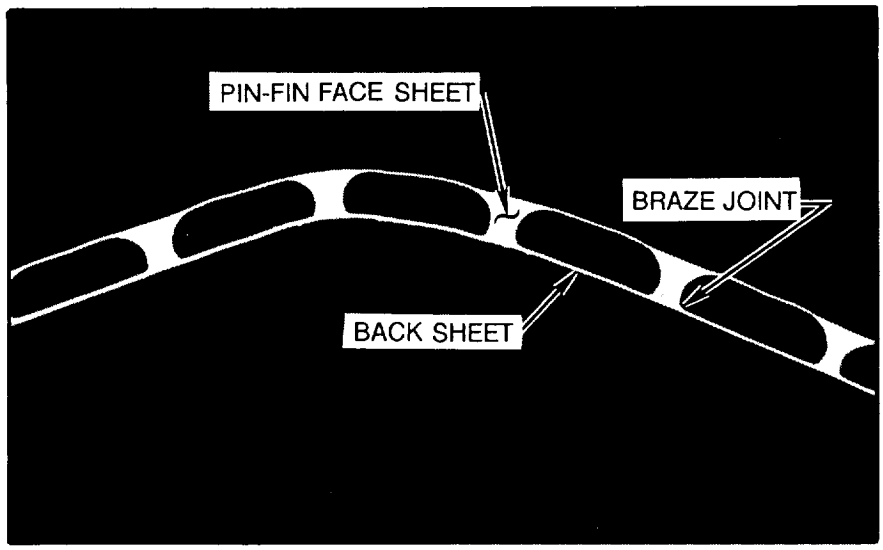

Figure 89. Section From Pin-Fin Cooling Jacket Bend Test Specimen

trailing edges are not detrimental to the structural integrity at design pressures, and no design changes were made.

An additional design issue was the fuel-injection tube penetration through the internal beams and the internal bypass that results from pressure differences across the beam and was observed during pressure testing of the partial-length struts. This issue was resolved by a redesign. A washer and sleeve configuration permits a more secure and repeatable braze joint. Figure 92 shows the redesign. The sleeve provides a long, high-pressure-drop flow path that minimizes leakage. The brazed washer allows for the maximum possible radial misalignments of tube and hole centers while providing a positive seal. This, in turn, allows loosening of assembly tolerances and reduces the need for the extensive hand-fitting required in assembly of the PL struts.

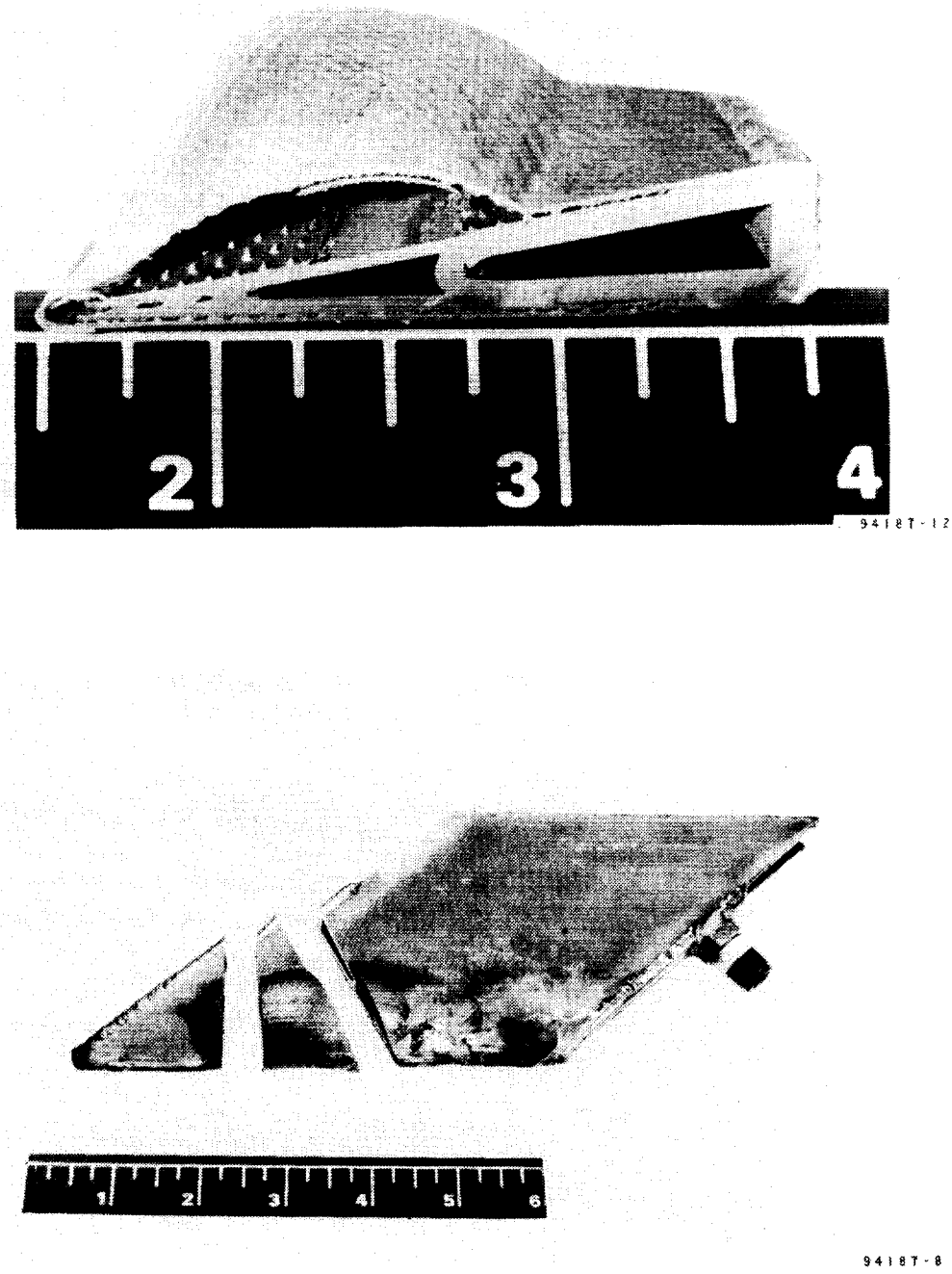

Figure 90. Leading Edge Test Specimen After 2750-psig Rupture

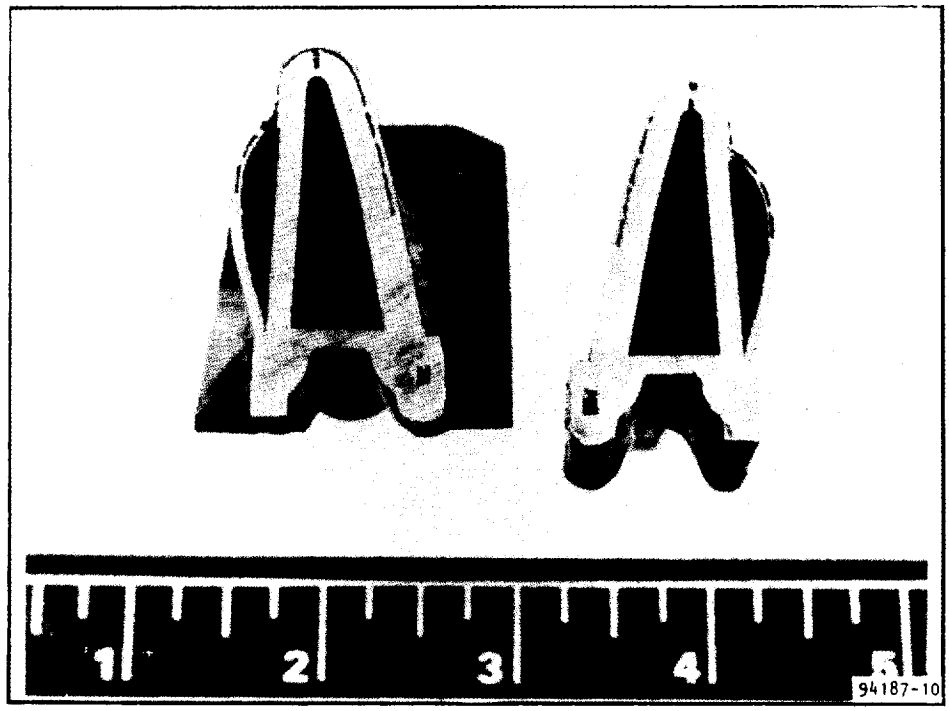

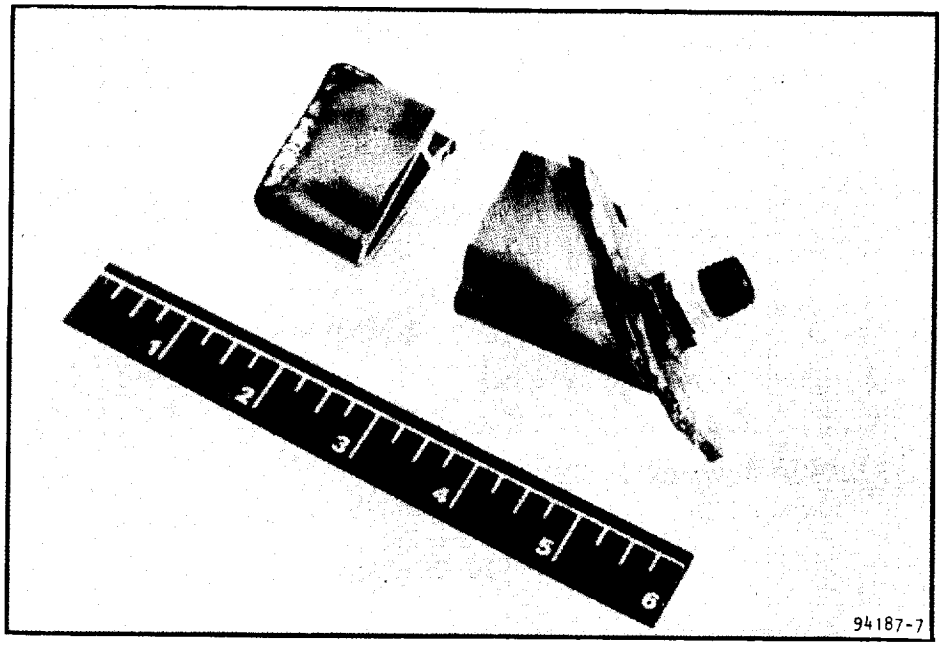

F-60425

Figure 91. Trailing Edge Test Specimen After 2900-psig Rupture

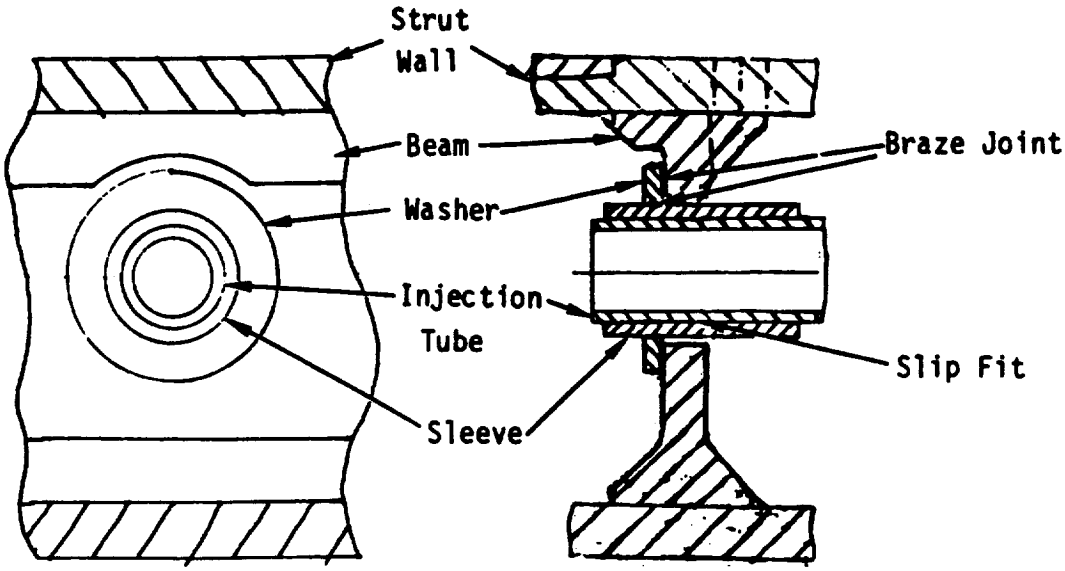

New Configuration

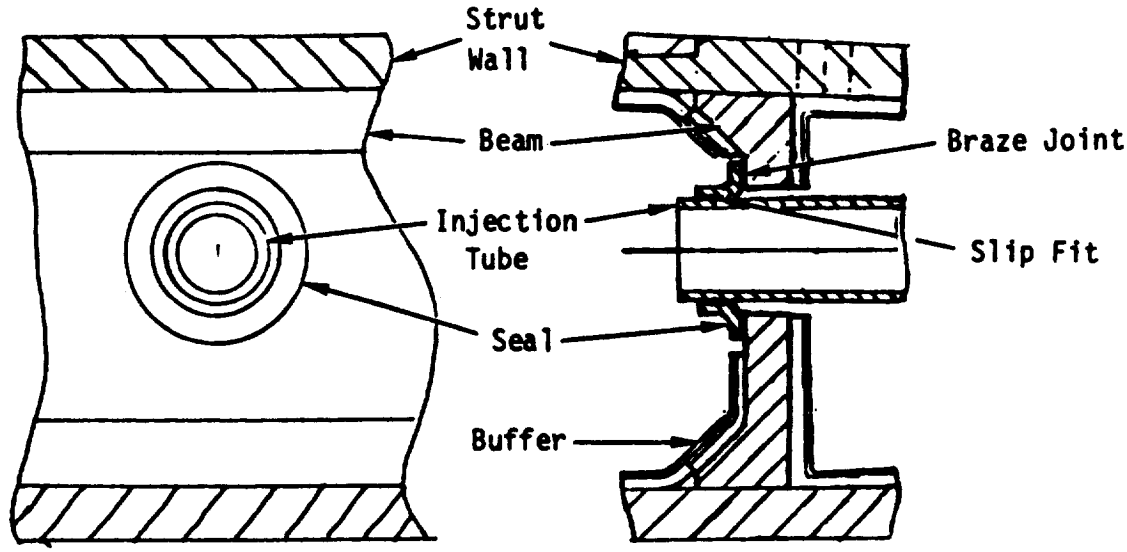

(Buffer Removed For Clarity)

Old Configuration

B-17183

Figure 92. Comparison of Old and New Seal Design

5. TASK 3 – PARTIAL LENGTH (PL) STRUT FABRICATION

This effort provided for evaluation and selection of fabrication methods for the full-length (FL) strut. Specifically, two struts of partial-length and full-scale cross section were fabricated to assess forming, machining, photochemical milling (PCM), fixturing, brazing, and assembly techniques.

Because of the anticipated longer lead times for the FL strut components, portions of the two efforts were somewhat parallel. Other manufacturing operations were delayed, pending results from the PL strut work. All assembly operations, however, were first performed on the partial-length struts. The sequencing of the critical manufacturing efforts applicable to both the PL and FL struts is presented in Table 21.

TABLE 21

FABRICATION SEQUENCE FOR THE PARTIAL- AND FULL-LENGTH STRUTS

INCO-718 Support Structure
Tool design and fabrication
Form and hot size skin
Fabricate leading edge insert
Assemble and braze strut body
Detail parts fabrication
Cooling jacket/support structure braze
Cooling Jacket Assembly
PCM pin-fin face plates
Assemble and braze
Form and hot size
Support Structure Assembly and Braze
Final assembly and braze
Final pressure test/hold
Ship to NASA

5.1 Design

The design features a full-scale cross section strut of 6-in. length. The selected length was judged to be a representative sample for developing FL strut manufacturing techniques. Figure 93 (Drawing 2300759) shows the PL strut assembly. Details and features are as shown and described for the FL strut.

As with the actual FL side strut, the PL strut cross sections were brazed assemblies, each consisting of an Inconel 718 support structure, Nickel 201 pin-fin cooling jacket subassemblies, and top and bottom cover plates to seal the ends of the assembly.

The support structure consisted of forward and aft sections. Each section included a formed wall and support beams, thermal buffers, and fuel injection tubes. The forward section, in addition, contained a leading edge insert for direct impingement cooling of the leading edge . The leading edge insert was machined from Inconel 718, and the coolant flow channels were generated by EDM.

The Nickel 201 cooling jacket assembly was a short version of the FL cooling jacket and consisted of forward and aft subassemblies. The pin-fin face plates were photochemically machined and brazed to 0.010-in.-thick Nickel 201 back sheets to make self-contained subassemblies. These were pressure-tested and holographically examined to verify structural integrity before they were formed to the appropriate section contour for brazing to the support structure. The machined top and bottom cover plates were brazed on during a third braze operation to complete the PL strut fabrication.

5.2 Support Structure

Fabrication of the Inconel 718 walls of the support structure was undertaken first. The material blanks were ground to final thickness, formed to the general shape of the respective sections, and then hot-formed into the precise shape required for brazing of the support structure assembly. Figure 94 shows the two PL forward strut walls on the form die. The leading and trailing edges of the structure must be formed to radii tighter than the material thickness. Additionally, the formed walls must be precisely contoured, to within brazing tolerances, for subsequent interfacing with the support structure stiffening beams and the cooling jacket subassemblies.

The forward wall was additionally machined at the leading edge for interfacing with the leading edge insert, as were the braze surfaces of the forward-to-aft wall joints. Figures 95 and 96 show the machined sections. The configuration of the

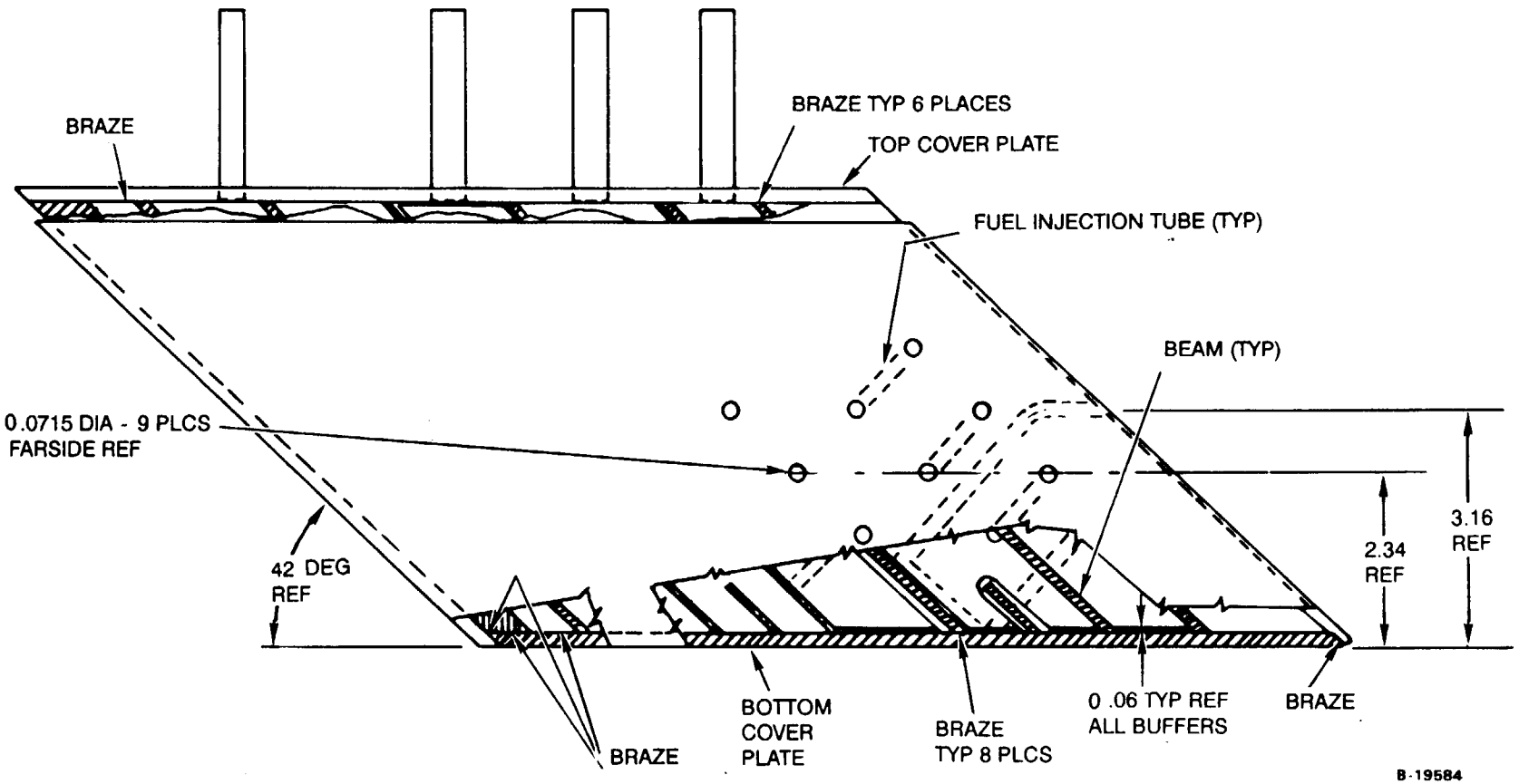

Figure 93. PL Strut Assembly

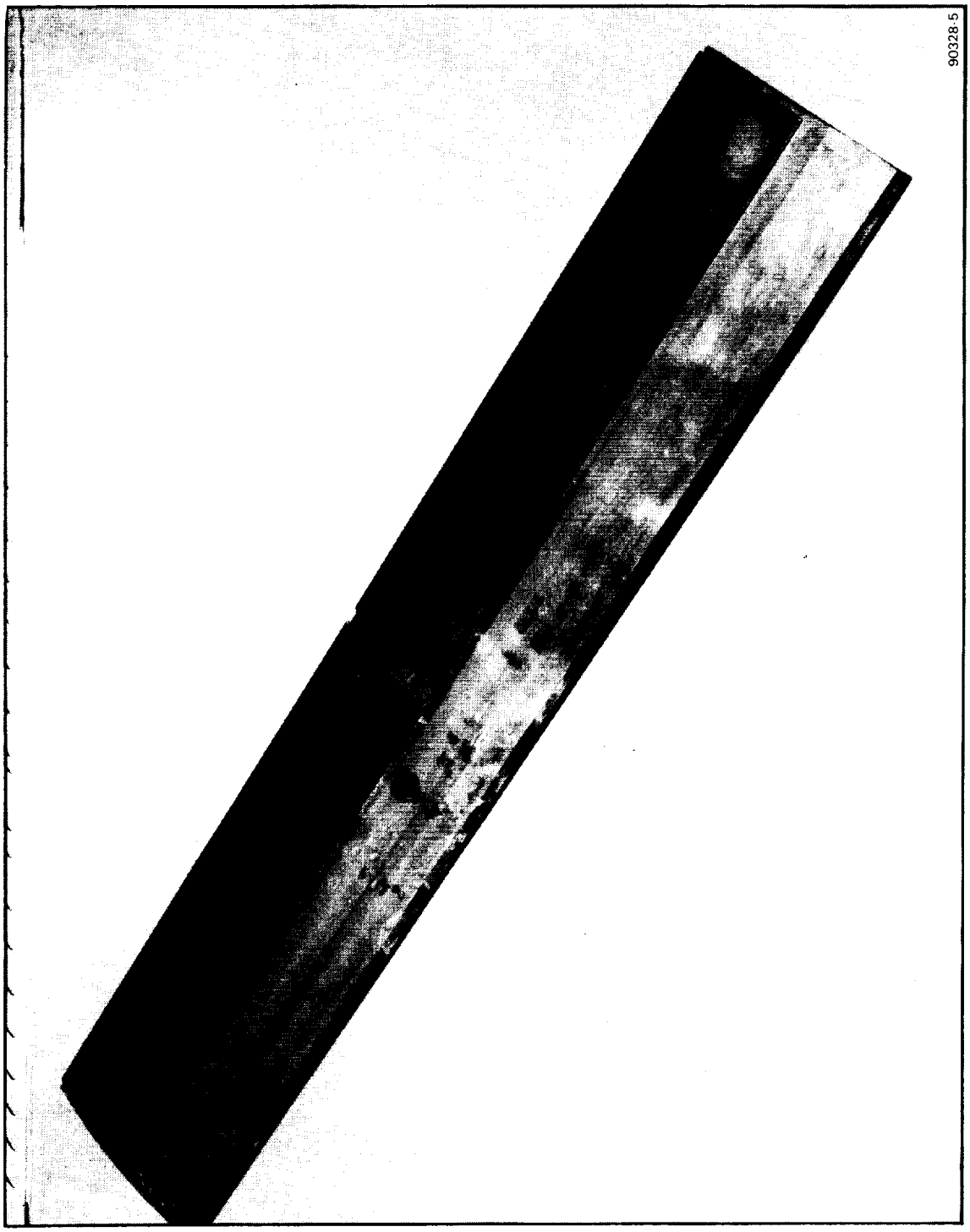

F-45659

Figure 94. Two Hot-Sized Partial-Length Forward Support Structures on Form Die

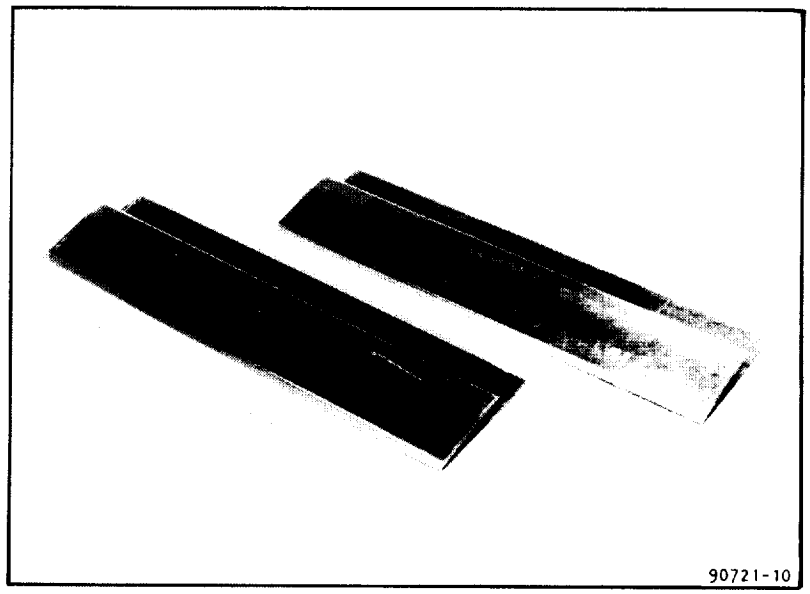

F-60407

Figure 95. Formed and Machined Inconel 718 Forward Support Structure Walls for Two PL Struts

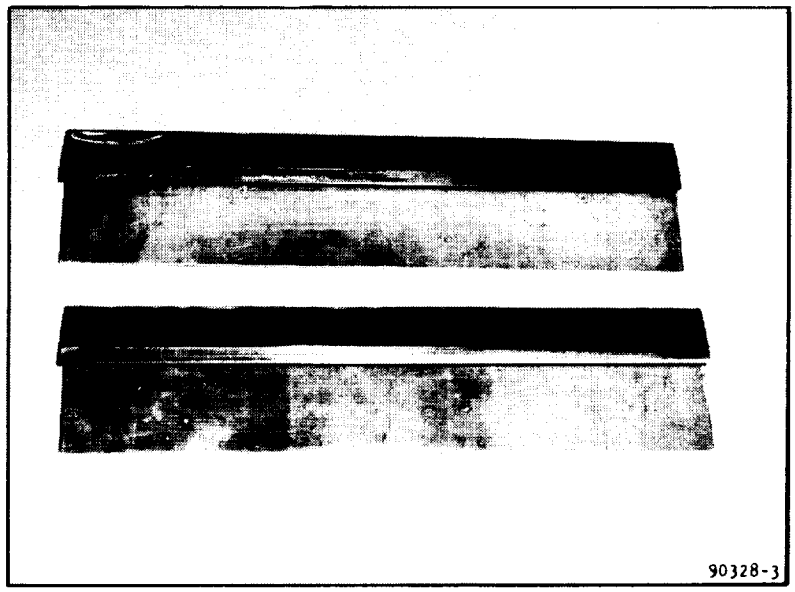

F-60408

Figure 96. Formed and Machined Aft Support Structure Walls for Two PL Struts

separate leading edge (LE) support structure section is shown in Figure 97. Figure 7 (Dwg. 195582, sheet 4 of 4) shows this part as Item 29; the two machined PL LE inserts and a closeup of the apex are presented in Figures 98 and 99. Machining of the leading edge coolant inlet holes proved developmental, because of the large length/diameter ratio. The final approach used round EDM'd holes in the rear and rectangular EDM'd holes at the front, rather than the initially planned all-rectangular holes. The LE's and the two wall sections were trial fitted, as shown in Figure 100. The sections are offset , as shown, to allow for 42-deg angle cuts at the top and bottom ends, and the faying surfaces were adjusted for a proper braze fit.

The major detail parts used in the first partial-length strut (PL1) are shown in Figures 101 and 102, and include the forward and aft support structures, and the leading edge.

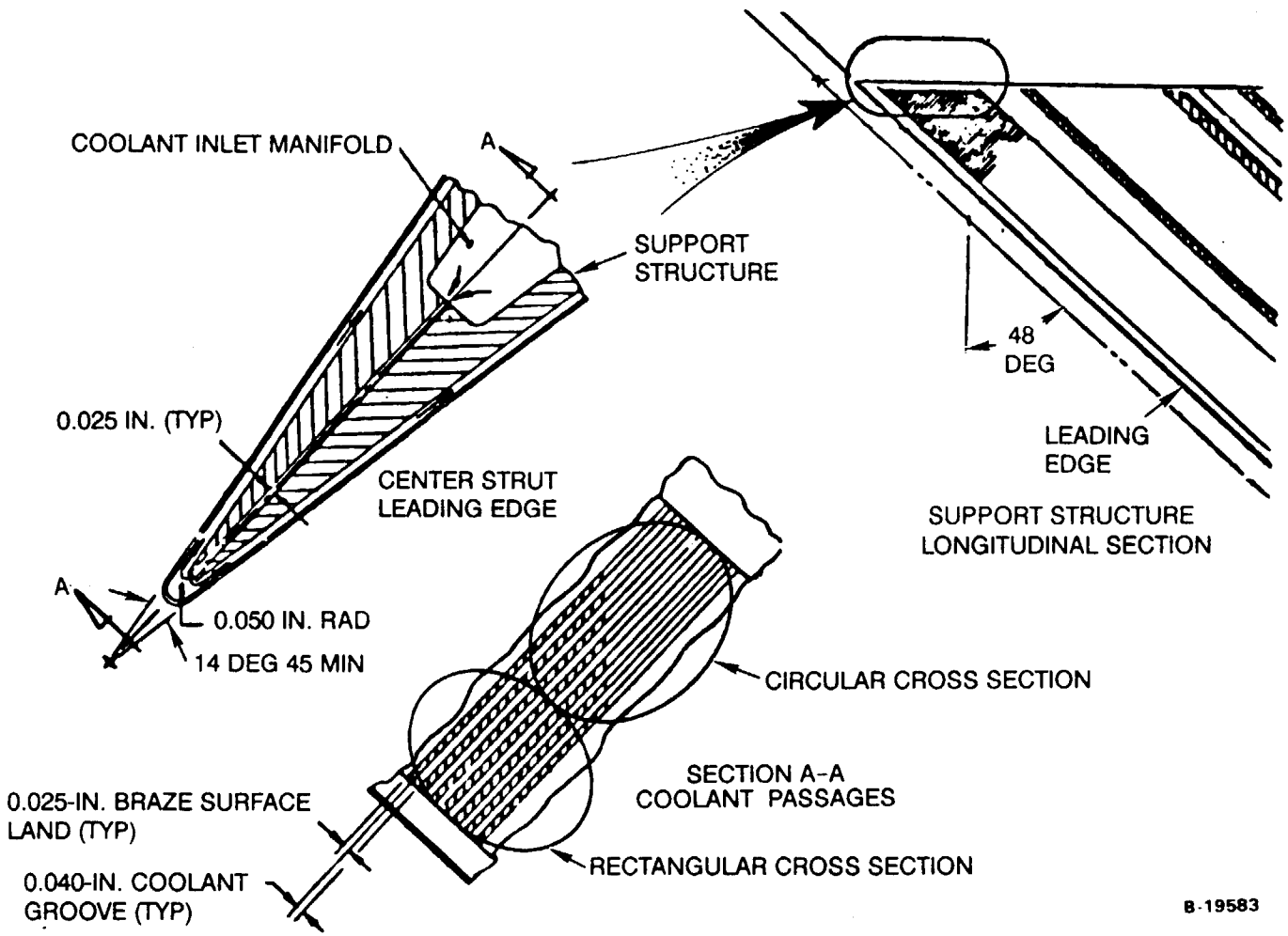

Figure 97. Leading Edge Configuration (Center Strut Shown – Typical for Side Struts)

ORIGINAL PAGE
BLACK AND WHITE PHOTOGRAPH

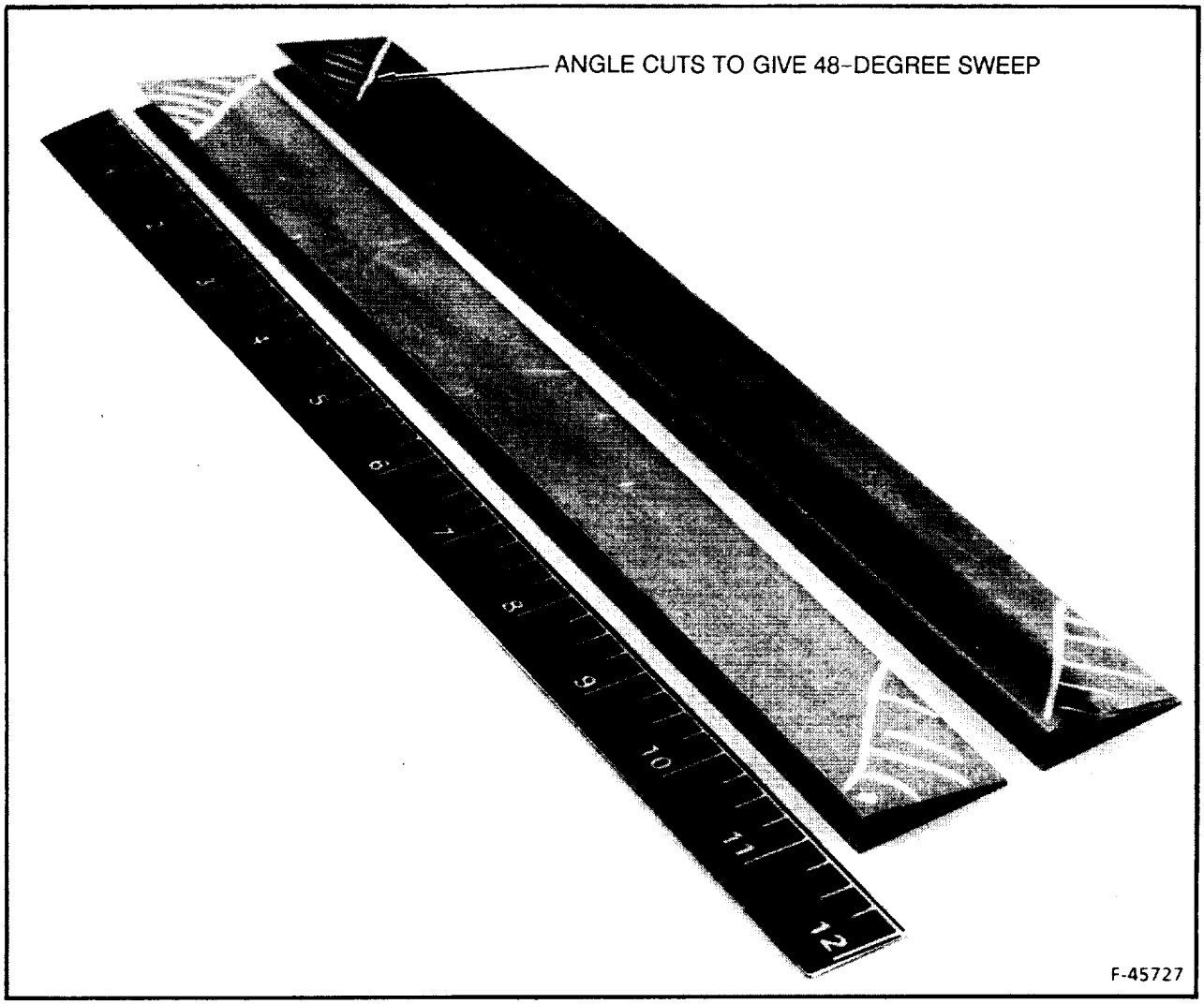

F-58505

Figure 98. Two Machined, Partial-Length Leading Edges

ORIGINAL PAGE
BLACK AND WHITE PHOTOGRAPH

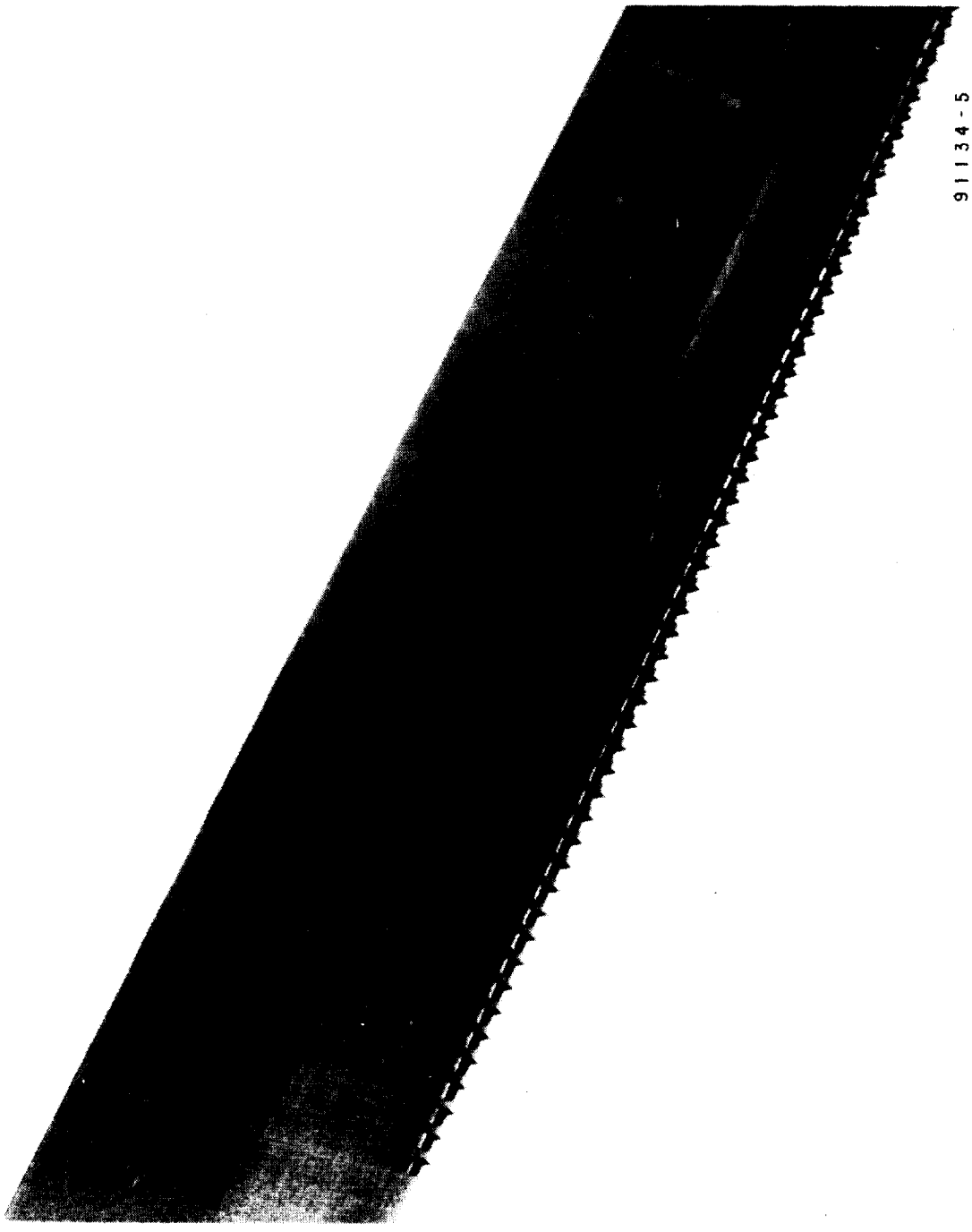

Figure 99. Closeup of Machined Partial-Length Leading Edge Support Structure Insert

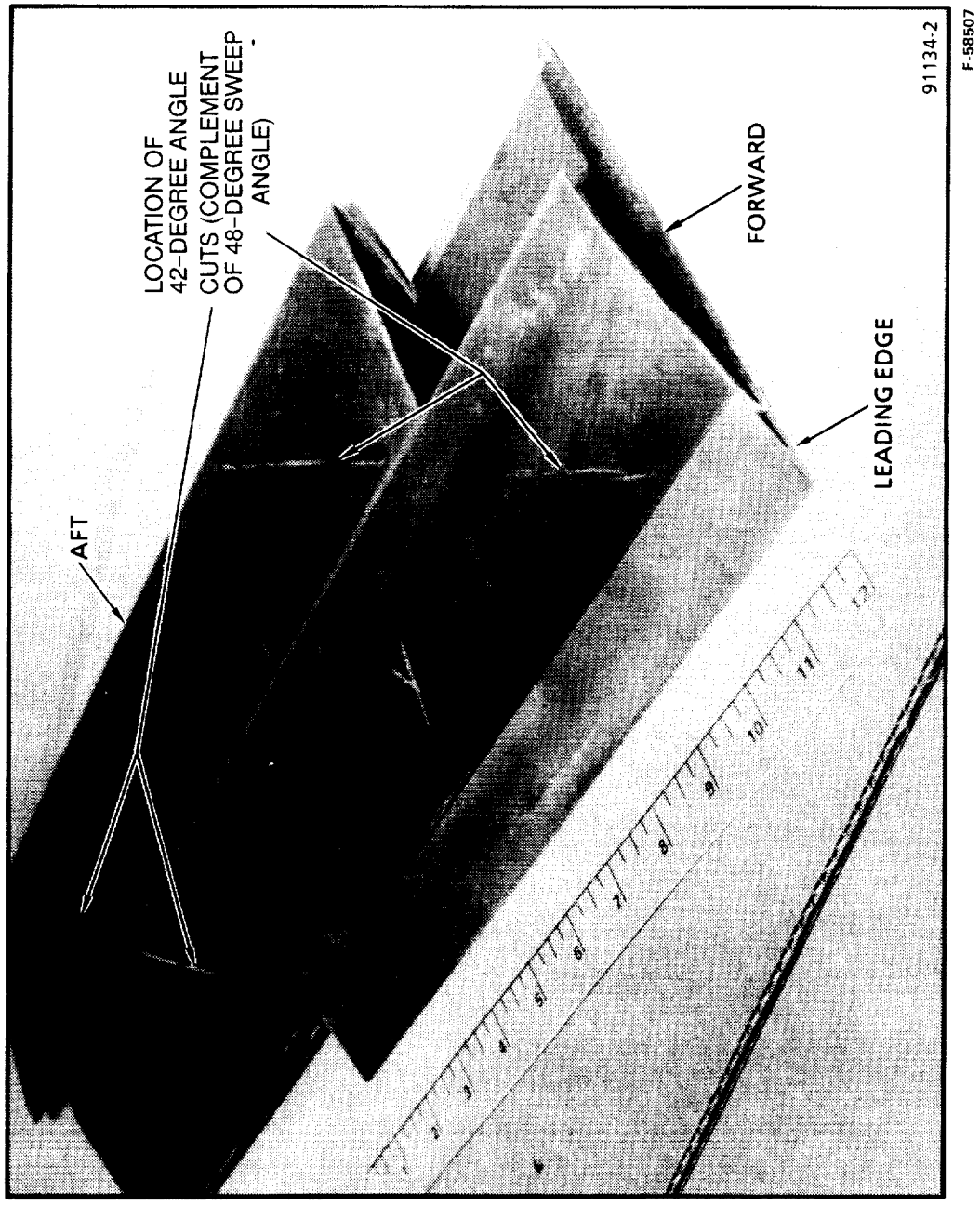

Figure 100. Fitup of Partial-Length Strut Leading Edge, Forward and Aft Support Structures (Parts Are Offset for Angle Cuts for Assembly with 48-deg Sweep)

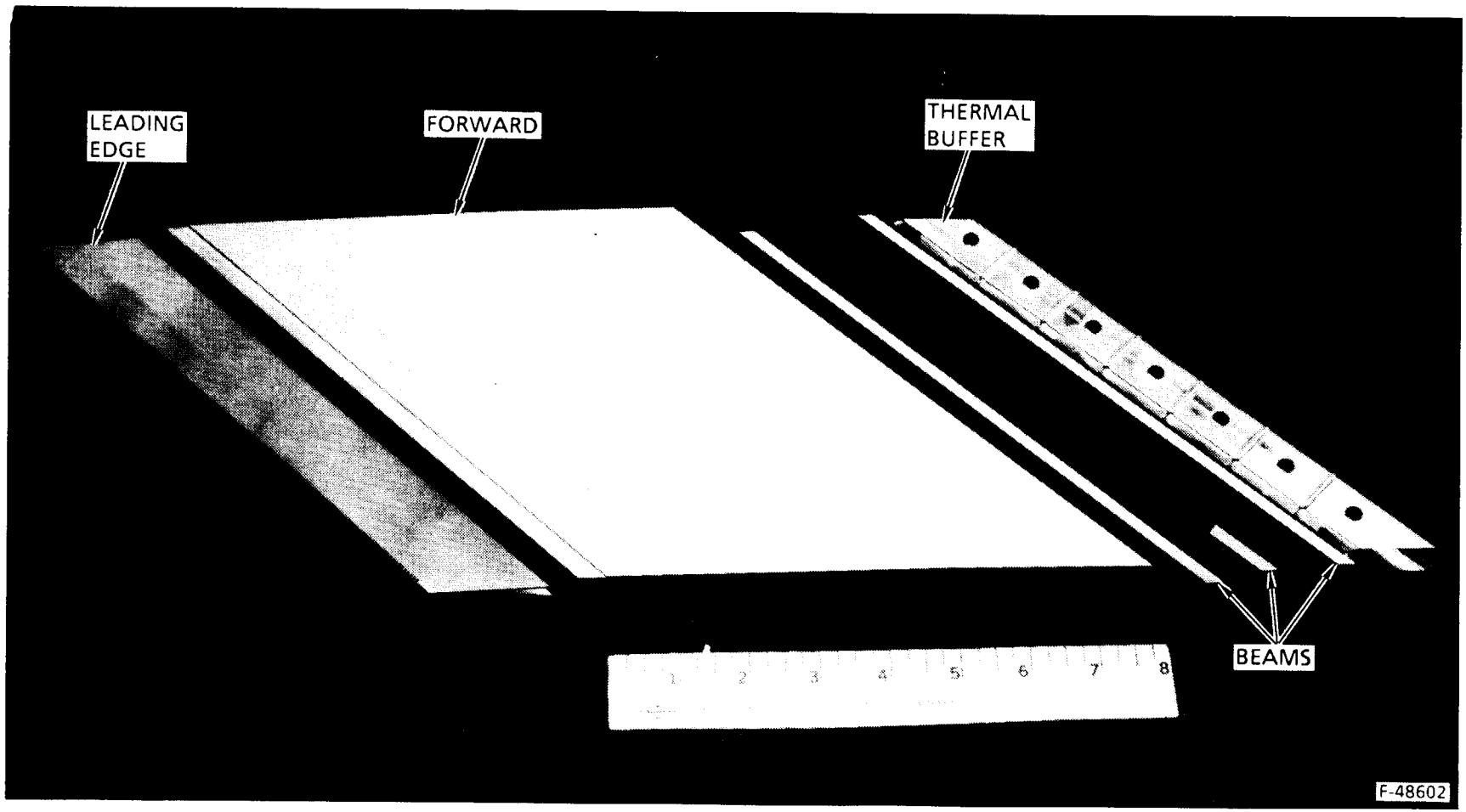

B-19604

Figure 101. Details of Forward Portion of Partial-Length Strut Support Structure

ORIGINAL PAGE
BLACK AND WHITE PHOTOGRAPH

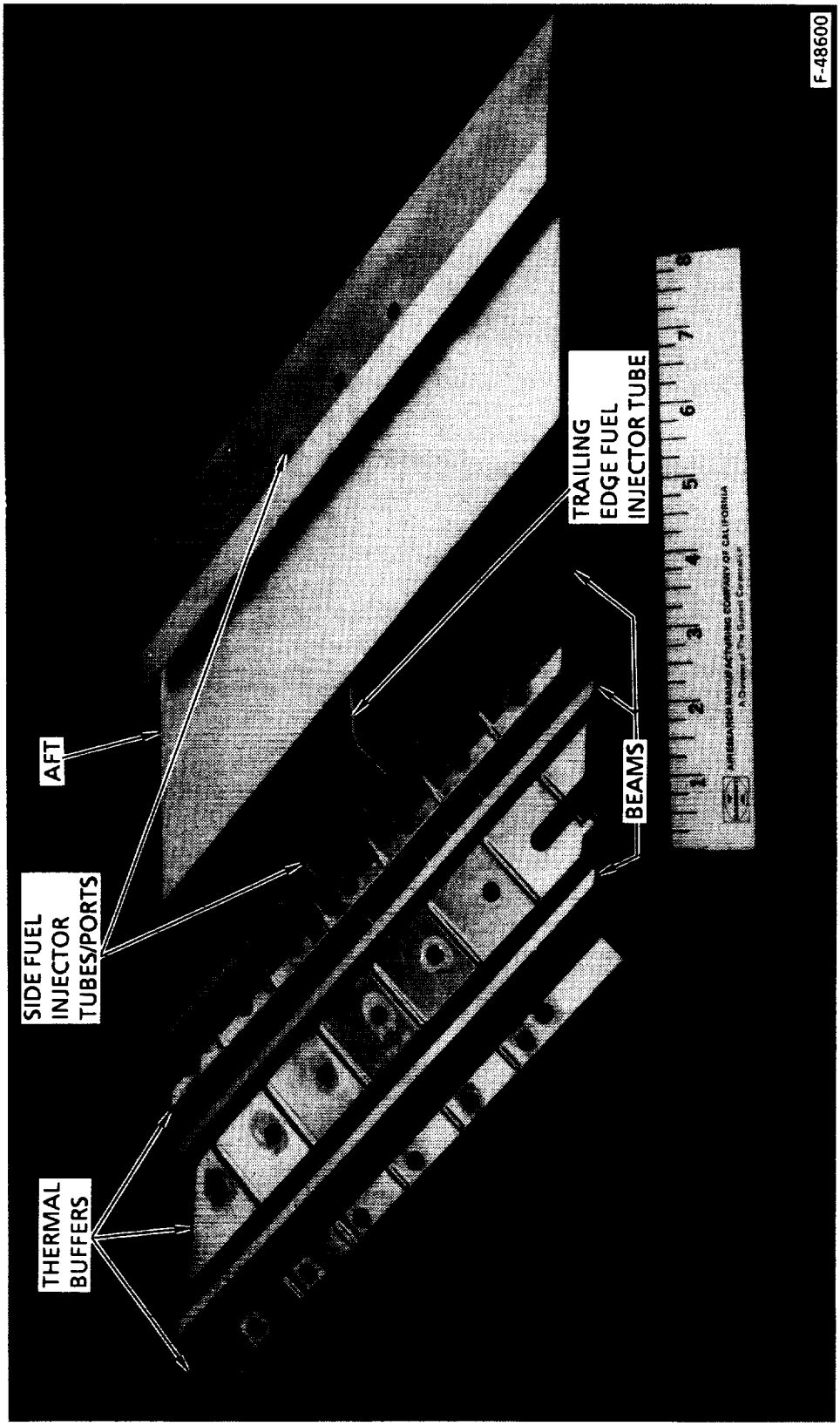

Figure 102. Details of Aft Portion of Partial-Length Strut Support Structure

As a first step in assembly, a support structure specimen, 2-in. wide, was brazed with Palniro 1 filler alloy at 2070°F to determine the proper pressure loading for brazing. The structure was placed in a sheet metal bag that was evacuated to produce a pressure loading from 0 to 1 atmosphere. Early tests on a crude model showed that a full vacuum loading of 14.7 psi at 2070°F led to deformations of 0.20 in. in the side wall between the supporting beams (Figure 103). A support structure test assembly, Figure 104, was brazed with a 10-psi load and had deflections on the order of 0.003 in., which were considered acceptable. As a check, this sample was rebrazed at 10-psi loading, and the previous result was confirmed.

To enhance brazeability, the Inconel 718 braze surfaces were electrolytic-nickel-plated to a thickness of 0.0002 to 0.0003 in. To evaluate adhesion of the plating, samples were plated and run through a braze cycle. Blistering occurred when only acid cleaning was used prior to plating. Glass-bead peening combined with acid-dip cleaning yielded an adherent plating and was specified for the struts.

Following these preliminary tests, the subassemblies of channel bulkheads, buffers, and fuel injection tubes were installed into the respective support structure sections (Figure 105). The two sections were joined and brazed to complete the support structure assembly for PL1 (Figure 106). After heat treatment and trimming the ends of the strut to length, three beam-to-body braze joints were seen to have line contact only.

A specially designed pressure test fixture that sealed the ends was used for low-pressure testing of the brazement. Holograms at 50 psi, Figures 107 and 108, showed an intermittent bond for one of the three marginally brazed beams. The strut was rebrazed after filler alloy slurry was applied to the beams. Figures 109 and 110 are the holograms after the rebraze. They indicate a satisfactory result.

In parallel with work on PL1, the second PL support structure was assembled and brazed. Supplemental braze alloy was used in the form of foil and slurry on the beam joints and the fuel injector tube penetrations. Braze voids at the fuel injectors were filled in a rebraze using Palniro 1. The structure was then satisfactorily pressure-tested to 460 psig, the limit of the fixture.

At this point, the PL1 and PL2 structures were available for assembly with the cooling jackets and the second-stage braze.

5.3 Cooling Jackets

As a first step, sample Nickel 201 pin-fin face plates for the forward cooling jacket were PCM'd to evaluate the artwork. The uniformity of the etched pattern over the specimen was excellent and the pin diameters and heights were to specification. The procedure was repeated for the aft jacket with satisfactory results. Following

ORIGINAL PAGE
BLACK AND WHITE PHOTOGRAPH

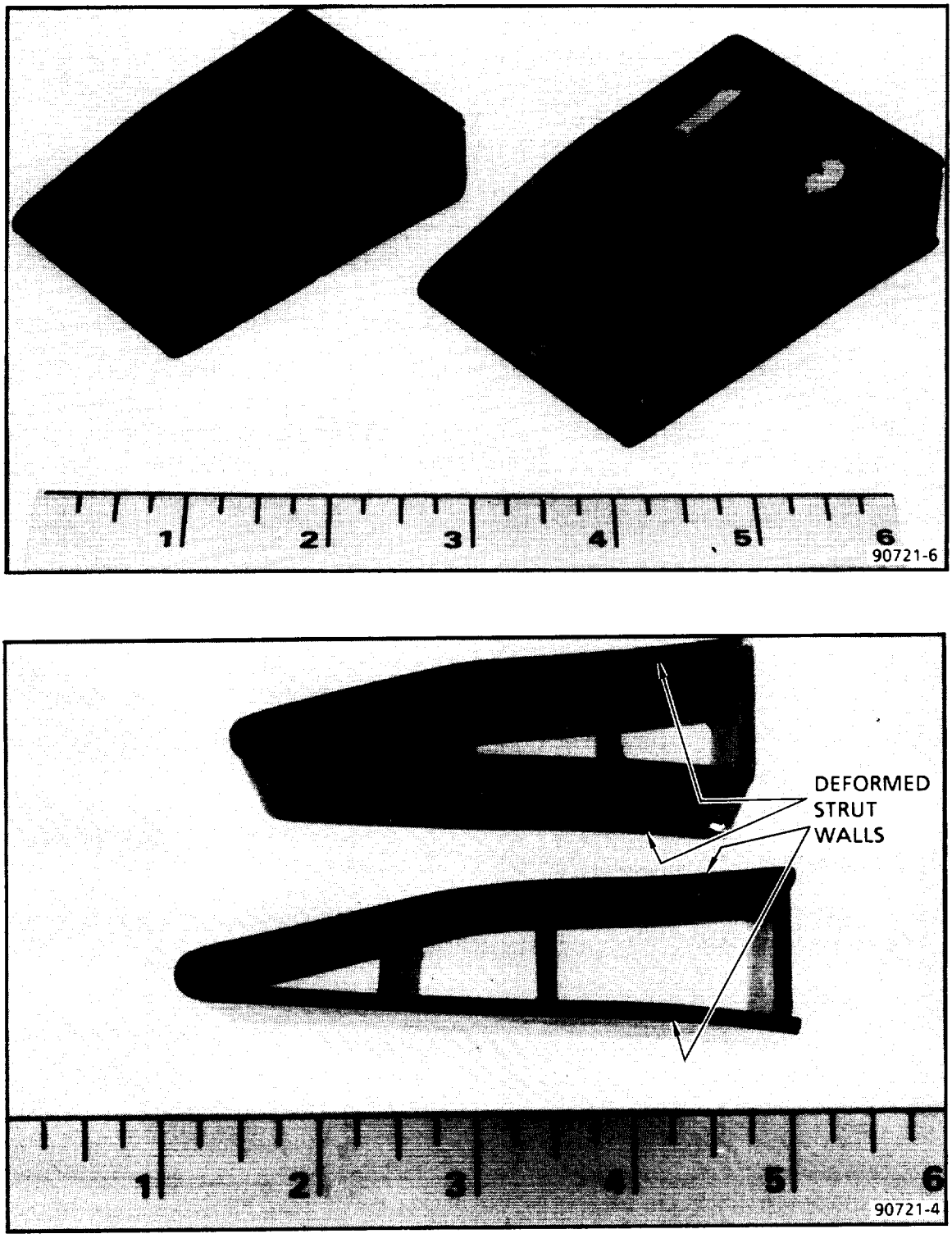

Figure 103. Support Structure Braze Loading Test Specimens

ORIGINAL PAGE
BLACK AND WHITE PHOTOGRAPH

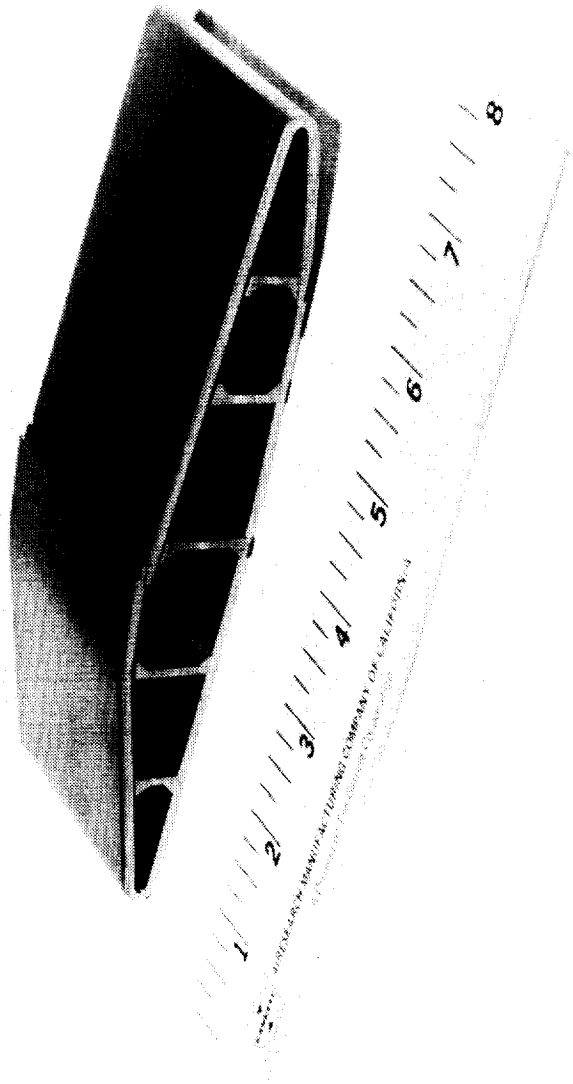

91636-7

Figure 104. Support Structure Braze Loading Test Assembly

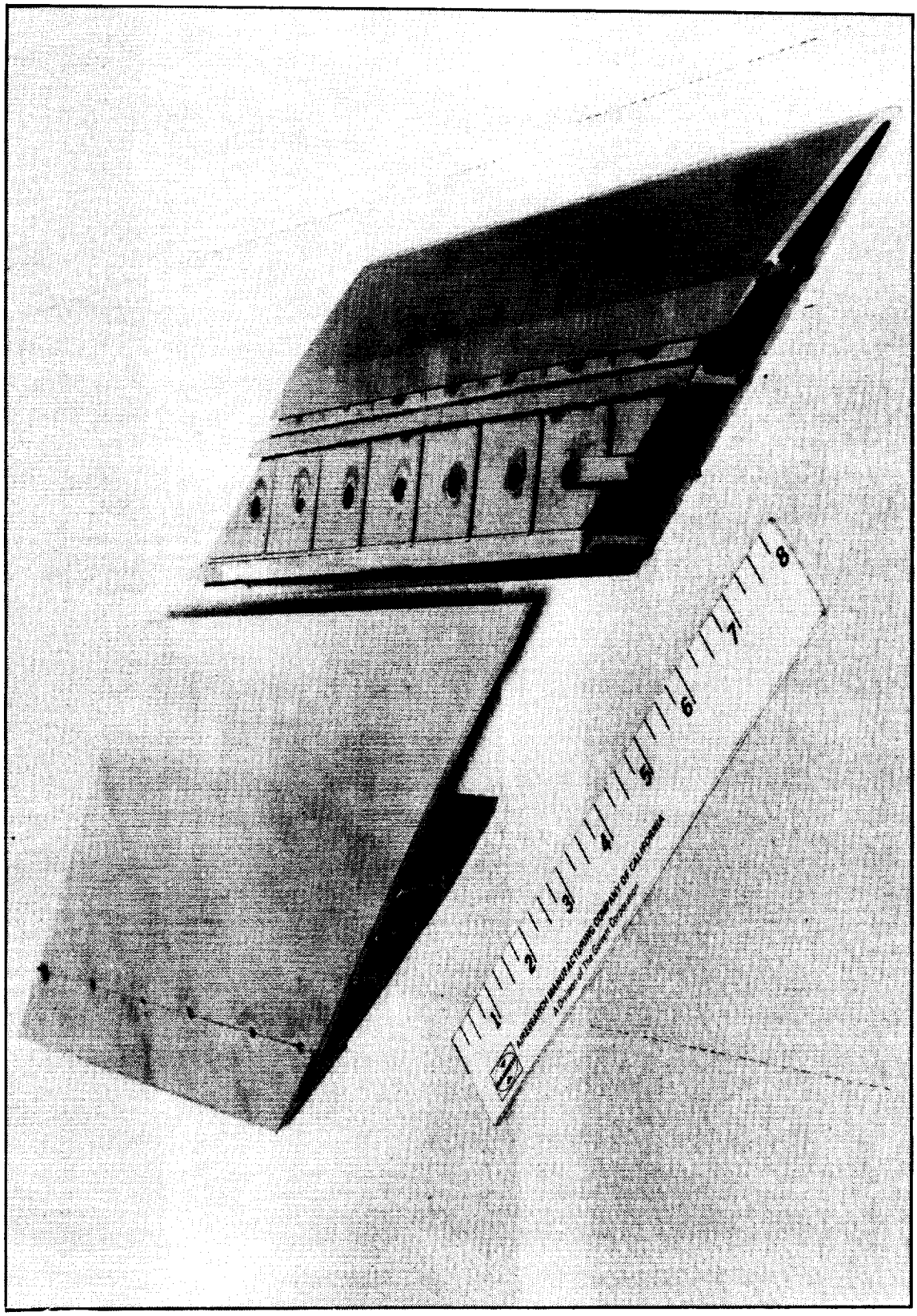

Figure 105. Assembled Forward and Aft Partial-Length Strut Details Prior to Braze

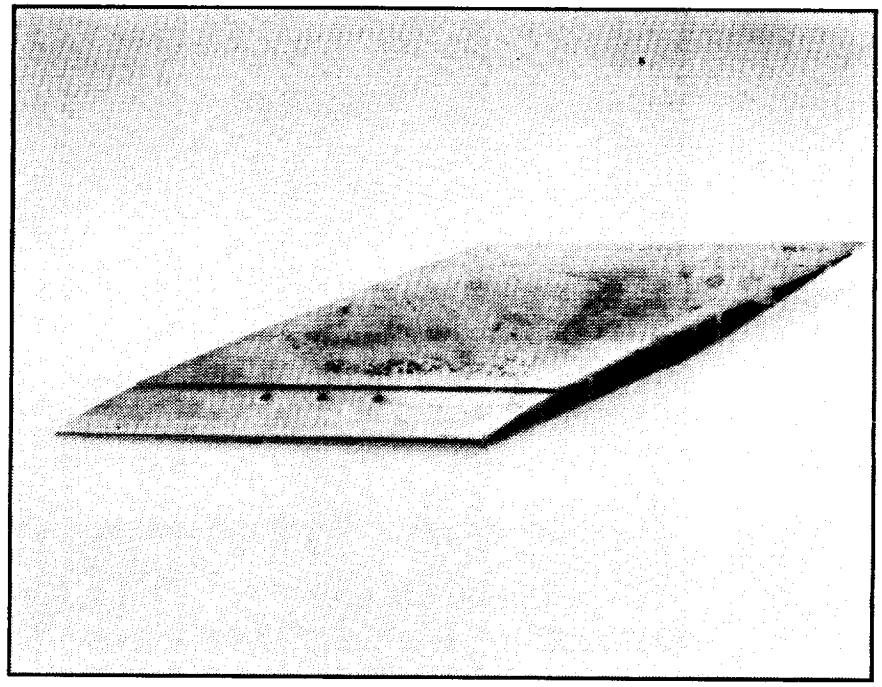

Figure 106. Brazed Partial-Length Strut (PL1)

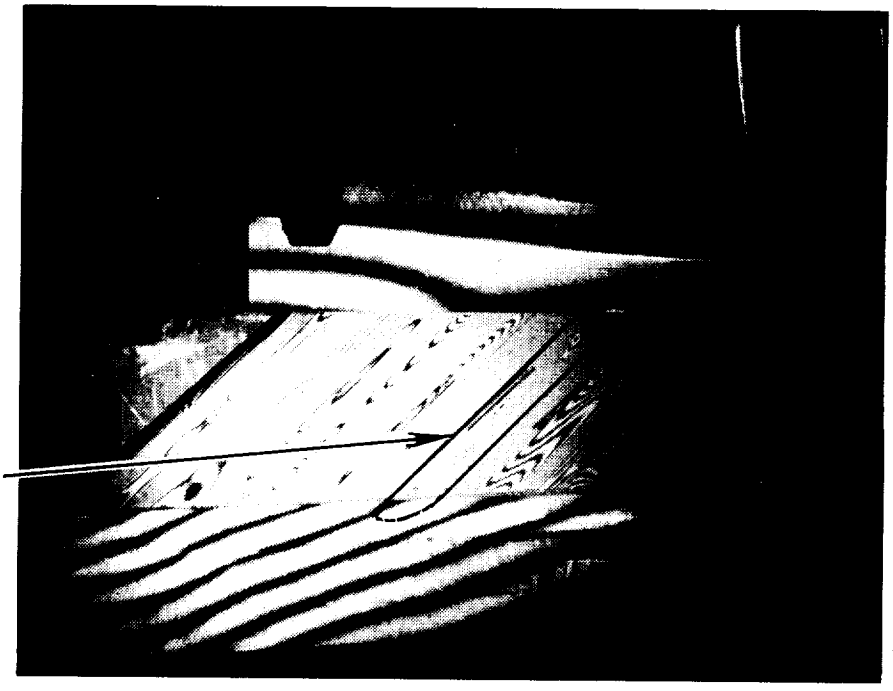

Figure 107. PL1 Hologram at 50 psi, Center Passage Side (One Beam with Intermittent Bond)

F-49933

Figure 108. PL1 Hologram at 50 psi, Sidewall Passage Side, After Rebraze of the Beams (No Indication of Unbonded Beams)

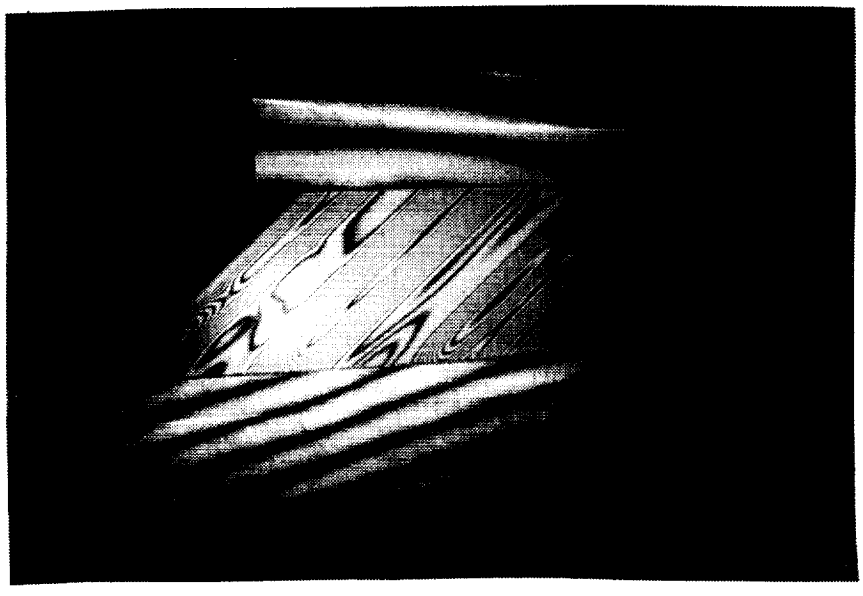

F-59251

Figure 109. PL1 Hologram at 50 psi, Center Passage Side, After Rebraze of the Beams (No Indication of Unbonded Beams)

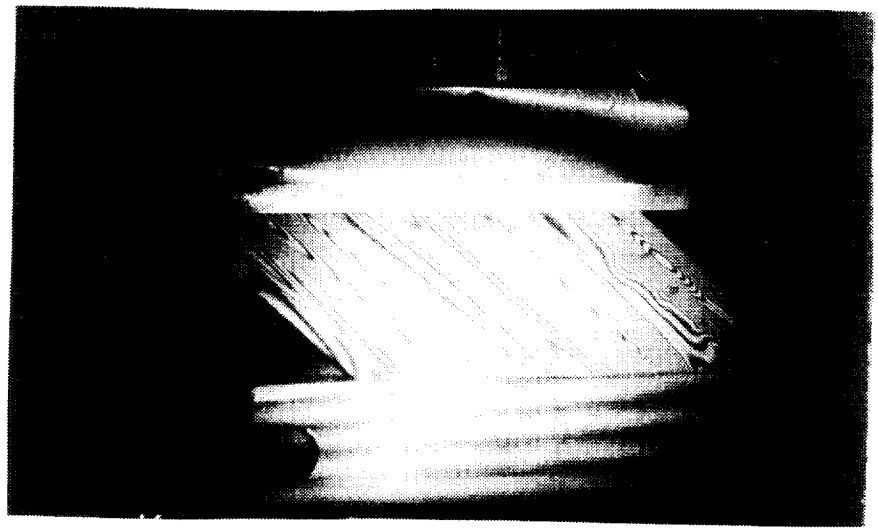

F-59252

Figure 110. PL1 Hologram at 50 psi, Sidewall Passage Side After Rebraze of the Beams (No Indication of Unbonded Beams)

this, the actual forward and aft face plates were etched. Figure 111 shows internal and external views of forward and aft face plates, respectively.

The aft jacket, which consists of a face plate, a cover plate, and 0.001-in. Palniro 1 filler alloy, was brazed without difficulty, Figure 112, and pressure-tested to 1500 psig. It was holographically pressure-tested to 1000 psig, Figure 113. No braze voids were found. X-ray examination shows no internal blockages by braze alloy, Figure 114.

In preparation for the next steps, a sample from an aft jacket assembly braze test was EDM'd in the flat to make the groove at the trailing edge. After EDM, the part was formed to the desired bend. During bending, the trailing edge groove narrowed approximately 50 percent (see Figure 115). For subsequent assemblies, the procedure was changed to form the jacket first and then machine the groove.

Dimensional inspection showed significant shrinkage of the brazed assemblies. A decrease of 0.060-in. was observed between two tooling holes approximately 10-in. apart. For the partial-length strut, this was acceptable; but if this shrinkage were proportionally larger for the full-length strut, the fuel injector pad holes would shift out of alignment.

Six series of tests were performed on samples of Nickel 201 sheet stock to determine the cause of the shrinkage. In each series of tests, the samples were subjected to the same braze temperature cycle. The test series included: tests with

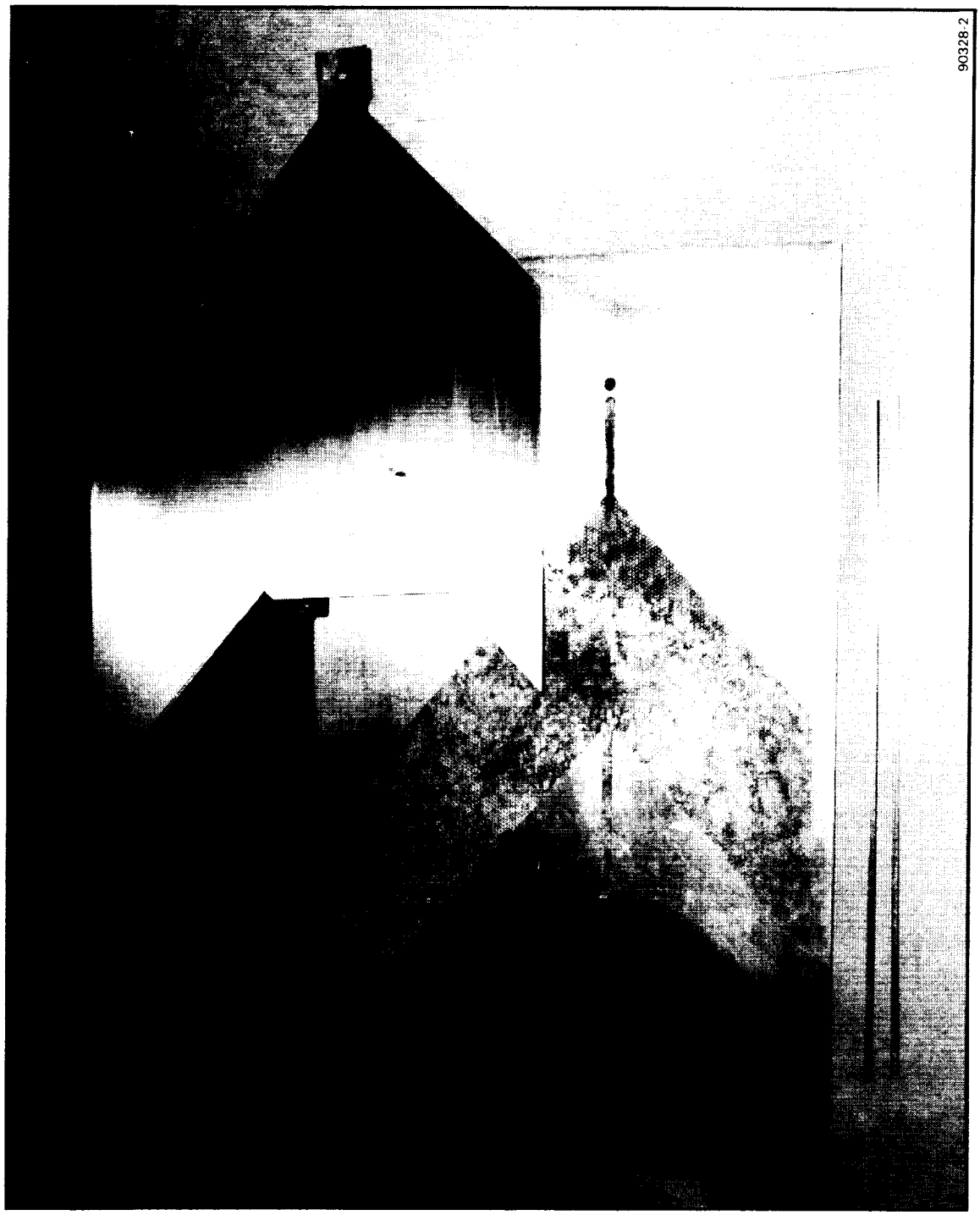

F-45660

Figure 111. Forward Cooling Jacket Pin-Fin Face Plates

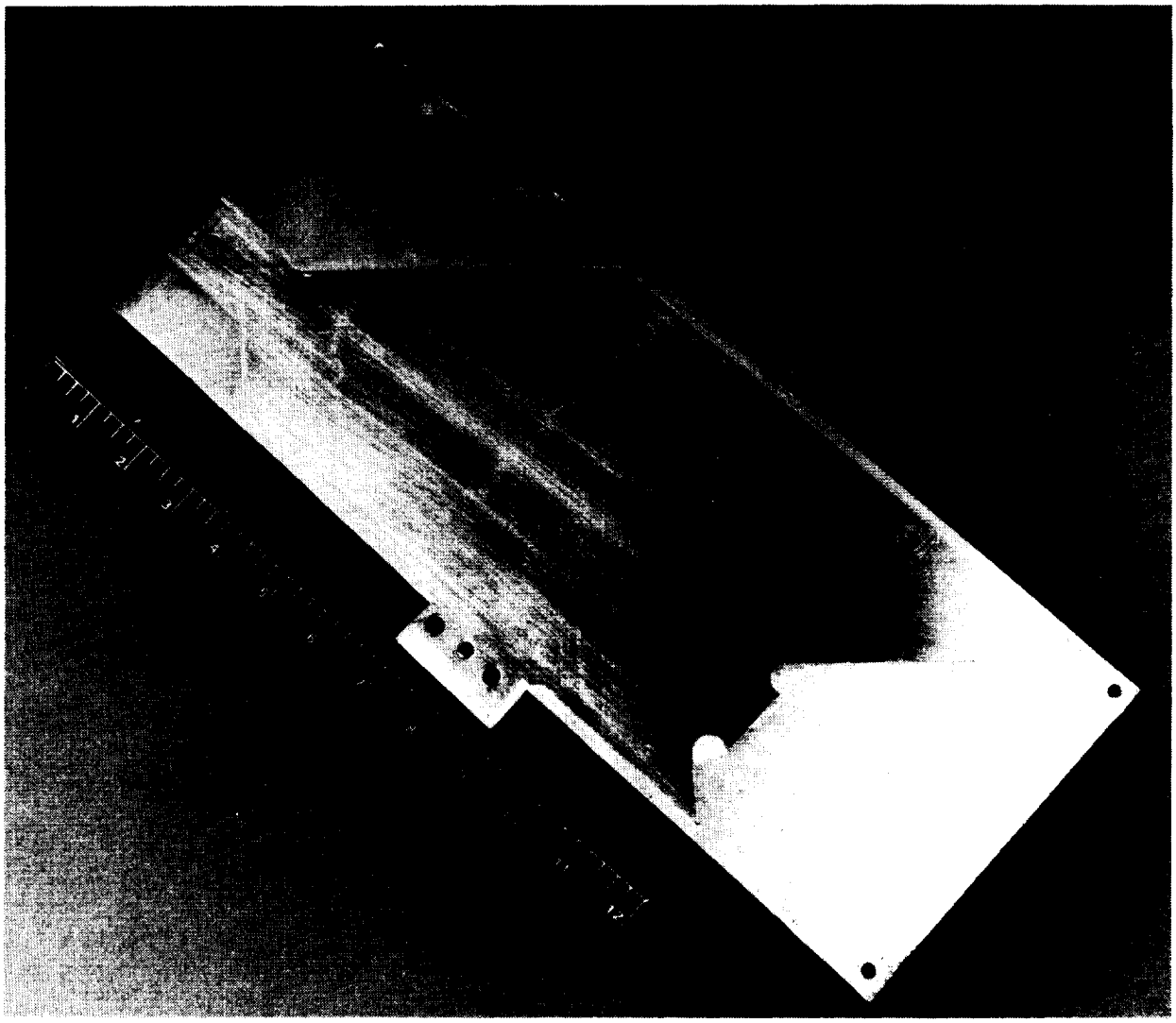

F-45728

Figure 112. Brazed Partial-Length Aft-Jacket Panel Assembly

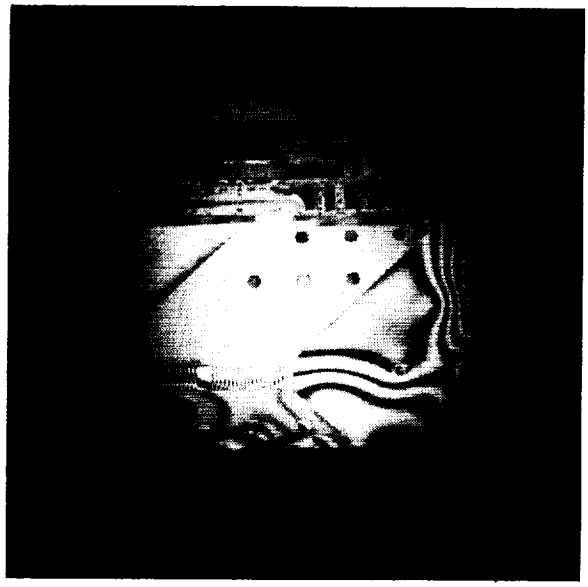

a. 500 PSIG

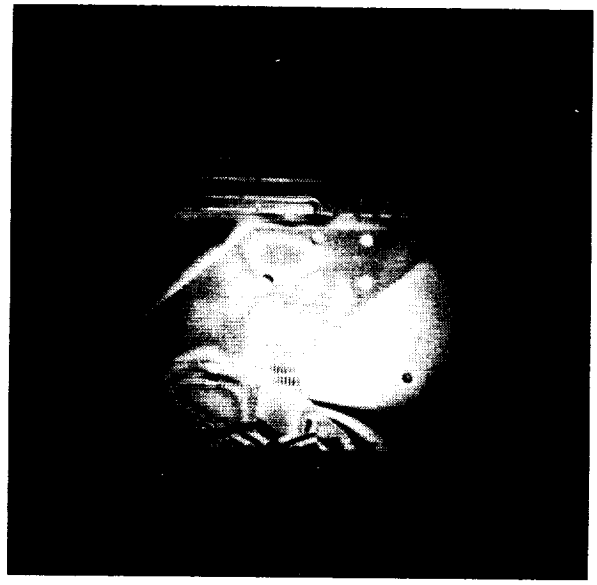

b. 1000 PSIG

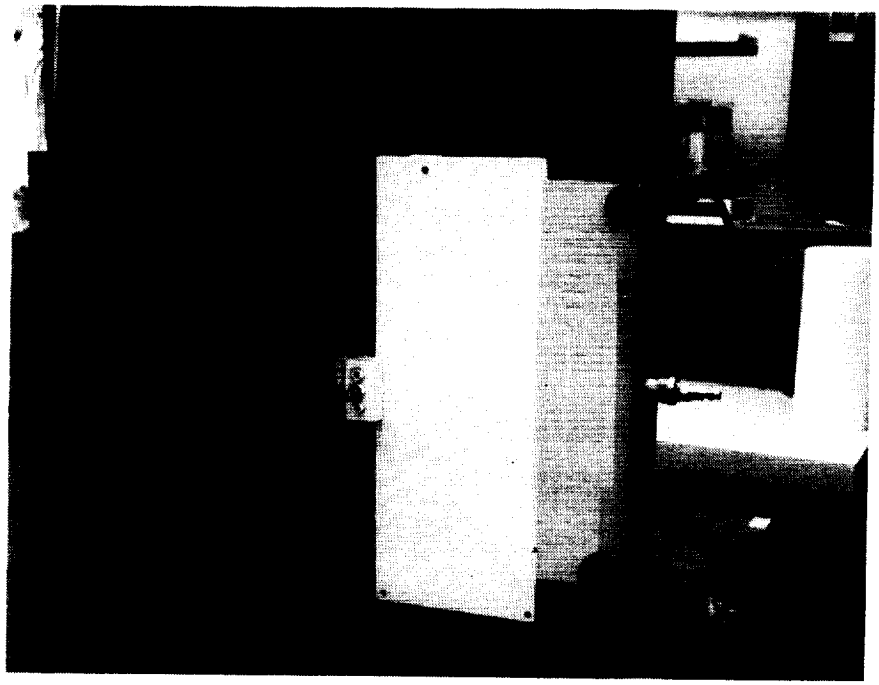

c. TEST SETUP

F-45726

Figure 113. Holographic Pressure Test of Aft-Jacket Panel Assembly (No Indication of Braze Voids)

NOTE: ALL INJECTOR HOLES ARE DRILLED AFTER BRAZE

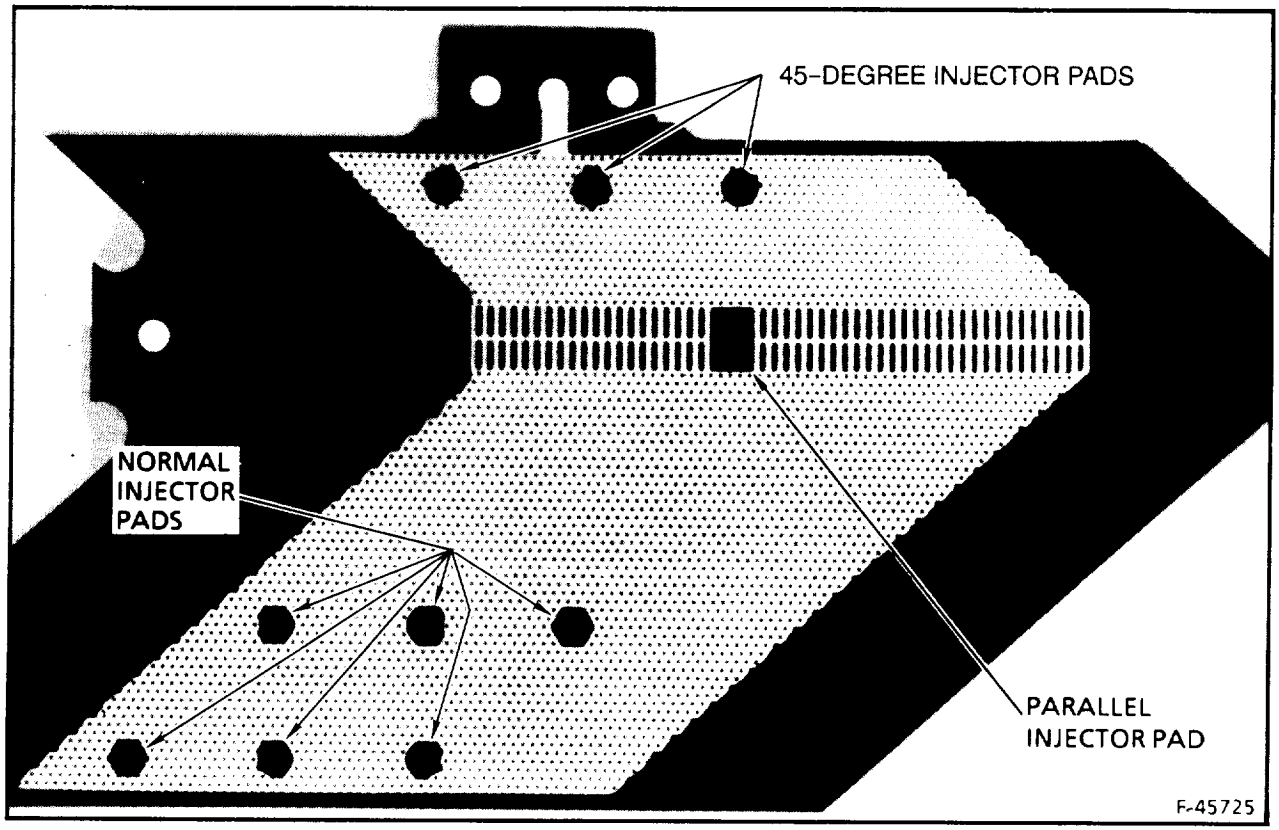

F-58506

Figure 114. X-Ray of Aft-Jacket Panel Assembly

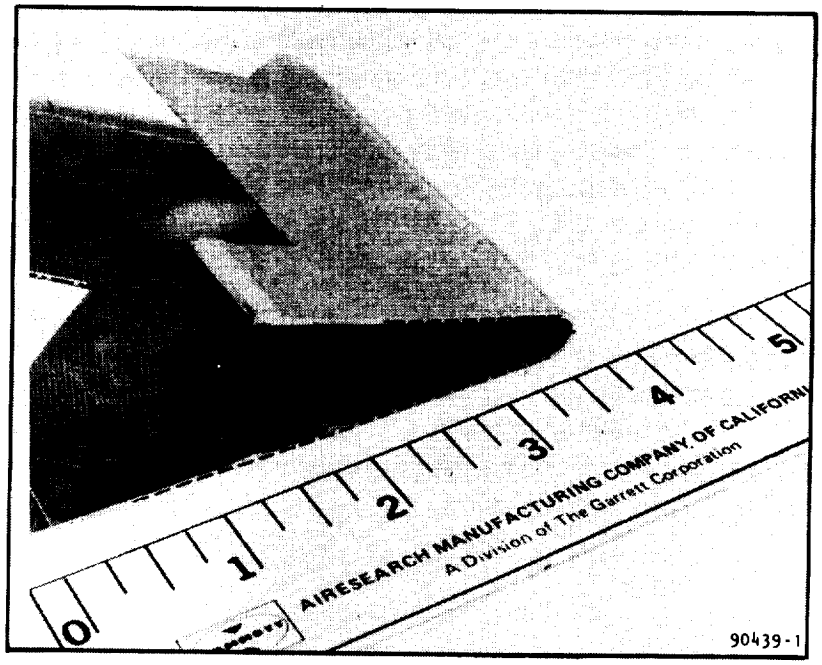

Figure 115. Aft-Jacket Bend Sample

F-60404

and without braze alloy, annealed and unannealed samples, samples before and after PCM (i.e., with and without pin fins), variations in the pressure history during the temperature cycle, and variations in slip sheet materials and orientation. Annealed PCM samples were annealed after PCM.

In the first series of tests, samples that were approximately 0.5 in. wide by 10 in. long were tested without braze alloy, slip sheets, and pressure forces. Annealed and unannealed samples with and without pin fins were tested. Test results indicated that shrinkage occurred only in the unannealed samples with pin fins. Consequently, it was thought that by annealing samples after PCM could be prevented.

In the second series of tests, annealed samples approximately 0.5 in. wide by 10 in. long were brazed using the same vacuum bag layup (Figure 116) and pressure history used during the PL cooling jacket braze operation. Samples with and without pin fins were tested. The results showed that all samples shrank from 0.020 to 0.030 in. in a 10-in. span. This suggested that the pressure load during the braze cycle was more significant than the annealed condition of the samples.

In the third series of tests, material samples (Figure 117) approximately 0.5 in. wide and 10 in. long were tested, without pressure loading, in a manner similar to the first series of tests. Again, test results indicated shrinkage occurred only in the unannealed sample with pin fins (the PCM'd sample).

In the fourth series of tests, samples approximately 2.0 in. wide and 12 in. long (Figure 118) were tested using the same vacuum bag layup used in the PL cooling jacket braze operation (Figure 116). In these tests, however, a pressure loading of 1 atm was maintained on the samples by evacuating the bag. Test results, which are similar to the results from the second series of tests, indicated that all of the samples shrank by 0.020 to 0.030 in.

In the fifth series of tests, two samples approximately 2.0 in. wide by 12 in. long (Figure 119) were vacuum bagged, as shown in Figure 116, and tested. In these tests, the pressure loading during the braze cycle was adjusted so that a pressure of 1 atm would be applied only while the samples were above 1900°F. The pressure during the balance of the cycle was 2 psi. In addition, the temperature history was slightly modified so that the temperature difference between the samples and the vacuum bag was less than 50°F during the cycle. Test results indicated no shrinkage in the test samples. Therefore, the modified temperature and pressure histories were selected for brazing the cooling jackets.

A PL forward jacket assembly was then brazed using the modified cycle, and the shrinkage reoccurred. Examination of the Refrasil cloth, a high-temperature fiber material used in the braze setup (Figure 116), indicated shrinkage of the cloth. This effect was not previously observed. Because of this unexpected shrinkage in the PL jacket and cloth, a sixth series of test samples was tested using the modified temperature and pressure histories. These samples incorporated various Refrasil

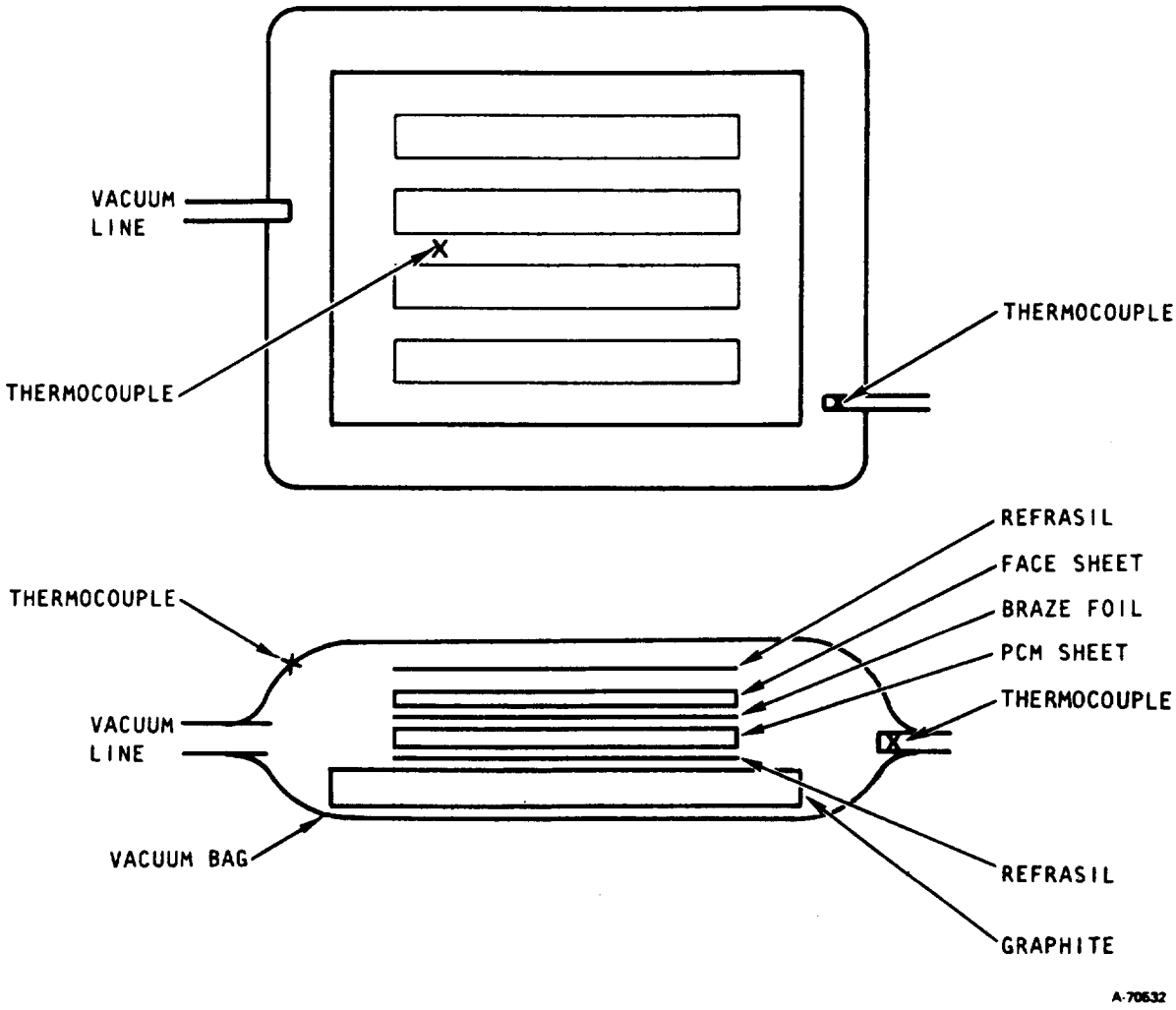

Figure 116. Setup of Jacket Panel Assembly for Brazing

weave orientations, annealed and unannealed sheet material, and the use of Fiberfrax and metallic slip sheets. The various combinations tested are shown in Figure 120. Test results indicated no shrinkage in any of the samples, indicating that the shrinkage in the second PL cooling jacket was probably caused by an unrecorded anomaly in pressure loading during the braze cycle.

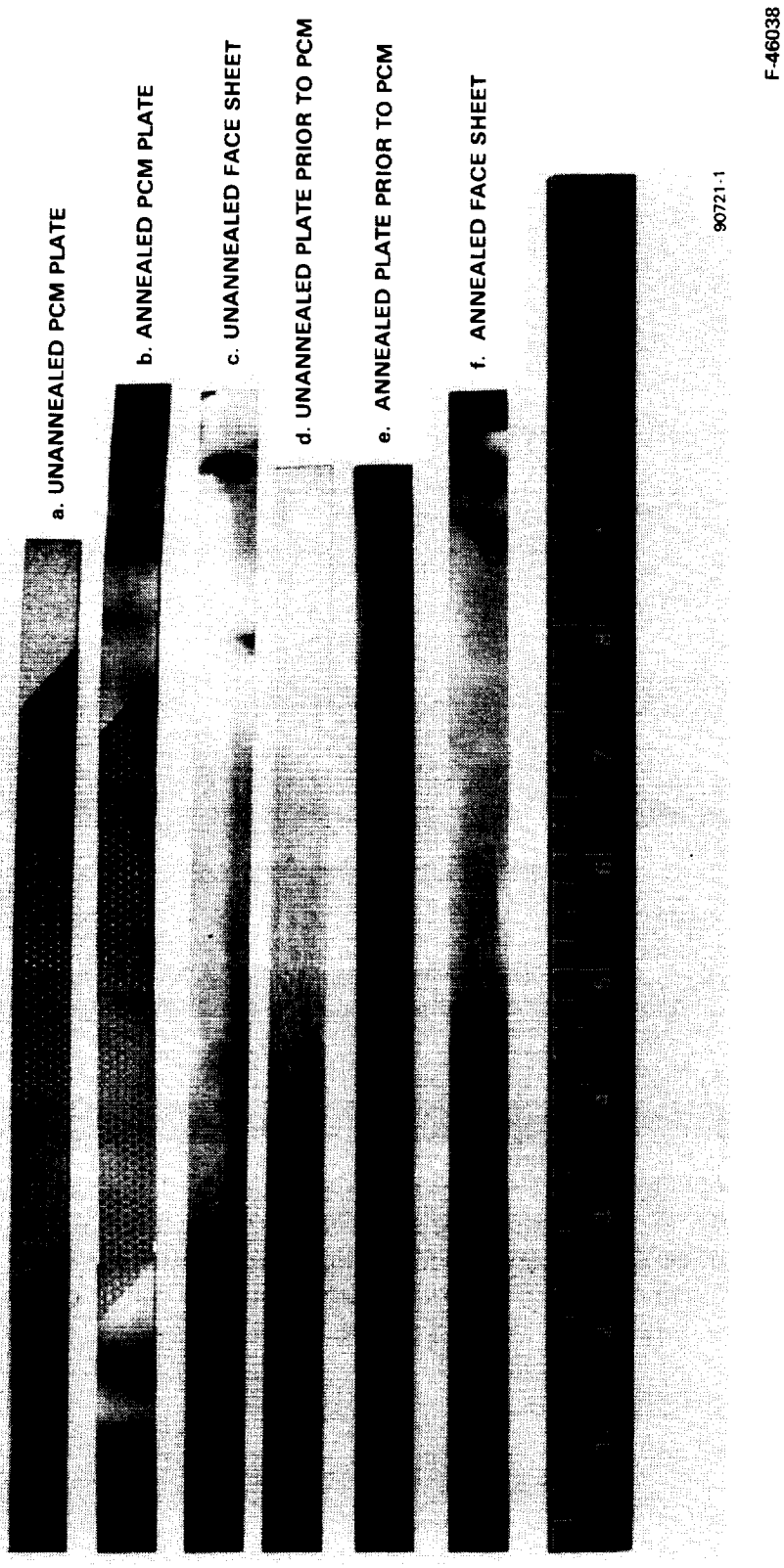

Figure 117. Bare, Unloaded Samples Exposed to Braze Cycle Temperature Profile

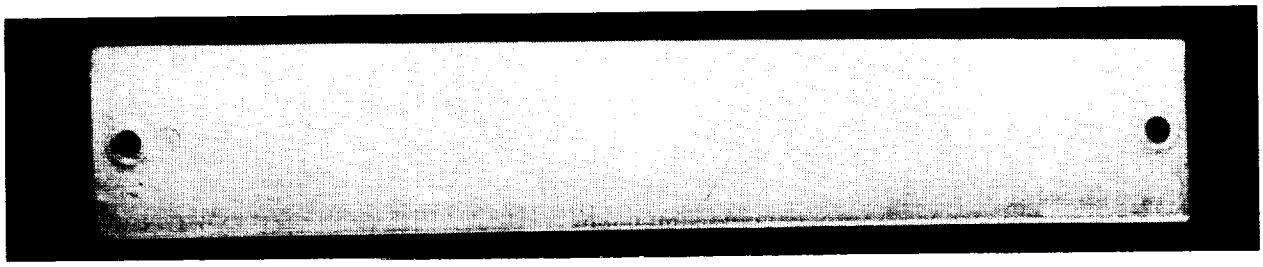

a. ANNEALED BRAZED SANDWICH SAMPLE

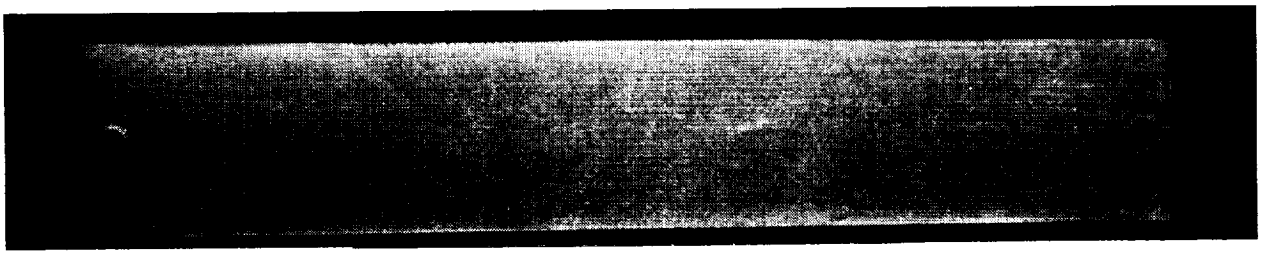

b. UNANNEALED BRAZED SANDWICH SAMPLE

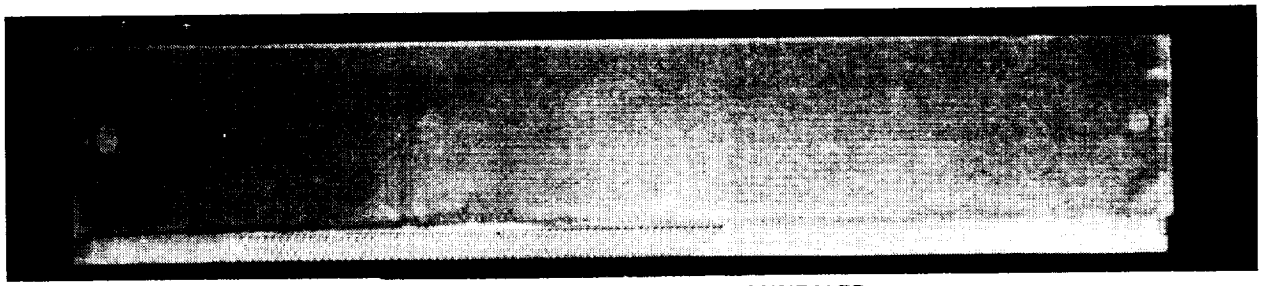

c. UNBRAZED SANDWICH - UNANNEALED

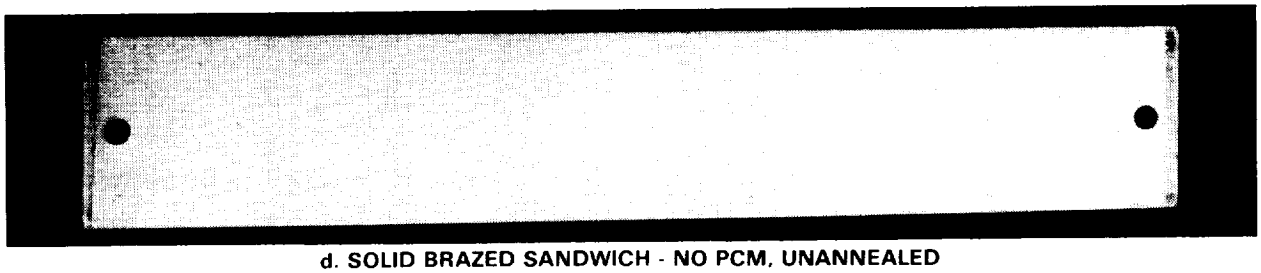

d. SOLID BRAZED SANDWICH - NO PCM, UNANNEALED

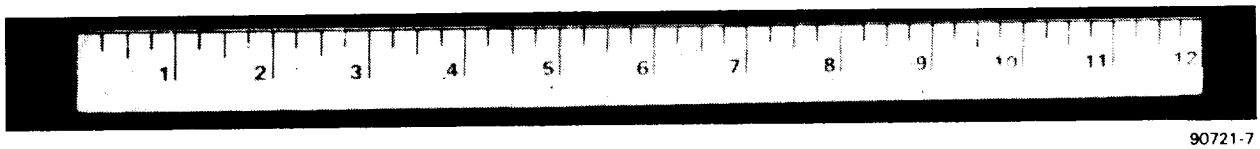

90721-7

F-46037

Figure 118. Samples Brazed in Original Vacuum Bag Layup

ORIGINAL PAGE
BLACK AND WHITE PHOTOGRAPH

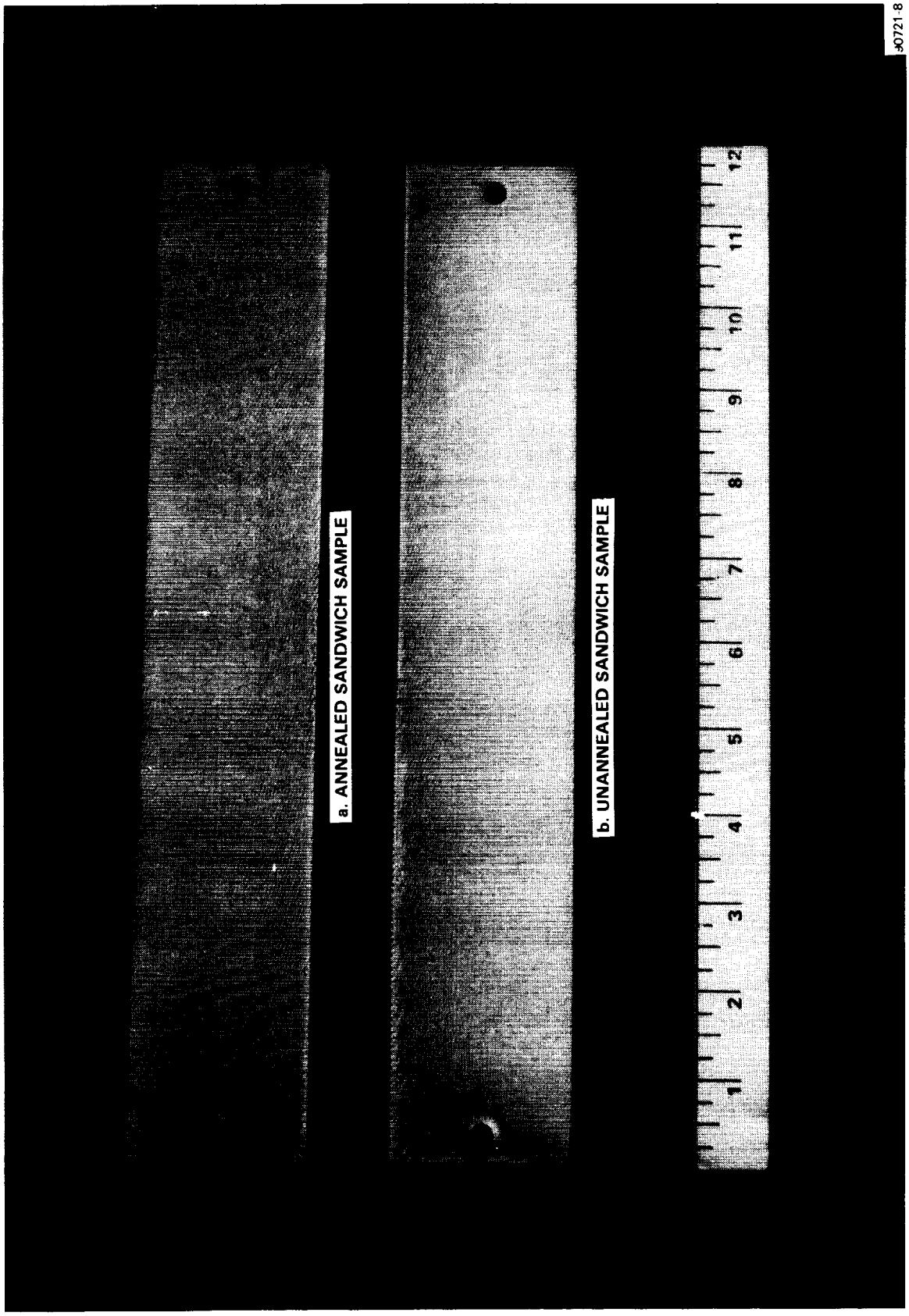

Figure 119. Samples Brazed in Modified Cycle

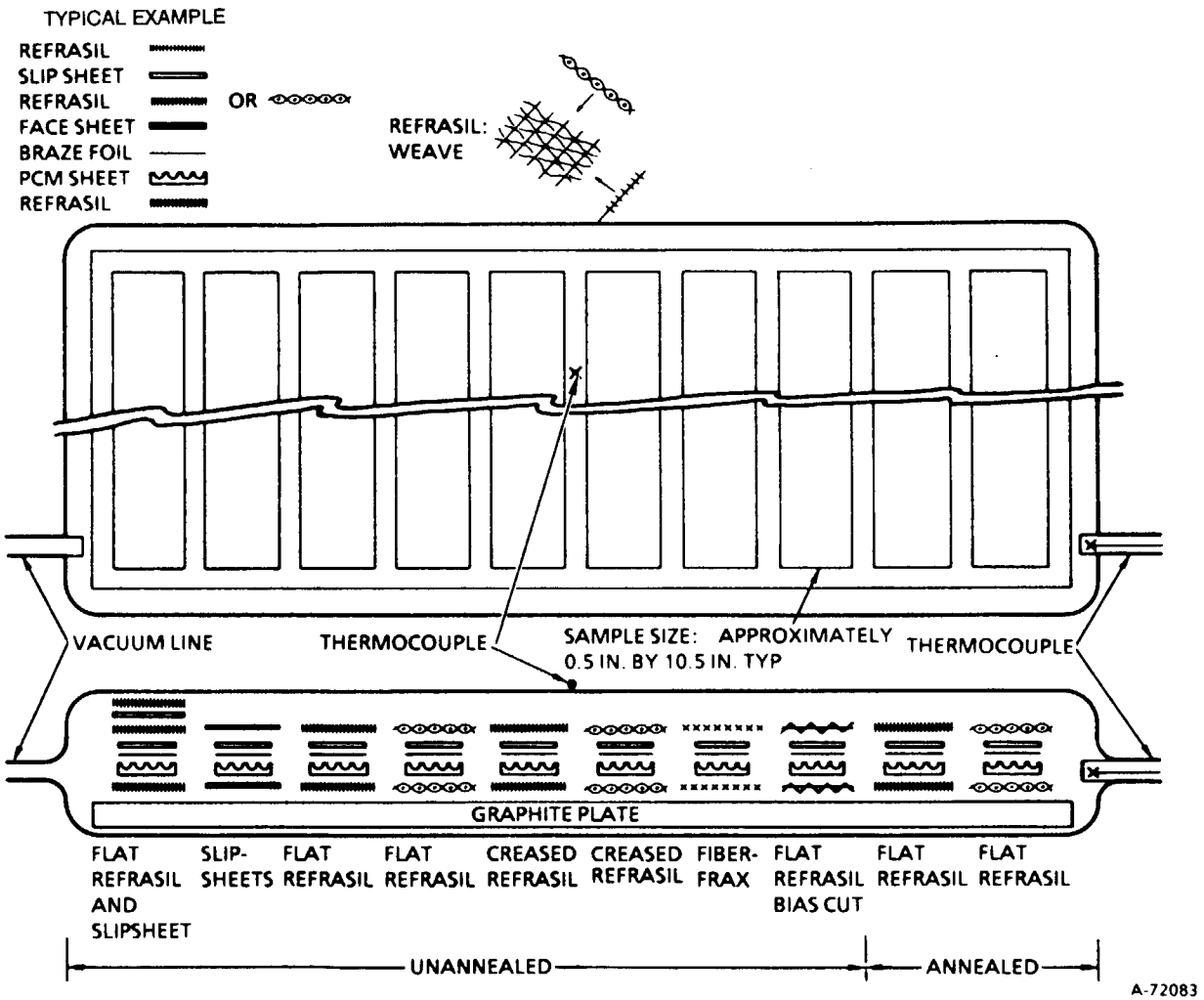

Figure 120. Setup for Braze Shrinkage Investigation with Multiple Test Samples

In order to confirm this conclusion, a test sample of the size of the forward PL cooling jackets was tested and no shrinkage occurred. Furthermore, no shrinkage occurred in a second set of PL forward and aft cooling jackets that were brazed using the modified temperature and pressure histories. Subsequently, these jackets were X-rayed and holographically pressure-tested to 500 psi. The aft panel displayed no blockage and the holographic tests, no indication of braze voids. The two forward panels had no blockage but had braze voids in some of the pin-fin to back sheet joints. Repair procedures were developed, as discussed below. Figure 121 shows the jacket panels during holographic tests.

To develop the braze-void repair procedure, a pin-fin sample was fabricated and artificially damaged. A 0.032-in.-diam hole was drilled 0.020 in. into the pin-fin plate starting from the cover plate side. This is deep enough to penetrate the cover plate, the braze joint, and 0.010 in. into the pin-fin. A 0.030-in.-diam wire was placed in the hole, braze alloy slurry was applied, and the jacket was rebrazed. Figure 122 shows a hologram of the sample pressurized at 250 psi. The repair area showed no more deflection than the surrounding brazed pin-fin joints. The two PL jackets were successfully repaired using this procedure. The repair areas were leak-tight and structurally sound.

At this point, the basic fabrication of the jackets was completed, and assembly with the support structure was started. Design changes in the cooling jackets, as discussed in para. 4.2.3, were not incorporated into the PL struts. Their implementation on the FL strut is described in para. 6.1.

5.4 Assembly

The PL1 cooling jackets were machined, drilled, and formed, using procedures described above, and were tack-welded to the Inco-718 support structure. Figure 123 shows the formed aft jacket, including a view into the trailing edge groove. The PL aft structure design included a representative, aft-facing fuel injection hole, as shown in Figure 124. The corresponding injector hole in the jacket was match-drilled. The three representative sidewall injector holes were directly drilled through the jacket and into the structure. After disassembly and cleaning, Palniro 7 filler alloy was applied, and the jackets were tacked to the body for brazing. Figure 125 shows the PL1 assembly after brazing. Items that are noted are discussed below.

Following brazing, the assembly was leak-tested. There were several leaks at the edges of the jackets, and braze voids between the jacket and the structure were noted in the area of the fuel tubes and the trailing edge of the aft jacket. A series of three braze repair cycles were used to stop the leaks.

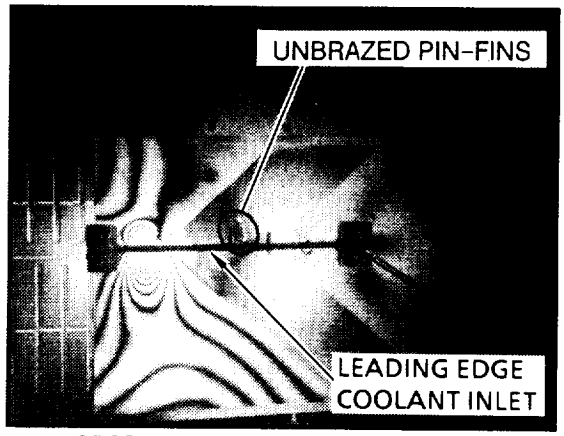

SECOND FORWARD JACKET 125 PSI

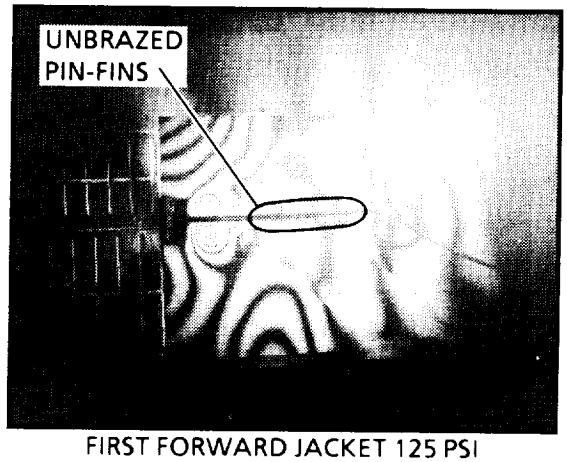

FIRST FORWARD JACKET 125 PSI

SECOND AFT JACKET 250 PSI (NO BRAZE VOIDS)

B-19609

Figure 121. Holographic Pressure Tests of Partial-Length Cooling Jackets

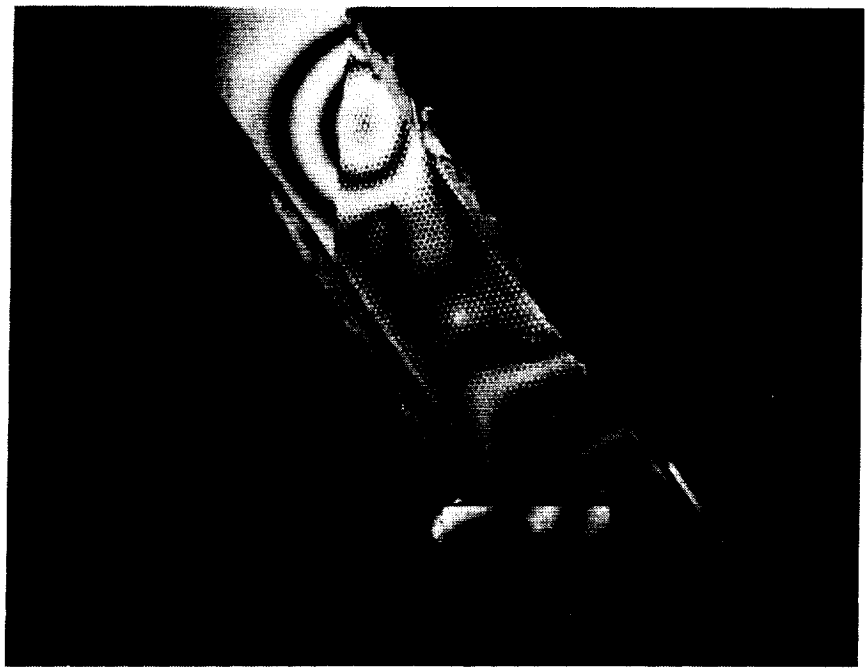

F-59253

Figure 122. Hologram of Repaired Panel Specimen at 250 psi (No Braze Voids)

The first repair used Palniro 7 and involved adding a cover plate to the leading edge, inserting additional filler alloy shim material at the trailing edge gap, inserting tube inserts into existing fuel tubes, applying slurry to seal the leaks at the edge of the jackets, and repeating the braze cycle. Leaks at the leading edge of the forward jacket, the trailing edge of the aft jacket, and at the fuel injector tubes were stopped with this cycle, but not the jacket-edge leaks. The second repair braze cycle to stop the leaks at the edge of the jackets was made at the same time the end covers were brazed to the support structure using Nioro at 1800°F.

The third repair braze cycle for the pin-hole leaks at the cooling jacket edges was a repeat of the cycle using Nioro. Upon completion of this cycle, the assembly was run through a final series of holographic tests. Figure 126 shows the test setup and holograms of the two sides. Maximum proof pressure was limited to 500 psig because of the voids near the leading edge and the 45-deg side fuel injection ports. Holography was limited to 250 psig as a safety precaution. The results for the PL1 assembly led to a number of changes in the stacking and brazing of the PL2 assembly. Important changes included the following:

- Hot-sizing of the formed cooling jackets on PL2 at 1 atm pressure loading and 1600°F for 45 min
- Increased number of fit-check inspections during stacking

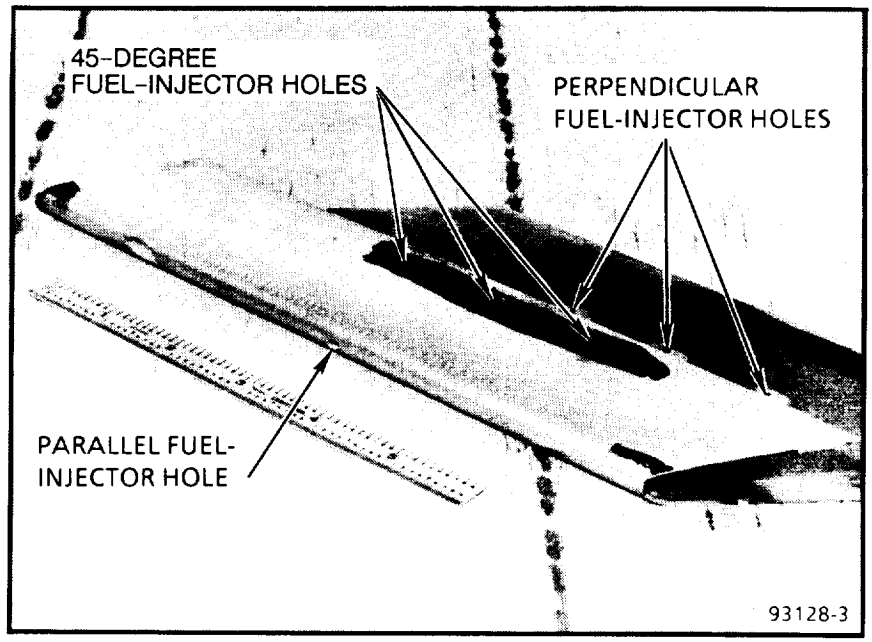

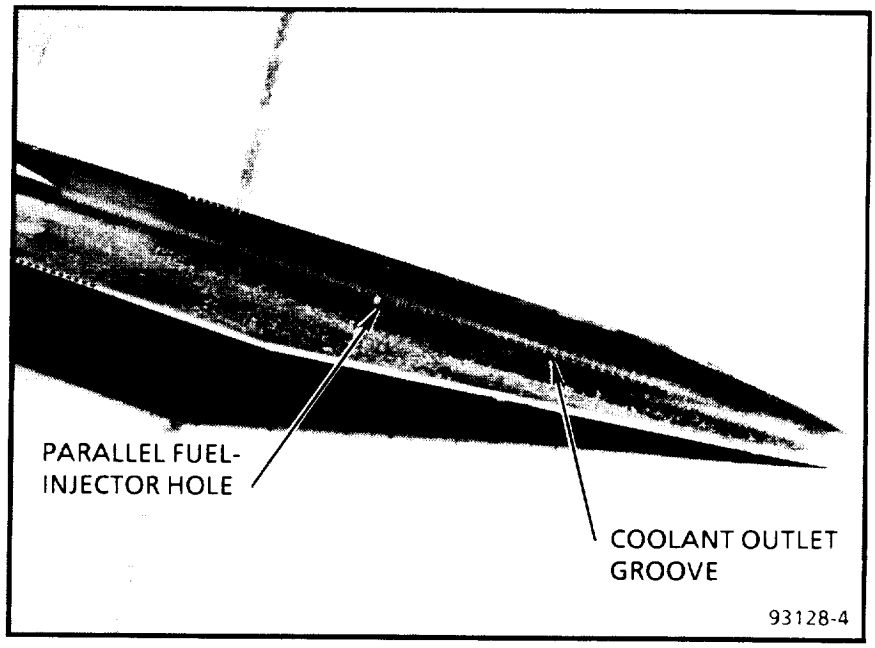

Figure 123. Formed Partial Length Aft Cooling Jacket (PL1)

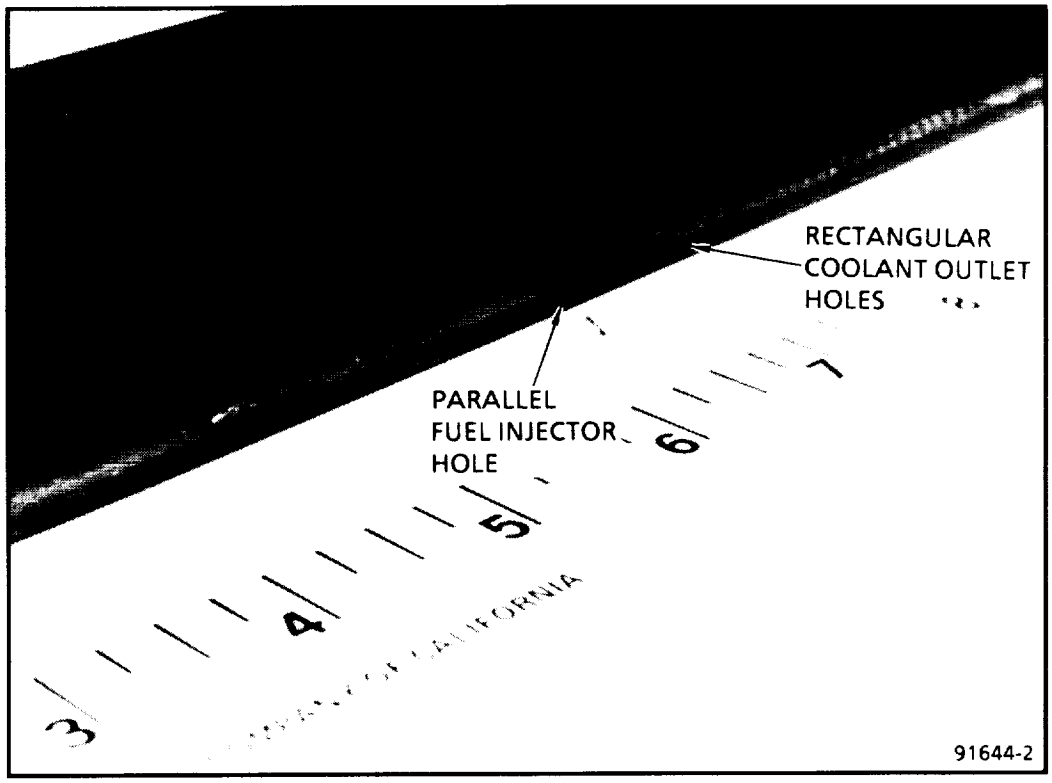

B-19610

Figure 124. Aft Support Structure Following EDM of Holes

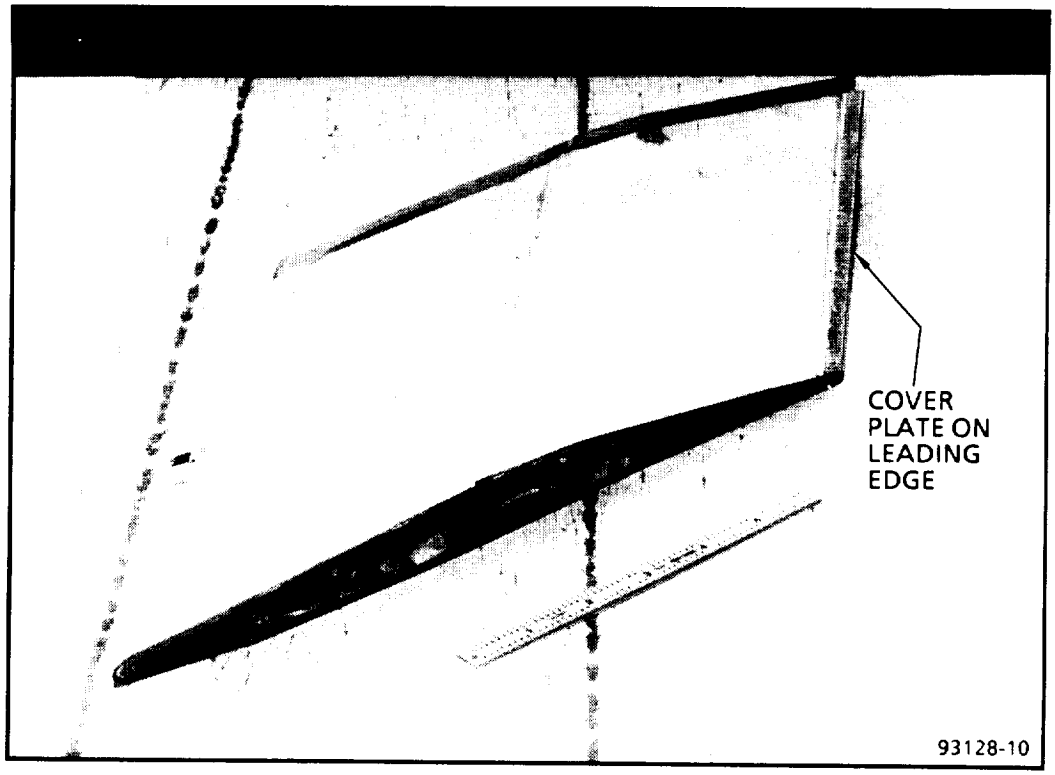

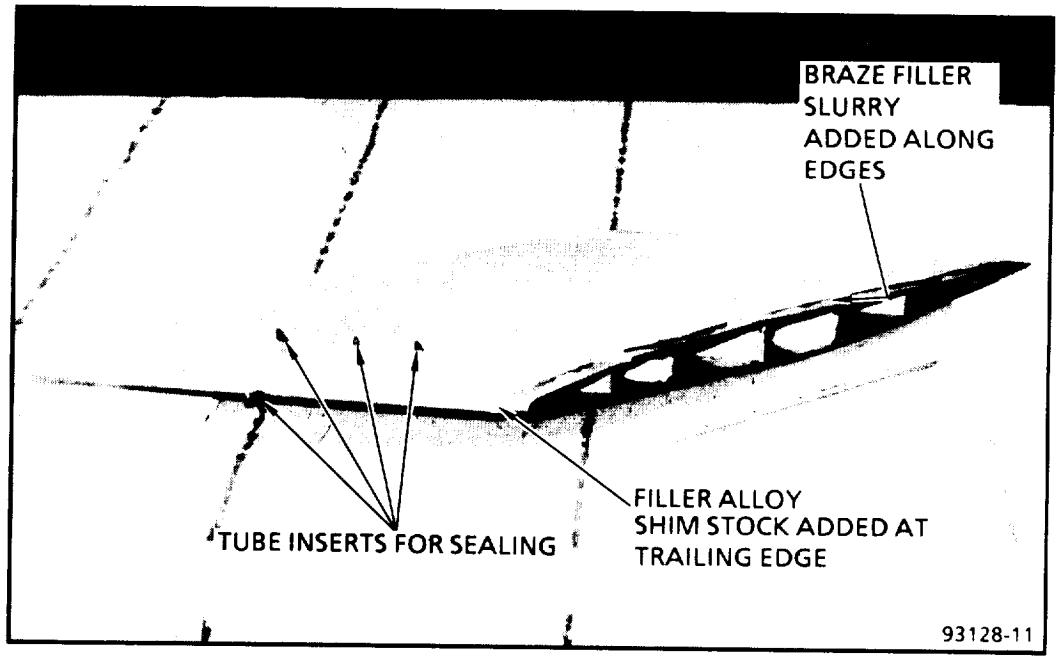

B-19611

Figure 125. Partial-Length Strut PL1 Brazed Assembly

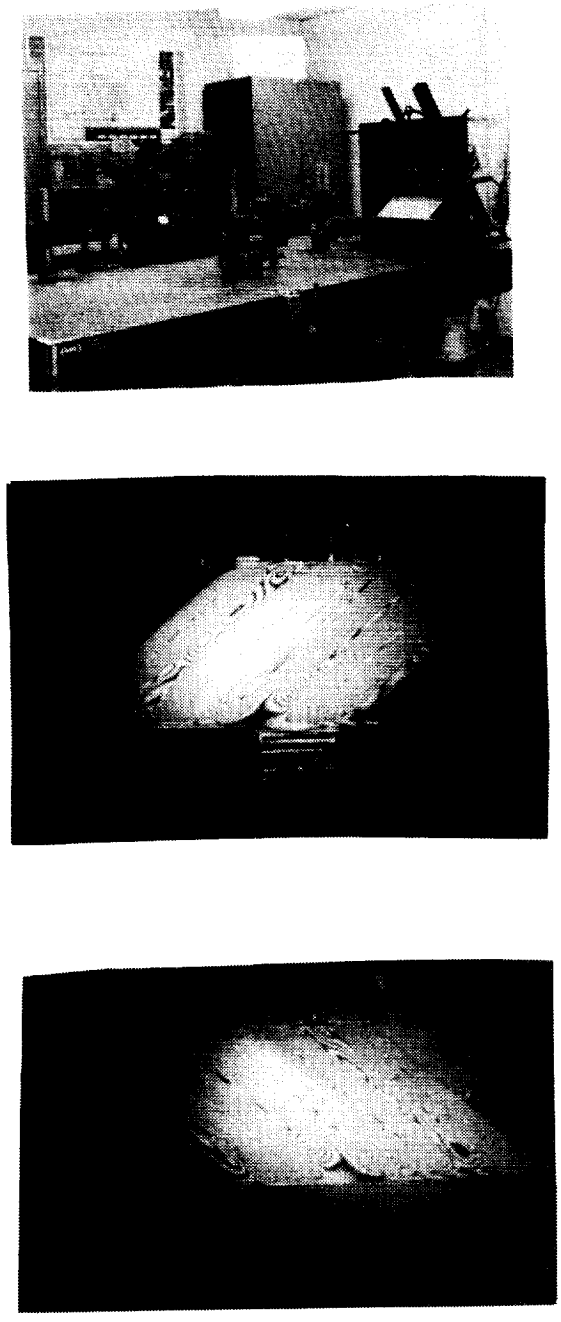

F-59254

Figure 126. Holographic Test Setup and Holograms of Partial-Length Strut PL1 (No Braze Voids)

- Improved fixturing during tack-welding of the jacket to avoid gaps created by the welds, and use of fewer welds to minimize the potentially detrimental restraints.

- More selectivity in application of slurry to minimize the potential for plugging coolant passages.

In general, PL1 established the brazing setup for the various stages and verified that correct and uniform temperatures were being maintained during the braze cycle. Rebrazing by adding filler alloy was shown to improve or repair deficient joints at all three stages of brazing.

The PL2 jacket-support structure assembly was brazed with Palniro 7 with the changes noted above, subsequently leak-tested at low pressure, and X-rayed. Holographic tests were omitted at this stage because of the difficulty of mechanically sealing the ends. There was no low-pressure leakage, but the X-rays showed plugging in the bottom 1 1/4 in. of the pin-fin material at the leading edge, in the slots at the trailing edge from the top of the pin-fin area to approximately 0.6 in. below the fuel injector tube, and in the crossover slot between the front and aft jackets on the center passage side. This side was facing down during the braze cycle. Figure 127 shows an X-ray calibration of the strut to facilitate identification of plugged areas. The observed plugging was not correctable short of grinding off both forward and aft jackets. Instead, the cover plates were added in the third braze cycle (Nioro) and the strut was pressure-tested. Figure 128 shows the PL2 assembly ready for test. Figure 129 shows holograms at 50 psig and at 1000 psig for 100 psid. For the latter, the reference hologram was taken at 900 psig, and the pressure was raised to 1000 psig for the difference hologram. The 1000 psig holograms indicate some localized anomalies, but no excessive deflections.

During the next step of testing, the pressure was raised to 1200 psig, and the aft-most beam joint separated. To continue the tests, the aft section of the assembly was cut away (Figure 130) and the fuel tubes plugged. The forward strut cavities were left unpressurized and the aft cavities were pressurized to 1750 psig. As a result of a fuel-tube plug leak, the test was stopped for the repair and then resumed. On repressurization after repair, a beam separated at 450 psig. The numerous pressurization cycles used in reaching 1750 psig apparently caused sufficient fatigue damage to produce the break.

Figure 131 shows holograms at 1500 psig referenced to 1450 psig (50 psi difference between exposures) that were made during the 1750-psig test series. When compared to the original set of holograms, deflections were generally larger during this second series of tests, indicating possible damage to the joints as a result of plastic deformation from the repeated pressure test loads following the aft joint separation.

The PL2 assembly was next sectioned and analyzed. The beam-to-wall joints measured 0.004 to 0.005 in. The braze void area along these joints varied from 5 to

ORIGINAL PAGE
BLACK AND WHITE PHOTOGRAPH

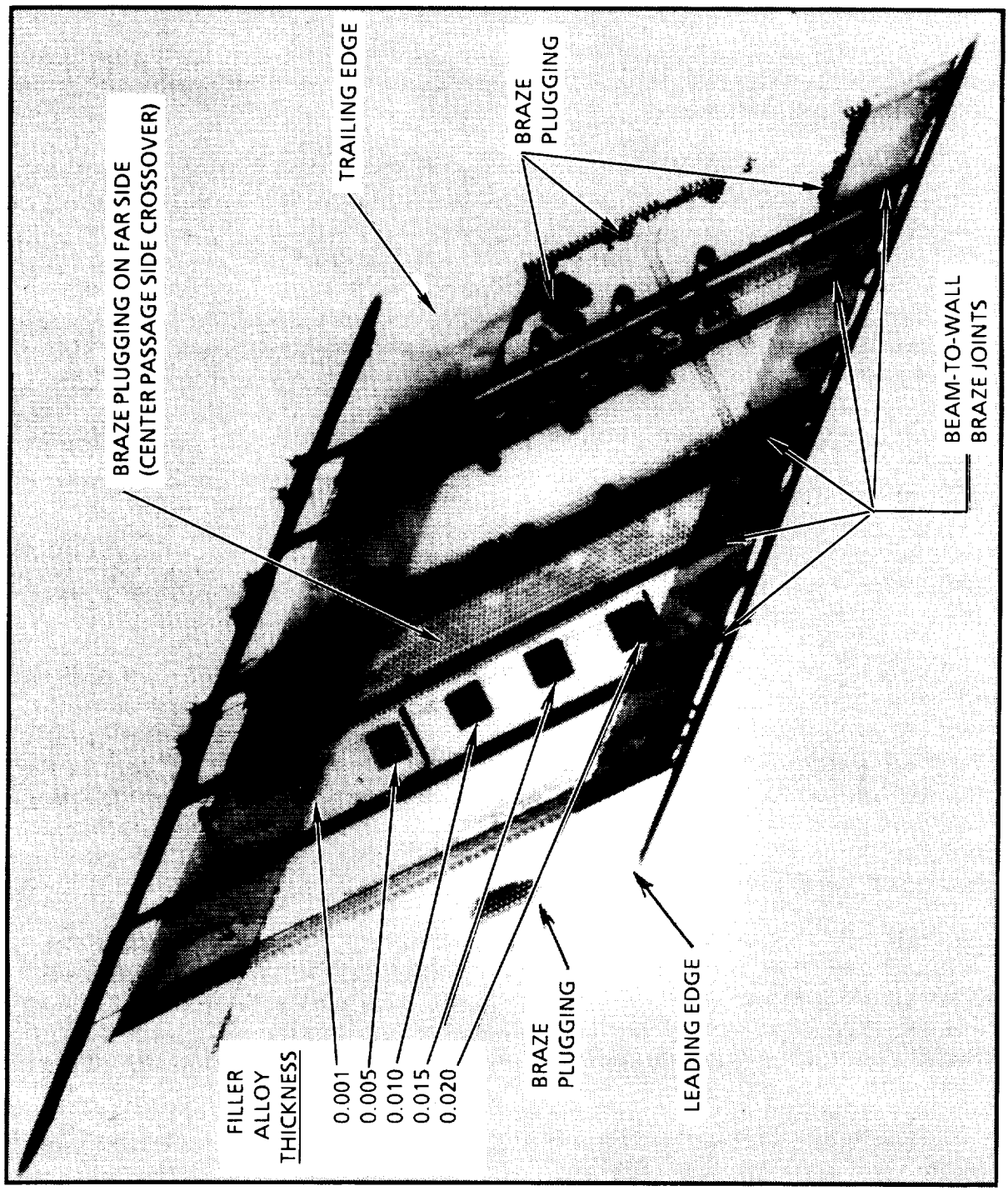

Figure 127. Calibration X-ray of Completed PL2 Assembly

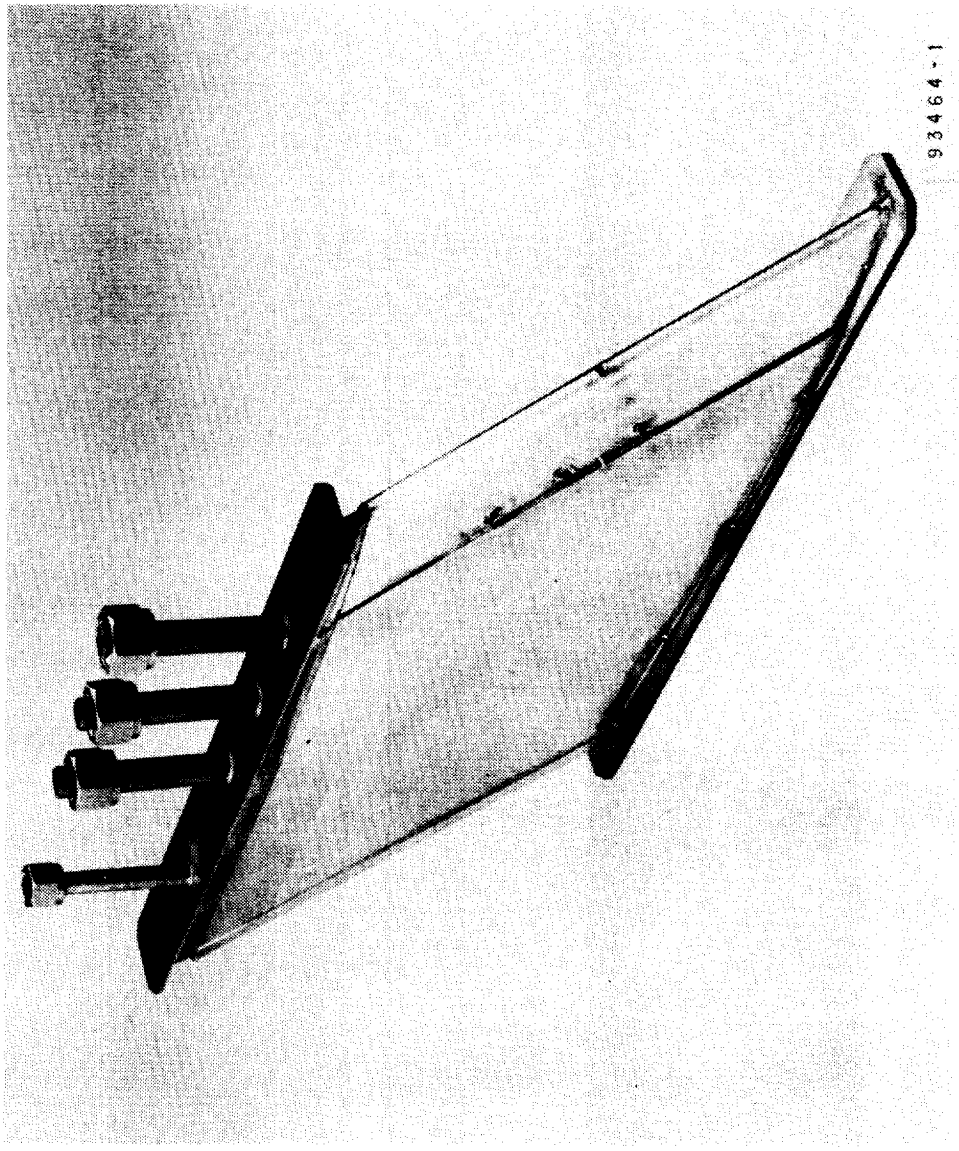

Figure 128. PL2 Assembly Ready for Pressure Test

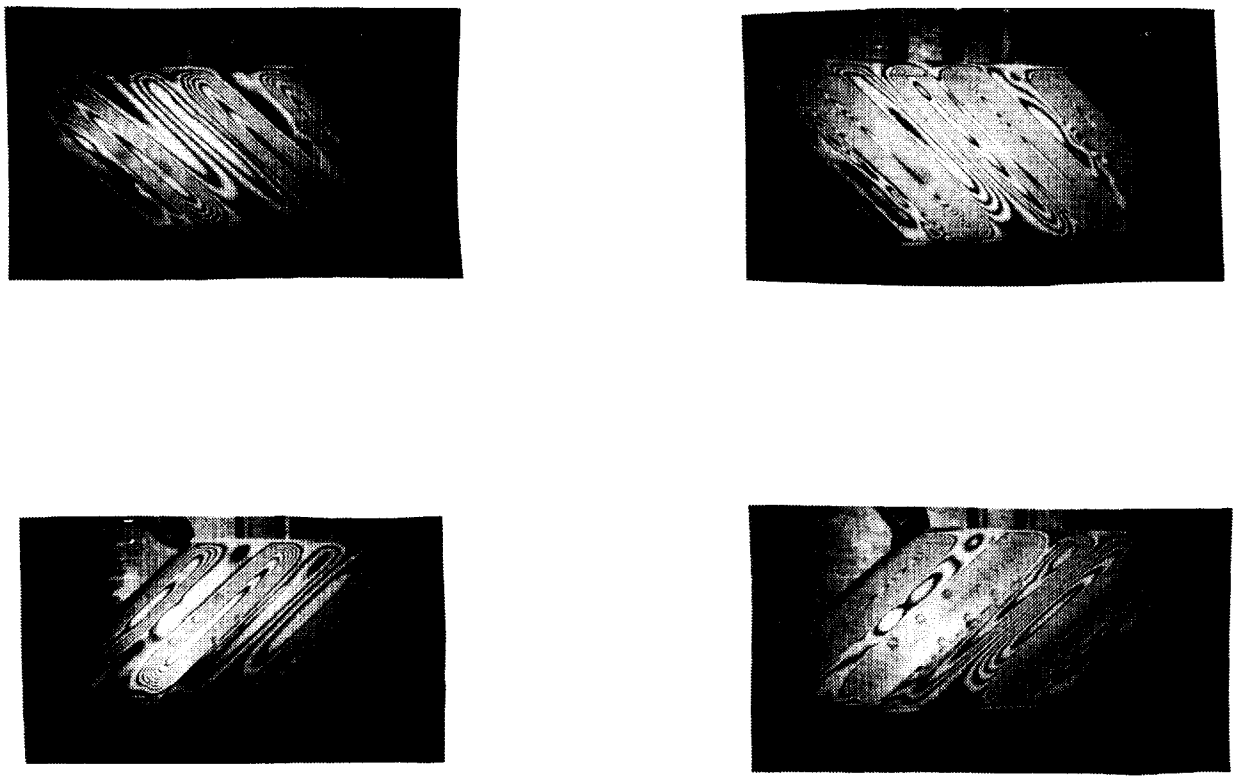

F-59255

Figure 129. Holograms of PL2 Assembly (No Braze Voids)

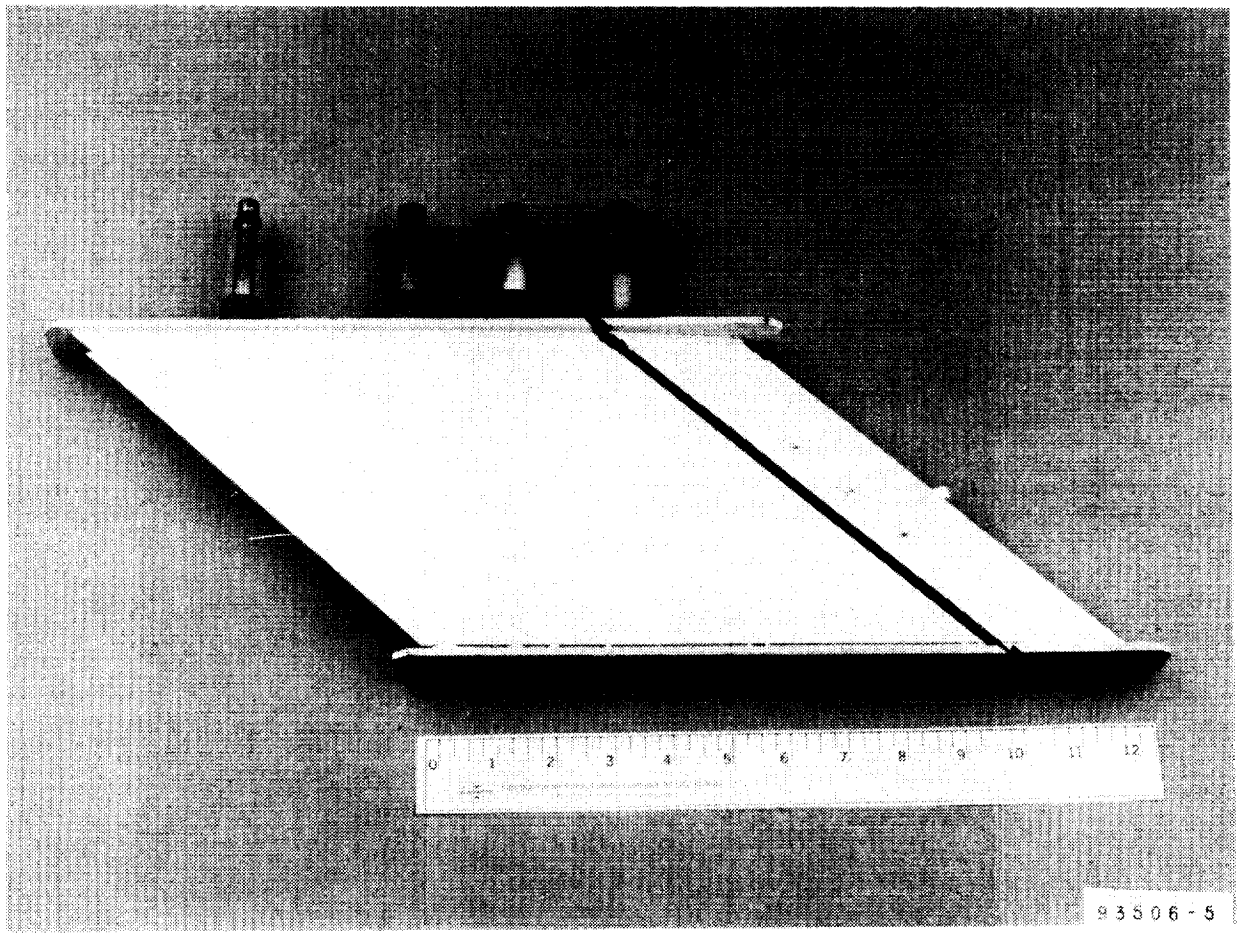

Figure 130. Removal of Aft-Beam Strut Section of PL2 Assembly

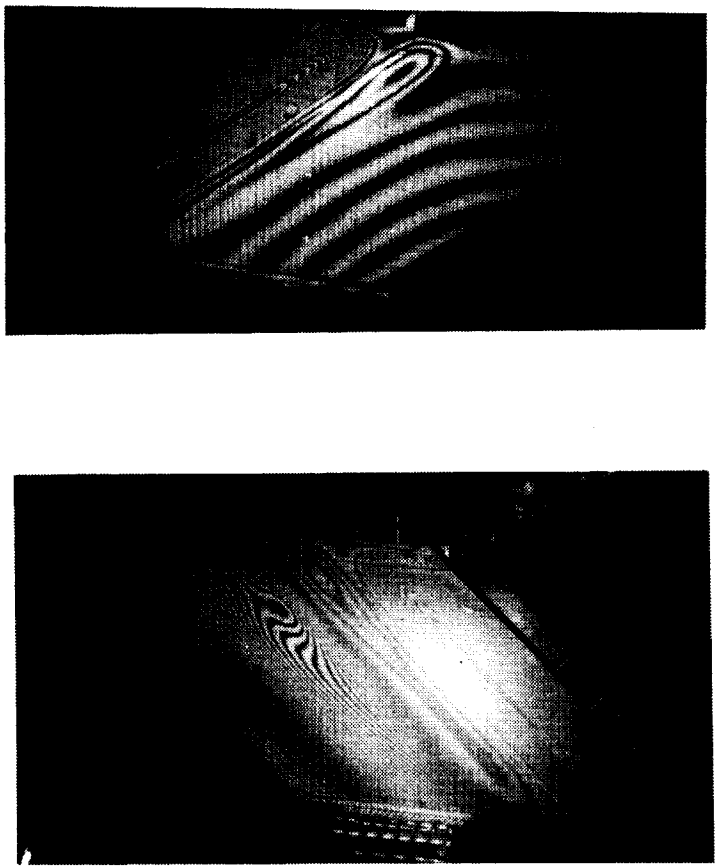

F-59256

Figure 131. Holograms of PL2 Assembly after Removal of Aft-Most Beam Section, at 1500 psig Referenced to 1450 psig (No Braze Voids)

75 percent. Selected beam joints that remained integral were tensile-tested, and showed strengths from 20 to 60 ksi (see Section 4).

The jacket-to-structure braze joint was also reviewed. The joint gap measured 0.003 to 0.005 in. and the void areas totaled approximately 20 percent. The hot-sizing of the cooling jacket prior to brazing thus reduced the braze void height and area versus the first strut, but was insufficient by itself to eliminate voids.

Figures 132 and 133 show two of the sections through the strut. Figure 132 shows the aft-most beam separation that occurred during the initial test series (at 1200 psig). This is the section that was cut away for the final pressure test series. Figure 133 is a section taken after the final test series and shows the beam separations that occurred at 450 psig after previous pressurization to 1750 psig. The joint sections in Figures 132 and 133 showed no evidence of being brazed—the result of large gaps that remained after assembly for brazing.

The results obtained from the two partial-length struts were used to define a series of investigations aimed at exploring each of the problem areas encountered. The parameters affecting the joining of specific features, alternative designs, and the manufacturing procedures were explored. These are discussed in Section 4, along with a number of other investigations that were undertaken to aid initial fabrication of the strut components and assemblies.

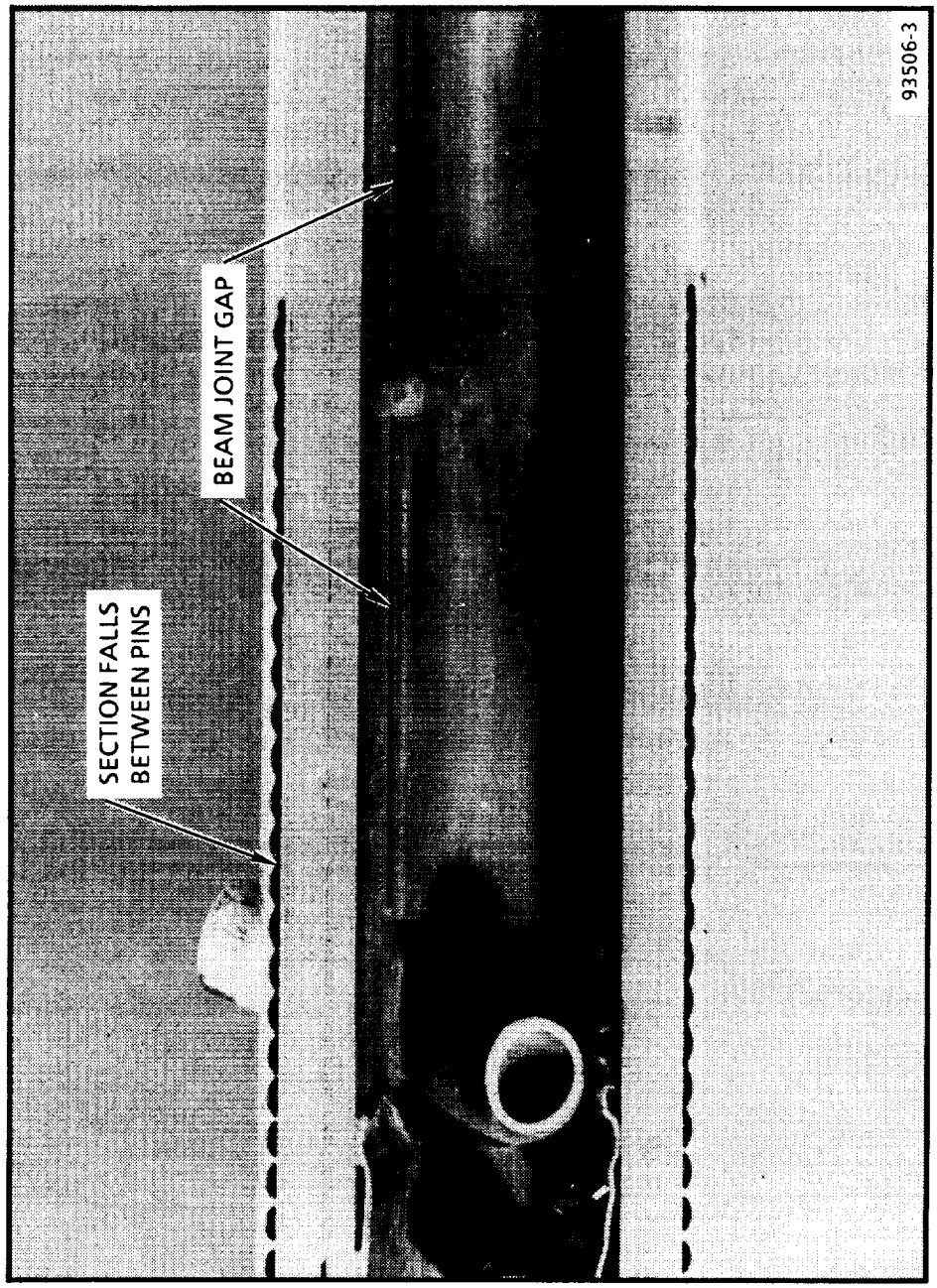

Figure 132. PL2 Aft-Most Beam Joint Gap After Initial Test Series

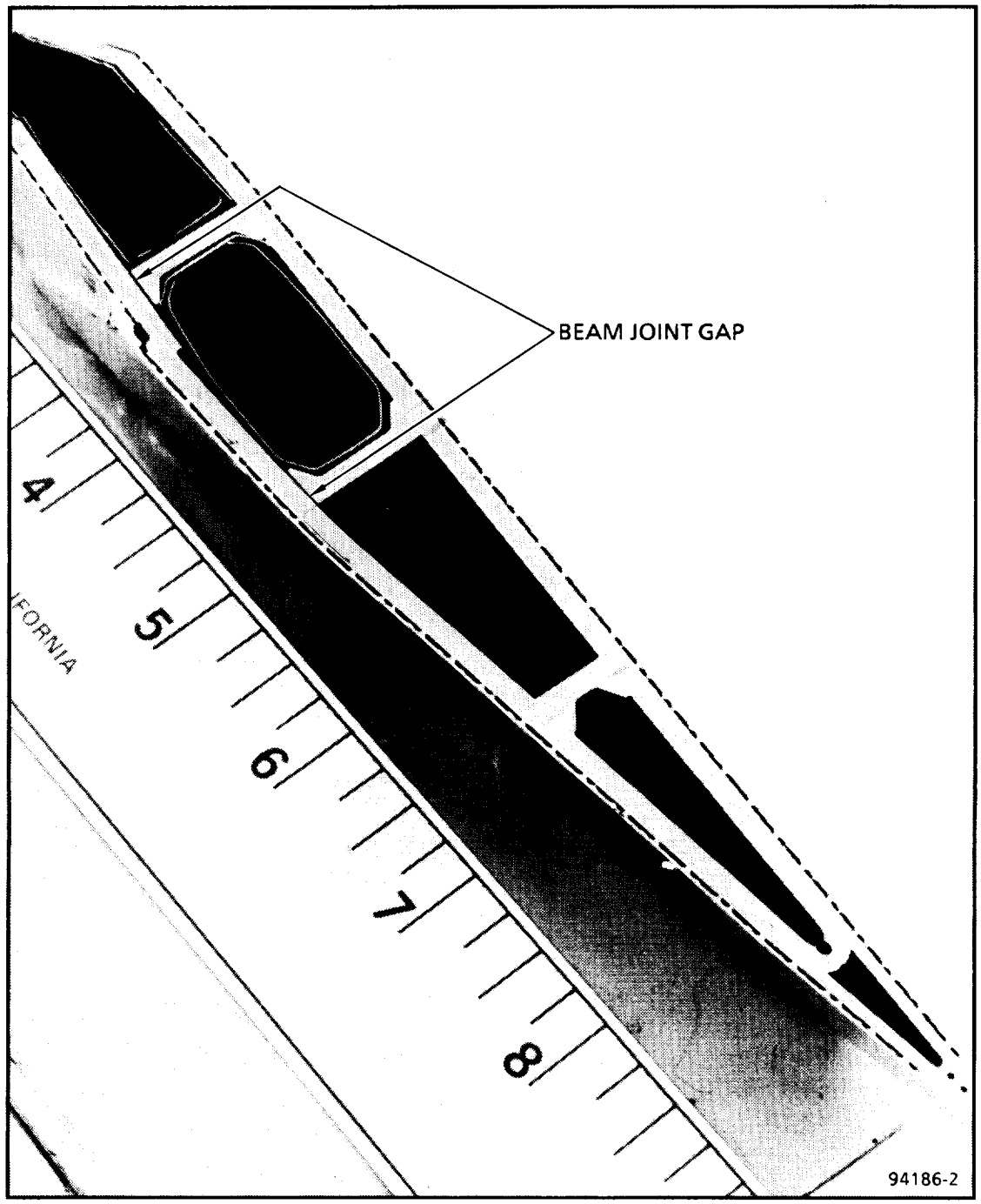

Figure 133. PL2 Assembly Showing Beam Joint Gap for the Two Aft Beams

6. TASK 3 – FULL-LENGTH (FL) STRUT FABRICATION

Many of the full-length strut components were fabricated in parallel with the partial-length struts. The experience with the PL assemblies and the results of the fabrication investigations, discussed in Section 4, led to a number of design changes in the FL components. The cooling jackets used the pin-fin patterns defined in Section 4, with a constant depth of 0.020 in., a 0.040-in.-dia. pin-fin on the sidewall passage side and a 0.030-in.-diam pin-fin on the center-passage side of the strut (the different pin-fin diameters are used to adjust the pressure drops to obtain the required coolant distribution, para. 4.2). Also, grooves were etched in the 0.010-in. cover plate of the cooling jacket to promote better braze alloy flow and filling of the gaps and to eliminate jacket-to-body voids as observed on the PL assemblies. The grooves were PCM'd, 0.005-in. deep and 0.035-in. wide with a 0.035-in. land. The groove pattern was designed to be parallel to the leading and trailing edges and was indexed to the pin-fin pattern, such that the grooves are located over the spaces between the pin-fins. This was done to make the cooling jacket assembly more flexible so that a better fit can be achieved during the forming and hot-sizing of the cooling jacket assembly to the structure.

As a refinement of the hot forming of the jackets, a hard fixture was developed to seat the cooling jackets to the support structure at the leading and trailing edges during hot-sizing and brazing. Figure 134 shows the design for this fixture. The pillow-block at one end is a sealed sheet metal tube that is gas-charged to a predetermined pressure at room temperature. The charge pressure, in turn, is calculated to exert a specified force, at hot-sizing or brazing temperature, on the stacked strut assembly. At temperature, the vacuum bag is fully evacuated to provide maximum load on the jacket-sidewall joints.

A number of runs were made with dummy parts, (see Figure 135). The conclusion from these was that the fixture by itself could not assure the requisite fits without applying higher loads than used. Control of the fixture and stacked parts at higher pressures would be developmental and risky.

As a result of this work, a coining tool for the critical forming of the leading edge was designed and fabricated. Forming of the more gently radiused trailing edge was judged sufficient as developed in previous efforts. Up to this point, the leading edges were formed into rubber. Figures 136 and 137 show the completed coining tool (the punch, i.e., the male die, is resting in the female die). After completion, the tool was shipped to NASA along with the other components.

As described previously, the strut assembly requires a series of three braze cycles using two major subassemblies: the cooling jackets and the Inconel 718 support structure. Table 22 outlines the fabrication sequences. After completion, these subassemblies were shipped to NASA Langley.

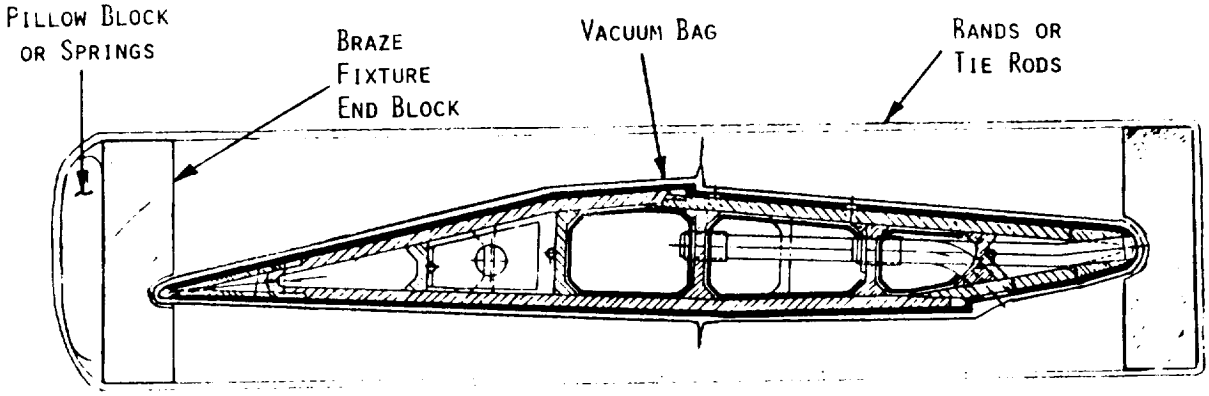

Figure 134. Design of Combination Hot-Sizing and Braze Fixture

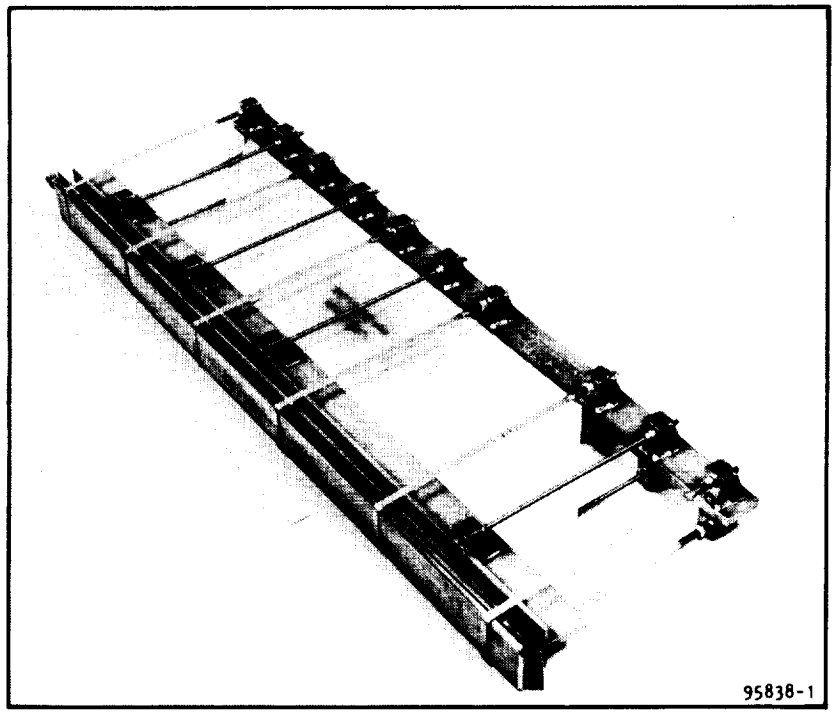

F-58714

Figure 135. Hot-Sizing/Braze Fixture with Dummy Part

ORIGINAL PAGE
BLACK AND WHITE PHOTOGRAPH

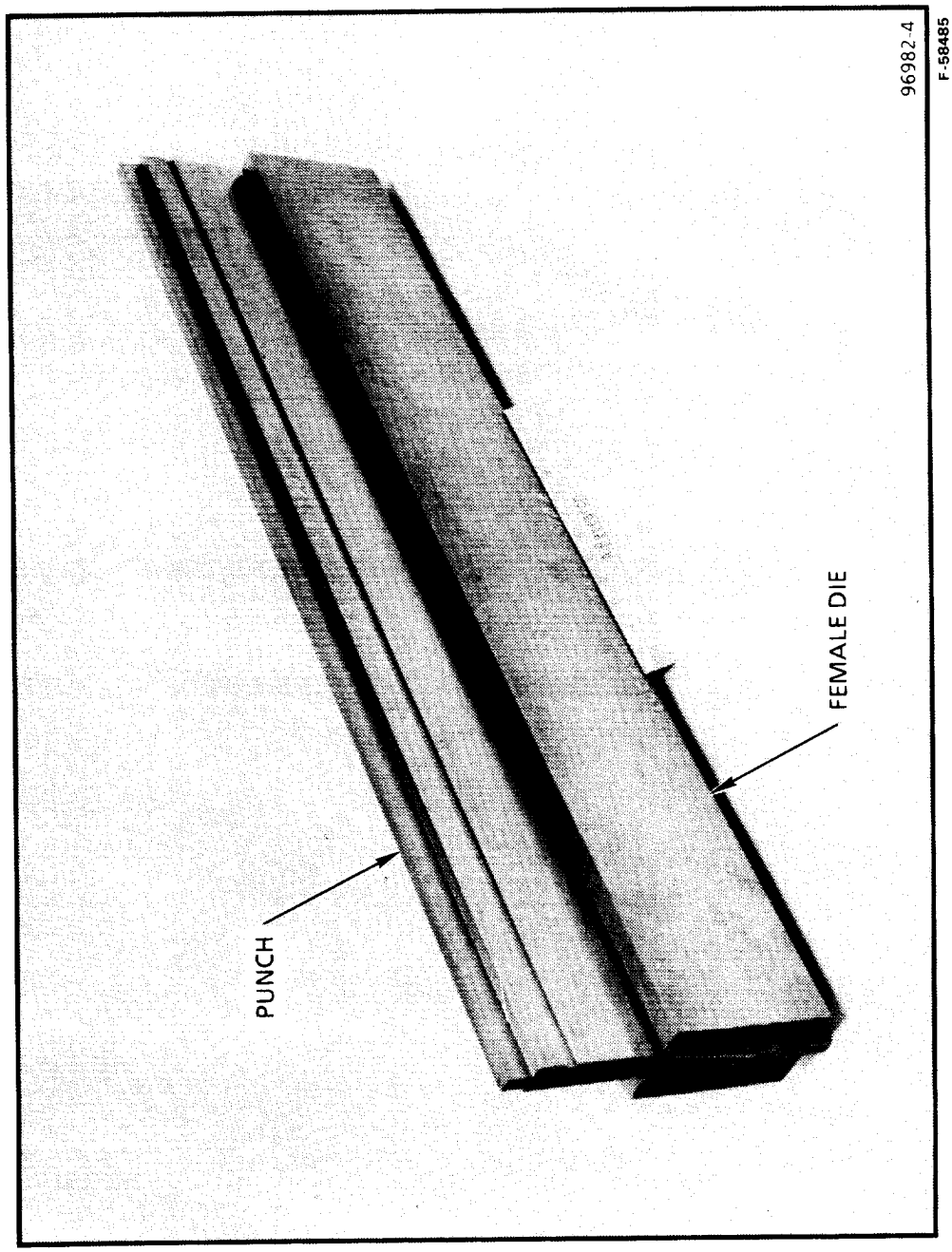

Figure 136. Jacket Leading Edge Coining Tool

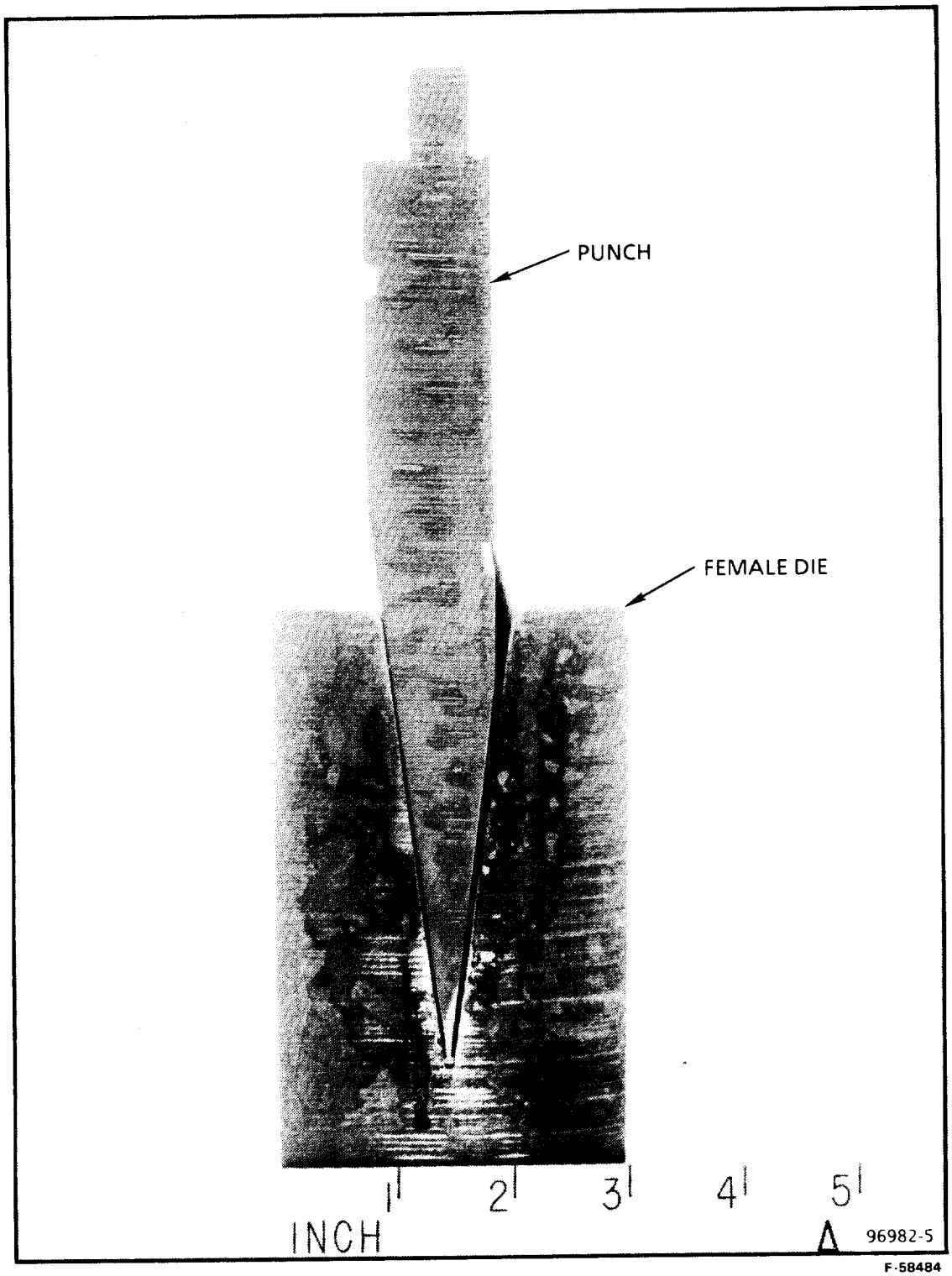

Figure 137. Jacket Leading Edge Coining Tool

TABLE 22

FABRICATION SEQUENCE FOR THE FULL-LENGTH STRUTS

INCO-718 Support Structure
Design and fabricate tools
Form and hot-size skin
Fabricate leading edge insert
Fabricate detail parts
Stack and braze
Cooling Jacket Assembly
Prepare PCM artwork
PCM the pin-fin face plates
Stack face plates with cover sheets
Braze
Leak and pressure test
Machine
Form and hot-size to support structure
Final Assembly
Fit cooling jacket to support structure
Stack cooling jackets and support structure
Braze
Leakage test
Braze end plates
Final pressure test

The artwork and the process scaleup from PL to FL for PCM of the forward and aft pin-fin face plates were verified using nickel material blanks – sheets of the same size and thickness as used for the final face plates. Several sample parts were fabricated to obtain the required pin-fin geometry and tolerances. PCM process variables were changed and tested with sample parts. Variables modified were the type of photo-resistant material (photo-resist), artwork edge factor allowance, and material surface condition. Nickel-201 samples verified that the process could produce the required jacket dimensions and tolerances. However, full-length jackets etched from Ni-200 (substituted for Ni-201 because of availability) had poor photo-resist adhesion. This resulted in cone-shape pins rather than pins of the proper diameter (see Figure 138). When the surface was first etched to roughen it, the proper pin geometry was obtained for both the sample and full-length jackets. Figures 139, 140, and 141 show the completed forward and aft jacket panels after PCM.

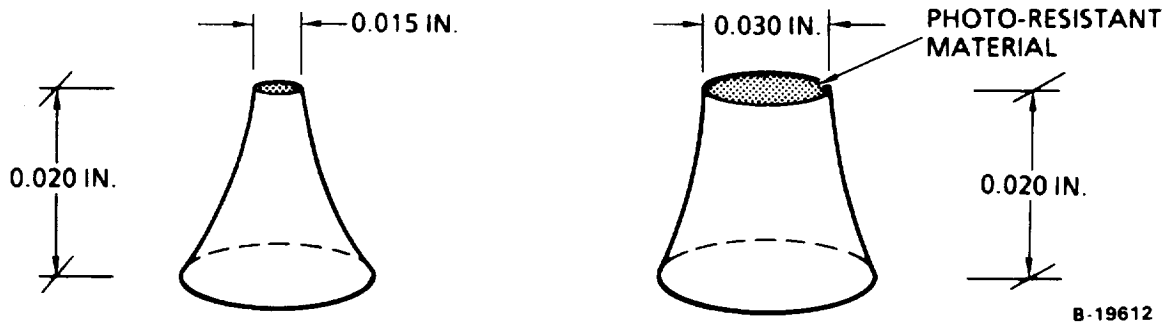

Figure 138. Effect of Loss of Photo-Resistant Materials on Pin-Fin Tips

Both panels were inspected, first dimensionally, then for uniformity of pin-fin height. The latter was accomplished indirectly by ink-coating the braze surface and pressing it on a sheet of paper on a granite surface plate. Both panels showed irregularities. To reduce these, the plates were hand-lapped on a granite surface plate and periodically checked by inking and printing.

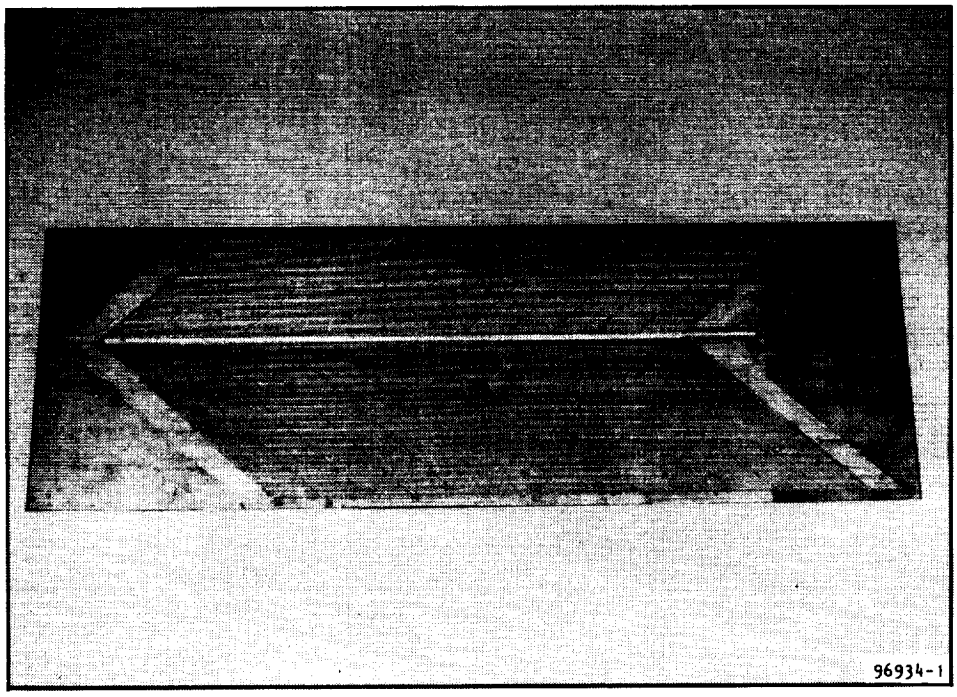

F-58715

Figure 139. Completed Forward Jacket PCM Panel

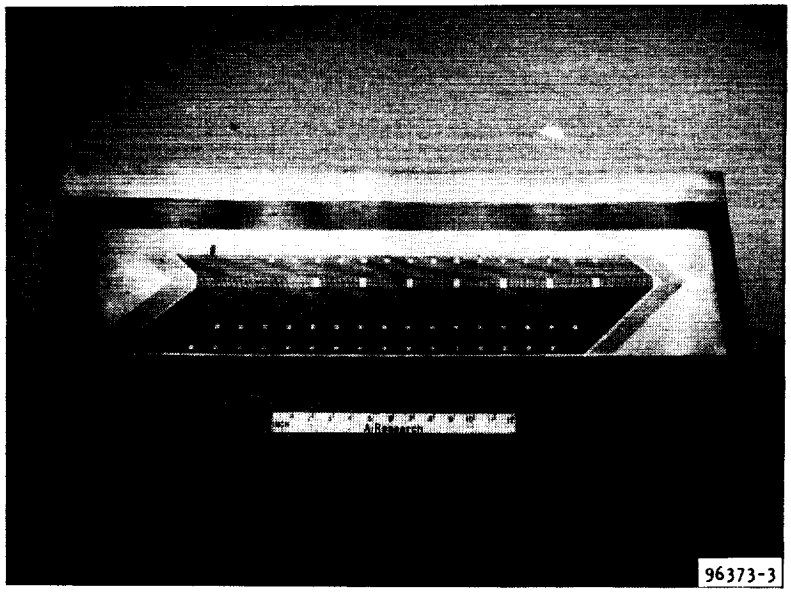

F-60405

Figure 140. Completed Aft Jacket PCM Panel

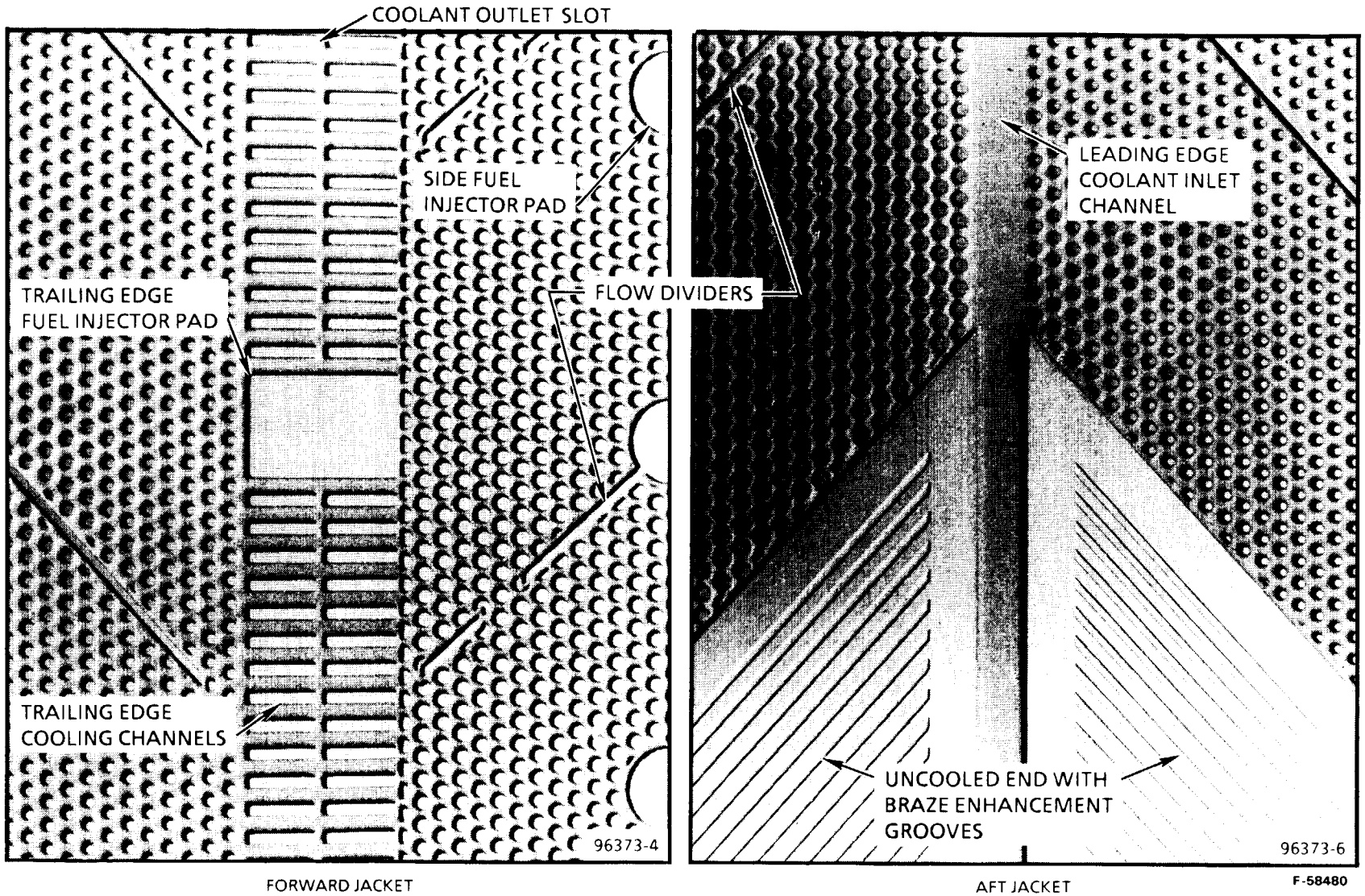

ORIGINAL PAGE
BLACK AND WHITE PHOTOGRAPH

Figure 141. Details of Forward and Aft Jacket PCM Panels

The lapped panels were then stacked and brazed using the procedures described in Sections 4 and 5. Figure 142 shows application of braze foil during stacking of the forward jacket. Following brazing, the jackets were X-rayed, proof-pressure tested, and holographically inspected. Figures 143 and 144 show a three-view sequence of X-rays of the forward and aft jackets. There is no evidence of braze filler plugging in either jacket. Figures 145 and 146 show sets of holograms for the two jackets. Both sets were taken at 840 psig, using reference holograms at 800 and 760 psig (40-and 80-psi difference between exposures), respectively. Use of small pressure differences greatly improved resolution compared to an ambient pressure reference. Both sets of holograms show sound brazing without evidence of voids. During the tests, the jackets were mounted on a special vacuum chuck, shown in Figure 147. Additionally a truss fixture, shown in Figure 148, was used to support the jacket over the gap of the leading edge coolant inlet channel. Figure 149 shows the forward jacket during the holographic tests, mounted on the vacuum chuck and with the truss installed.

Following successful pressure testing, grooves were PCM'd in the 0.010-in. back sheet of the aft jacket (not done on the forward jacket), and the coolant outlet slot at the trailing edge was opened. Figure 150 shows the jacket after PCM of the grooves and before opening the cooling outlet slot. The fuel-injector pads and the slot are printed through the back sheet, but remain flush with the surface, since the pads and the edges of the slot will be brazed to the support structures (see also Figure 141). The forward jacket was completed by brazing rails along the spanwise edges to form the coolant crossover to the aft jacket. These rails are shown in Sections T-T and U-U, sheet 2, of drawing 195582 (Figure 7). Figure 151 shows the as-delivered panel. Grooves on the back sheet will be PCM'd after delivery to NASA.

6.2 Support Structure

The main components of the support structure are the leading edge, the forward and aft walls, beams/bulkheads, thermal buffers, and fuel-injector tubes.

6.2.1 Walls. — The first steps in support structure fabrication were the forming and machining of the forward and aft wall sections. Final sizing was done hot and under load. Small test specimens were used to develop the procedures. Parts were brake-formed to the approximate leading- and trailing-edge radii, fixtured to mandrels, and hot-sized by application of ambient pressure to an evacuated steel-bag retort. The specimens, fixtured on the Inco-718 hot-sizing mandrels, are shown in Figure 152.

The FL dies were machined of Inconel 718 to match the thermal expansion of the Inco-718 wall sections during hot-sizing. They are shown in Figure 153. One each of the FL wall sections was formed; these wall sections along with their respective male and female forming dies are shown in Figure 154. Two each of the forward and aft wall sections for the

ORIGINAL PAGE
BLACK AND WHITE PHOTOGRAPH

Figure 142. Application of Braze Foil During Stacking of the Forward Jacket for Brazing

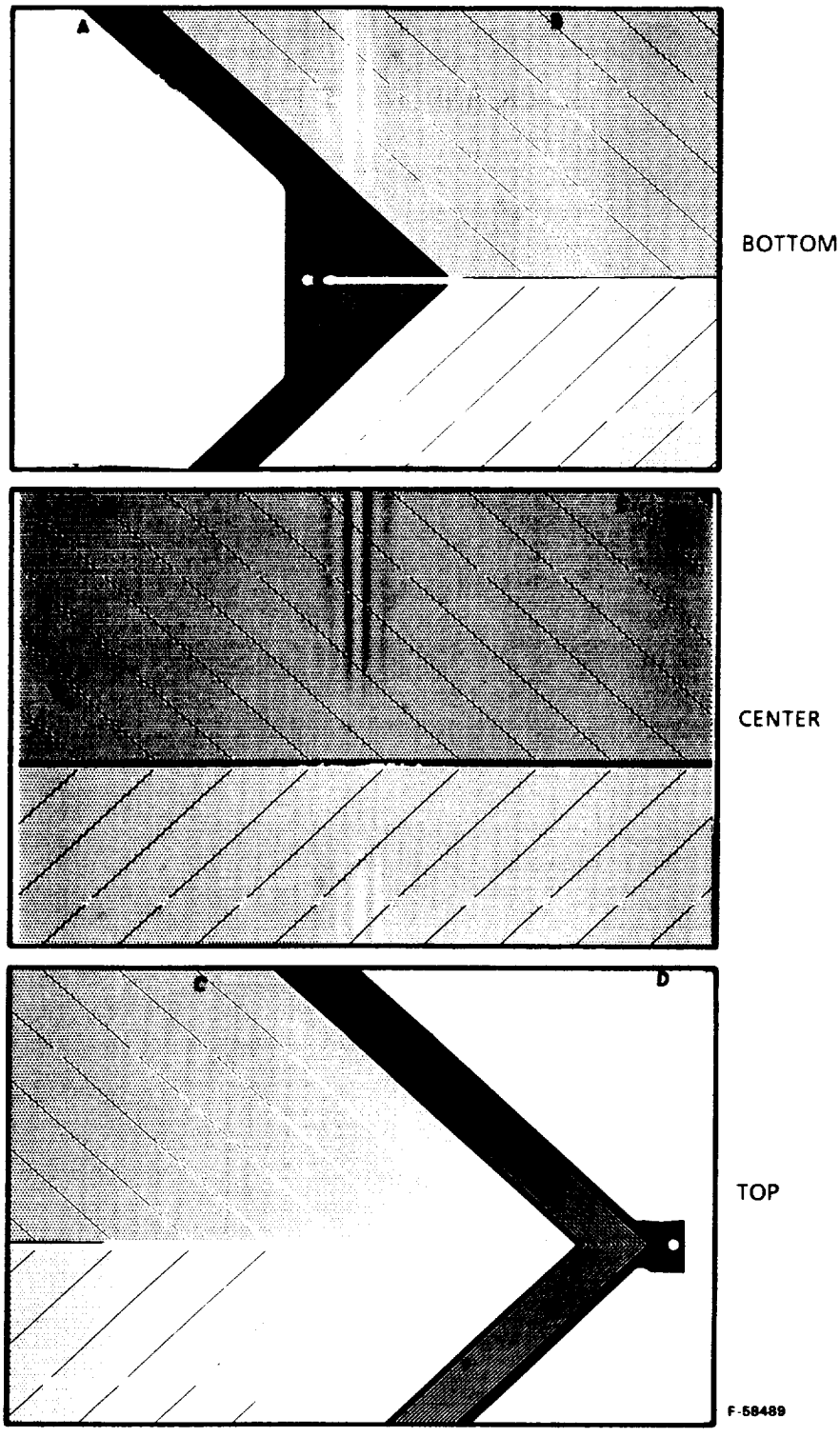

Figure 143. X-Ray of Brazed Full-Length Forward Coolant Jacket

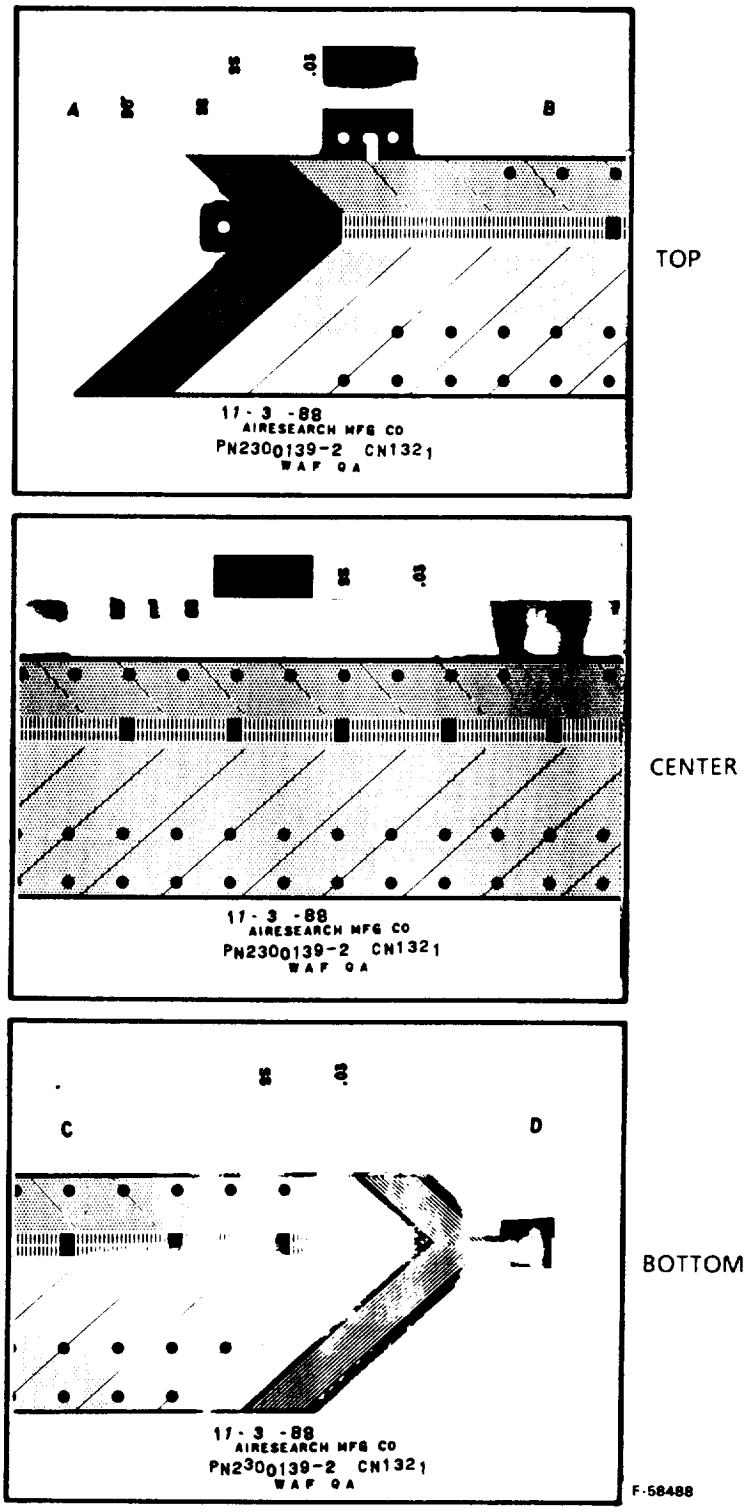

Figure 144. X-Ray of Brazed Full-Length Aft Coolant Jacket

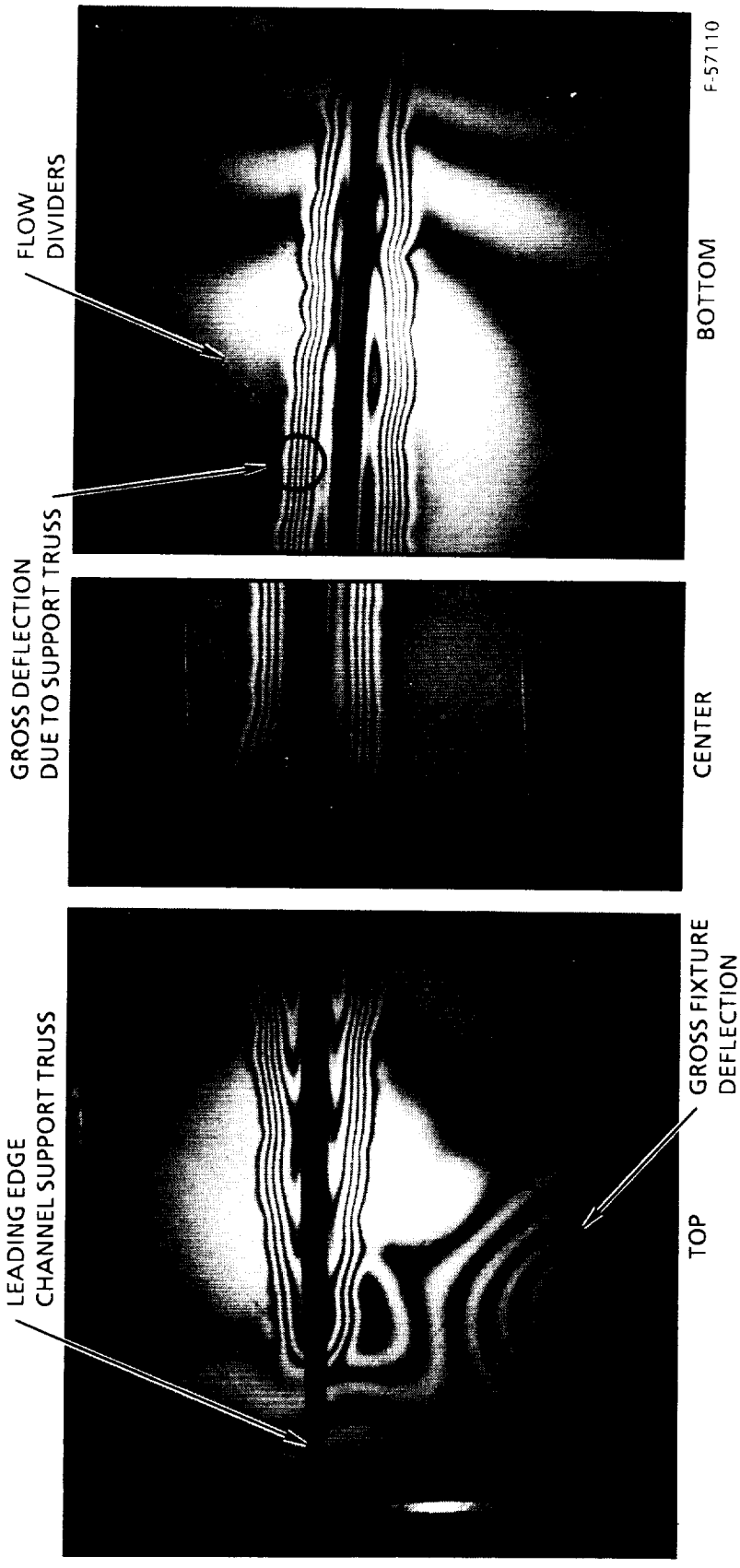

Figure 145. Brazed Forward Jacket Hologram after 1050-psig Proof Pressure, at 840 psig and 40 psid. No Indication of Braze Voids

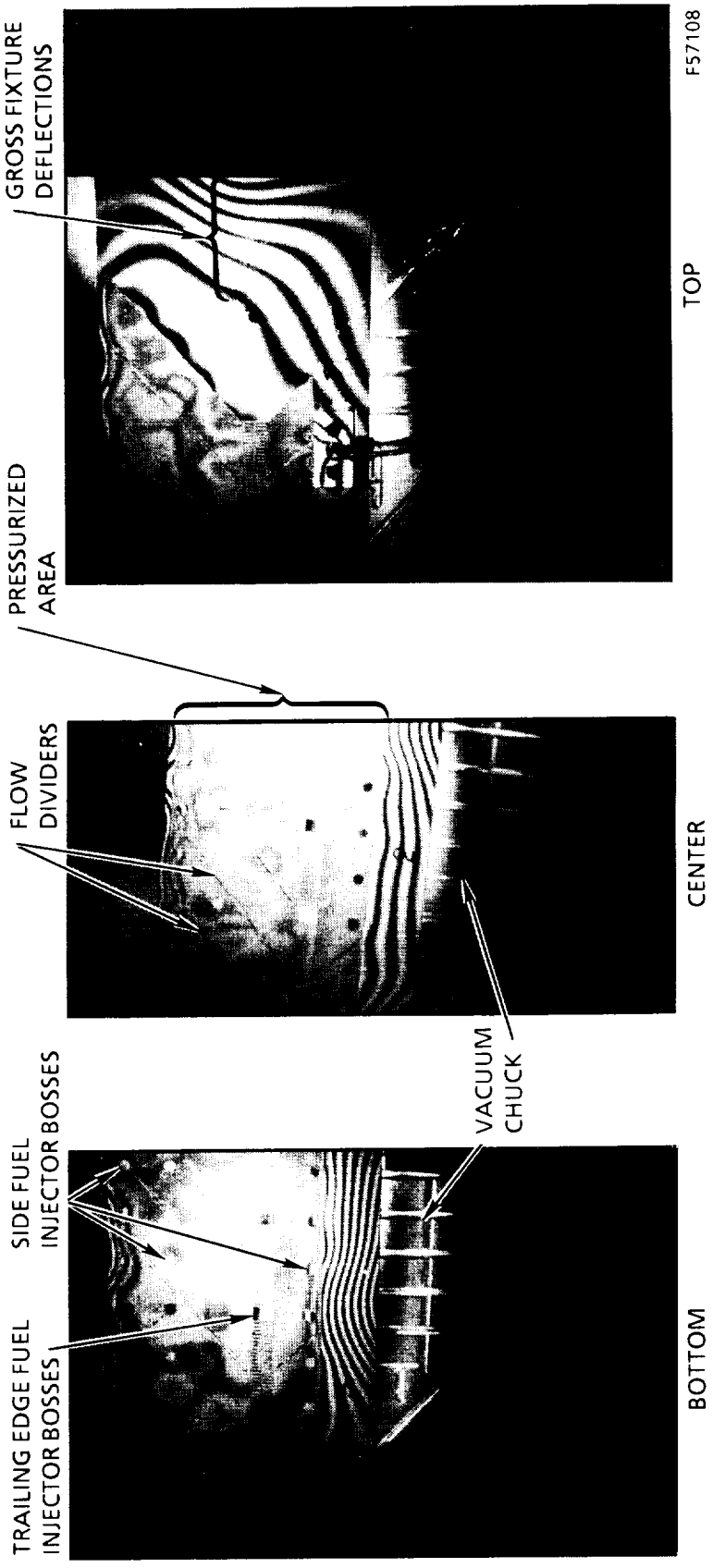

Figure 146. Brazed Aft Jacket Hologram after 1050-psig Proof Pressure, at 840 psig and 80 psid. No Indication of Braze Voids

ORIGINAL PAGE
BLACK AND WHITE PHOTOGRAPH

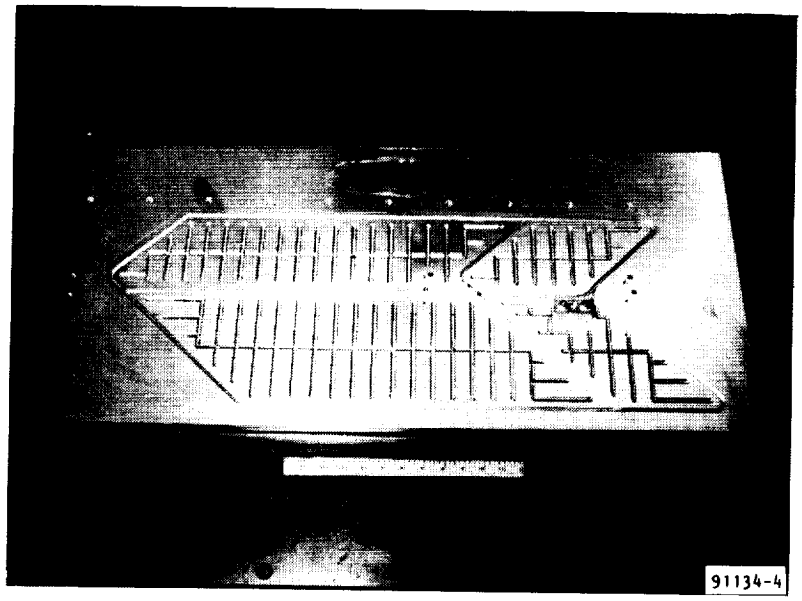

F-60406

Figure 147. Vacuum Chuck for Cooling Jackets

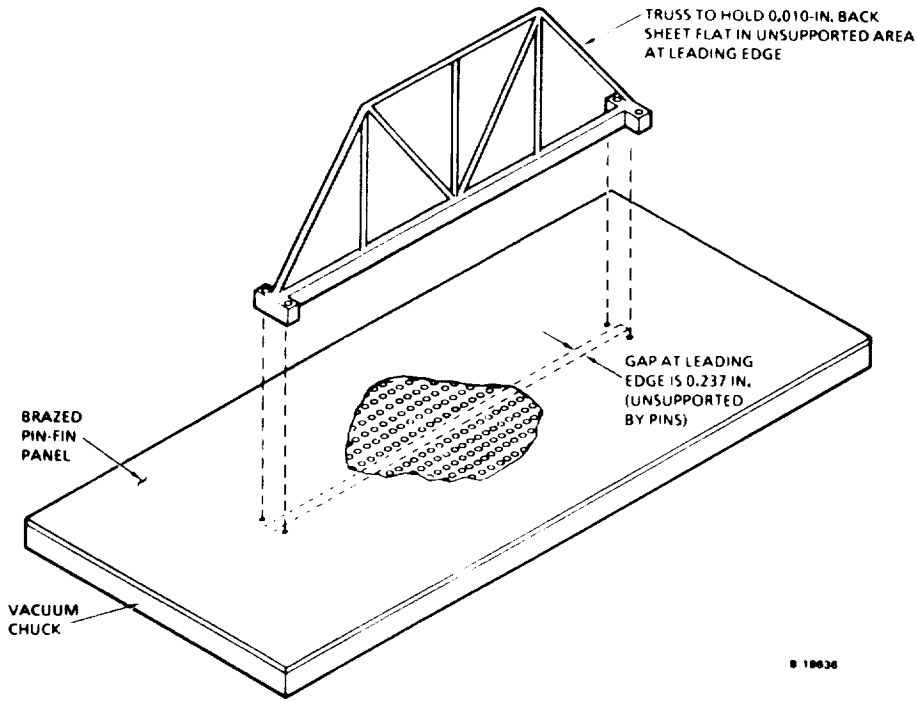

Figure 148. Assembly of Truss to Forward Jacket for Holographic Testing

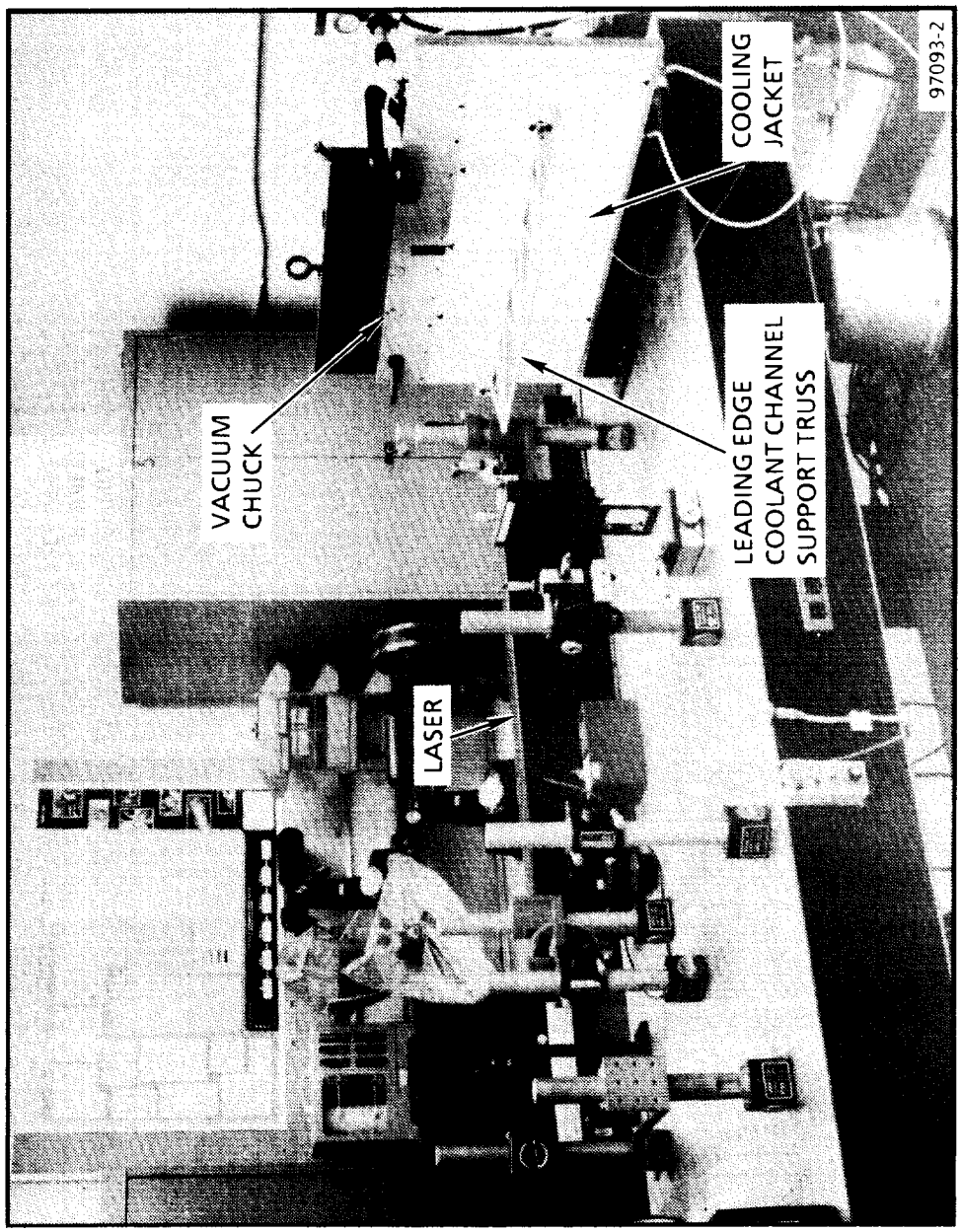

Figure 149. Holographic Test Setup with Forward Jacket on Vacuum Chuck and with Support Truss Installed

ORIGINAL PAGE
BLACK AND WHITE PHOTOGRAPH

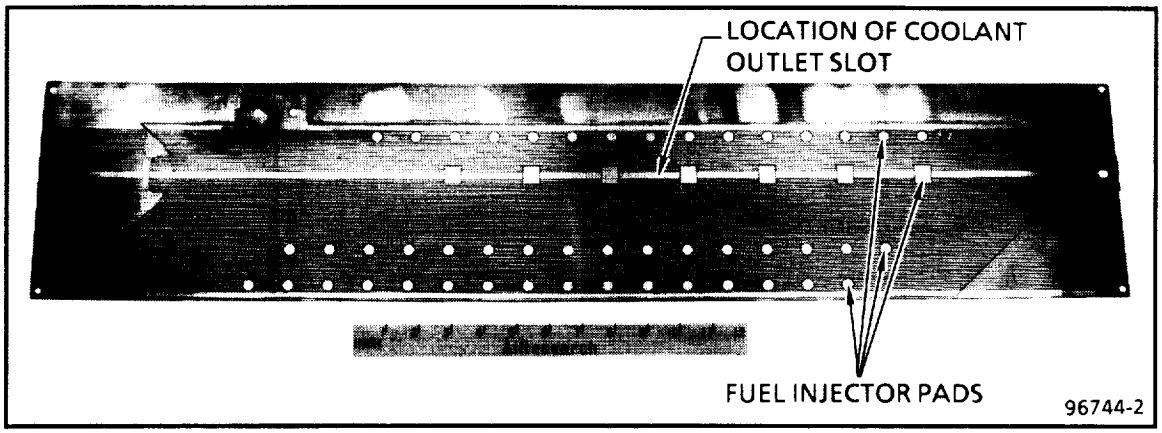

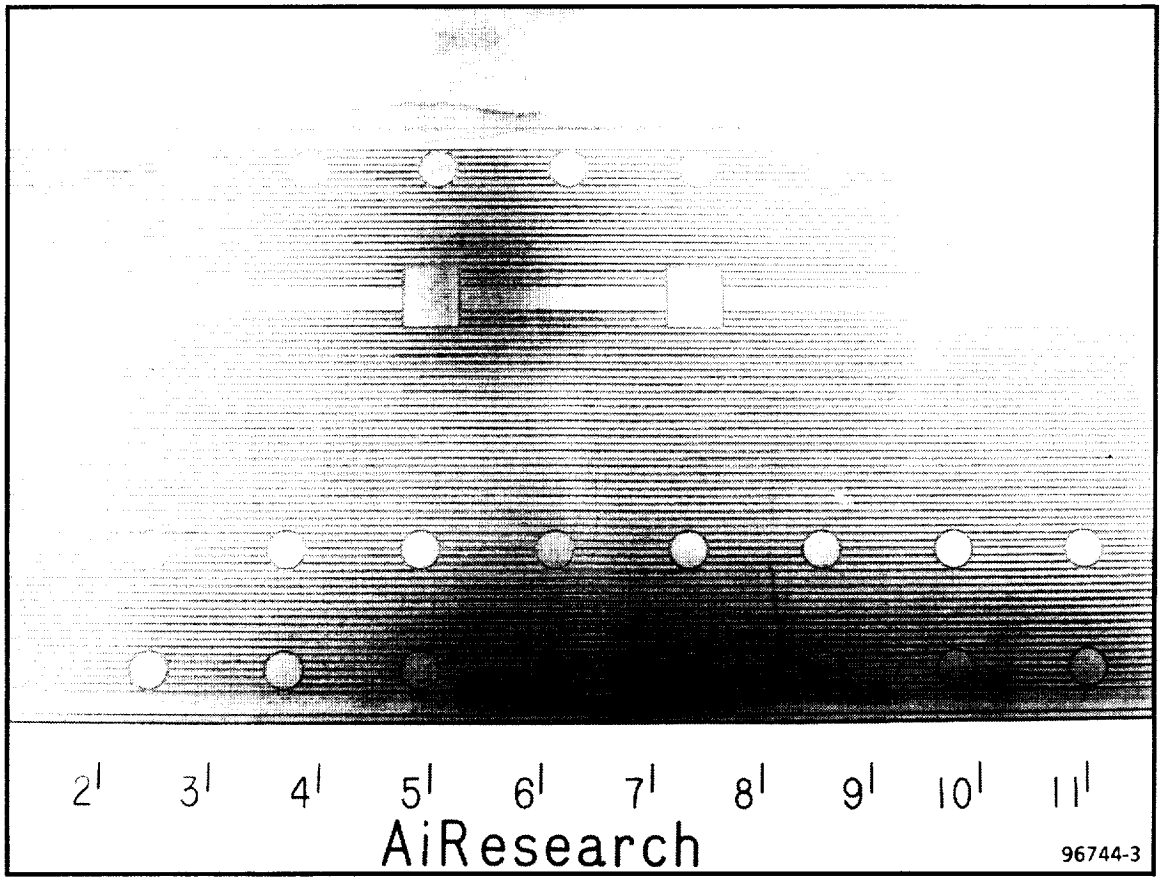

B-19614

Figure 150. PCM Grooves (0.005-in. Deep x 0.035-in. Wide) in Back Sheet of Aft Cooling Jacket

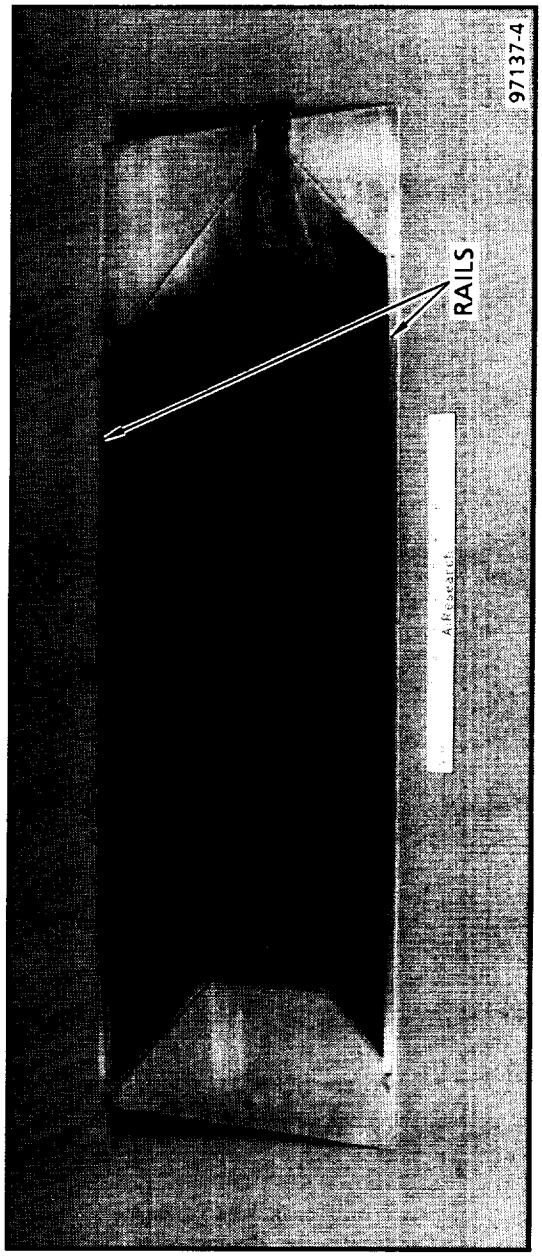

Figure 151. Forward Cooling Jacket After Brazing Two Rails

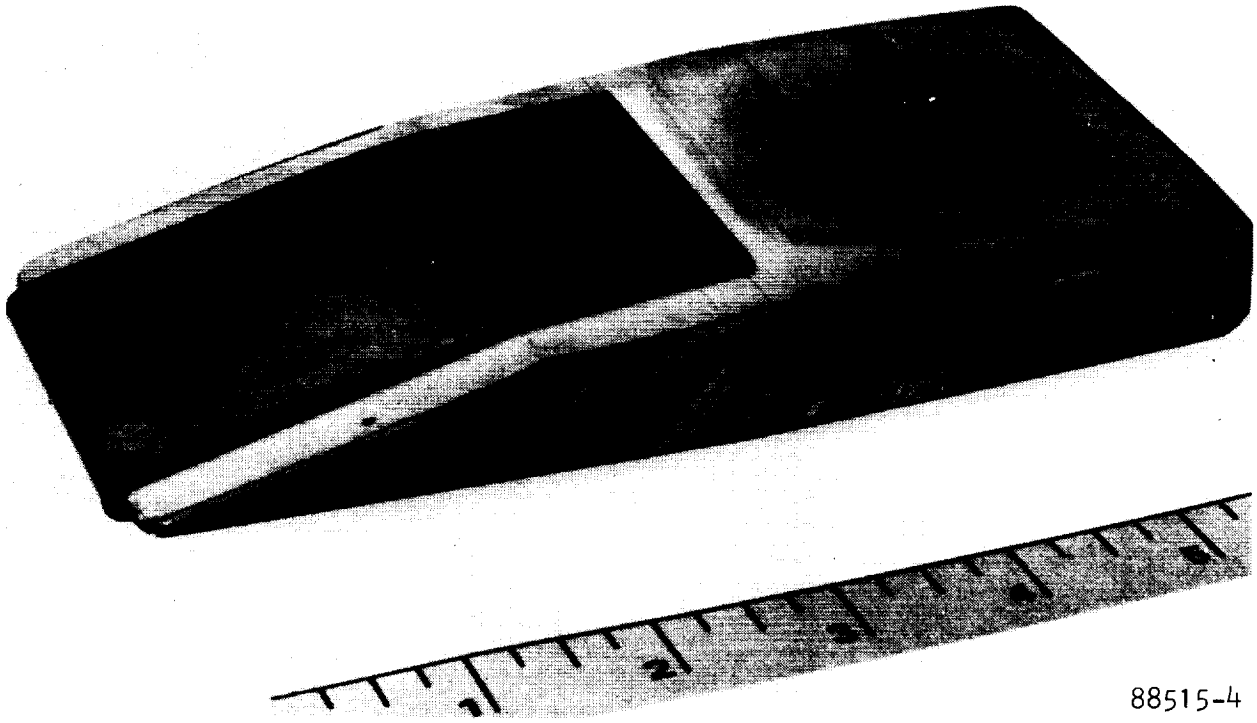

a. FORWARD SECTION

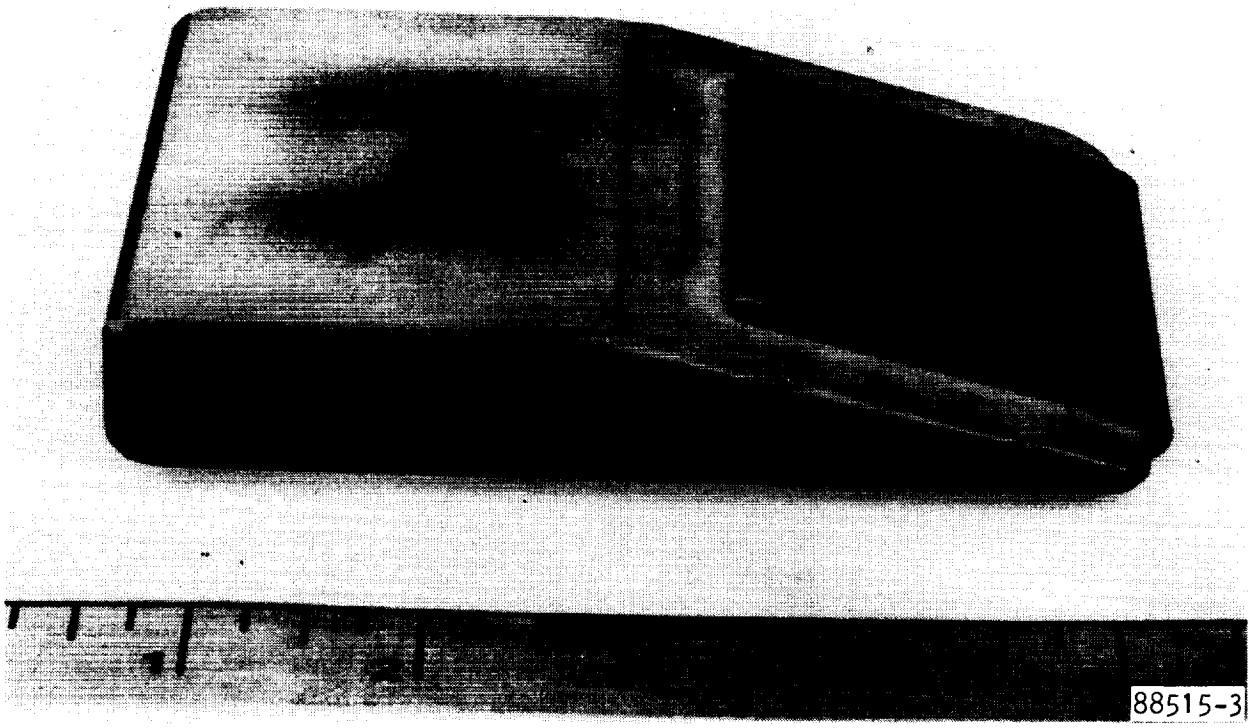

b. AFT SECTION

F-40603

Figure 152. Inconel 718 Support Structure Hot-Sizing Tests

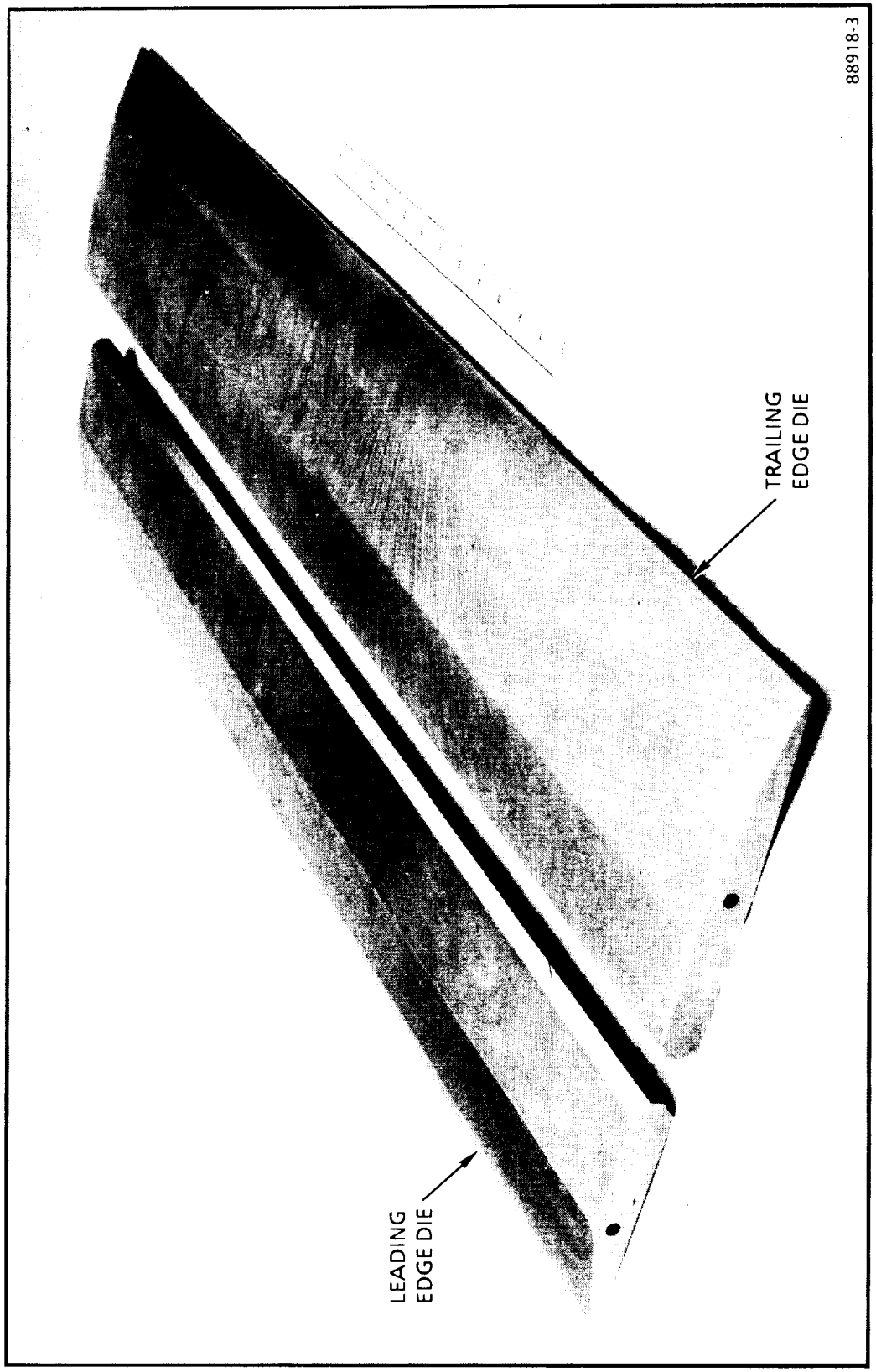

Figure 153. Inconel 718 Hot-Sizing Dies for Full-Length Strut Support Structure Sections

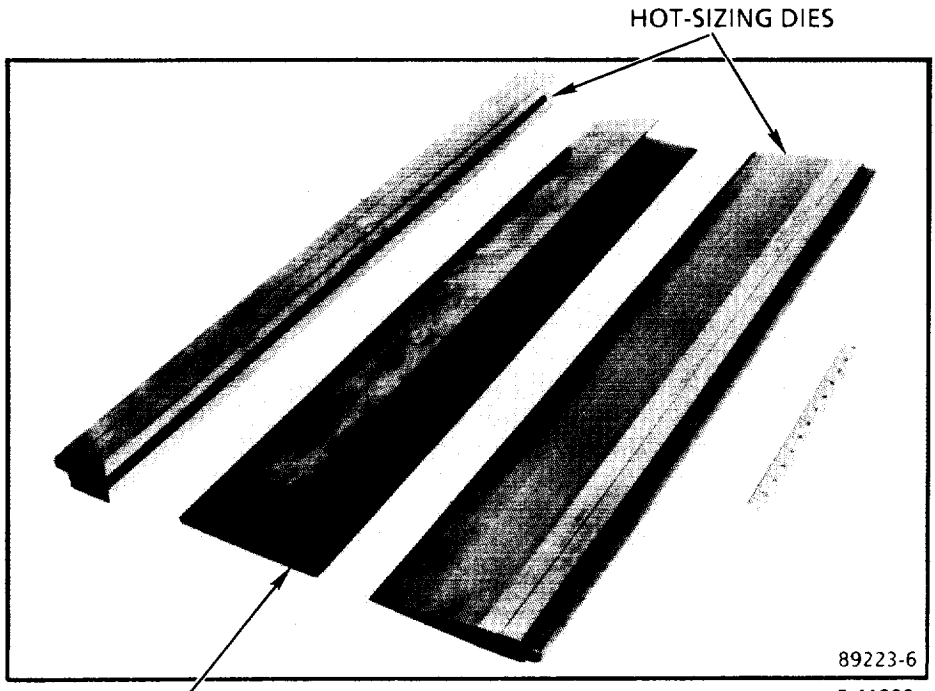

a. FORWARD SECTION

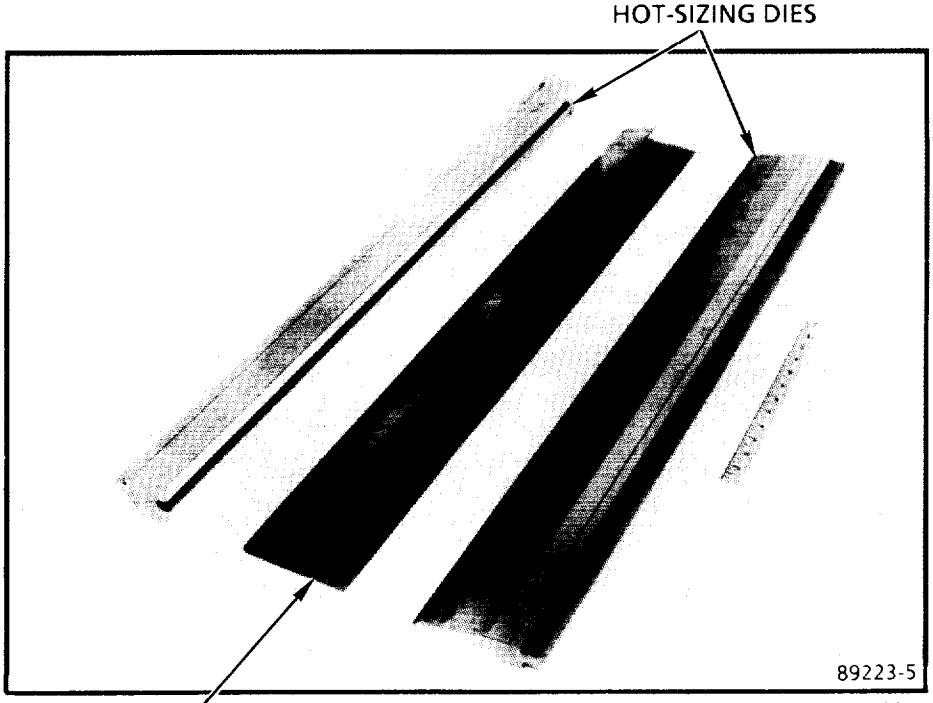

b. AFT SECTION

Figure 154. Hot-Sized Inconel 718 Support Structure Sections and Hot-Sizing Dies

PL struts were also formed using the FL dies. An as-formed forward section is shown in Figure 155. Two aft sections, after hot-sizing and still on the Inconel 718 FL sizing die, are shown in Figure 156.

After hot sizing, the braze surfaces were machined. Holes were cut using EDM. The five FL beams are shown in Figure 157. The beam flanges are closely toleranced and machined to match the wall contours and provide the needed braze fits. As with the PL struts, the Inconel-718 braze surfaces were electrolytic-nickel-plated to a thickness of 0.0002 to 0.0003 in. to enhance brazeability.

6.2.2 Leading edge. – In parallel with wall fabrication, the separate leading edge section was machined and the coolant holes were drilled and EDM'd. This is an all-machined part. Figure 158 shows the completed part.

6.2.3 Buffers. – (See Figure 12.) The purpose of the buffers is to reduce convective heat transfer between the hot fuel and the slowly responding support structure by means of the relatively stagnant gas layer between the walls and the buffers. Analysis by NASA-Langley (ref. 4) had shown large gradients at startup and shutdown, with the walls either initially cold or hot and a rapid change in fuel temperature.

Fabrication of the buffers started with tooling tryout pieces. A special die (Figure 159) was fabricated to simultaneously form the flanges and the dimples that space the buffers off the structural surfaces. A set of buffers for the partial-length strut is shown in Figure 160. The buffers have peripheral ridges to minimize flow bypassing and 0.250-in.-diam holes between the ridges to provide venting along the length. EDM was used to trim the buffers to length and angle for subsequent assembly into the structure sections. A complete set of buffers for the full-length strut is shown in Figure 161.

6.2.4 Assembly. – All detail parts were closely inspected before, during, and after stacking for braze. Experience with test articles and the PL struts had emphasized the critical need for close braze fits and sound joints in this highly-loaded structure. The multiplicity of shallow-angled faying surfaces places greater demands than usual on accurate fitups of parts as stacked. Minimal compensation is possible in the braze cycle. Figures 162 and 163 show the forward and aft assemblies, as stacked. The forward assembly includes the leading edge section. After stacking, the joint gap between the center beams and the support structure wall ranged up to 0.007 in., mainly as a result of an overall spanwise bow in the wall. To pull the parts together and straighten the assembly, nine holes were drilled through the wall into the center of the beam and plug-welded along the length of the center beam. A test piece was first fabricated to evaluate the welds, especially because of the need to weld through the gold-based filler alloy. Results were satisfactory in terms of both the quality of the weld and the fit. The machining and welding were then done on the fully-assembled part ready for brazing and were successful in straightening the assembly.

A manufacturing mockup of the sidewall-side fuel injector area was used to ensure smooth assembly and close mechanical and braze fits. This was necessary because the tube angles are compoundly shaped and must install into a confined space and have braze-fits with the aft wall and beam (see Section 4 for a sketch of this area).

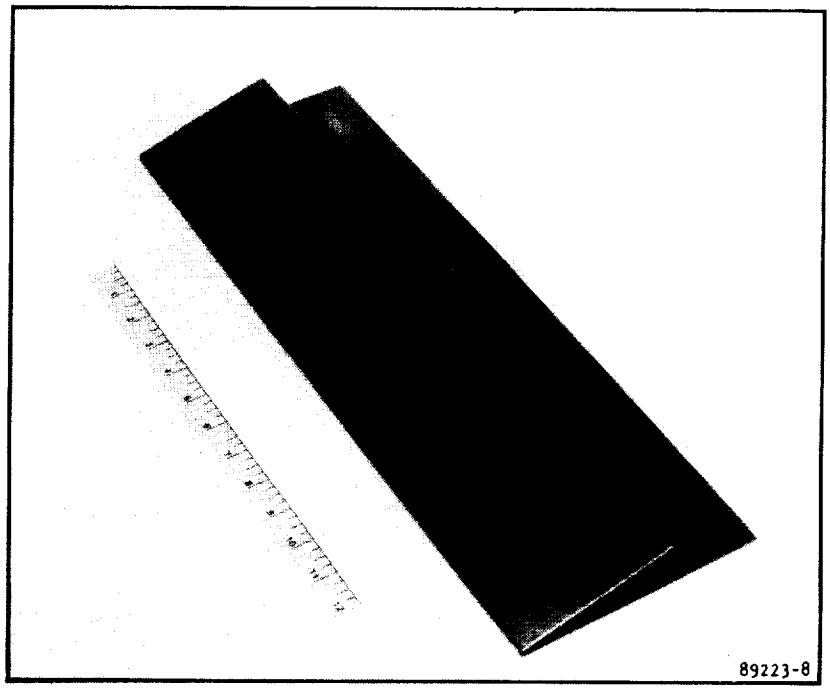

F-58716

Figure 155. Hot-Sized Inconel Forward Section Support Structure (Partial-Length)

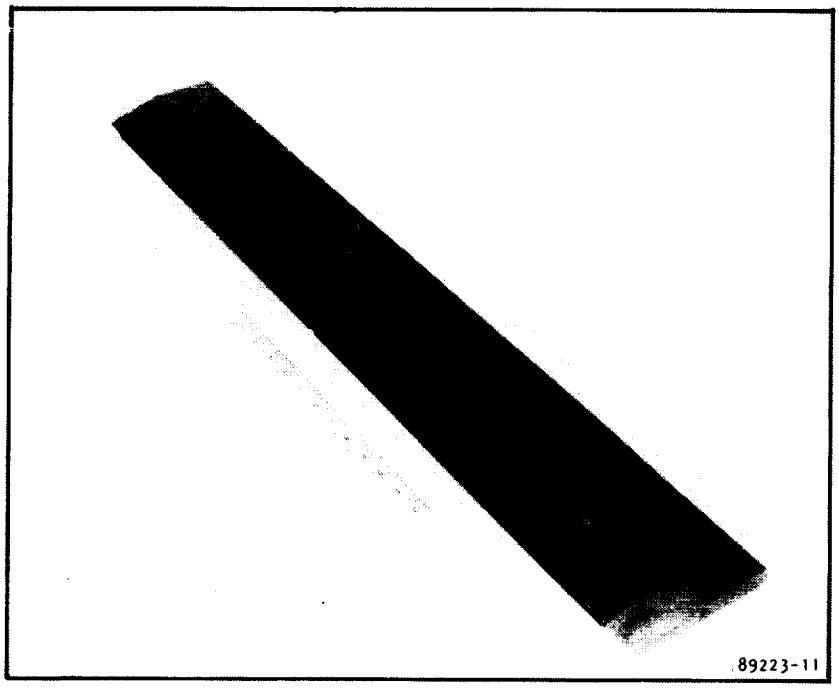

F-58717

Figure 156. Hot-Sized Inconel 718 Aft Section Support Structures (Partial-Length) on FL Hot-Sizing Die

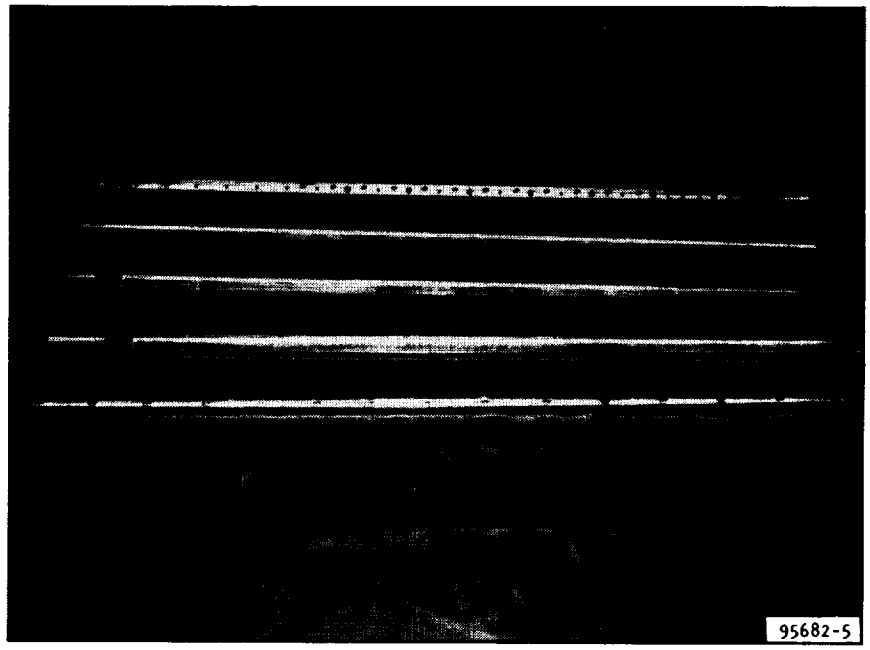

F-58718

Figure 157. Complete Set of Beams for Full-Length Strut

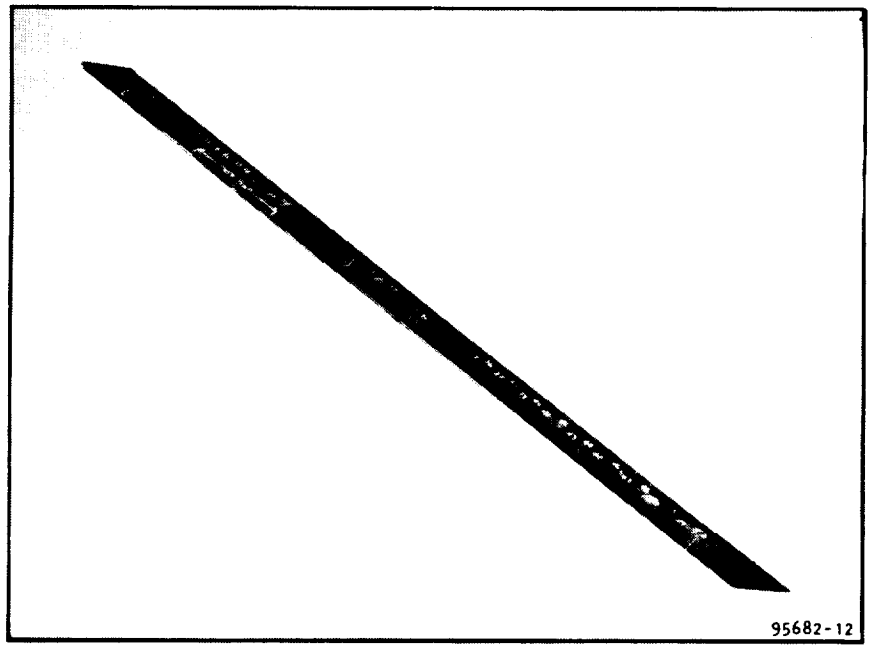

F-60399

Figure 158. Completed Leading Edge Support Structure Section

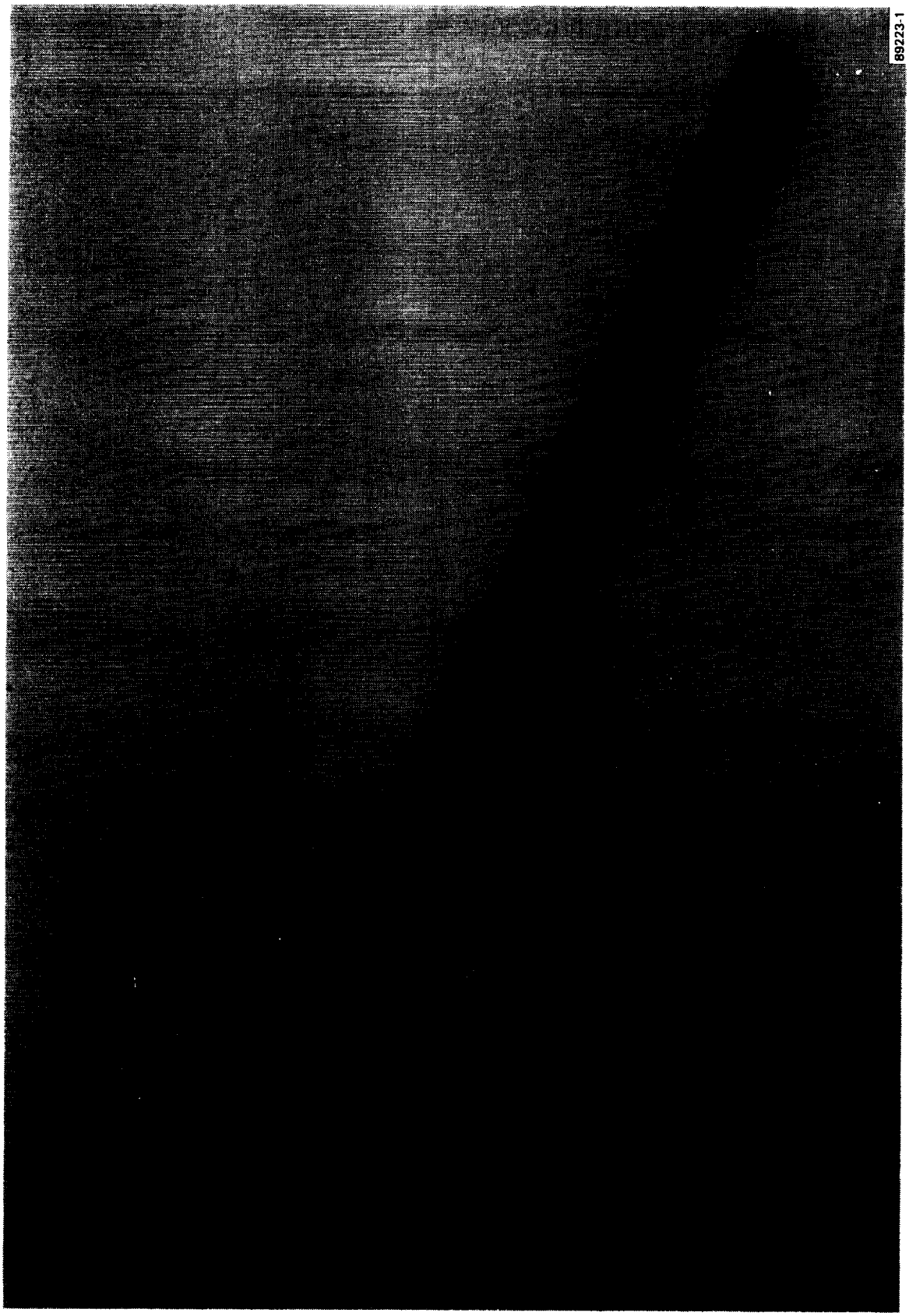

Figure 159. Thermal Buffer Forming Die (Female)

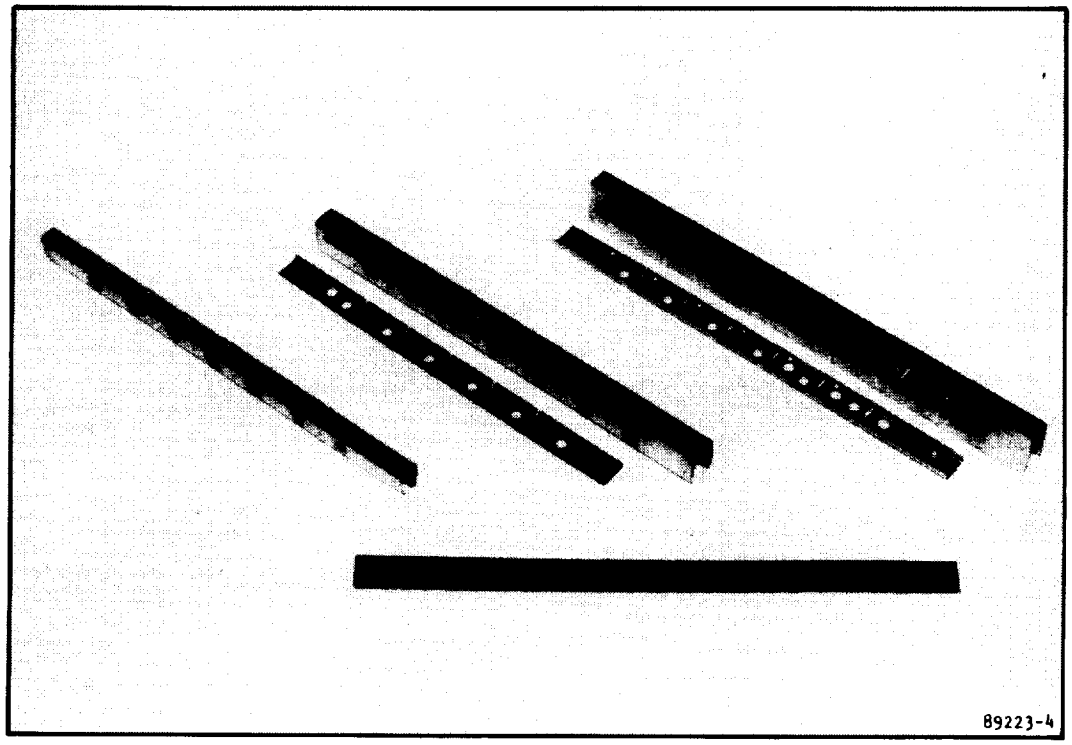

F-60400

Figure 160. Set of Formed Buffers for Partial-Length Strut

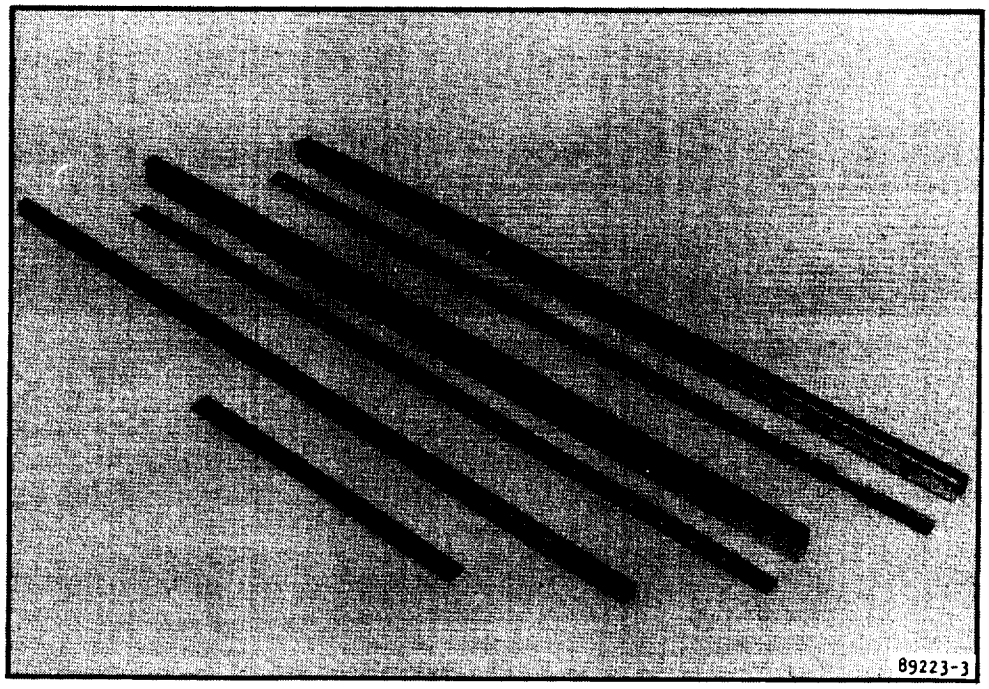

F-60401

Figure 161. Formed Buffers for Full-Length Strut

ORIGINAL PAGE
BLACK AND WHITE PHOTOGRAPH

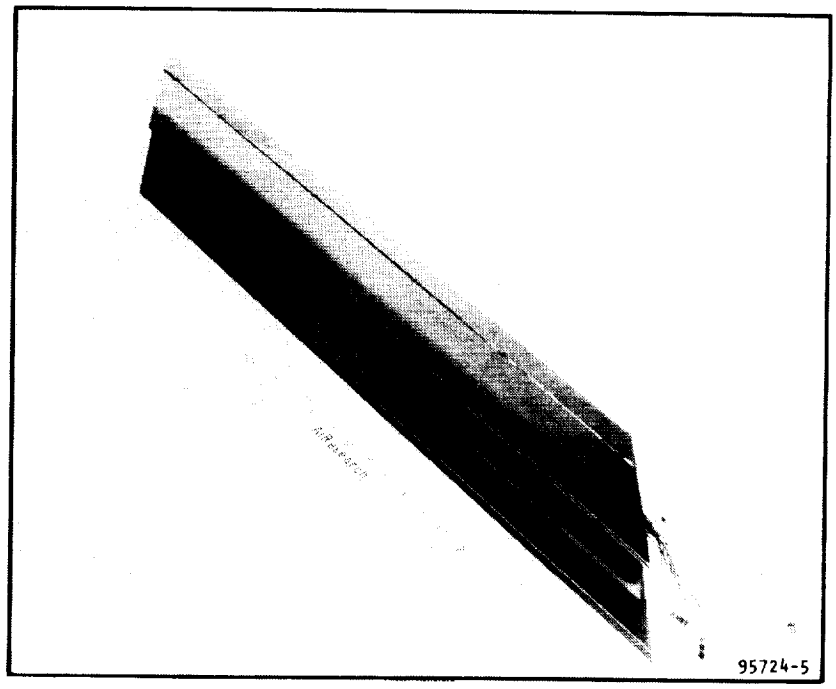

F-58710

Figure 162. Forward Support Structure Assembly, Stacked for Brazing

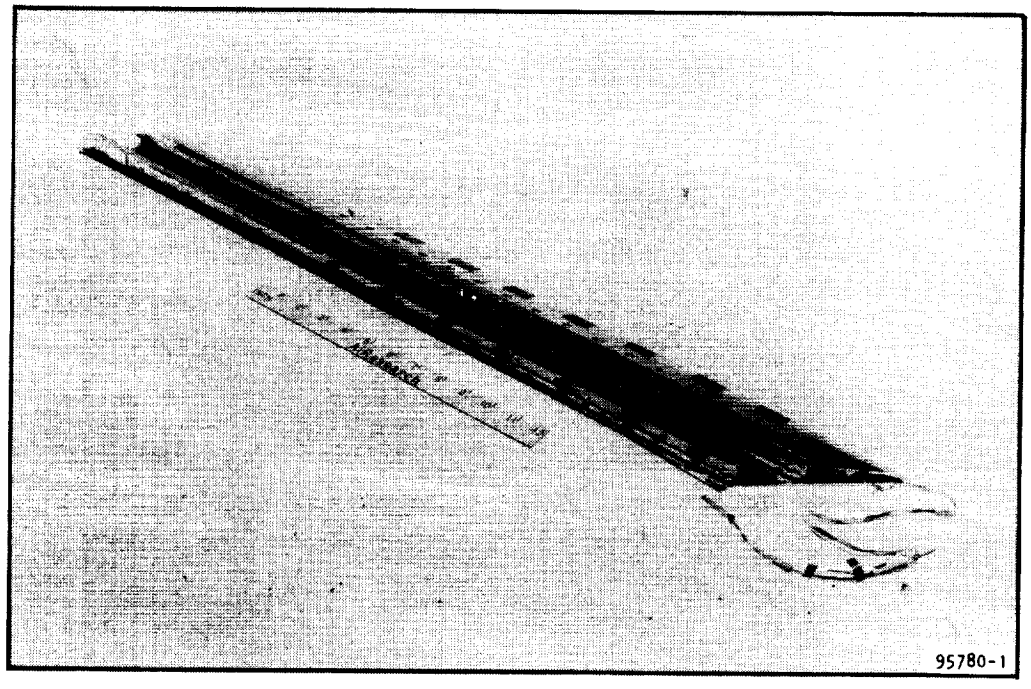

F-60402

Figure 163. Aft Support Structure Assembly, Stacked for Brazing

The two main assemblies were brazed in a bag retort following the procedures developed during PL strut fabrication. Figure 164 shows the two sides of the as-brazed assembly and a head-on view of the trailing edge showing the coolant holes. These were EDM'd after holography of the assembly. Temporary cover plates were brazed on as part of this assembly to facilitate leakage and pressure testing. Figure 165 shows an end view taken before the temporary cover plates were added in one of the rebraze cycles.

Three furnace rebraze cycles with Palniro 1 were used to fill in thinly brazed structural joints and to eliminate minor leaks. The assembly was then proof-pressure tested to 1050 psig and holographically inspected to 840 psig with a 50 psi difference pressure (reference hologram at 790 psig).

Figure 166 shows the resulting holograms, for which the strut was photographed in three sections. The holograms show a structurally sound assembly.

Dimensional inspection of the brazed assembly for accuracy and smoothness of contours showed some bowing and rippling. Various methods were considered to reduce this condition, including flame spraying, mechanical straightening, and furnace cycling under load. A furnace anneal cycle followed by hand-dressing of affected areas was selected as the most conservative approach. One of the critical areas is the junction of the leading edge tip section and the forward support structure. Experience with the PL struts and test sections had shown slight fit or angular mismatches at this junction to be a potential source of jacket-structure braze voids. Results of the dressing were judged satisfactory for subsequent braze assembly.

This completed the manufacture of the support structure assembly. Figure 167 shows the completed cooling jackets and the support structure.

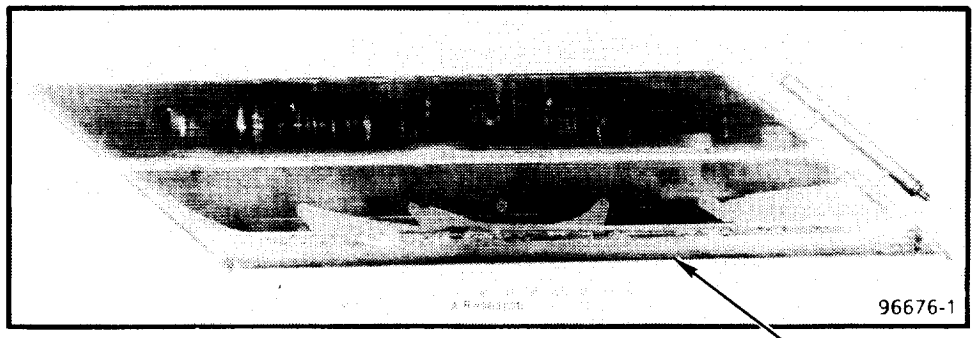

a. Center-Passage Side

LEADING EDGE

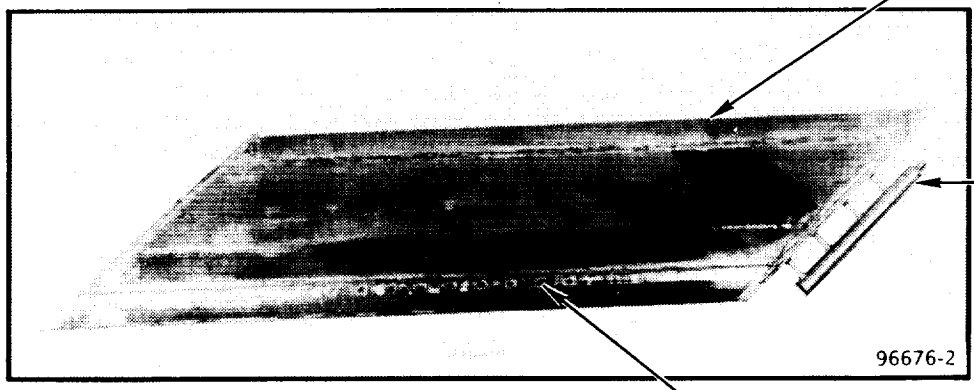

PRESSURE
TEST MANIFOLD

45-DEGREE FUEL INJECTORS

b. Sidewall Passage Side

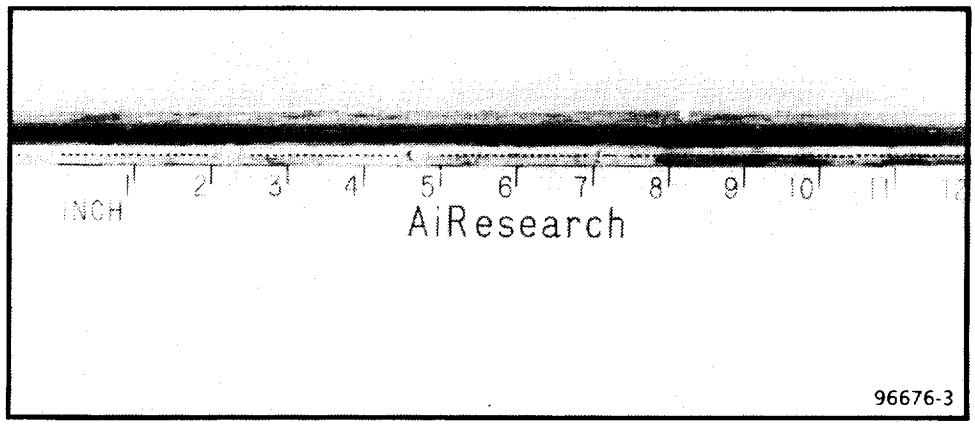

F-58482

c. Leading Edge

Figure 164. Brazed Full-Length Support Structure

Figure 165. Cross Section View of Full-Length Support Structure After Braze

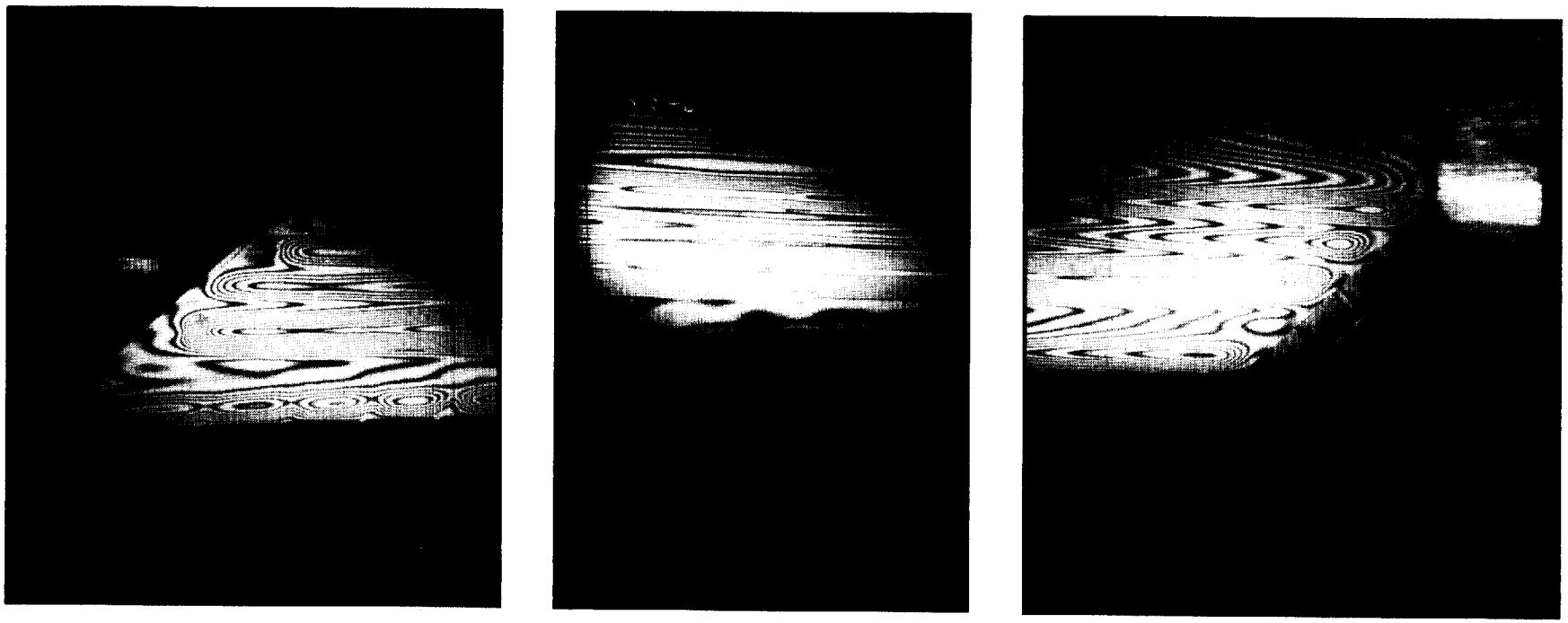

F-57109

Figure 166. Full-Length Support Structure Holograms of Sidewall Passage Side, at 840 psig and 50 psid (No Braze Voids)

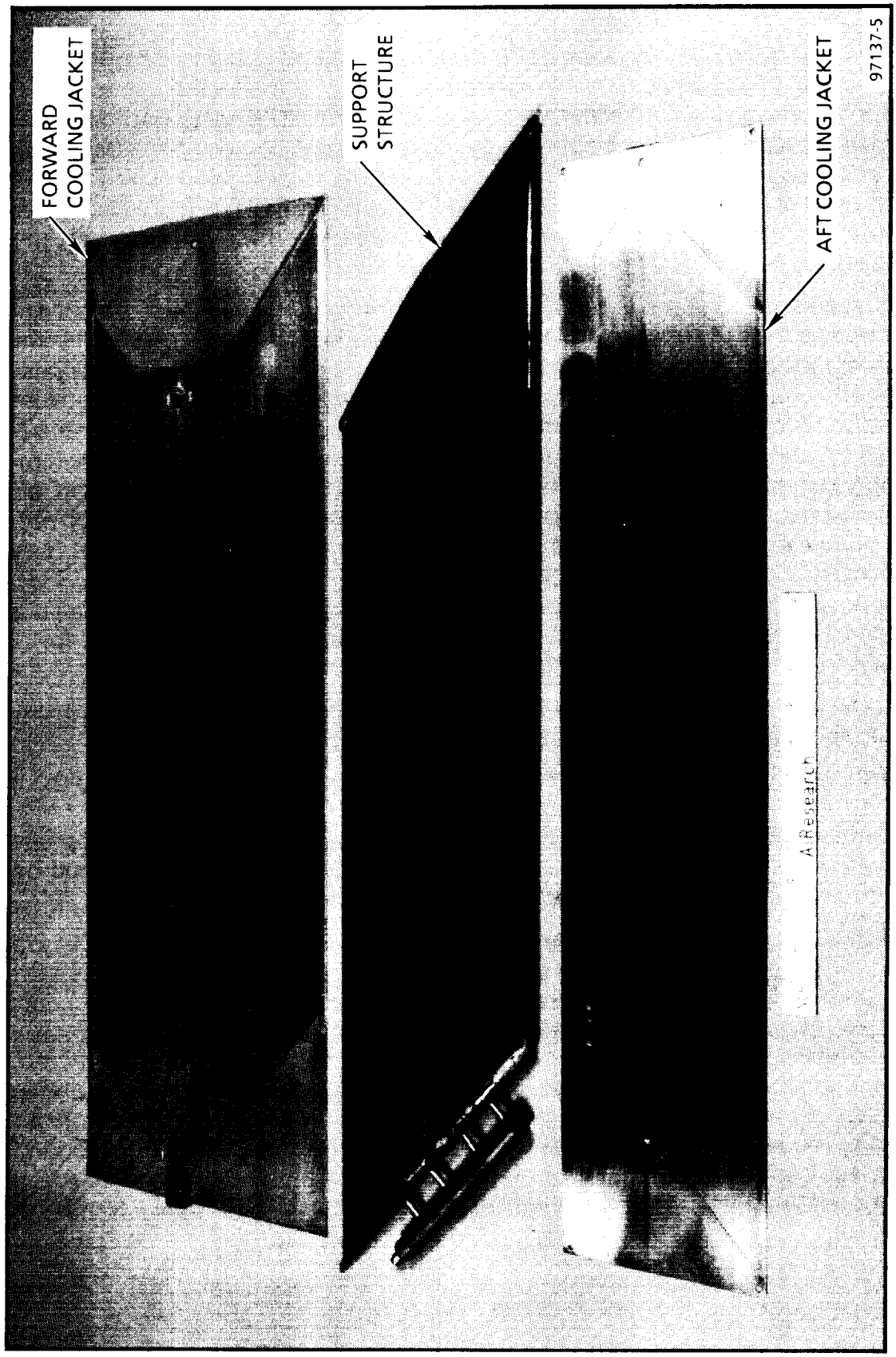

Figure 167. Completed Full-Length Strut Subassemblies

7. CONCLUDING REMARKS

The fabrication concepts used in the strut grew out of cost and schedule tradeoffs of sheet-metal-based versus machining-based designs for the support structure. Other fabrication approaches were eliminated because of relatively large tooling costs or high-risk development that were inappropriate for a one-only assembly. The underlying assumption was that formed sheet metal can be made forgiving of relatively loose tolerances by use of pressure-loaded hot-sizing and brazing operations to obtain the needed braze fits. On this assumption, the sheet metal assembly showed significant advantages and was selected.

Actual experience showed that the accommodation of tolerances was limited by the bulk of material and the stoutness of the structure required for strut pressure containment. Additionally, fabrication was complicated by: (1) distortions in the as-brazed subassemblies that required considerable effort to eliminate; (2) machined faying surfaces that had been retained to assure the precise fits needed for high-strength brazements; and (3) an increased number of parts and faying surfaces to accommodate the more incremental assembly required by the sheet-metal-type design. The combination of these factors essentially negated the expected advantage of the formed concept. Development was highly serial along each step of the way, since each operation was a first, especially in regard to the scale-up to the full-length from the partial-length strut. By means of the careful progression from operation to operation, a sound support structure was successfully produced.

The cooling jackets were developed to the stage of successful completion of the brazed assemblies. Scaleup to full-length from partial-length again required adjustments in processing, but was generally less sensitive than the support structure.

The overall hardware experience on the program indicates that improved producibility of the current design requires substantial commitments for tooling and automation of operations, and developmental hardware to establish and verify methods and processes. Thus, for a one-of-a-kind strut, machining of the support structure is probably a more cost-effective approach, offering an overall-reduced schedule and cost risk.

Fabrication requirements of the cooling jackets are generally in hand and of acceptable risk. A simplification of the final assembly of the cooling jackets to the support structure, however, appears desirable and feasible. It involves eliminating the jacket cover sheets and brazing the pin-fin panels directly to the support structure, i.e., pin-fin tips directly to an Inconel-718 support structure. This would both reduce the number of braze steps and improve formability of the jackets. Cooling jacket assemblies that are self-contained for pressure were used in the design to facilitate verification of jacket integrity on a stand-alone basis and to limit the extent of rework solely to the jackets. This is now considered less beneficial than the resulting simplification of the direct braze. Experimental verification of structural performance will be required to substantiate feasibility of this jacket type.

In summary, the program was successful in producing proof-tested cooling jackets and support structure, and has defined the fabrication requirements for a fuel-injection strut of this type. Many of the issues that were speculative at the start of the program were clarified. These issues included the following:

- Fabrication feasibility of the sheet-metal support structure concept in terms of (1) pressure containment and (2) dimensional control. This was confirmed, but is not recommended for one-time development.

- Fabrication feasibility of the self-contained pin-fin cooling jackets in terms of (1) scale-up to full-length, (2) containment of high pressure (1500 psig proof), and (3) plugging by braze filler alloy. This was confirmed, although direct brazing to the support structure (see above) presents an attractive opportunity for further simplification.

- Verification of leading edge fabrication and low cycle fatigue performance. Basic fabrication was successfully demonstrated on the subelement level and full-length tooling was developed. A simplified method for LCF testing of the leading edge stagnation region was evolved and evaluated.

A number of paths were often attempted in resolving general processing and specific tooling, forming, handling, and brazing questions, leading to a focus on successful methods and governing constraints. The resulting data base provides a basis for manufacture of both the specific design used here and alternative designs that may be formulated for improved producibility or other applications.

8. REFERENCES

1. Hypersonic Research Engine Project—Phase II, Structures and Cooling Development, Final Technical Data Report. Data Item No. 55-7.18, NASA CR-112087, May 18, 1972.

2. Killackey, J.J., Katinszky E.A., Tepper, S., Vuigner, A.A., Wright, C.C., and Stockwell, G.G., Thermal-Structural Design Study of an Airframe-Integrated Scramjet, Prepared under Contract No. NAS1-13984 by AiResearch Manufacturing Company, The Garrett Corporation. NASA CR-159039, May 1980.

3. Buchmann, O.A., Summary Report, Thermal-Structural Design Study of an Airframe-Integrated Scramjet, NASA CR-3141, 1978.

4. Wieting, Allan R., and Guy, Robert W., Thermal-Structural Design/Analysis of an Airframe-Integrated Hydrogen-Cooled Scramjet, J. of Aircraft, Vol. 13, No. 3, March 1976, pp. 192 to 197.

5. Buchmann, O.A., Arefian, V.V., Warren, H.A., Vuigner A.A., and Pohlman, M.J., Advanced Fabrication Techniques for Hydrogen-Cooled Engine Structures, Prepared under Contract No. NAS1-14180 by AiResearch Manufacturing Company, The Garrett Corporation, NASA CR-3949, November 1985.

6. Buchmann, O.A., "Advanced Fabrication Techniques for Cooled Engine Structures," Recent Advances in Structures for Hypersonic Flight, NASA CP 2065, pp. 145 to 193, September 1978.

7. Tetelman, A.S. and McEvily, Jr., A.J., Fracture of Structural Materials, p. 377, John Wiley and Sons, Inc., 1967.

8. Hertzberg, Richard W., Deformation and Fracture Mechanics of Engineering Materials, p. 459, John Wiley and Sons, Inc., 1976.

NASA Contractor Report 181945
Distribution List
NAS1-16097

	No. Copies
NASA Langley Research Center Hampton, VA 23665-5225 Attn: 151/Research Information Office	2
139A/Technology Utilization Office	1
243/Harold N. Murrow	25
NASA Ames Research Center Attn: 202-3/Library Moffett Field, CA 94035	1
NASA Dryden Flight Research Facility Ames Research Center Attn: Library P. O. Box 273 Edwards, CA 93523	1
NASA Goddard Space Flight Center Attn: Library Greenbelt, MD 20771	1
NASA Marshall Space Flight Center Attn: AS24L/Library Marshall Space Flight Center, AL 35812	1
Jet Propulsion Laboratory Attn: 111-113/Library 4800 Oak Grove Drive Pasadena, CA 91103	1
NASA Lewis Research Center Attn: 60-3/Library 21000 Brookpark Road Cleveland, OH 44135	1
NASA John F. Kennedy Space Center Attn: NWSI-D/Library Kennedy Space Center, FL 32899	1
National Aeronautics and Space Administration Attn: RM Washington, DC 20546-0001	1
NASA Scientific and Technical Information Facility P. O. Box 8757 Baltimore/Washington International Airport, MD 21240	19 plus original

Report Documentation Page

1. Report No.	2. Government Accession No.	3. Recipient's Catalog No.
NASA CR 181945		

4. Title and Subtitle	5. Report Date
Development and Fabrication of Structural Components for a Scramjet	March 1990
	6. Performing Organization Code
7. Author(s)	8. Performing Organization Report No.
O. A. Buchmann	89-62543
	10. Work Unit No.
	505-80-31-01
9. Performing Organization Name and Address	11. Contract or Grant No.
AiResearch Los Angeles Division Allied-Signal Aerospace Company 2525 W. 190th Street Torrance, CA 90509	NAS1-16097
	13. Type of Report and Period Covered
12. Sponsoring Agency Name and Address	Contractor Report (Final) March 1980–May 1989
National Aeronautics and Space Administration Langley Research Center Hampton, VA 23665-5225	14. Sponsoring Agency Code

15. Supplementary Notes

Langley Technical Monitor: H. Murrow

16. Abstract

This report documents the final phase of a program broadly directed toward design and development of long-life (100 hours and 1,000 cycles with a goal of 1,000 hours and 10,000 cycles) hydrogen-cooled structures for application to scramjets. Previous phases of the program resulted in (1) an overall engine design and (2) analytical and experimental characterization of selected candidate materials and concepts. The latter efforts indicated that the basic life goals for the program can be reached with available means.

The main objective of the effort reported here was an integrated, experimental evaluation of the results of the previous program phases. The fuel injection strut was selected for this purpose, including fabrication development and fabrication of a full-scale strut. Testing of the completed strut was to be performed in a NASA-Langley wind tunnel. In addition, conceptual designs were formulated for a heat transfer test unit and a flat panel structural test unit.

Tooling and fabrication procedures required to fabricate the strut were developed, and fabrication and delivery to NASA of all strut components, including major subassemblies, were completed.

17. Abstract	18. Abstract
Regeneratively cooled structure Scramjet Thermal protection system Fuel injection strut	UNCLASSIFIED-UNLIMITED

19. Security Classif. (of this report)	20. Security Classif. (of this page)	21. No. of pages	22. Price
UNCLASSIFIED	UNCLASSIFIED	234	